TECHNISCHE UNIVERSITÄT MÜNCHEN

Department Chemie

Lehrstuhl für Biotechnologie

Characterization of the essential Hsp90 co-chaperone Sgt1 in *S. cerevisiae*

Christopher Marius Dodt

Vollständiger Abdruck der von der Fakultät für Chemie der Technischen Universität München zur Erlangung des akademischen Grades eines Doktors der Naturwissenschaften (Dr.rer.nat.) genehmigten Dissertation.

Vorsitzender:	Prof. Dr. Matthias Feige
Prüfer der Dissertation:	1. Prof. Dr. Johannes Buchner
	2. Prof. Dr. Michael Sattler

Die Dissertation wurde am 29.10.2020 bei der Technischen Universität München eingereicht und durch die Fakultät für Chemie am 08.12.2020 angenommen.

Content

Summary

In *Saccharomyces cerevisiae* the Hsp90 machinery is assisted by twelve co-chaperones. Sgt1 is among those co-chaperones and essential for yeast viability. During the course of research on Sgt1 the question about the essential biological role remained unanswered. Moreover, the integration into the chaperone network stayed incomplete. This thesis addressed those to major open questions.

The C-terminal SGS domain of Sgt1 was demonstrated to harbor solely the essential *in vivo* function. Using NMR structural data of the SGS domain were obtained showing two stable helices separated by a turn. Additionally, two transient helices one located before and one after the helix-turn-helix motif were revealed. Further dissection of these structural elements concerning their role in yeast viability displayed that the stable helix II ranging from residue 351-365 is the most crucial structure. The combination of NMR data and *in vivo* analysis suggests a conformational switch within this helix II at serine 361, which most likely is regulated by phosphorylation.

Physical and genetic interactome analyses of Sgt1 and of the essential SGS domain indicate a biological role in protein folding and ribosome assembly. Interestingly, the SGS domain displayed interactors from a broad spectrum of chaperone classes suggesting cooperative action on protein folding. Moreover, the combination of genetic and physical interaction data strongly implies a role in ribosome-associated protein folding. Cell cycle resolved interaction studies of the SGS domain yielded a differential set of enriched proteins. However, the annotation of biological roles indicates a consistent function during cell cycle progression of the essential domain.

The integration of Sgt1 into the chaperone network revealed unprecedented interaction between Sgt1 and Hsp90. *In vitro* analysis strongly suggests that Hsp90 utilizes an extended binding interface comprising not only the NTD but at least an additional domain for Sgt1 interaction. Furthermore, the interaction with Hsp90 is not solely mediated by the CS domain of Sgt1 but also the CS-SGS-inter-domain linker seems to participate in stable binding. Additionally, the *in vitro* data indicates different interaction modes depending on the conformational state of Hsp90, of which the AMP-PNP-induced closed state is the preferred one for Sgt1 interaction.

The analysis of the interplay with the Hsp70 system showed that Sgt1 most likely directly interacts with Hsp40 instead of Hsp70. The interaction is mediated by the essential SGS domain of Sgt1. The quaternary complex formation between Sgt1, Hsp40, Hsp70 and Hsp90 suggests a bridging function of Sgt1. Moreover, *in vivo* experiments indicate that the phosphorylation of the conformational switch of Sgt1 implements a preference for the Hsp70 system.

Extended *in vitro* analysis on the integration of Sgt1 into the Hsp90 co-chaperone network and the Hsp70 system tempt to speculate about a combined chaperone cycle of both machineries mediated

by Sgt1. In brief, Sgt1 enters the Hsp70 system by interacting with Hsp40. By facilitating a bridging complex between Hsp90 and Hsp40/Hsp70, Sgt1 transfers to the Hsp90 machinery. Trimeric complex formation with TPR-containing co-chaperones allows simultaneous action. Acceleration of the conformational cycle of Hsp90 by Aha1 drives the conformation-specific binding of Sgt1. Ultimately, Sba1 competes for binding to closed Hsp90 releasing Sgt1.

Zusammenfassung

In *Saccharomyces cerevisiae* wird die Hsp90-Maschinerie von zwölf Co-Chaperonen unterstützt. Sgt1 gehört zu diesen Co-Chaperonen und ist essentiell für die Lebensfähigkeit von Hefe. Im Verlauf der Forschung an Sgt1 blieb die Frage nach der wesentlichen biologischen Rolle unbeantwortet. Zudem blieb die Integration in das Chaperon-Netzwerk unvollständig. Diese Arbeit befasst sich mit diesen wichtigen offenen Fragen.

Es konnte gezeigt werden, dass die C-terminale SGS-Domäne von Sgt1 die essentielle *in vivo* Funktion trägt. Mit Hilfe von NMR wurden Strukturdaten der SGS-Domäne erlangt, die zwei stabile Helices zeigen, die durch einen Turn getrennt sind. Zusätzlich wurden zwei transiente Helices, eine vor und eine nach dem Helix-Turn-Helix-Motiv, nachgewiesen. Weiteres Sezieren dieser Strukturelemente hinsichtlich ihrer Rolle für die Lebensfähigkeit von Hefe zeigte, dass die stabile Helix II im Bereich von Aminosäure 351-365 die wichtigste Struktur ist. Die Kombination von NMR-Daten und *in vivo* Experimenten lässt auf einen Konformationsschalter innerhalb dieser Helix II bei Serin 361 schließen, der höchstwahrscheinlich durch Phosphorylierung reguliert wird.

Physikalische und genetische Interaktom-Analysen von Sgt1 und der essentiellen SGS-Domäne deuten auf eine biologische Rolle bei der Proteinfaltung und dem Ribosomenaufbau hin. Interessanterweise zeigte die SGS-Domäne Interaktoren aus einem breiten Spektrum von Chaperonen, die auf eine kooperative Funktion bei der Proteinfaltung schließen lassen. Darüber hinaus deutet die Kombination von genetischen und physikalischen Interaktionsdaten stark auf eine Rolle bei der ribosomen-assoziierten Proteinfaltung hin. Zellzyklus-aufgelöste Interaktionsstudien der SGS-Domäne ergaben unterschiedliche angereicherte Proteine. Dennoch deutet die Annotation der biologischen Rollen auf eine konsistente Funktion während des Zellzyklus hin.

Die Integration von Sgt1 in das Chaperon-Netzwerk zeigte eine neuartige Interaktion zwischen Sgt1 und Hsp90. Die *In-vitro* Analyse deutet stark darauf hin, dass Hsp90 eine erweiterte Bindungsstelle nutzt, die nicht nur die NTD, sondern mindestens eine zusätzliche Domäne für die Interaktion mit Sgt1 umfasst. Darüber hinaus wird die Interaktion mit Hsp90 nicht nur durch die CS-Domäne von Sgt1 vermittelt, sondern auch der CS-SGS-Interdomänen-Linker scheint an einer stabilen Bindung beteiligt zu sein. Zusätzlich weisen die *in vitro* Daten auf unterschiedliche Interaktionsmodi in Abhängigkeit des Konformationszustands von Hsp90 hin, von denen der AMP-PNP-induzierte geschlossene Zustand der bevorzugte für die Sgt1-Interaktion ist.

Die Analyse des Zusammenspiels mit dem Hsp70-System zeigte, dass Sgt1 höchstwahrscheinlich direkt mit Hsp40 anstelle von Hsp70 interagiert. Die Interaktion wird durch die essentielle SGS-Domäne von Sgt1 vermittelt. Die quaternäre Komplexbildung zwischen Sgt1, Hsp40, Hsp70 und

Hsp90 legt eine Brückenfunktion von Sgt1 nahe. Darüber hinaus deuten *in vivo* Experimente darauf hin, dass die Phosphorylierung des Konformationsschalters von Sgt1 eine Präferenz für das Hsp70-System implementiert.

Erweiterte *In-vitro* Analysen über die Integration von Sgt1 in das Hsp90-Co-Chaperon-Netzwerk und das Hsp70-System verleiten zu Spekulationen über einen kombinierten Chaperonzyklus beider Maschinerien, der durch Sgt1 vermittelt wird. Zusammengefasst, Sgt1 tritt in das Hsp70-System ein, indem es mit Hsp40 interagiert. Der Eintritt in den Hsp90-Zyklus wird durch die Ausbildung eines Brückenkomplexes zwischen Hsp90 und Hsp40/Hsp70 ermöglicht. Die Bildung eines trimeren Komplexes mit TPR-haltigen Co-Chaperonen ermöglicht eine gleichzeitige Funktionsausübung der Co-Chaperone. Die Beschleunigung des Konformationszyklusses von Hsp90 durch Aha1 treibt die konformationsspezifische Bindung von Sgt1 voran. Was zur bevorzugten Bindung an geschlossenes Hsp90 führt. Letztendlich konkurriert Sba1 um die Bindung an geschlossenes Hsp90, wobei Sgt1 freigesetzt wird.

1. Introduction

1.1. Protein folding

Proteins are one of the major groups of macromolecules and are involved in almost every cellular function. An average mammalian cell expresses 10,000-20,000 different protein species, which further can be modified in function (Bekker-Jensen et al., 2017, Kulak et al., 2017).

The linear polypeptide chain consisting of proteogenic amino acids needs to adopt a unique, thermodynamically stable three-dimensional structure to reach the functional active state (Hartl and Hayer-Hartl, 2009). Pioneer work by Anfinsen showed the spontaneous refolding of a small protein *in vitro* implicating that the information of the native conformation of a protein is encoded in its primary sequence (Anfinsen, 1973). However, if a protein consisting of 100 amino acids, would explore all possible conformations, the protein would need more than 10^{30} seconds to reach the optimal state. This implies that, reaching the native state by random sampling would exceed the life time of the universe (Levinthal, 1968). Hence, proteins must populate folding intermediates on their way to the native state (Dinner et al., 2000, Dobson, 2003). Folding to the native state of small proteins is well understood by now (Dobson and Karplus, 1999, Hartl and Hayer-Hartl, 2009). Yet, the major fraction of proteins consists of more than 100 amino acids and forms multi-domain proteins prone to inefficient folding, if unassisted (Brockwell and Radford, 2007). Moreover, molecular crowding, the tremendous concentration of macromolecules, impinges the folding *in vivo* and enhances folding intermediates, misfolded states and aggregates (Ellis and Minton, 2006).

The folding of proteins depends on many weak, noncovalent interactions of amino acids both close and far away in the primary sequence (Brockwell and Radford, 2007, Dobson, 2003, Fersht, 2000). Hydrophobic forces are crucial in driving chain collapse and the burial of nonpolar amino acids in the core of the folded structure, further restricting the possible conformational states during folding (Dinner et al., 2000). Thus, protein folding is not considered to occur along a linear pathway but rather sampling on the free-energy landscape towards the thermodynamically favorable state. The folding funnel describes an energy landscape, on which polypeptides travel downhill to adopt their native fold (Balchin et al., 2016, Balchin et al., 2020, Dill and MacCallum, 2012, Dinner et al., 2000). During their folding process proteins often overcome multiple local minima representing folding intermediates to reach their native fold. However, kinetically trapped folding intermediates tend to stably misfold leading to potential harmful protein aggregates (Balchin et al., 2020, Dinner et al., 2000). Partially structured polypeptides exposing hydrophobic patches are typically prone to aggregate in a concentration-dependent manner (Chiti and Dobson, 2006). Albeit, the major fraction of aggregates is amorphous, some form a structurally stable cross-β-structure, so called amyloid

fibrils (Balchin et al., 2016). Protein aggregation and especially the formation of amyloid fibrils are connected to various disease, e.g. mutations in superoxide dismutase are linked to amyotrophic lateral sclerosis, poly-Q tracts linked to Huntington's disease and amyloid-beta (Aβ) as well tau to Alzheimer's disease (Shahheydari et al., 2017, Soto and Pritzkow, 2018, Vacchi et al., 2020).

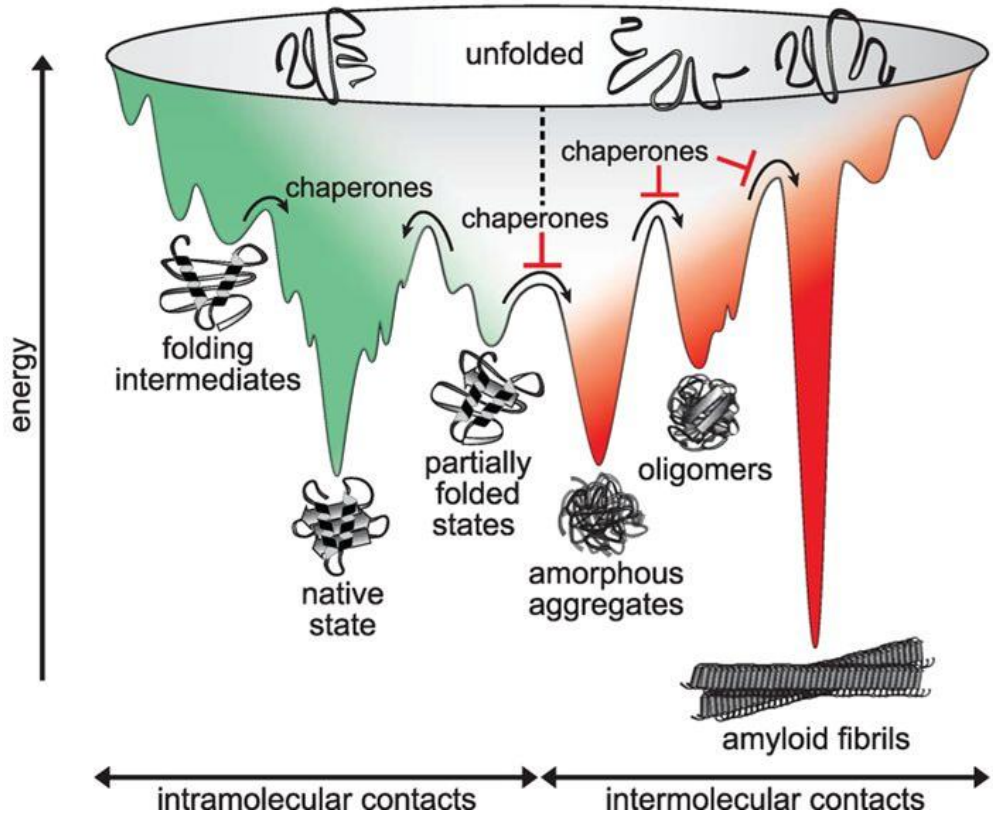

Figure 1: Protein folding funnel. An unfolded polypeptide samples along the potential free-energy landscape during folding. Partially folded states or folding intermediates overcome kinetic barriers by chaperone assistance to reach the native state (green). The unfolded protein or partially folded states collapse into unfavorable energy minima leading to various forms of aggregates of which amyloid fibrils might be thermodynamically the most stable (red). Adapted from (Balchin et al., 2016).

1.2. The Proteostasis network (PN)

The increasing number of age-related proteinopathies demonstrates the importance of the balance between maintaining protein homeostasis and proper proteasomal degradation (Higuchi-Sanabria et al., 2018, Labbadia and Morimoto, 2015, Taylor, 2011). The interconnected pathways of synthesis, folding, maintaining and degrading proteins is referred to as the proteostasis network (Jayaraj et al., 2020). Since the conformational flexibility is often part of the functionality, proteins typically do not adopt one rigid native folded state. Moreover, a fraction of about 30 % of the proteome are considered intrinsically disordered or partially unstructured (Dunker et al., 2008). Environmental stress and genetic variation challenge the proteostasis network. A molecular machinery exists to

prevent detrimental interactions and toxic aggregates (Roth et al., 2014, Olzscha et al., 2011). The proteostasis network evolved to control quality not only on a given time point in a protein's life, but also has generated specific factors to control cellular distribution and localization (Moehle et al., 2019, Hetz et al., 2015).

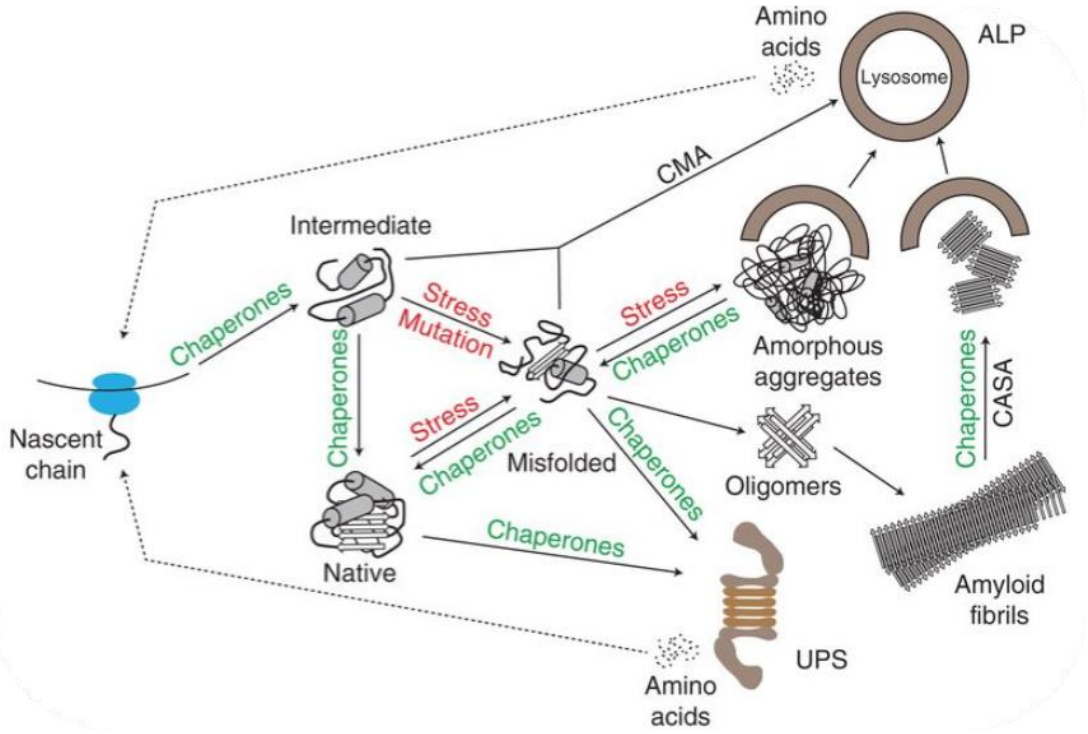

Figure 2: Proteostasis network. Chaperones fulfill the central role in the proteostasis network. Ribosome-associated chaperones contact the emerging nascent chain to prevent misfolding and aggregation. Downstream of these early acting chaperones cytosolic or compartment-specific chaperones assist in folding and maintain the structural conformation counteracting environmental or mutational stress. Misfolded or aggregated proteins are selectively targeted for degradation by the ubiquitin-proteasome system (UPS) or autophagy-lysosomal pathway (ALP) assisted by chaperones. Adapted from (Jayaraj et al., 2020) by permission of Cold Spring Harbor Laboratory Press.

The earliest interaction in the quality control system occurs at the ribosomal exit tunnel and is involved in the surveillance of *de novo* synthesizing proteins (Deuerling, 2019). Although, small proteins may undergo folding within the ribosomal exit tunnel (Nilsson et al., 2015, Holtkamp et al., 2015), the majority of proteins folds co- or/and post-translational assisted by molecular chaperones (Doring et al., 2017, Deuerling, 2019). In eukaryotic cells preeminently two chaperone systems act on *de novo* synthesizing proteins. These are the heterodimeric nascent polypeptide-associated complex (NAC) and the ribosome-associated complex (RAC) consisting of a specialized Hsp70/Hsp40 chaperone system.

The nascent polypeptide-associated complex NAC consists of an α- and a β-subunit, which are evolutionarily conserved among eukaryotes (Wiedmann et al., 1994, Gamerdinger, 2016, Kramer et al., 2019). The limited structural data of NAC indicates a location of the protein complex in close proximity to the nascent peptide tunnel exit (Nyathi and Pool, 2015, Pech et al., 2010, Wegrzyn et al., 2006). Its equimolar abundance relative to ribosomes points to the involvement in protection of *de*

novo synthesizing proteins acting as an ATP-independent chaperone (Raue et al., 2007, Preissler and Deuerling, 2012, Duttler et al., 2013). Additionally, NAC seems to act as a counterpart for ribosomal-Sec61 association (Gamerdinger et al., 2015). Localization of the ribosome to the endoplasmic reticulum (ER) is mediated by the Sec61 complex, which shows low nanomolar association, even if no signal peptide is present (Jungnickel and Rapoport, 1995, Borgese et al., 1974). In that regard, NAC is crucial for the localization of the ribosome (Moller et al., 1998). Moreover, evidence is given that NAC not only prevents misdirection to the ER but also promotes the localization to mitochondria (Gamerdinger et al., 2015, del Alamo et al., 2011).

The ribosome-associated complex (RAC) is the second chaperone system involved in the folding of newly synthesizing proteins in eukaryotes. RAC has been extensively studied in yeast, in which RAC consists of the Hsp40 protein Zuo1 and the ATPase-inactive Hsp70 isoform Ssz1. This module recruits the ribosome-associated yeast Hsp70s Ssb1/2 to the ribosomal exit tunnel and stimulates Ssb's ATPase and thereby association with the emerging polypeptide (Preissler and Deuerling, 2012). In mammals RAC recruits a cytosolic Hsp70 variant (Hsp70L1 in humans), which in contrast to Ssb cannot bind to the ribosome by itself (Preissler and Deuerling, 2012, Zhang et al., 2017). Studies on the interactome of Ssb showed that the chaperone is associated with approx. 80 % of cytosolic, nuclear and mitochondrial proteins as well as 40 % of ER-targeted proteins, indicating a role in distribution and location of target substrate proteins (Doring et al., 2017, Willmund et al., 2013). Although, a ribosome-associated Hsp70 like Ssb is missing in higher eukaryotes, it is thought, that the recruitment of cytosolic Hsp70 by RAC compensates this function (Jaiswal et al., 2011).

In prokaryotes only one ribosome-associated chaperone is present, the trigger factor (TF). TF acts as an ATP-independent holdase in close proximity to the ribosomal exit tunnel protecting newly-synthesized proteins from aggregation (Deuerling et al., 1999, Teter et al., 1999, Kramer et al., 2019).

To balance the steady state of proteins within a cell, degradation pathways counteract the protein synthesis. The degradation of proteins not only recycles no longer needed proteins, but also protects the cell from toxic aggregates by degrading misfolded proteins. This branch of the eukaryotic PN consist of mainly two machineries, the ubiquitin-proteasome system (UPS) and the autophagy-lysosomal pathway (ALP) (Forster et al., 2013, Cohen-Kaplan et al., 2016, Dikic, 2017, Varshavsky, 2017).

The ubiquitin-proteasome system (UPS) depends on the covalent modification of target proteins with the small protein ubiquitin by an ATP-dependent cascade. Three enzymes, termed E1, E2 and E3, participate in the covalent modification of a target protein. E1 activates the ubiquitin by the use of ATP, next the ubiquitin-conjugating enzyme E2 takes over the activated ubiquitin and in the last step

the ubiquitin ligase E3 covalently links ubiquitin via an isopeptide bond to a specific target protein (Zheng and Shabek, 2017, Finley, 2009, Varshavsky, 2017). Degradation of the ubiquitinylated protein is performed by the 26 S proteasome, which consists of the catalytic core unit 20 S and the 19 S cap which provides ATP-dependent unfolding of the target protein (Dong et al., 2019, Bhattacharyya et al., 2014). Since the proteasome requires ubiquitinylated, unfolded substrate, the UPS alone is not able to clear aggregates, so that cooperation with the disaggregating chaperone machinery is necessary (Esser et al., 2004).

In contrast to the UPS the autophagy-lysosomal pathway (ALP) is sufficient to clear aggregates on its own. The ALP removes aggregates by encapsulation of the insoluble inclusions with a membrane structure and subsequent fusion with the lysosome (Galluzzi et al., 2017). Also, ALP can be assisted by chaperones. In case of the chaperone-assisted selective autophagy (CASA) chaperones recruit the autophagy machinery to the insoluble deposit (Arndt et al., 2010, Carra et al., 2008, Gamerdinger et al., 2009). A second autophagy process, in which chaperones directly translocated the target protein into the lysosome by binding to the receptor LAMP2A, is referred as to chaperone-mediated autophagy (CMA) (Kaushik and Cuervo, 2018).

The central hub connecting every branch and fulfilling folding and conformational maintenance is accomplished by molecular chaperones.

1.3. Molecular chaperones

By definition molecular chaperones assist in the folding and maintaining of the conformational integrity and assembly of other proteins without being part of its final structure (Hartl et al., 2011, Ellis, 1990, Ellis, 2006, Dingwall and Laskey, 1990). Due to the fact that a temperature upshift increases the expression of certain chaperones, they are mostly referred as to heat shock proteins (Hsps) (Ritossa, 1962, Ritossa, 1996). Chaperones are most often grouped according to their molecular mass: Hsp40, Hsp60, Hsp70, Hsp90, Hsp100 and small heat shock proteins (sHsps).

1.3.1. Small heat shock proteins

Proteins of the small heat shock class share a central α-crystallin domain (ACD) (Caspers et al., 1995). The ACD, the only structurally folded domain of sHsps, is flanked by two flexible regions, the N-terminal region (NTR) and the C-terminal region (CTR). The CTR consisting of mostly polar and charged residues is suggested to be necessary for the solubility of the protein even under extremely high protein concentrations (Smulders et al., 1996, Horwitz, 2003). The ACD is the site of

dimerization and also seems to be involved in client binding, as well as binding to non-client proteins like the Hsp70 co-chaperone Bag3 (Mainz et al., 2015, Rauch et al., 2017, Delbecq et al., 2015). The variable NTR contains a high number of hydrophobic amino acids. It is also involved in client interaction (Cox et al., 2018, Sluchanko et al., 2017, Bloemendal, 1977) and in the formation and dynamics of oligomers as suggested by Braun and Jehle (Braun et al., 2011, Jehle et al., 2011). Extensive studies on the client interaction could so far not clearly define one mode of action for sHsp, the chaperone activity more likely depends on the client/sHsps pair as well as specific tissue localization and cellular conditions (Rogalla et al., 1999, Cox et al., 2016, Mymrikov et al., 2017, Mymrikov et al., 2020)

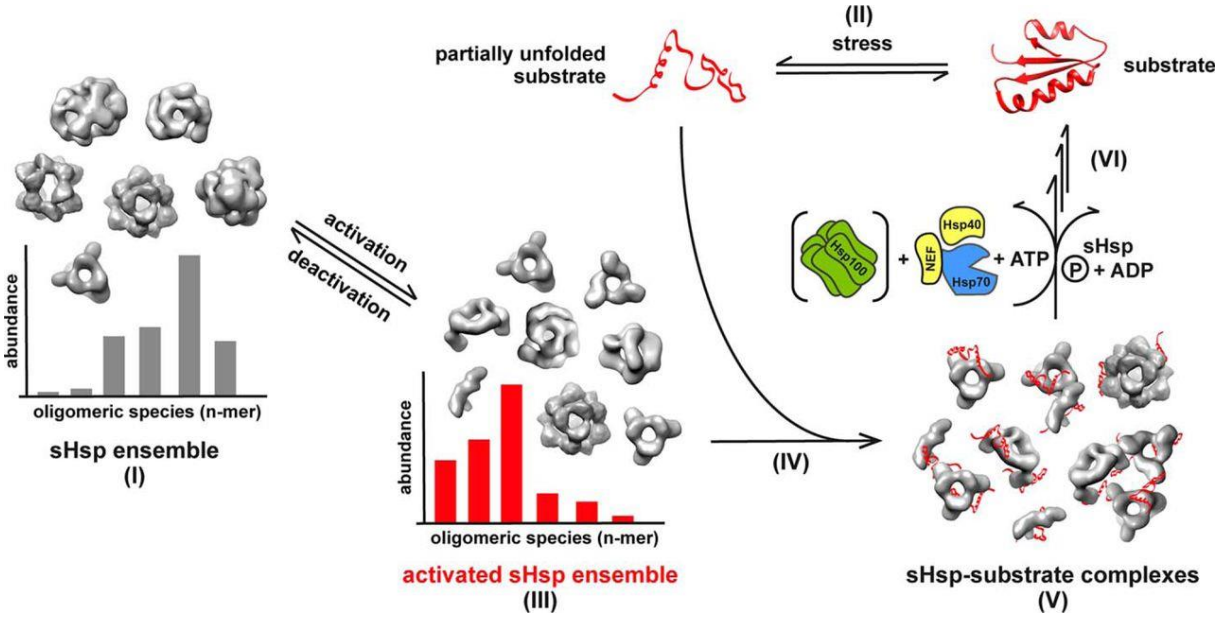

Figure 3: Mode of function of sHsps. Small heat shock proteins occur in a dynamic equilibrium of various oligomeric states. Upon activation due to stresses or phosphorylation, the oligomeric species shift towards smaller ones buffering un/mis-folded proteins as holdase in a refolding competent state for downstream chaperones like Hsp70. Adapted from (Haslbeck et al., 2019).

The ATP-independent holdases are involved in the implementation of various constitutive roles like maintaining the integrity of the eye lens (Haslbeck et al., 2016, Kaiser et al., 2019) and regulation of cytoskeletal elements (Dubinska-Magiera et al., 2014, Sugiyama et al., 2000). Apart from the constitutive functions, small heat shock proteins are highly sensitive to changes in cellular conditions to prevent protein aggregation upon environmental stresses (Haslbeck et al., 2005). The change of the oligomer organization induces domain accessibility and activity. By this, sHsps respond to heat stress (Haslbeck and Vierling, 2015, Haslbeck et al., 1999), changes in pH (Fleckenstein et al., 2015, Rajagopal et al., 2015) and oxidative stress as well as metal-induced stresses (Preville et al., 1999, Kaiser et al., 2019, Mainz et al., 2012, Karmakar and Das, 2011). Additional to the response to stresses or their constitutive functions, the activity of small heat shock proteins and their oligomeric state can be regulated by phosphorylation (Jovcevski et al., 2015, Peschek et al., 2013).

1.3.2. Chaperonins (Hsp60)

The Hsp60 family of chaperones occurs as a large double-ring complex consisting of seven to nine subunits per ring depending on the species. Further, chaperonins are divided in two classes; Group I chaperonins like the prokaryotic GroEL/GroES, mitochondrial Hsp60/Hsp10 and Rubisco subunit binding protein which occurs in chloroplast. The archaeal thermosomes and eukaryotic TCP-1 ring complex (TRiC), or chaperonin-containing TCP-1 (CCT) are classified as group II chaperonins (Horwich and Willison, 1993, Hayer-Hartl et al., 2016, Lopez et al., 2015). The main difference between the two groups of chaperonins is the necessity of a co-chaperonin in case of group I (e.g. GroES in *E.coli* assists GroEL), while group II has a built-in lid replacing the co-chaperonin (Douglas et al., 2011). A single subunit consists of three domains: the apical domain (A domain) providing the client interaction site, an intermediate domain (I domain) bridging the A domain and the equatorial domain (E domain), which contributes inter- and intra-ring contacts as well as the ATP-binding site (Klumpp et al., 1997, Ditzel et al., 1998, Waldmann et al., 1995). During the ATP-driven conformational cycle of the ring system the apical domain switches its exposed surface from a hydrophilic one, which initially binds substrates, to a charged cavity, which allows the client to fold in isolation (Gupta et al., 2014, Clare et al., 2012, Gruber and Horovitz, 2016, Saibil et al., 2013). For chaperonins of the group I encapsulation of the client protein within the cavity of the Hsp60-ring depends on the co-chaperonin (Hayer-Hartl et al., 2016). Sequential binding of ATP to the other ring releases the folded substrate or allows not fully folded substrate to re-cycle (Lin et al., 2008, Sharma et al., 2008). In case of TRiC/CCT, the cavity only partially closes allowing the consecutive folding of single domains of multi-domain proteins (Russmann et al., 2012). Moreover, the subunits of TRiC/CCT are eight paralogous proteins, which differ in ATP affinity as well as recognition sites leading to an asymmetric complex (Joachimiak et al., 2014, Rivenzon-Segal et al., 2005, Kalisman et al., 2012). Whether the two rings function in a sequential manner or whether both chambers can be capped at once still remains a matter of ongoing research (Taguchi, 2015).

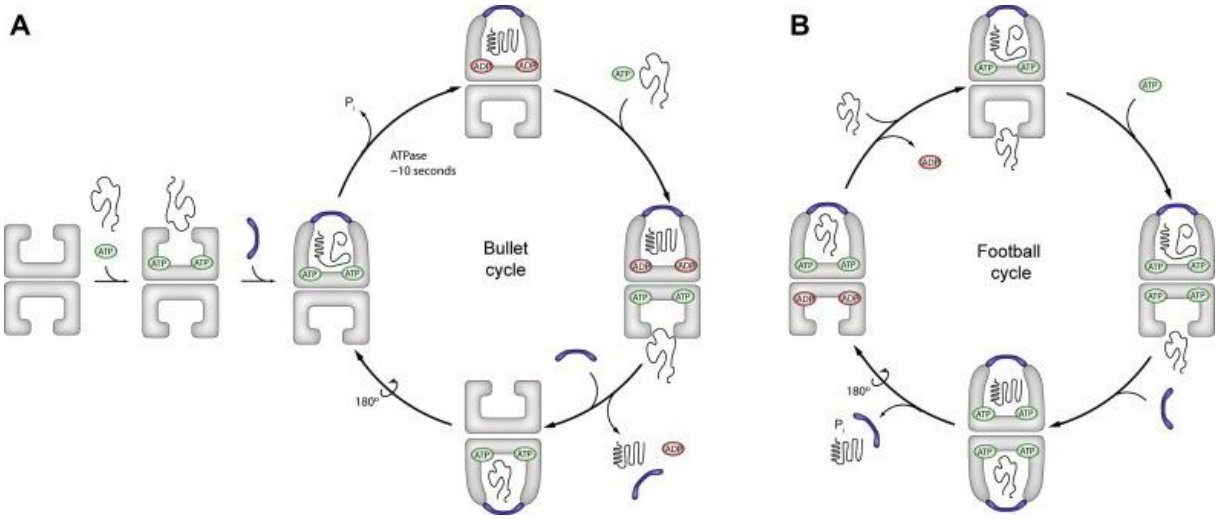

Figure 4: GroEL/GroES cycle. (A)The bullet cycle: only one chamber at a time is occupied by substrate. ATP hydrolysis and subsequent binding of the opposing ring to ATP and a substrate releases the folded client. In blue GroES. (B) The football cycle: both cavities are occupied by substrate at the same time. (Skjaerven et al., 2015) With Permission from FEBS Letter, John Wiley and Sons.

The chaperonin TRiC/CCT is able to promote client folding by itself. However, a hetero-hexameric chaperone, Prefoldin (PFD/Gim), assists in the progression of productive folding cycles (Gestaut et al., 2019, Siegert et al., 2000). The ATP-independent chaperone Prefoldin binds via an electrostatic interface to TRiC/CCT enabling the alignment of both substrate chambers to modify the folding environment of the client protein (Gestaut et al., 2019).

1.3.3. Hsp100

The class of Hsp100 disaggregases is not present in metazoa, but in all non-metazoan eukaryotes, some archaea and eubacteria (Erives and Fassler, 2015, Sweeny and Shorter, 2016). Hsp100 belongs to the class of AAA^+ ATPases forming a hexameric, asymmetric ring-like structure. The most prominent representatives of Hsp100's are the yeast Hsp104 and the bacterial ClpB (Parsell et al., 1994, Wendler et al., 2009, Yokom et al., 2016, Gates et al., 2017, Duran et al., 2017). In the case of Hsp104 one protomer is composed of an N-terminal domain (NTD), followed by two nucleotide binding domains (NBD1 and NBD2), which derive from different classes of AAA^+ ATPase families (Erzberger and Berger, 2006). Nevertheless, both contain an arginine finger residue crucial for ATP hydrolysis and conserved tyrosine residues within the axial channel of the hexameric ring required for substrate binding and translocation (Sweeny and Shorter, 2016). A short C-terminal domain completes the protomer. ATP-hydrolysis drives major conformational changes which lead to the extraction of proteins from aggregates by unfolding and translocation through the inner axial channel by a ratchet-like mechanism (Sweeny et al., 2015, Gates et al., 2017). The ATP-driven cycle of Hsp104 allows disaggregation or resolubilization of proteins from different structural conditions, like

phase-transitioned gels, disordered aggregates, pre amyloid oligomers, amyloids and prions (DeSantis et al., 2012, DeSantis and Shorter, 2012, Lo Bianco et al., 2008, Kroschwald et al., 2015, Glover and Lindquist, 1998, Shorter and Lindquist, 2004, Klaips et al., 2014). These abilities of Hsp104 demonstrate its importance in maintaining or resolving membraneless organelles like P-bodies or stress granules (Kroschwald et al., 2015, Wallace et al., 2015), enabling proteasomal degradation (Lee and Goldberg, 2010, Preston et al., 2018, Ruan et al., 2017). Also its involvement in longevity is discussed (Andersson et al., 2013, Hanzen et al., 2016, Saarikangas and Barral, 2015). The class of Hsp100 chaperones cooperates with the Hsp70 and sHsp systems to increase disaggregase capacities (Kaimal et al., 2017, Shorter and Lindquist, 2008).

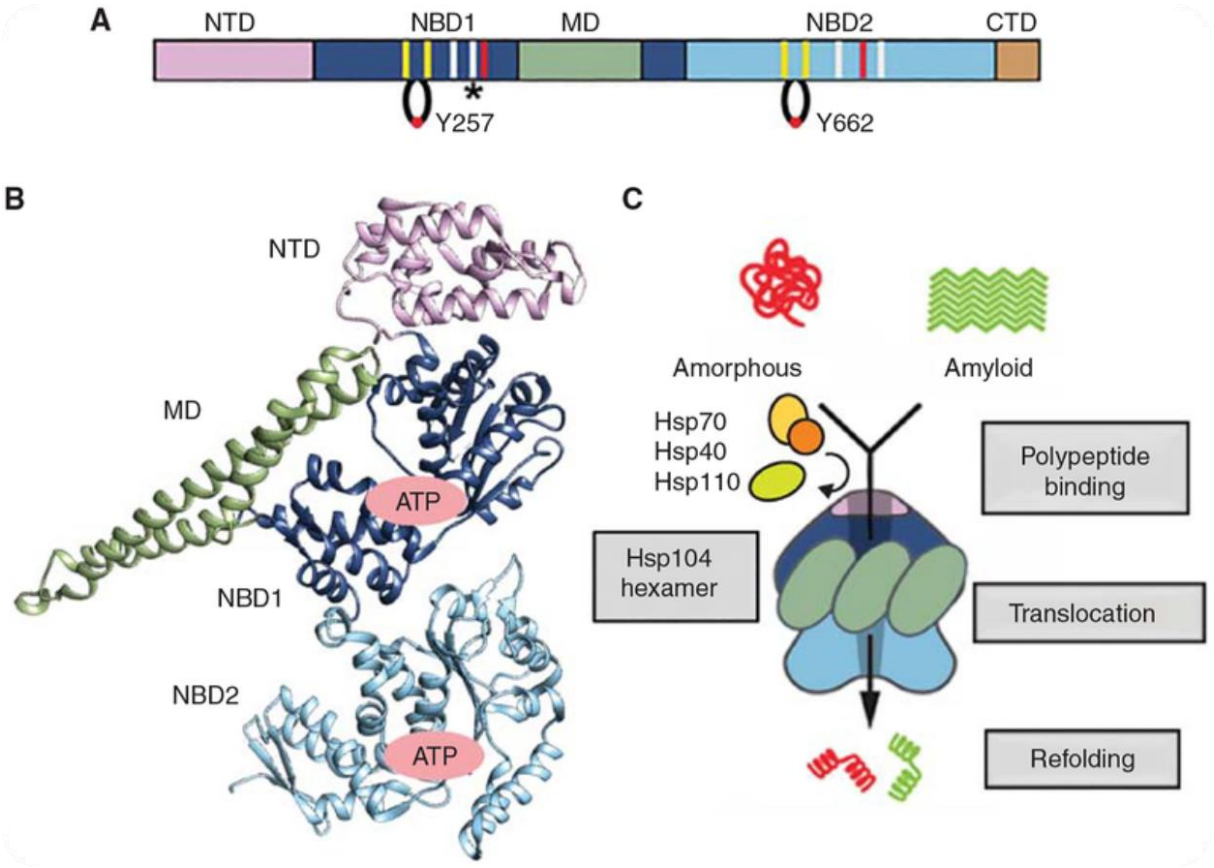

Figure 5: Structure and function of Hsp104. (A) Sketched domain structure of Hsp104. N-terminal domain (magenta), followed by the two nucleotide binding domains (dark blue and light blue), which are linked by the middle domain (green), completed by the C-terminal extension (orange). In the NBDs noteworthy features are highlighted: In yellow Walker A and B-motif, in white Sensor 1 and 2, in red the arginine finger, the asterisk indicates a putative new arginine involved in ATP-hydrolysis (Gates et al., 2017), loops indicated the conserved tyrosine residues. (B) ClpB protomer crystal structure (PDB 1QVR) (Lee et al., 2003). The bacterial homolog is colored according to A. (C) The cartoon illustrates the function of Hsp104 machinery in concert with the Hsp70 machinery. Color code as in A. Adapted from (Shorter and Southworth, 2019) by permission of Cold Spring Harbor Laboratory Press.

1.3.4. Hsp70

Members of the Hsp70 family cooperate with all above-mentioned chaperone systems, like sHsps, chaperonins and Hsp100. Additionally they play a role in protein degradation, underlying the versatility of the proteins class (Rosenzweig et al., 2019). Hsp70 is present throughout all kingdoms of life, from a few Hsp70 homologues in bacteria up to 13 Hsp70s in humans. The molecular chaperone protects cells from a wide range of proteotoxic stresses by its ability of promiscuously binding to a diverse set of client proteins (Zuiderweg et al., 2017, Mayer, 2000, Mayer and Bukau, 2005, Rosenzweig et al., 2017). Besides the classical function of a chaperone, Hsp70 performs also more distinct function. Hsp70's function in *de novo* folding of proteins emerging from the ribosomal tunnel was mentioned above. A downstream chaperone to which Hsp70 can transfer client proteins for further maturation is Hsp90, which will be discussed in section 1.4. (Scheufler, 2000, Röhl et al., 2015). If downstream transfer of client proteins fails, the client can either undergo another Hsp70 cycle or can be targeted for degradation by the Hsp70 co-chaperone and E3-ligase CHIP (carboxy terminus of Hsc70 interacting protein) (Ballinger, 1999, Stankiewicz et al., 2010, Hohfeld et al., 2001, Connell, 2001). Moreover, Hsp70 is involved in protein translocation. First, Hsp70 binds newly-synthesized proteins to keep them in a translocation-competent state (Craig, 2018). Second, compartment-specialized Hsp70 isoforms drive the translocation process across the membrane. In association with the translocon-apparatus Hsp70 generates enough inward pulling force by increasing entropy to facilitate translocation (Craig, 2018, Goloubinoff and Rios, 2007). As mentioned before Hsp70 can cooperate with Hsp100 chaperones functioning together in protein disaggregation. In metazoa, Hsp100 is absent, so that the disaggregase function is fulfilled by the coordinated action of Hsp70 and its co-factors, a J-domain protein and a nucleotide exchange factor (NEF) (Nillegoda, 2015, Shorter, 2011, Gao, 2015, Scior, 2018). Additionally, Hsp70 plays a role in assembly and disassembly of protein complexes. The most prominent example is the uncoating of clathrin-coated vesicles during endocytosis (Sousa, 2016, Sousa and Lafer, 2015, Ungewickell, 1995).

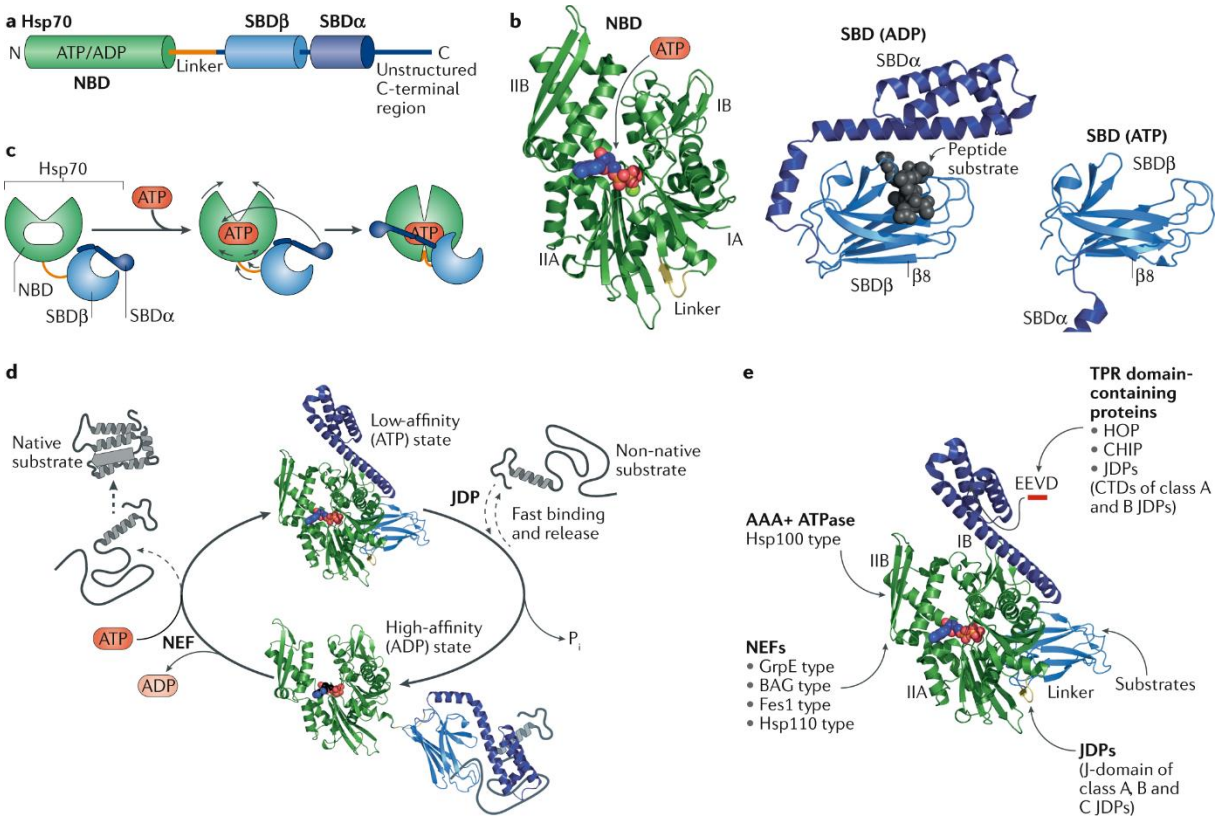

Figure 6: Structure and function of Hsp70. (A) Schematic presentation of Hsp70 domain structure. The N-terminal NBD (green) is linked to the SBD (light blue β-subunit, dark blue α-subunit) by a flexible linker followed by the unstructured C-terminal extension. (B) Left: Crystal structure of Hsp70's NBD bound to ATP (PDB 4B9Q)(Kityk et al., 2012). Middel: Structure of the SBD in high affinity state with bound substrate peptide depicted in black spheres. (PDB 1DKX) (Zhu, 1996). Right: SBD in the low affinity open state (PDB 4B9Q)(Kityk et al., 2012). (C) Presentation of the conformational changes induced by ATP binding. After rotation of the NBD lobes, the lower crevice opens, where subsequentially the interdomain linker docks, ultimately, leading to the detachment of the lid. (D) Simplified Hsp70 cycle. JDP (J-domain protein/Hsp40) assisted substrate binding leads to ATP-hydrolysis and closing of the lid reaching the high affinity state. Subsequent, nucleotide exchange assisted by nucleotide exchange factors (NEF) releases the substrate and resets Hsp70 in the low affinity state. (E) Crystal structure of Hsp70 (PDB 4B9Q) with indications of interaction sites for substrates and co-chaperones. Adapted from (Rosenzweig et al., 2019) by permission of Springer Nature.

The members of the Hsp70 class all share major structural features. The archetype consists of a nucleotide binding domain (NBD), which can be further divided in four sub domains IA, IB, IIA and IIB, the substrate binding domain (SBDβ) and the lid SBDα. The NBD is linked to the SBDβ by an interdomain linker region. Hsp70s display an unstructured C-terminal tail, which harbors the EEVD motif at its very end in eukaryotes (Flaherty et al., 1990, Rosenzweig et al., 2019). The domains of Hsp70 traverse major conformational rearrangements driven by ATP-hydrolysis, defining different states of substrate processing (Kityk et al., 2015). Binding of ATP to the NBD leads to a rotation and conformational change in the NBD, which in turn dislocates the SBDα-lid from SBDβ setting Hsp70 in an open conformation. The ATP-bound, open state of Hsp70 is the low-affinity state with respect to substrate binding. The basal ATPase activity of Hsp70 is low with approximately 1 ATP molecule per 6-40 min (Kityk et al., 2015, Kityk et al., 2012).Substrate binding to the hydrophobic binding pocket of the SBDβ releases the SBD from the NBD. Subsequent ATP-hydrolysis leads to the docking of the lid SBDα to SBDβ setting Hsp70 in the high affinity state (Mayer, 2000, Zhu, 1996). Substrate release is

triggered by nucleotide exchange and consequential entering the open state (Mayer et al., 2000, Buczynski et al., 2001). Especially, substrates exposing a peptide of five to seven amino acids with a hydrophobic core flanked by charged residues is recognized by Hsp70 (Rudiger et al., 1997). Patches of hydrophobic amino acids are usual shielded from the environment in the core of a native folded protein. Exposure of these sequences elucidates the promiscuous binding of Hsp70 to unfolded proteins (Rosenzweig et al., 2019). Despite the conservation of the peptide-binding configuration the diversity of substrate binding is further increased by variability of substrate orientation as well as the differing preferences of distinct Hsp70 family members (Morshauser, 1999, Pellecchia, 2000, Jiang et al., 2005, Zahn, 2013, Clerico et al., 2015, Rosenzweig et al., 2017, Gragerov and Gottesman, 1994).

1.3.5. Hsp40/JDP (J-domain containing proteins)

The Hsp40 proteins are co-chaperones of the Hsp70 machinery. All members of the co-chaperone family share a J-domain. Due to this they are referred to as J-domain containing proteins (JDPs). The archetype of JDPs is the bacterial Hsp40 DnaJ (Kampinga and Craig, 2010, Rosenzweig et al., 2019). The protein family is divided into three subclasses A, B and C. The class A JDPs share the architecture of DnaJ, which consists of an N-terminal J-domain, an α-helical hairpin domain of about 70 amino acids, followed by a glycine/phenylalanine-rich domain (G/F-rich). A linker connecting the G/F-rich domain to two C-terminal β-sandwich domains (CTDI and CTDII), completed by an C-terminal dimerization domain. In comparison to class B JDPs, class A comprises a zinc-finger-like region (ZFLR) inserted into the CTDI (examples class A: DnaJ (bacterial), Ydj1 (yeast), DNAJ1 to 4 (human); examples class B: CbpA (bacterial), Sis1 (yeast), DNAJB1,4,5 (human)(Cheetham and Caplan, 1998). Proteins belonging to class C only share the J-domain and show otherwise no further conservation (Kampinga and Craig, 2010).

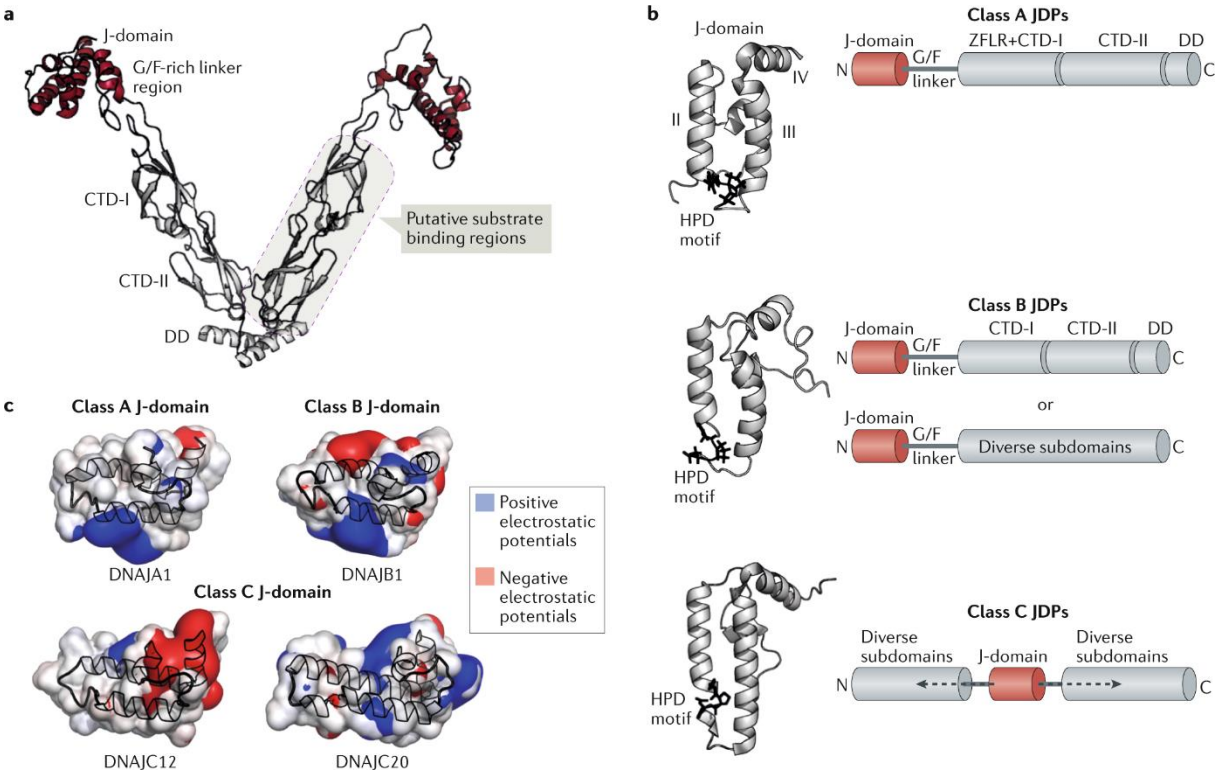

Figure 7: Structure of J-domain containing proteins. (A) Crystal structure of bacterial DnaJ (PDB 4J80), domain architecture is indicated (DD, dimerization domain; CTD, C-terminal domain; G/F-rich, glycine-phenylalanine rich domain; ZFLR, zinc-finger-like region). (B) Schematic domain organization of the three different JDP-classes. Structure of the J-domain with highlighted HPD.motif. (C) J-domains representative of all three classes display the electrostatic surfaces. Adapted from (Rosenzweig et al., 2019) by permission of Springer Nature.

The class A and B JDPs function as dimers, except the human ER-located ERdj3, which was shown to form tetramers (Chen et al., 2017, Ramos et al., 2008, Feige and Hendershot, 2011, Otero et al., 2014). The chaperones preferentially bind hydrophobic, linear sequences of around 8 amino acids. However, the preferences of substrate binding patches differ between the diverse JDPs (Rudiger et al., 2001, Li and Sha, 2003, Lee et al., 2002, Feifel et al., 1998, Jiang et al., 2019). Each protomer can bind stretches of the substrate with in CTDI and CTDII, additional, in class A JDPs the ZFLR is involved in substrate binding. Yet, these binding sites are not universal applicable (Jiang et al., 2019). Moreover, the G/F-rich domain is involved in substrate binding (Perales-Calvo et al., 2010, Yan and Craig, 1999). Binding to the substrate protein leads to the unfolding of the client and even disruption of secondary structural elements within the client (Jiang et al., 2019).

The mode of bound substrate is highly compatible for the subsequent transfer to Hsp70. Binding of the Hsp40 co-chaperone is mediated by its J-domain. Particularly, the conserved histidine-proline-aspartate (HPD) motif is crucial for complex formation (Suh et al., 1998, Suh et al., 1999, Kityk et al., 2018). Additional contacts between the C-terminal domain of Hsp70 and the CTDs of Hsp40 are reported (Jiang et al., 2019, Suzuki et al., 2010, Li et al., 2006). Besides the transfer of the predisposed client to Hsp70, the binding of JDPs to Hsp70 increases its ATPase activity and shifting Hsp70 in a non-equilibrium substrate binding state called ultra-affinity state (Los Rios and Barducci,

2014, Cyr et al., 1992, Liberek et al., 1991). Due to the substrate specifity of Hsp40, JDP-interaction dictates a specialized function to Hsp70 chaperones and adds another level of functional diversity to the Hsp70 chaperone system (Kampinga and Craig, 2010, Craig et al., 2006, Craig and Marszalek, 2017).

1.3.6. Nucleotide exchange factors (NEF) of Hsp70

NEFs form a heterogeneous class of Hsp70 co-chaperones. The functional related NEFs cluster in four structural unrelated protein families (Harrison et al., 1997, Takayama et al., 1999, Sondermann, 2001, Polier et al., 2008). In eukaryotes three distinct families are present, Bag (Bcl2-associated athanogene)-type, Hsp110s and Armadillos. The fourth class of NEFs originates from bacteria, the GrpE-type, and is also present in mitochondria and chloroplasts. Despite, their structural diversity and their different binding modes to Hsp70, their mode of action is in all cases the stabilization of the open conformation of the nucleotide binding domain of Hsp70 (Schuermann, 2008, Harrison et al., 1997, Yan et al., 2011, Wu et al., 2012). The stabilization of the open NDB allows rapid exchange from ADP to ATP, leading to the reset of HSp70 in the open, low affinity conformation and ultimately, to client release (Rosam, 2018, Gassler et al., 2001, Gowda, 2018). In addition, some NEFs block the substrate binding domain of Hsp70 to prevent unproductive rebinding of the client protein (Gowda, 2018, Rosam, 2018, Wu et al., 2012).

Different affinities of NEFs to Hsp70 and, as a consequence, varying exchange rates fine-tune the time of interaction between Hsp70 and client protein. Additionally, NEFs with further interaction domain can target Hsp70 to a specific localization or pathway (Gassler et al., 2001, Brehmer, 2001, Luders et al., 2000, Gamerdinger, 2009, Minoia, 2014).

Hence, similar to JDPs, NEFs add another level of regulation to the Hsp70 system. The tripartite Hsp70-JDP-NEF machinery is a plastic network with tremendous functional diversity.

1.4. Hsp90

The molecular chaperone Hsp90 is one of the most abundant proteins in the cell (Welch and Feramisco, 1982). Except for archaea, Hsp90 is conserved in all kingdoms of life (Chen et al., 2006, Gupta, 1995). In bacteria usually only one copy of Hsp90 is present (e.g. HtpG (high temperature protein G) in *E.coli*), whereas eukaryotes express at least two copies of Hsp90, one constitutively expressed e.g. 82 kDa heat shock cognate protein (Hsc82) and one heat-inducible isoform e.g. 82 kDa heat shock protein (Hsp82) in yeast (Johnson, 2012). The two isoforms exhibit to some degree functional specifity, albeit their high sequence and structural similarity (Morano et al., 1999, Millson et al., 2007, Girstmair et al., 2019). In eukaryotes, Hsp90 is essential also under normal growth conditions, meaning that at least one isoform has to be expressed, in contrast to bacteria (Borkovich et al., 1989, Bardwell and Craig, 1988). In metazoans organelle-specific variants of Hsp90 are expressed, TRAP1 (tumor necrosis factor receptor associated protein 1) in mitochondria, Grp94 (glucose-regulated protein 94) in the ER and cHsp90 in chloroplasts (Gupta, 1995, Marzec et al., 2012, Ho Yeong et al., 1995, Im, 2016, Inoue et al., 2013, Lin and Cheng, 1997).

Hsp90 acts as a downstream chaperone operating at a late stage of client maturation and is responsible for the folding, activation and assembly of clients (Balchin et al., 2016, Biebl and Buchner, 2019). The first identified client proteins in complex with Hsp90 were steroid hormone receptors (SHRs) and viral Src kinase (v-Scr) (Brugge et al., 1981, Dougherty et al., 1984). The diverse set of clients ranging from transcription factors, kinases to a variety of signal transducers reflecting central hubs of all biological pathways illustrates the importance of Hsp90 in cellular regulation (Echeverría et al., 2011, Zhao et al., 2005, McClellan et al., 2007).

1.4.1. Structure and conformational cycle of Hsp90

Members of the Hsp90 family consist of three domains: an N-terminal nucleotide binding domain (NTD), a middle domain (MD) and the C-terminal domain (CTD). The CTD is the dimerization site which is essential for the formation of the functional homodimer *in vivo* (Wayne and Bolon, 2007, Harris et al., 2004). Additionally, eukaryotic family members except TRAP1 display a charged, flexible linker between the NTD and the MD affecting conformational dynamics and Hsp90 function (Hainzl et al., 2009, Jahn et al., 2014, Tsutsumi et al., 2012, Ho Yeong et al., 1995). In the case of cytosolic, eukaryotic Hsp90s the CTD harbors at its very end the amino acid sequence methionine-glutamic acid-glutamic acid-valine-aspartic acid (MEEVD) mediating binding to co-chaperones containing a tetratricopepetide repeat domain (TPR) (Assimon et al., 2015, Scheufler, 2000, Prodromou et al., 1999, Chen et al., 1998).

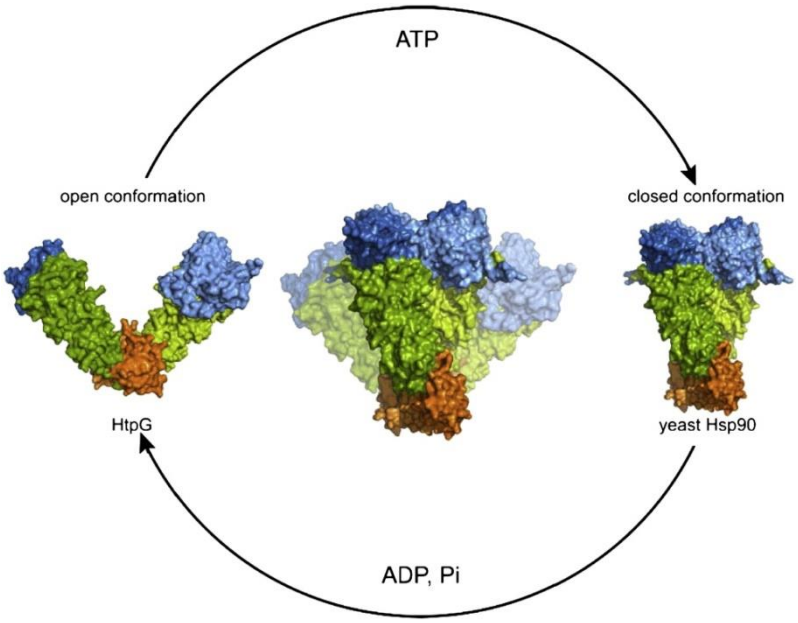

Figure 8: Structure of Hsp90. Crystal structure of the *E.coli* Hsp90 in the open conformation (left, PDB 2IOQ) and of the closed yeast Hsp90 (right, PDB 2CG9). The three domains of each protomer are indicated by color, NTD, blue; MD, green, CTD, orange. Adapted from (Li et al., 2012) with permission from *Elsevier.*

Hsp90 belongs to the GHKL split ATPase superfamily (gyrase subunit B, histidine kinase and DNA mismatch repair protein MutL) (Dutta and Inouye, 2000). Formation of the active ATPase requires substantial conformational rearrangements of the NTD and MD (Meyer et al., 2003, Cunningham et al., 2008). ATP binds with low affinity (K_D approx. 400 µM) to the NTD, which favors ADP-binding (K_D approx. 10 µM) implicating the need of an ATP excess in cells for proper function (Prodromou et al., 1999, Scheibel et al., 1997). Binding of ATP to the NTD induces the rearrangement of a conserved loop, the lid region, to close over the ATP binding pocket. Subsequently, the NTDs dimerize (closed state 1) and associate with the MD (closed state 2) (Ali et al., 2006, Cunningham et al., 2008, Hessling et al., 2009). The association of the NTD with the MD leads to the repositioning of a conserved arginine residue of the MD (Arg380 in yeast) necessary for ATP-hydrolysis (Meyer et al., 2003, Prodromou et al., 2000, Cunningham et al., 2012). After ATP-hydrolysis and release of ADP + P_i, the Hsp90 dimer resets to its open, v-shaped conformation (Shiau et al., 2006, Dollins et al., 2007). While early reports suggest an essential character for the ATPase activity of Hsp90 (Obermann et al., 1998, Panaretou et al., 1998), mutational analysis implicate that sampling the conformational states and allowing defined dwell times in specific states is essential (Zierer et al., 2016). Traversing major conformational rearrangements to gain ATPase activity is the rate limiting step of ATP-hydrolysis leading to a slow hydrolysis rate of approximately 1 ATP min^{-1} for yeast and 0.1 ATP min^{-1} for human Hsp90 (Hessling et al., 2009, McLaughlin et al., 2002, Scheibel et al., 1997). Notably, the bacterial Hsp90 works in a deterministic, ratchet-like mechanism, while eukaryotic Hsp90 samples all conformations even in the absence of nucleotides (Shiau et al., 2006, Southworth and Agard, 2008, Graf et al., 2009, Ratzke et al., 2012, Mickler et al., 2009).

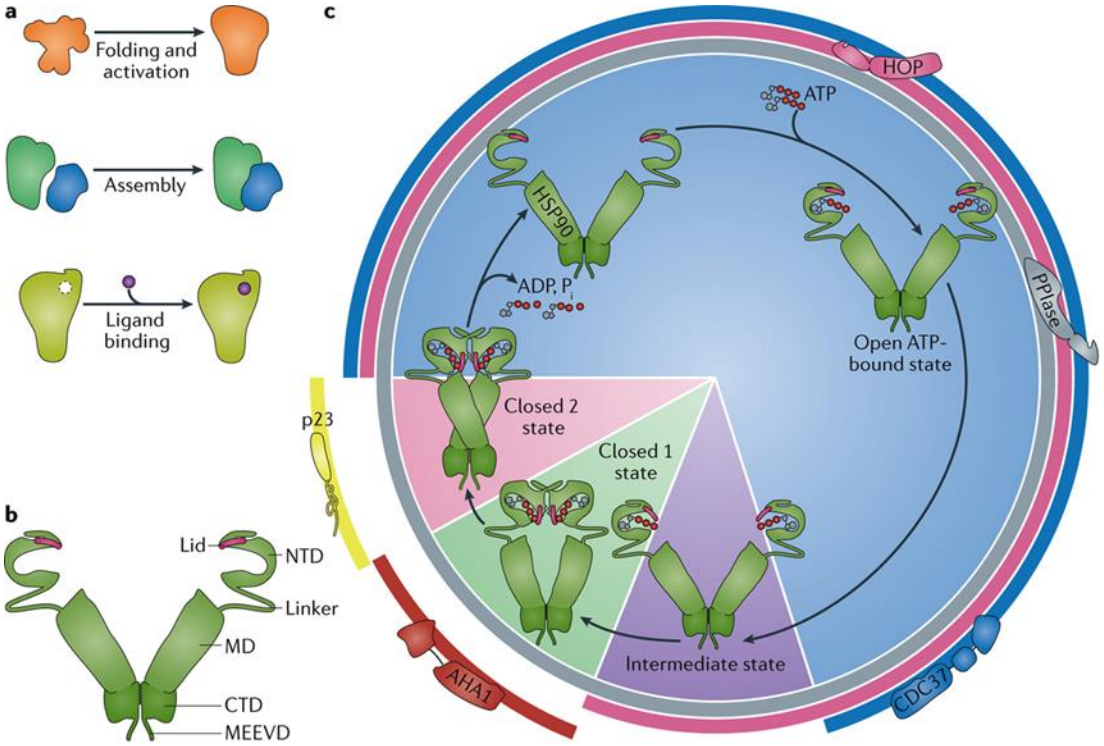

Figure 9: Function and cycle of Hsp90. (A) Sketch of the possible actions of Hsp90 on client proteins. (B) Schematic view of the domain organization of Hsp90. (C) Conformational cycle of Hsp90 and effective period of co-chaperone action. Hsp90 traverses different conformational states, starting with the open state, which can be stabilized by Hop/Sti1 and also Cdc37 acts early in the cycle as client recruiter, upon ATP-binding the lid closes (intermediate state), following N-N-dimerization (closed 1 state) can be accelerated by Aha1 leading to the closed 2 state, which can be stabilized by p23/Sba1. Subsequent, ATP-hydrolysis and release resets the cycle. Adapted from (Schopf et al., 2017) by permission of Springer Nature.

1.4.2. Hsp90 co-chaperones

For eukaryotic, cytosolic Hsp90 a plenitude of helper proteins have been identified regulating different aspects of Hsp90 such as the ATPase cycle, client interaction and posttranslational modifications (Biebl and Buchner, 2019, Schopf et al., 2017). Co-chaperones emerged during evolution from bacteria harboring no known Hsp90 co-chaperone over unicellular eukaryotes (yeast displays 12 Hsp90 co-chaperones) to humans with over 20 co-chaperones (Biebl and Buchner, 2019). In case of organelle-specific Hsp90s, only for Grp94 an assisting protein was reported (Liu et al., 2010, Rosenbaum et al., 2014, Van Anken et al., 2009).

Hsp90 utilizes all three domains for co-chaperone interaction (Li et al., 2012). Co-chaperones can bind simultaneously probably acting synergistically or compete for a defined binding site not only with other co-chaperones but also with client proteins (Biebl and Buchner, 2019, Schopf et al., 2017).

Several co-chaperones containing a TPR domain binds to the C-terminal MEEVD motif of Hsp90. (Scheufler et al., 2000, Chen et al., 1998, Brinker et al., 2002). One of these co-chaperones is the adaptor protein Hop/Sti1, Hsp70/90-organizing protein (human), stress inducible protein 1 (yeast). Hop/Sti1 harboring three TPR domains mediates the interaction between Hsp90 and Hsp70 by

binding via its TPR domains to C-terminal motifs of both molecular chaperones. This complex facilitates downstream transfer of client proteins from Hsp70 to Hsp90 (Chen and Smith, 1998, Johnson et al., 1998, Wegele et al., 2006, Röhl et al., 2015). Hop/Sti1 displays additional two aspartic acid and proline rich (DP) domains, which are involved in client activation (Flom et al., 2007, Schmid et al., 2012). The co-chaperone also acts as modulator of Hsp90's ATPase cycle. By binding to the CTD and MD, Hsp90 is locked in the open, client accepting conformation thereby inhibiting the ATPase activity as a non-competitive inhibitor (Prodromou et al., 1999, Richter et al., 2003, Li et al., 2011, Schmid et al., 2012). Notably, in systems lacking the adaptor protein as well as in yeast direct interaction between Hsp90 and Hsp70 is reported (Genest et al., 2015, Kravats et al., 2018). Some TPR-containing co-chaperones are cis/trans PPIases (peptidyl-prolyl-cis-trans-isomerases) like cyclophilins (e.g. Cyp40, Cpr6, Cpr7) and the FK506-binding protein family of PPIases (e.g. FKBP51 and FKBP52), which all display an intrinsic chaperone activity independent of Hsp90 (Ratajczak and Carrello, 1996, Riggs et al., 2004, Bose et al., 1996, Freeman et al., 1996, Pirkl and Buchner, 2001). In yeast two Cyp40-related PPIase co-chaperones are present, the cyclosporin-sensitive proline rotamase 6 (Cpr6) and Cpr7. Alike the two FKBPs, Cpr6 and Cpr7 seemingly act in different ways on client proteins (Hutchison et al., 1993, Smith et al., 1993, Duina et al., 1996, Duina et al., 1998, Mayr et al., 2000, Zuehlke and Johnson, 2012). Cpr7 depleted yeast shows a growth defect, which led to the discovery of the cyclophilin 7 suppressor (Cns1) co-chaperone (Dolinski et al., 1998). This TPR-containing co-chaperone is together with Cdc37 and Sgt1 one of three essential co-chaperones in yeast and displays overlapping functions with Cpr7 (Tesic et al., 2003, Tenge et al., 2015). Recent research revealed Cns1's involvement in chaperoning the eukaryotic elongation factor 2 (eEF2) connecting Hsp90 to protein translation (Schopf et al., 2019). The co-chaperone protein phosphatase 5 (PP5, in yeast Ppt1, protein phosphatase T 1) binds to the CTD of Hsp90 and acts as modulator of the phosphorylation state of client proteins, the co-chaperone Cdc37 and Hsp90 (Wandinger et al., 2006, Vaughan et al., 2008, Shelton et al., 2017b, Ramsey and Chinkers, 2002, Yang et al., 2005). Furthermore, a TPR-containing E3-ligase ,carboxy-terminus of Hsc70 interacting protein (CHIP), interacts with Hsp90 via the MEEVD motif targeting partially folded clients for proteasomal degradation (Connell, 2001, Demand et al., 2001, Paul and Ghosh, 2014)

Cdc37 is a client-specific co-chaperone recruiting kinases to Hsp90 (Grammatikakis et al., 1999, Hunter and Poon, 1997, Stepanova et al., 1996). In yeast Cdc37 belongs to the essential co-chaperones. The complex of Cdc37, Hsp90 and client kinase was recently solved by cryogenic electron microscopy confirming previous findings that Cdc37 contacts the NTD and MD (Siligardi et al., 2002, Eckl et al., 2013, Eckl et al., 2015). Surprisingly, Cdc37 wraps around one Hsp90 protomer while the kinase is bound between the clamp of the two Hsp90 monomers. The two kinase lobes are torn apart facing opposite sides of the Hsp90 dimer (Verba et al., 2016). A co-chaperone also

suggested to bind to the NTD and MD is the activator of Hsp90 ATPase protein 1 (Aha1). As the name implies Aha1 acts as a strong accelerator of the ATPase activity by facilitating NTD-dimerization and thereby tuning the dwell time clients bound to Hsp90 (Meyer et al., 2004, Retzlaff et al., 2010, Panaretou et al., 2002, Koulov et al., 2010, Li et al., 2013). In yeast another activator of the ATPase activity of Hsp90 is the co-chaperone high-copy Hsp90 suppressor 1 (Hch1). In higher eukaryotes Hch1 was lost during evolution. Remarkably, the posttranslational phosphorylation of Hsp90 at residues Tyrosine 627 in human functionally substitutes Hch1 (Zuehlke et al., 2017). In contrast, the co-chaperone p23/Sba1 (prostaglandin E synthase 3/increased sensitivity to benzoquinine ansamycins 1) inhibits Hsp90's ATPase activity by binding to the closed 2 state (Ali et al., 2006, Richter et al., 2004, McLaughlin et al., 2006). Besides, p23/Sba1 involvement in chaperoning, the co-chaperone fulfills Hsp90-independent functions such as chromatin remodeling and ribosome biogenesis (Echtenkamp et al., 2011, Echtenkamp et al., 2016, Bose et al., 1996, Freeman et al., 2000, Weikl et al., 1999, Weaver et al., 2000). The two Hsp90 co-chaperones, protein interacting with Hsp90 1 (Pih1) and TPR-containing protein associated with Hsp90 (Tah1), act in concert to promote the formation of RuvB-like 1-Ruvb2-Tah1-Pih1 (R2TP)-complexes which are required for nucleolar ribonucleoprotein biogenesis (Zhao et al., 2008, Kakihara and Houry, 2012).

1.4.3. The Hsp90 co-chaperone Sgt1

Sgt1 (Suppressor of G2 allele of *skp1*) was first identified as a suppressor of the thermo-sensitive growth of *skp1-4* (Suppressor of kinetochore protein mutant 1) (Kitagawa et al., 1999). The mutant allele of SKP1 was reported to arrest the cell cycle in the G2 phase and leading to chromosomal missegregation (Connelly and Hieter, 1996, Stemmann and Lechner, 1996). Notably, during the study Kitagawa and colleagues isolated the thermo-sensitive mutants *sgt1-3* and *sgt1-5* of Sgt1 which arrest cells in G2 phase or G1 phase, respectively (Kitagawa et al., 1999). Sgt1 is one of the three essential Hsp90 co-chaperones in yeast and is conserved in all eukaryotes (Kitagawa et al., 1999, Schopf et al., 2017, Eckl et al., 2014, Filipek and Lesniak, 2018, Zabka et al., 2008). Interestingly, higher eukaryotes harbor two Sgt1 isoforms (Niikura and Kitagawa, 2003, Azevedo et al., 2006, Zou et al., 2004). Structurally a three domain architecture consisting of an N-terminal TPR (tetratricopeptide repeat) domain, a CS (Chord-containing proteins and Sgt1) domain and a C-terminal SGS (Sgt1 specific) domain is conserved, expect for nematodes which lack the TPR domain (Eckl et al., 2014, Haslbeck et al., 2013).

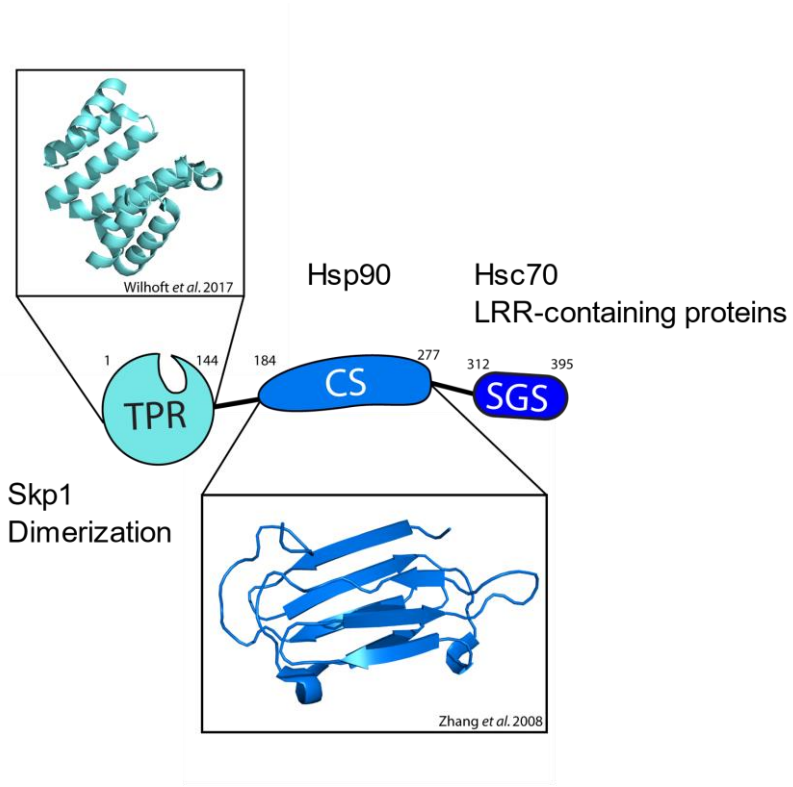

Figure 10: Domain architecture of Sgt1. Sgt1 consists of three domains: TPR, CS and SGS (numbers indicated domain boundaries of the yeast protein). Interaction partner of the single domains are indicated. Available structural information of the TPR (PDB 5AN3) and CS (PDB 2JKI) domain is displayed.

The TPR domain of Sgt1 was recently crystalized in complex with the BTB (BR-C, ttk and bab) domain of Skp1 confirming previous findings that the TPR domain is the site of Skp1 interaction (Willhoft et al., 2017, Bansal et al., 2004, Kitagawa et al., 1999). The direct interaction with Skp1 links Sgt1 to the assembly of the kinetochore and the assembly of SCF (Skp1-Cullin-F-box) E3 ligase complexes (Kitagawa et al., 1999, Bansal et al., 2004, Steensgaard et al., 2004, Davies and Kaplan, 2010, Lingelbach and Kaplan, 2004). Moreover, the TPR domain is necessary for dimerization in yeast and plant Sgt1; Albeit Sgt1 can form higher orders of oligomers; the dimer is the prevalent form in solution (Willhoft et al., 2017, Nyarko et al., 2007). Notably, the human homologue does not dimerize (Nyarko et al., 2007). The ability of yeast Sgt1 to dimerize was reported to be crucial for kinetochore assembly and can be negatively regulated by phosphorylation (Bansal et al., 2009a, Bansal et al., 2009b).

Initial studies suggest that the TPR domain also mediates the interaction with Hsp90 similar to other TPR-containing co-chaperones (Bansal et al., 2004). However, structural studies revealed that the CS domain of Sgt1 facilitates interaction with the NTD of Hsp90 (Zhang et al., 2008, Lee et al., 2004b, Catlett and Kaplan, 2006). Despite the structural homology of the CS domain of Sgt1 to the one of p23/Sba1, both co-chaperones are thought to bind to different regions of the NTD of Hsp90 (Zhang et al., 2008). Yet, studies on nematode Sgt1 suggests that Sgt1 binds to two different region of Hsp90

NTD dependent on the conformational state of Hsp90 (Eckl et al., 2014). Noteworthy, human and *C.elegans* Sgt1 prefer binding to Hsp90 in the presence of ATP while yeast Sgt1 preferentially binds to apo-Hsp90 (Eckl et al., 2014, Lee et al., 2004b, Catlett and Kaplan, 2006).

The SGS domain is considered mostly unstructured with a degree of helical propensities (Lee et al., 2004b). Interaction with the molecular chaperone Hsp70 is mediated by the SGS domain (Noel et al., 2007, Spiechowicz et al., 2007). Furthermore, phosphorylation of Sgt1 mostly occurs within the SGS domain (Bansal et al., 2009a, Martins et al., 2009, Martins and Sunkel, 2009, Liu et al., 2012). The C-terminal domain is also reported to be required for the interaction with LRR (leucine rich repeat) containing proteins (Dubacq et al., 2002, Azevedo et al., 2006).

The interaction with LRR-containing proteins assigns Sgt1 an involvement in the cAMP-pathway in yeast due to its interaction with the adenylyl cyclase Cyr1 (Dubacq et al., 2002), while in human or plant the innate immune response depends on Sgt1 interaction with LRR-containing proteins, especially with resistance genes (R-genes) and nucleotide-binding oligomerization domain-like receptors (NLRs) (Azevedo et al., 2006, da Silva Correia et al., 2007, Kadota et al., 2008, Kadota et al., 2010, Mayor et al., 2007, Meldau et al., 2011, Muskett and Parker, 2003, Shirasu, 2009). Since most of Sgt1's interaction partners share a LRR motif, Sgt1 is considered to be a specific client recruiter co-chaperone for LRR-containing proteins (Stuttmann et al., 2008, Taipale et al., 2014). However, Sgt1 seems to have a general impact on Hsp90-dependent client maturation (Sahasrabudhe et al., 2017).

In view of Sgt1's involvement in cell cycle progression, in particular kinetochore assembly and maturation of SCF E3 ligases, it is not surprising that Sgt1 is related to a variety of disease, such as cancer and neurodegenerative disease (Gao et al., 2013, Ogi et al., 2015, Spiechowicz et al., 2006, Kitagawa et al., 1999).

Up to now, Sgt1 is assigned to various pathways and its involvement in specific aspects is extensively studied. However, its essential function and interplay within the chaperone network remains still enigmatic.

1.4.4. Hsp90 co-chaperone cycle

Some of the aforementioned co-chaperones display a binding-specifity towards a distinct conformational state of Hsp90. The model of this co-chaperone-assisted Hsp90 cycle starts with the open state of Hsp90. At this point, Hop/Sti1 binds to Hsp90 inhibiting the ATPase activity (Richter et al., 2003, Hessling et al., 2009) and facilitates client transfer, either from Hsp70 or via spontaneous binding or by client recruiting co-chaperones, like the kinase-specific Cdc37 (Wegele et al., 2006,

Johnson et al., 1998, Kravats et al., 2018). In fact, Hop/Sti1 is also involved in the maturation of kinases (Lee et al., 2004a, Taipale et al., 2014, Sahasrabudhe et al., 2017, Biebl et al., 2020). Additional binding of another TPR-containing co-chaperone like one of the PPIases to the CTD is possible (Biebl and Buchner, 2019). Subsequent binding of Aha1 displaces Hop/Sti1 and accelerates the ATPase cycle by facilitating N-terminal dimerization of the Hsp90 protomers (Li et al., 2011, Li et al., 2013). Also the binding of a second PPIase, ATP and p23/Sba1 breaks up Hop/Sti1 binding, driving the cycle to the closed 2 state (Li et al., 2011). In case of an Aha1-driven transition, p23/Sba1 displaces Aha1 and stabilizes the closed 2 state. Sequentially, ATP-hydrolysis takes place and ADP+P_i, substrate and remaining co-chaperones are released (Biebl and Buchner, 2019, Schopf et al., 2017). Furthermore, additional co-chaperones can act on the Hsp90 cycle providing the optimal maturation machinery in a client-specific manner.

1.4.5. Posttranslational modification of Hsp90

Posttranslational modifications (PTM) add another layer of Hsp90 regulation. Not only Hsp90 can be posttranslationally modulated, but also its co-chaperones and clients (Sima and Richter, 2018, Backe et al., 2020). Among the numerous modifications of Hsp90 are phosphorylation, acetylation, methylation, S-nitrosylation and SUMOylation (Sima and Richter, 2018, Mayer and Le Breton, 2015, Prodromou, 2016). The PTMs confer not merely local effects, but rather modify intradomain communication acting as conformational switches (Morra et al., 2009, Retzlaff et al., 2009, Soroka et al., 2012).The dynamic editing of PTMs fine-tunes the Hsp90 machinery (Scroggins and Neckers, 2007, Mollapour and Neckers, 2012).

Phosphorylation, one of the most frequent modifications, was reported to decrease Hsp90 chaperone activity and slows down the ATPase cycle. However, depending on the position and client, phosphorylation also positively effects maturation (Mollapour et al., 2011, Soroka et al., 2012, Nguyen et al., 2017, Lu et al., 2014). Notably, phosphorylation in the CTD modulates the binding of TPR-containing co-chaperones (Assimon et al., 2015, Muller et al., 2013). Dynamic regulation by acetylation of Hsp90 is mediated by histone acetyltransferases (HAT) and histone deacetylases (HDAC). The states of acetylation favor different sets of co-chaperones modifying client maturation as reported for SHRs (Scroggins et al., 2007, Cohen and Yao, 2004, Aoyagi and Archer, 2005, Murphy et al., 2005, Bali et al., 2005, Suuronen et al., 2008). Lysine methylation at position K594 leads to an alteration of the ATPase cycle, co-chaperone regulation and overall conformational cycle (Rehn et al., 2020). Interestingly, methylation of Hsp90 seems to be important for the maintenance and function of skeletal muscles (Donlin et al., 2012, Abu-Farha et al., 2011). The S-nitrosylation of Hsp90 occures in the CTD and impairs the ATPase activity and chaperoning function of Hsp90 (Martínez-Ruiz et al.,

2005, Retzlaff et al., 2009). Modification with the small ubiquitin like modifier (SUMO) protein at the NTD of Hsp90 recruits Aha1 and surprisingly, increases drug binding (Mollapour et al., 2014).

1.4.6. Hsp90 clients

Other than molecular chaperones like Hsp70 which preferentially bind to hydrophobic patches, Hsp90 does not display a defined pattern of substrate recognition. The diversity of protein families depending on Hsp90, and concomitantly, the presence of stringent clients as well as Hsp90-independent members within these protein families make it difficult to define an Hsp90 client (Taipale et al., 2010, Taipale et al., 2012). Furthermore, a bipartite differentiation into client and non-client protein is challenged since a continuous range of Hsp90-binding affinities has been reported (Taipale et al., 2012).

Hsp90 was first identified in complex with client proteins of the SHR class and kinase family (Brugge et al., 1981, Dougherty et al., 1984). Interestingly, a large scale study revealed that only 7 % of the human transcription factors, to which SHRs belong, depend on Hsp90, whereas 60 % of the human kinome are Hsp90-dependent (Taipale et al., 2012). Notably, 30 % of E3 ubiquitin ligases have been reported to be Hsp90-dependent (Taipale et al., 2012). Hsp90 clients require different function of Hsp90. Clients of the steroid hormone receptors (SHR) family seem to require Hsp90 for ligand binding (Pratt and Dittmar, 1998, Kirschke et al., 2014). Furthermore, proteins like soluble guanylyl cyclase, inducible nitric oxide synthase or β- and γ-globins acquire their heme insertion competent state in an Hsp90-dependent manner (Ghosh et al., 2011, Ghosh and Stuehr, 2012, Ghosh et al., 2018). Assembly of protein complexes such as the aforementioned R2TP complexes demand Hsp90 action (Zhao et al., 2008). In case of stringent clients of the kinase family, Hsp90 supports ATP binding, thereof stabilization and activation of the kinase (Boczek et al., 2015, Eckl et al., 2016, Grammatikakis et al., 1999). Moreover, p53, the guardian of the genome, requires Hsp90 for stability and activation (Blagosklonny et al., 1996, Nagata et al., 1999, Walerych et al., 2004, Dahiya et al., 2019, Lane, 1992).

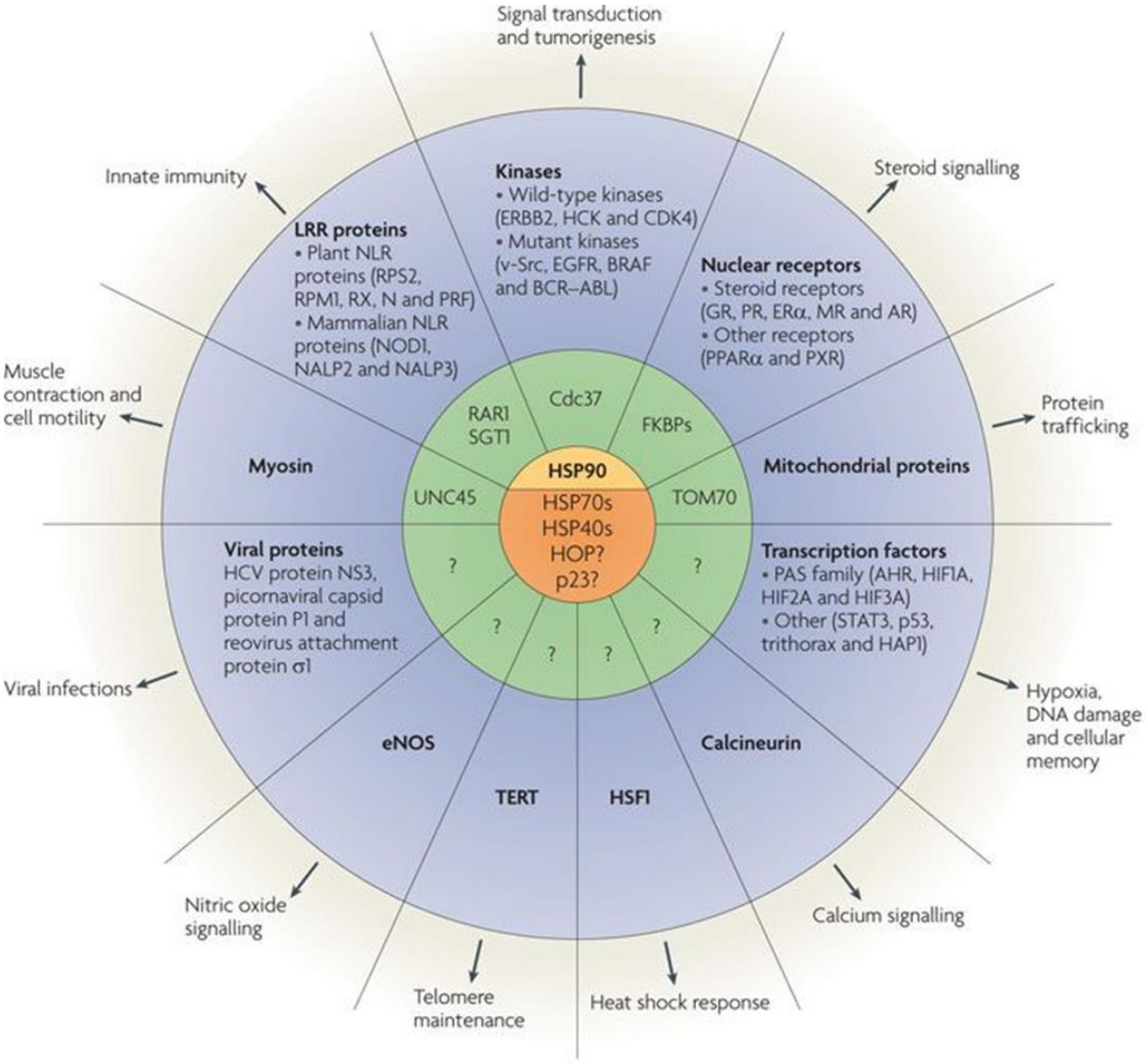

Figure 11: Client spectrum of Hsp90. Hsp90 associates with a diverse set of clients with the help of core chaperones (orange) and further co-chaperones (green) linking Hsp90 to central hubs of cellular processes. Adapted from (Taipale et al., 2010) by permission of Springer Nature.

Client binding to Hsp90 is affected by different aspects such as the conformational state of Hsp90, the co-chaperone set acting in a client-specific manner and posttranslational modifications of Hsp90 (Karagoz, 2014, Lorenz et al., 2014, Biebl and Buchner, 2019, Backe et al., 2020). The major client interaction site of Hsp90 is the MD as revealed by mutational as well as structural studies (Bohen and Yamamoto, 1993, Nathan and Lindquist, 1995, Lorenz et al., 2014, Verba et al., 2016, Radli and Rüdiger, 2018). In addition to the MD, also the CTD and NTD of Hsp90 are involved in client interaction (Hagn et al., 2010, Park et al., 2011, Eckl et al., 2015, Karagoz, 2014).

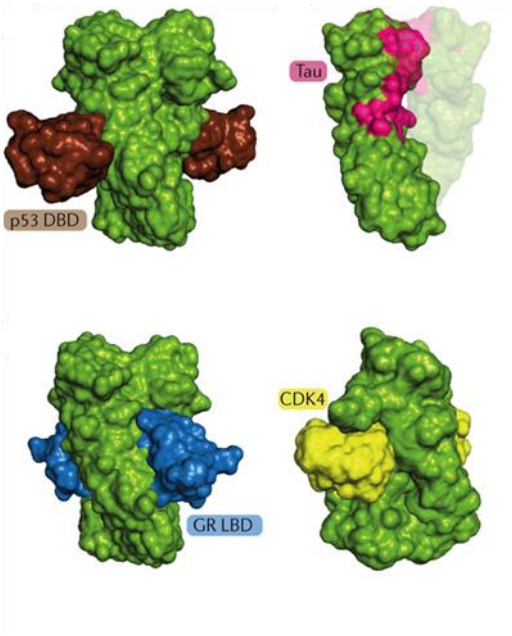

Figure 12: Client interactions with Hsp90. Binding of indicated client proteins to Hsp90 (green). In case of p53 (Hagn et al., 2010), Tau (Karagoz, 2014) and GR (Lorenz et al., 2014) interaction data were mapped onto yeast Hsp82 (PDB 2CG9). CDK4 binding to human Hsp90β according to Verba *et al.* (Verba et al., 2016) (PDB 5FWL). Adapted from (Schopf et al., 2017) by permission of *Springer Nature.*

1.4.7. Hsp90 in diseases

Overlooking the list of client proteins Hsp90s involvement in a variety of diseases is not surprising. Cancer cells display increased cell proliferation accompanied by upregulation of protein synthesis challenging the proteostasis network. Mutation of proto-oncogenic proteins leading to the active oncogenic protein often increases their chaperone dependence (Hanahan and Weinberg, 2011). Besides proto-oncogenic or oncogenic client proteins of Hsp90 such as v-Src, ErbB2, HIF1, the most noted is p53. The tumorsuppressor is mutated in more than 50 % of human cancer cases (Miyata et al., 2013, Whitesell and Lindquist, 2005, Schulz-Heddergott and Moll, 2018). Hsp90 may promote genetic variation by buffering the destabilizing effect of mutations (Rutherford and Lindquist, 1998). In fact, upregulation of Hsp90 among other chaperones is often reported for cancer cells and correlates with a negative prognosis (Calderwood and Gong, 2016, Calderwood et al., 2006, Pick et al., 2007, Dimas et al., 2018). The addiction of cancer cells for Hsp90 and the opportunity of specific inhibition of Hsp90 due to its unique binding mode of ATP to the NTD raises the therapeutic relevance (Prodromou et al., 1997, Whitesell et al., 1994, Whitesell et al., 1998, Chiosis et al., 2002, Heske et al., 2016, Zuehlke et al., 2018, Sidera and Patsavoudi, 2014). Concomitant with the increasing age of our society, neuropathies become more frequent. A central hallmark of neuropathies is the aggregation of proteins. Hsp90 is associated with neuropathies such as Huntington's, Alzheimer's, amyotrophic lateral sclerosis and Parkinson's (Brehme et al., 2014, Lackie

et al., 2017). Proteins connected with these disease such as Tau, amyloid β and α-synuclein are among the clients of Hsp90, however the function of Hsp90 in maturation and disease onset is not fully understood as well as the therapeutic approach of inhibition (Evans et al., 2006, Dickey et al., 2006, Dickey et al., 2007, Chen et al., 2014, Falsone et al., 2009, Putcha et al., 2010, Daturpalli et al., 2013). Additionally, Hsp90 co-chaperones, in particular Aha1, CHIP and Cyp40, seem to be also involved in neuropathies (Shelton et al., 2017a, Gong et al., 2004, Baker et al., 2017, Jinwal et al., 2013). Moreover, Aha1 plays a crucial role in cystic fibrosis, which is caused by mutation of the cystic fibrosis transmembrane conductance regulator (CFTR). Selective disruption of the Hsp90-Aha1 complex in this case seems to be a promising therapeutic approach (Loo et al., 1998, Koulov et al., 2010, Wang et al., 2006, Stiegler et al., 2017, Mijnders et al., 2017). Furthermore, Hsp90 is involved in viral infections. Viral proteins display a high rate of synthesis and mutation requiring chaperones to buffer the instability (Geller et al., 2012, Geller et al., 2013). Besides viral infections, protozoans like *Leishmania donovani* (leishmaniasis) and *Plasmodium falciparum* (malaria) dependent on Hsp90 during their infectious life cycle as a consequence specific inhibition of parasite Hsp90 can be used as treatment (Roy et al., 2012, Hombach et al., 2015, Wiesgigl and Clos, 2001).

In view of the variety of diseases Hsp90 is linked to, it is not surprising that therapeutic agents targeting Hsp90 are of great interest and part of a multitude of clinical approaches (Zheng et al., 2018, Criado-Marrero et al., 2018, Garcia-Carbonero et al., 2013).

2. Objective

This study focuses on the characterization of the essential Hsp90 co-chaperone Sgt1. Applying *in vitro* and *in vivo* techniques, this study aims to reveal Sgt1's essential function in yeast and its interplay with the Hsp90 and Hsp70 machinery.

So far, different functions could be assigned to the different domains of Sgt1. Using plasmid shuffling the contribution of Sgt1's domains to yeast viability will be assessed. Based on these results further analysis will be performed to determine the minimal structural element providing the essential function of Sgt1. Moreover, mutational analysis with Sgt1-related thermo-sensitive strains will additionally provide insights into the biological role of the domains of Sgt1. In addition to these *in vivo* experiments, a synthetic genetic array screen will be carried out to identify genetic interactors of Sgt1 among the pool of Hsp90 co-chaperones and a broad spectrum of chaperones, which will allow positioning of Sgt1 within the chaperon-network.

The *in vivo* analysis will be further supported by *in vitro* experiments, in particular the dissection of the chaperone interaction of Sgt1. Therefore, the proteins will be recombinant expressed and purified. Complex formation of Sgt1 with the Hsp90 machinery as well as the Hsp70 machinery will be probed by analytical ultracentrifugation. Moreover, *in vitro* characterization of the interaction of Sgt1 and Hsp90 in combination with the complex formation experiments will provide the integration of Sgt1 into the Hsp90 co-chaperone cycle.

Until now, structural information about the TPR and the CS domain of Sgt1 are available. Hence, this study will aim on gaining structural insights into the SGS domain using NMR spectroscopy. Additionally, the conformational dynamics of Sgt1 will be addressed by Hydrogen/deuterium exchange-mass spectrometry.

Interactome analysis of Sgt1 will be carried out using *in vivo* pull-down experiments coupled to MS/MS measurements. The experiments will identify pathways Sgt1 is involved in and further expand our knowledge about the biological function of Sgt1. Moreover, cell cycle state-resolved experiments using agents for yeast cell synchronization will provide a detailed look at Sgt1's interactome specificity during cell cycle progression.

In sum, the thesis will expand the picture of the essential Hsp90 co-chaperone Sgt1. It will allow classing Sgt1 within not only the Hsp90 chaperone system but also the extended chaperome. Additionally, the essential structural features will be revealed and their relevance considering the chaperone cycle.

3. Material and Methods

3.1. Material

Table 1: Chemicals

Chemicals used in this study	
5-fluoroorotic acid (5'-FOA)	Thermo Fisher, Waltham, USA
Acetic acid	Roth, Karlsruhe, Germany
Acrylamid/Bis solution 38:2 (40% w/v)	Serva, Heidelberg, Germany
Adenine	Sigma, St. Louis, USA
Adenosine-5'-diphosphate (ADP) disodium solution	Roche, Mannheim, Germany
Adenosine-5'-triphosphate (ATP) disodium solution	Roche, Mannheim, Germany
Adenylyl Imidodiphosphat (AMP-PNP)	Roche, Mannheim, Germany
Agar Agar	Serva, Heidelberg, Germany
Agarose	Serva, Heidelberg, Germany
Alanine	Sigma, St. Louis, USA
Ammonium chloride-^{15}N	Cortecnet, Voisins-Le Bretonneux, France
Ammonium persulfate (APS)	Roth, Karlsruhe, Germany
Ampicillin sodium salt	Roth, Karlsruhe, Germany
Arginine	Sigma, St. Louis, USA
Asparagine	Sigma, St. Louis, USA
Aspartic acid	Sigma, St. Louis, USA
ATTO488-maleimide	ATTO-TEC, Siegen, Germany
Bacto-peptone	BD Biosciences, Franklin Lakes, USA
Bacto-tryptone	BD Bioscience, Franklin Lakes, USA
Biotin	Sigma, St. Louis, USA
Boric acid	Sigma, St. Louis, USA
Bradford solution	Serva, Heidelberg, Germany
Bromphenolblue S	Serva, Heidelberg, Germany
Calcium chloride	Sigma, St. Louis, USA
Canavanine	Sigma, St. Louis, USA
Cobalt chloride	Sigma, St. Louis, USA
Coomassie Brilliant Blue R-250	Serva, Heidelberg, Germany
Copper chloride	Sigma, St. Louis, USA
Deoxynucleotide triphosphates (dNTPS)	New England Biolabs, Beverly, USA
Deoxyribonucleic acid, single stranded from salmon testes (ssDNA)	Sigman, St Louis, USA
D-Glucose-^{13}C	Merck, Darmstadt , Germany
Dimethyl sulfoxide (DMSO)	Merck, Darmstadt, Germany
di-Potassium hydrogen phosphate	Merck, Darmstadt, Germany
di-Sodium hydrogen phosphate	Merck, Darmstadt, Germany
Dithiothreitol (DTT)	Roth, Karlsruhe, Germany
Doxycycline	Sigma, St. Louis, USA
Ethanol	Merck, Darmstadt, Germany
Ethylenediaminetetraactetic acid (EDTA)	Merck, Darmstadt, Germany
Formaldehyde	Sigma, St. Louis, USA

Galactose	Merck, Darmstadt, Germany
Geneticin (G418)	Thermo Fisher, Waltham, USA
Glucose	Merck, Darmstadt, Germany
Glutamic acid	Sigman, St. Louis, USA
Glutamine	Sigma, St. Louis, USA
Glycerol	Roth, Karlsruhe, Germany
Glycine	Roth, Karlsruhe, Germany
Histidine	Sigma, St. Louis, USA
Hydroxyurea	Sigma, St. Louis, USA
Hygromycin B (Hyg)	Thermo Fisher, Waltham, USA
Imidazole	Sigma, St. Louis, USA
Iron chloride	Merck, Darmstadt, Germany
Isoleucine	Sigma, St. Louis, USA
Isopropyl β-D-1-thiogalactopyranoside (IPTG)	Serva, Heidelberg, Germany
Kanamycine sulfate	Roth, Karlsruhe, Germany
LB medium	Serva, Heidelberg, Germany
Leucine	Sigma, St. Louis, USA
Lithium acetate	Roth, Karlsruhe, Germany
Lysine	Sigma, St. Louis, USA
Magnesium chloride	Merck, Darmstadt, Germany
Magnesium sulfate	Merck, Darmstadt, Germany
Manganese chloride	Sigma, St. Louis, USA
Methanol	Merck, Darmstadt, Germany
Methionine	Sigma, St. Louis, USA
Milk powder	Roth, Karlsruhe, Germany
Molybdic acid	Sigma, St. Louis, USA
N-(2-Hydroxyethyl)-piperazine-N‘-2-ethanesulfonic acid (HEPES)	Roth, Karlsruhe, Germany
Niacinamide	MP Biomedicals, Santa Ana, USA
Nickel sulfate	Sigma, St. Louis, USA
Nocodazole	Sigma, St. Louis, USA
Nourseothricin (clonNAT)	Jena Bioscience, Jena, Germany
Phenylalanine	Sigma, St. Louis, USA
Phenylmethylsulfonyl fluoride (PMSF)	Sigma, St. Louis, USA
Polyethylene (20) sorbitan monolaurate (Tween 20)	Merck, Darmstadt, Germany
Polyethylene glycol (PEG) 3350	Sigma, St. Louis, USA
Potassium chloride	Roth, Karlsruhe, Germany
Potassium dihydrogen phosphate	Merck, Darmstadt, Germany
Proline	Sigma, St. Louis, USA
Protease inhibitor Mix G, HP	Serva, Heidelberg, Germany
Pyridoxine	Merck, Darmstadt, Germany
Radicicol	Roth, Karlsruhe, Germany
Riboflavin	Merck, Darmstadt, Germany
S-Aminoethyl-L-cysteine (Thialysine)	Sigma, St. Louis, USA
Serine	Sigma, St. Louis, USA
Sodium chloride	Merck, Darmstadt, Germany
Sodium dihydrogen phosphate	Merck, Darmstadt, Germany
Sodium dodecylsulfate (SDS)	Serva, Heidelberg, Germany
Sodium hydroxid	Roth, Karlsruhe, Germany

Tergitol Type NP-40 (NP-40)	Merck, Darmstadt, Germany
Tetramethylethylenediamine (TEMED)	Roth, Karlsruhe, Germany
Thiamine	Merck, Darmstadt, Germany
Threonine	Sigma, St. Louis, USA
Tris-(2-carboxyethyl)phosphine (TCEP)	Roth, Karlsruhe, Germany
Tris-(Hydroxymethyl)-aminomethane (TRIS)	Roth, Karlsruhe, Germany
Tryptophane	Sigma, St. Louis, USA
Uracil	Sigma, St. Louis, USA
Valine	Sigma, St. Louis, USA
Xylencyanol	Serva, Heidelberg, Germany
Yeast extract	Serva, Heidelberg, Germany
Yeast Nitrogen Base (YNB) -amino acids	BD Biosciences, Franklin Lakes, USA
Yeast Nitrogen Base (YNB)- amino acids - ammonium sulfate	BD Biosciences, Franklin Lakes, USA
Zinc chloride	Merck, Darmstadt, Germany
α-factor	Bachem, Basel, Swiss
β-mercaptoethanol	Roth, Karlsruhe, Germany

Table 2: Enzymes, Standards and Kits

Enzymes, standards and kits used in this study	
1 kB DNA ladder	Peqlab, Erlangen, Germany
α-GAPDH	Sigma, St. Louis, USA
α -GFP	Roche, Mannheim, Germany
α -Hsp90	Pineda
α -mouse-POD	Sigma, St. Louis, USA
Antarctic Phosphatase	New England Biolabs, Beverly, USA
α -PGK	Thermo Fisher, Waltham, USA
α -rabbit-POD	Sigma, St. Louis, USA
α -Sgt1	Pineda
α -Ssa1	Pineda
α -Ydj1	Pineda
BamHI-HF	New England Biolabs, Beverly, USA
Dnase I	AppliChem PanReac, Darmstadt, Germany
DpnI	New England Biolabs, Beverly, USA
Go-Taq DNA polymerase	New England Biolabs, Beverly, USA
Immersol 518F	Zeiss, Jena, Germany
Q5 High-fidelity DNA polymerase	New England Biolabs, Beverly, USA
SalI-HF	New England Biolabs, Beverly, USA
Stain G	Serva, Heidelberg, Germany
SUMO-protease (ULP-1)	Maximilian Biebl
T4 DNA liagse	New England Biolabs, Beverly, USA
T4 DNA polymerase	New England Biolabs, Beverly, USA
T4 Polynucleotide kinase	New England Biolabs, Beverly, USA
TEV-Protease	Maximilian Fottner
Triple Color Protein Standard III	Serva, Heidelberg, Germany
Western Bright ECL Spray	Advansta, Menlo Park, USA
Wizard Miniprep kit	Promega, Madison, USA
Wizard PCR product purification and gel extraction kit	Promega, Madison, USA

Table 3: Consumables

Consumables used in this study	
Amicon Ultra Centrifugal filter units	Merck, Darmstadt, Germany
Cuvette, PS	Brand, Wertheim, Germany
GFP-Trap agarose beads	Chromotek, Martinsried, Germany
Glass beads	Roth, Karlsruhe, Germany
PCR tubes	Biorad, Munich, Germany
PD-10 columns	GE Healthcare, Chicago, USA
PE Tubes	Greiner&Söhne, Nürtingen, Germany
PVDF membranes	Roth, Karlsruhe, Germany
Reaction tubes	Sarstedt, Nürnberg, Germany
TG PRIME gradient gels	Serva, Heidelberg, Germany

Table 4: Columns

Chromatography columns used in this study	
HiLoad 16/60 Superdex 200 pg	GE Healthcare, Chicago, USA
HiLoad 16/60 Superdex 75 pg	GE Healthcare, Chicago, USA
HiPrep 26/10 desalting column	GE Healthcare, Chicago, USA
HisTrap FF 5 mL	GE Healthcare, Chicago, USA
Resource-Q (6 mL)	GE Healthcare, Chicago, USA

Table 5: Devices

Devices used in this study	
ACQUITY M-class UPLC	Waters Crop., Milford, USA
Äkta FPCL	GE Healthcare, Chicago, USA
Analytical ultracentrifuge XL-A equipped with fluorescence detection system	Beckman Coulter, Brea, USA AVIV Biomedical, Lakewood, USA
Avanti J-25, J26XP, JXN30 with rotors JA-10 and JA-25.50	Beckman Coulter, Brea, USA
Bandelin Sonopuls HD2200	Branson, Danbury, USA
Benchtop Centrifuge 5418	Eppendorf, Hamburg, Germany
BioDoc II	Biometra, Göttingen, Germany
Cell Disruption System Basic Z	Constant Systems, Warwick, UK
Chirascan V100 Circular Dichroism spectrometer	AppliedPhotophysics, Leatherhead, UK
Electrophoresis Power Supply-EPS1001	GE Healthcare, Chicago, USA
Electrophoresis Power Supply-EPS3501XL	GE Healthcare, Chicago, USA
Electrophoresis Power Supply-EPS601	GE Healthcare, Chicago, USA
Eppendorf Thermomixer compact	Eppendorf, Hamburg, Germany
Eppendorf ThermoStat plus	Eppendorf, Hamburg, Germany
Eppendorft Centrifuge 5810	Eppendorf, Hamburg, Germany
Fastblot B44	Biometra, Göttingen, Germany
Freezer Ultra-low temperature C760	New Brunswick Scientific, Edison, USA
Hamamatsu 4792-95 digital camera	Hamamatsu Photonics,Hamamatsu, Japan
Heraeus Biofuge stratos	Thermo Scientific, Waltham, USA
Hoefer Mighty Small dual gel caster	Hoefer, Holliston, USA
Homogenizer Heidolph DIAX 900	Heidolph, Kelheim, Germany
HTS PAL Leap robot	Leap Technologies, Aabenraa, Denmark

Huber compatible control	Peter Huber Kältemaschinenbau, Offenburg, Germany
Image Quant 3000, LAS 4000	GE Healthcare, Chicago, USA
Incubator Binder KB 115	Binder, Tuttlingen, Germany
Incubator Certomat BS-1	Sartorius, Göttingen, Germany
Incubator Mytron WB	Mytron, Heiligenstadt, Germany
Magnetic stirrer Heidolph MR 3001	Heidolph, Kelheim, Germany
Mighty Small II SE 250/SE 260 electrophoresis unit	Hoefer, Holliston, USA
PCR cycler BioRad T-100 thermal cycler	BioRad, Munich, Germany
PHERAstar FSX	BMG Labtech, Ortenberg, Germany
pH-Meter 538 MultiCal	WTW, Weilheim, Germany
Platform shaker Heidolph Polymax 2040	Heidolph, Kelheim, Germany
Sartorius 1409 MP	Sartorius, Göttingen, Germany
Sartorius BL310	Sartorius, Göttingen, Germany
Sartorius universal	Sartorius, Göttingen, Germany
Shaking device Certomat SII, GFL 3005	Sartorius, Göttingen, Germany
Spectrophotometer Nanodrop ND-1000 UV/Vis	Peqlab, Erlangen, Germany
Spectrophotometer Varian Cary 50/100 Bio UV/Vis	Varian, Palo Alto, USA
Synapt G2-S mass spectrometer	Waters Crop., Milford, USA
Ultrospec 1100pro	GE Healthcare, Chicago, USA
Universal 320R	Hettich Lab, Tuttlingen, Germany
Vortex Heidolph REAX top	Heidolph, Kelheim, Germany
Zeiss Axiovert 200	Zeiss, Jena, Germany
Zeiss FluoArc	Zeiss, Jena, Germany
Zeiss Plan-NEOFLUAR 63x	Zeiss, Jena, Germany

Table 6: Software

Software used in this study	
Adobe CS2	Adobe Systems, San Jose, USA
DynamX	Waters Corp., Milford, USA
Endnote x9	Thomson Reuters, New York, USA
Microsoft Office	Microsoft, Redmond, USA
NEBaseChanger	http://nebasechanger.neb.com/
NEBuilder	http://nebuilder.neb.com/
Origin 9.1	OriginLab, Northampton, USA
ProtParamTool	ExPasy
Pymol	Schrödinger, Cambridge, USA
SedFit	Peter Schuck
Sednterp	John Philo
SedView	David B. Hayes, Walter F. Stafford
Serial Cloner	Serial Basics, USA
Simple PCI	Compix Inc., Cranberry Township, USA
STRING Database	//string-db.org/

Table 7: Standard solutions

Standard solutions used in this study		
Solution	Concentration	Ingredients
Agarose Solution	0.8-2 % (w/v) 100 mL 2 µL	Agarose TAE (1x) Serva DNA Stain G
Blocking solution	5 % (w/v)	Milk powder in TBS-T
DNA loading buffer	50 % (v/v) 10 mM 0.2 % (w/v) 0.2 % (w/v)	Glycerol EDTA pH 8.0 Bromphenolblue Xylecyanol
Separating gel buffer (4x)	250 mM 0.8 % (w/v)	Tris/acetate pH 8.0 SDS
Stacking gel buffer (2x)	250 mM 0.4 % (w/v)	Tris/acetate pH 8.0 SDS
TAE (50X)	2 M 50 mM	Tris/acetate pH 8.0 EDTA
Fairbanks A	2.5 g 250 mL 80 mL Ad 1 L	Coomassie Brilliant Blue R-250 Ethanol Acetic acid H_2O
Fairbanks D	250 mL 80 mL Ad 1 L	Ethanol Acetic acid H_2O
Laemmli sample buffer (5x)	312.5 mM 10 % /w/v) 50 % (v/v) 2.5 % (v/v) 0.05 % (w/v)	Tris pH 6.8 SDS Glycerol B-mercaptoethanol Bromphenolblue
PBS (10x)	40 mM 160 mM 1.15 M	KH_2PO_4 Na_2HPO_4 NaCl pH 7.4
TBS (10x)	250 mM 30 mM 1.5 M	Tris pH 7.6 KCl NaCl
TBS-T	0.1 % (v/v)	Tween-20 in TBS(1x)
SDS running buffer (10x)	250 mM 2 M 1 % (w/v)	Tris pH 6.8 Glycine SDS
Western Blot transfer buffer	36 g 7.6 g 500 mL 0.3 % (w/v) Ad 2.5 L	Glycine Tris Methanol SDS H_2O pH 8.3

Table 8: Medium for bacterial handling

Media for *E. coli* growth used in this study		
Name		Composition
LB		20 g/L LB-powder
2YT		16 g/L Bacto Tryptone 10 g/L Yeast extract 5 g/L NaCl
Minimal medium (M9)	100 mL	10xM9 33.7 mM Na_2HPO_4 x 2 H_2O 22 mM KH_2PO_4 8.55 mM NaCl 9.35 mM NH_4Cl (^{15}N)
	1 mL	1 M $MgSO_4$
	0.3 mL	1M $CaCl_2$
	1 mL	Biotin (1 mg/mL)
	1 mL	Thiamin (1 mg/mL)
	20 mL	20 % D-Glucose (^{13}C)
	10 mL	Trace elements solution (100x)
	Ad 1 L	H_2O
Trace elements solution (100x)		13.4 mM EDTA 3.1 mM $FeCl_3$-$6H_2O$ 0.62 mM $ZnCl_2$ 76 µM $CuCl_2$-$2H_2O$ 42 µM $CoCl_2$-$2H_2O$ 162 µM H_3BO_3 8.1 µM $MnCl_2$-$4H_2O$
Agar		20 g/L for plates
Antibiotics		50 µg/mL Kanamycin 100 µg/mL Ampicillin 50 µg/mL Chloramphenicol

Table 9: Medium for yeast handling

Media for *Saccharomyces cerevisiae* growth used in this study	
Name	Composition
YPD	10 g/L Yeast extract 20 g/L Peptone 20 g/L Glucose
SD	6.7 g/L YNB-AA 2 g/L amino acid drop out mix 20 g/L Glucose
Amino acid drop-out mix	0.5 g Adenine, 2 g Alanine, 2 g Arginine, 10 g Leucine, 2 g Lysine, 2 g Methionine, 2 g Asparagine, 2 g Aspartic acid, 2 g Glutamic acid, 2 g Glutamine, 2 g Glycine, 2 g Histidine, 2 g Isoleucine, 2 g Phenylalanine, 2 g Proline, 2 g Serine, 2 g Threonine, 2 g Tryptophane, 2 g Uracil, 2 g Valine

Antibiotics and amino acid analogous	200 µg/mL G418 100 µg/mL Nourseothricin (clonNAT) 50 µg/mL Thialysine 50 µg/mL Canavanine 200 µg/mL HygromycinB

Table 10: Bacterial strains

E.coli strains used in this study		
E. coli strain	Genotype	Source
BL21 (DE3) Codon Plus	F$^-$*ompT* *hsdS*($r_B^-m_B^-$)*dcm*$^+$ Tet^r*gal* λ(DE3) *endA* Hte [*arg*U *ile*Y *leu*W Cam^r]	Stratagene, La Jolla, USA
Rosetta BL21	F$^-$*ompT* *hsdS*($r_B^-m_B^-$) gal*dcm* (DE3) pRARE (Cam^R)	Merck Millipore, Darmstadt, Germany
XL-1 blue	F$^-$ϕ80(Δ*lacZ*)ΔM15 Δ*lac*X74 *hsd*R(r_K^- m_K^-) Δ*rec*A1398 *end*A1 *ton*A	Invitrogen, Carlsbad, USA

Table 11: Yeast strains

Yeast strains used in this study		
Strain	Genotype	source
BY4741	MATa *his3Δ1 leu2Δ0 met15Δ0 ura3Δ0*	EUROSCARF, Frankfurt, Germany
R1158	MATa *URA3::CMV-tTA his3Δ1 leu2Δ0 met15Δ0*	Dharmacon, Lafayette, USA
tetO7-SGT1	MATa *pSGT1::kanR-tetO7-TATA URA3::CMV-tTA his3Δ1 leu2Δ0 met15Δ0*	Dharmacon, Lafayette, USA
Y8205	MATα *can1Δ::STE2pr-Sp-his5 lyp1Δ::STE3pr-Sp-LEU2 his3Δ1 leu2Δ0 ura3Δ0*	C. Boone
Y8205 *tetO7-SGT1*	MATα *can1Δ::STE2pr-Sp-his5 lyp1Δ::STE3pr-Sp-LEU2 his3Δ1 leu2Δ0 ura3Δ0 pSGT1::natR-tetO7-TATA URA3::CMV-tTA*	This study
sgt1Δ [SGT1]	MATa *his3Δ1 leu2Δ0 met15Δ0 ura3Δ0 sgt1::hygNT* [p416-GPD-SGT1^{wt}]	This study
sgt1-3	MATa *his3Δ1 leu2Δ0 met15Δ0 ura3Δ0 sgt1-3::kanMX*	EUROSCARF, Frankfurt, Germany
sgt1-5	MATa *his3Δ1 leu2Δ0 met15Δ0 ura3Δ0 sgt1-5::kanMX*	EUROSCARF, Frankfurt, Germany
skp1-3	MATa *his3Δ1 leu2Δ0 met15Δ0 ura3Δ0 skp1-3::kanMX*	EUROSCARF, Frankfurt Germany
skp1-4		K. Kitagawa
Single deletion mutants	BY4741 *goi Δ::kanMX*	EUROSCARF, Frankfurt, Germany
DAmP strains	BY4741 *goi -DAmP::kanMX*	Dharmacon, Lafayette, USA

Table 12: Plasmids

Plasmids used in this study		
Plasmid	Insert/Cloning Site	Source
pET28b		Merck Biosciences, Schwalbach, Germany
p415-GPD		Addgene, Cambridge, USA
p413-GAL1		Addgene, Cambridge, USA
pET-SUMO-mod	His_6-SUMO, BbsI/BamHI	Oliver Lorenz
pET28-yHsp90	NdeI/BamHI	Klaus Richter
pET28-hHsp90β	NdeI/BamHI	Klaus Richter
pET-SUMO-hHsp70	BamHI/XhoI	Eva Kriehuber
pET-SUMO-Ydj1	BamHI/XhoI	Oliver Lorenz
pET28-Sgt1		Sandrine Stiegler
pET28-Sgt1-S233C		Sandrine Stiegler
pET-SUMO-TEV-$Sgt1^{WT}$	BamHI	This study
pET-SUMO-Sgt1-S361D	BamHI	This study
pET-SUMO-Sgt1-S233C	BamHI	This study
pET-SUMO-Sgt1-H59A	BamHI	This study
pET-SUMO-Sgt1-TPR	BamHI	This study
pET-SUMO-Sgt1-CS	BamHI	This study
pET-SUMO-Sgt1-SGS	BamHI	This study
pET-SUMO-Sgt1-TPR-CS	BamHI	This study
pET-SUMO-Sgt1-TPR-L-SGS	BamHI	This study
pET-SUMO-Sgt1-CS-SGS	BamHI	This study
pET-SUMO-Sgt1-TPR-S109C	BamHI	This study
pET-SUMO-Sgt1-TPR(S109C)-L-SGS	BamHI	This study
pET-SUMO-Sgt1-CS-S233C	BamHI	This study
pET-SUMO-Sgt1-CS(S233C)-SGS	BamHI	This study
pET-SUMO-Sgt1-SGS-S312C	BamHI	This study
pET-SUMO-Sgt1-TPR-CS(S233C)	BamHI	This study
pET-SUMO-Sgt1-TPR-H59A	BamHI	This study
pET-SUMO-Sgt1-SGS-S361D	BamHI	This study
pET-SUMO-Skp1	BamHI	This study
pET-SUMO-Sugt1B	BamHI	This study
pET-SUMO-Sugt1A	BamHI	This study
p413-GAL1-$Sgt1^{WT}$	SalI/BamHI	This study
p413-GAL1-TPR	SalI/BamHI	This study
p413-GAL1-CS	SalI/BamHI	This study
p413-GAL1-SGS	SalI/BamHI	This study
p413-GAL1-TPR-CS	SalI/BamHI	This study
p413-GAL1-CS-SGS	SalI/BamHI	This study
p413-GAL1-TPR-L-SGS	SalI/BamHI	This study
p413-GAL1-Sgt1-H59A	SalI/BamHI	This study
p413-GAL1-Sgt1-Y190R/F201R	SalI/BamHI	This study
p413-GAL1-TPR-H59A	SalI/BamHI	This study
p413-GAL1-TPR(H59A)-CS	SalI/BamHI	This study
p413-GAL1-TPR(H59A)-L-SGS	SalI/BamHI	This study

p413-GAL1-CS-Y190R/F201R	SalI/BamHI	This study
p413-GAL1-TPR-CS(Y190R/F201R)	SalI/BamHI	This study
p413-GAL1-CS(Y190R/F201R)-SGS	SalI/BamHI	This study
p415-GPD-Sgt1^{WT}	SalI/BamHI	This study
p415-GPD-TPR	SalI/BamHI	This study
p415-GPD-CS	SalI/BamHI	This study
p415-GPD-SGS	SalI/BamHI	This study
p415-GPD-TPR-CS	SalI/BamHI	This study
p415-GPD-CS-SGS	SalI/BamHI	This study
p415-GPD-TPR-L-SGS	SalI/BamHI	This study
p415-GPD-Sgt1-S361D	SalI/BamHI	This study
p415-GPD-SGS-S361D	SalI/BamHI	This study
p415-GPD-Sgt1-Y190R/F201R	SalI/BamHI	This study
p415-GPD-Sgt1-H59A	SalI/BamHI	This study
p415-GPD-Sgt1-372	SalI/BamHI	This study
p415-GPD-Sgt1-371	SalI/BamHI	This study
p415-GPD-Sgt1-370	SalI/BamHI	This study
p415-GPD-Sgt1-369	SalI/BamHI	This study
p415-GPD-Sgt1-368	SalI/BamHI	This study
p415-GPD-Sgt1-367	SalI/BamHI	This study
p415-GPD-Sgt1-366	SalI/BamHI	This study
p415-GPD-Sgt1-365	SalI/BamHI	This study
p415-GPD-Sgt1-321-372	SalI/BamHI	This study
p415-GPD-Sgt1-337-372	SalI/BamHI	This study
p415-GPD-Sgt1-M358P	SalI/BamHI	This study
p415-GPD-Sgt1-G349P	SalI/BamHI	This study
p415-GPD-Sgt1-P352G	SalI/BamHI	This study
p415-GPD-Sgt1-349-352allA	SalI/BamHI	This study
p415-GPD-Sgt1-F343P	SalI/BamHI	This study
p415-GPD-Sgt1-GFP	SalI/BamHI	This study
p415-GPD-Sgt1(S361D)-GFP	SalI/BamHI	This study
p415-GPD-SGS-GFP	SalI/BamHI	This study
p415-GPD-GFP	BamHI/XhoI	Florian Schopf
p416-GPD-Sgt1^{WT}	SalI/BamHI	This study

3.2. Bacterial and cloning methods

3.2.1. Plasmid purification from *E.coli*

Amplification of DNA-plasmids was performed by growing an *E. coli* overnight culture with the respective antibiotics. Cells were pelleted and the plasmid was purified using Wizard plus SV Minipreps DNA purification system according to the manufacturer's instruction. The isolated plasmid was sequenced and stored at – 20 °C until further usage.

3.2.2. Agarose gel electrophoresis

Agarose gel electrophoresis was carried out for analytic separation of DNA. The samples were mixed with 1 x DNA-loading buffer and loaded on a 1 % agarose gel in 1 x TAE (40 mM Tris acetate, 1 mM EDTA, pH 8.0) supplemented with 2 µL/ 100 mL Serva DNA Stain G. Electrophoresis was performed at a constant current of 120 V in 1 x TAE-buffer for 25 min. 1 kb DNA ladder was used as standard. The separated DNA was detected under UV light.

3.2.3. Restriction digest and dephosphorylation of plasmid DNA

Restriction enzymes and buffers were purchased from New England Biolabs. Following the manufacturer's instruction, 1 µg plasmid was digested in CutSmart buffer at 37 °C overnight. The digested plasmid was subsequently treated with Antarctic Phosphatase according to the manufacturer's protocol. As per specification of the Wizard PCR product purification and gel extraction kit, the digested and dephosphorylated plasmids were purified.

3.2.4. Sequence and ligation independent cloning (SLIC)

Jeong *et al.* (Jeong et al., 2012) described a cloning technique which depends on the 3'-5' exonuclease function of the T4 DNA polymerase and the design of homologous sequence overlaps between the vector and the insert.

The insert was generated by standard Q5-polymerase chain reaction (PCR) according to the manufacturer's instruction. All primers used for SLIC were designed using the NEBuilder online tool. Following table displays the PCR mixture and set up. The enzymes and buffers were purchased from New England Biolabs.

Table 13: PCR mixture for standard Q5-PCR

32.6 µL	H_2O
1 µL	template (final concentration between 1-10 ng)
1 µL	dNTPs (10 mM)
10 µL	5 x Q5 Reaction Buffer
2.5 µL	primer 1 (10 µM)
2.5 µL	primer 2 (10 µM)
0.4 µL	Q5 DNA polymerase

Table 14: PCR program for standard Q5-PCR

step	temperature [°C]	time
initial denaturation	98	3 min
35 x Cycles	98	10 s
	50-72	30 s
	72	30 s/kb
final extension	72	4 min

The amplified PCR product was purified using the Wizard PCR product purification and gel extraction kit.

The SLIC reaction was assembled as shown in table 13. The reaction was started by adding T4 DNA polymerase. After incubation for 2.5 min at room temperature, the reaction was stopped by transfer on ice. Next, the reaction mixture was used for *E.coli* transformation (section 3.2.6.).

Table 15: Restriction digestion

x µL (100 ng)	digested vector DNA
1 µL	NEB buffer 2.1
x µL (40 ng)	insert
0.4 µL	T4 DNA polymerase
ad 10 µL	H_2O

3.2.5. Site directed mutagenesis and ligation

Standard Q5-PCR as described in section 3.2.4. was used for the insertion, substitution or deletion of a site-specific fragment according to the manufacturer's protocol. All primers for site directed mutagenesis were generated using the NEBaseChanger online tool producing blunt-ended linear plasmids. Table 16 shows the reaction mixture for ligation of linearized plasmids. The reaction was incubated for 5 min at room temperature and then stopped by chilling on ice. The whole mixture was used for *E.coli* transformation. All enzymes and buffers were purchased from New England Biolabs.

Table 16: Ligation mixture

1 µL	PCR-product
0.5 µL	DnpI
0.5 µL	T4 DNA ligase
0.5 µL	T4 PNK
1 µL	10 x T4 Ligase buffer
ad 10 µL	H_2O

3.2.6. *E.coli* transformation

Chemical competent *E.coli* strains were generated as described in (Hanahan and Meselson, 1983). For transformation, 100 µL of competent cells were supplemented with 1-2 µL plasmid DNA or 10 µL cloning reaction mixture and incubated for 10 min on ice. Afterwards, the cells were heat shocked at 42 °C for 1 min and again chilled on ice for 5 min. Next, cells were recovered in 1 mL LB_0 medium at 37 °C for 1 h. Cells were then plated onto LB-plates containing the required antibiotics for plasmid selection and incubated for 1 day at 37 °C.

3.2.7. DNA sequencing

Validity of plasmid DNA was confirmed by sequencing using the services of Eurofins Genomics (Ebersberg, Germany) or GENEWIZ (Leipzig, Germany).

3.3. Yeast methods

3.3.1. Nomenclature of *Saccharomyces cerevisiae* genes and proteins

Yeast wild-type genes are indicated by capital letters (e.g. GOI1, gene of interest 1). Mutant genes are written in lowercase, italic letter (e.g. *goi1, gene of interest 1*). The deletion of the entire open reading frame is indicated by *Δ* (*goiΔ, deletion mutant of the gene of interest 1*). Yeast proteins start with a capital letter (e.g. Poi1, protein of interest 1).

3.3.2. Yeast transformation

Yeast transformation was performed as described by Gietz and Woods (Gietz and Woods, 2002) in a slightly modified way. In brief, yeast cells were grown over night in the respective medium (wild-type yeast was grown in YPD) and reinoculated in 50 mL to a starting OD_{600}=0.2. Yeast growth continued for approximately two cell division cycles at 30 °C (thermo-sensitive (ts) mutants were grown at 25 °C). Afterwards, cells were harvested by centrifugation at 3000 x g for 5 min, washed once with 25 mL sterile H_2O, subsequently washed with 1 mL 0.1 M lithium acetate and then resuspended in 0.5 mL 0.1 M lithium acetate. 50 µL of the cell suspension was used for a single transformation reaction,

therefore, cells were spun down and the supernatant was discarded. The following transformation mix was added in the given order.

Table 17: LiAc-transformation mix

240 µL	50 % PEG 3350 (w/v)
36 µL	1 M lithium acetate
10 µL	ssDNA (10 mg/mL)
x µL	plasmid DNA or PCR product
74-x µL	H_2O

For PCR-derived linear DNA for chromosomal integration, 50 µL of the PCR product were used and for plasmid DNA transformation, 1-2 µg of plasmid DNA were used. The cells supplemented with the transformation mixture were mixed by vortexing and incubated for 30 min at 30 °C. Afterwards, cells were heat shocked for 30 min at 42 °C. For a plasmid transformation, cells were then spun down, washed with 1 mL sterile H_2O and ultimately 200 µL of the suspension was plated onto selective plates.

In case of a chromosomal integration and selection for antibiotic resistances, cells were allowed to recover after heat shock in 1 mL YPD at 30 °C (ts-mutants 25 °C, respectively) for 2-4 h. Hereinafter, cells were washed with 1 mL H_2O, resuspended in 200 µL H_2O and the whole suspension was plated on selective plates.

Plates were incubated for 3 days at 30 °C, 25 °C in case of ts-strains respectively.

3.3.3. Knop-PCR for chromosomal integration

For the purpose of chromosomal deletions, N-terminal or C-terminal tagging, a PCR-based method described by Janke *et al.* (Janke et al., 2004) was used. The so-called Knop-toolbox consist of a variety of plasmids for all kind of tags or deletions with different selections markers and delivers an modular primer design, which allows quick and easy chromosomal modifications in yeast.

The Knop-PCR was conducted according to the following scheme.

Table 18: PCR-mixture for Knop-PCR

5 µL	10 x buffer 2 (500 mM Tris-HCl, 22.5 mM $MgCl_2$, 160 mM NH_4SO_4, 20 % DMSO, 1 % Triton-X100, pH 9.2)
1 µL	dNTPS (10 mM)
2.5 µL	S_x-Primer (10 µM)
2.5 µL	S_y-Primer (10 µM)
1 µL	cassette plasmid (100 ng/µL)
0.5 µL	Go-Taq polymerase
0.4 µL	Q5 DNA polymerase
42.1 µL	H_2O

Table 19: PCR-program for Knop-PCR

step	temperature [°C]	time
initial denaturation	98	3 min
10 x cycles	98	30 s
	54	30 s
	68	2 min 40 s
20 x cycles	98	30 s
	54	30 s
	68	2 min 40 s +20 s/cycle

The PCR product was transformed into yeast according to section 3.3.2.

3.3.4. Serial dilution spot assay

Yeast cells were grown overnight at a permissive temperature in 5 mL of the respective media. Next, 5 OD_{600} units were harvested (3000 x g, 2 min), washed with 1 mL sterile H_2O and then resuspended in 0.5 mL sterile H_2O. From this cell suspension (OD_{600}=10) a 10-fold serial dilution was prepared starting with OD_{600}=1, if not otherwise indicated. 5 µL of each dilution step were spotted onto plates as indicated.

3.3.5. Synthetic genetic array screening (SGA)

SGA screening was performed as previously described by Tong *et al.* (Tong and Boone, 2006) using the Y8205 query strain. To screen the knock-down of the essential gene SGT1, a strain harboring SGT1 under the control of the repressible tet-off system (Mnaimneh et al., 2004) in the background of Y8205 was generated. Therefore, R1158 tetO7-SGT1 was mated with Y8205. Using the swapping method the kanMX resistance cassette was changed against the natMX cassette (Tong and Boone, 2006). After sporulation the final query strain Y8205 tetO7-SGT1 was selected on -Arg -Lys -Leu -Ura +Can +Thia +cloNAT.

Starting with Y8205 tetO7-SGT1 a manual screen including Hsp90 co-chaperones deletion mutants and a diverse set of yeast chaperone deletion mutants was set up. Deletion mutants were obtained from the EUROSCARF library. The haploid double mutants were selected on -His -Arg -Lys –Ura +Can +Thia +G418 +clonNAT. Synthetic genetic interaction was scored using spot assays in the presence or absence of 10 µg/mL doxycycline.

3.3.6. Microscopy and localization experiments

Microscopy experiments were performed using a Zeiss Axiovert 200 equipped with a Zeiss Plan-NEOFLUAR 63x.1.25 oil 440461 objective and a FluoArc system. Images were recorded using a Hamamatsu 4792-95 digital camera and processed with Simple PCI 5.3 software.

Localization of C-terminal GFP-tagged Sgt1 and domain constructs were conducted using aforementioned equipment. The wild-type BY4741 yeast strain was transformed with a p415-GPD plasmid expressing the GFP-fusion proteins. Yeast cells were grown to log phase at 30°C in the required SD medium and localization was analyzed by microscopy. Using ImageJ Cell Counter cells displaying nuclear or cytoplasmic localization of the GFP signal were quantified. Percentage of total cells classified in the indicated category for the indicated Sgt1 constructs were plotted showing the mean of three independent experiments.

3.3.7. Yeast cell cycle synchronization

Yeast cell cycle synchronization/arrest was obtained using α-factor, nocodazole or hydroxyurea following the previously described protocol with slight modifications (Rosebrock, 2017). In brief, yeast cells were grown over night in 5 mL of the respective medium and reinoculated in 50 mL starting with an OD_{600}= 0.2. Growth was prolonged until the culture reached OD_{600}=0.6. Then the pheromone or chemical was added (α-factor to a final concentration of 25 ng/mL, nocodazole 15 µg/mL and hydroxyurea 200 mM) inducing cell cycle arrest. The arrest was monitored by microscopy and cells were harvested or release when >95% of the culture showed the typical morphology. Release was obtained by washing the cells twice in pre-warmed medium.

3.3.8. GFP-Pull-down

For a GFP pull-down experiment yeast cells carrying GFP-tagged Sgt1 constructs or GFP on a plasmid were grown to log-phase and about 40 OD_{600} units were harvested. In case of cross-link experiments cells were resuspended in 1 % formaldehyde, incubated for 10 min and afterwards quenched with 0.5 M glycine.

For the pull-down, cells were then resuspended in IP-Buffer (50 mM TRIS, 100 mM NaCl, 5 mM $MgCl_2$, 0.15 % NP-40, 2 mM PMSF, 2x protease inhibitor mix HP, 1 mM DTT) and lysed by glass bead

disruption. Cell lysate was cleared by centrifugation at 14,000 x g for 10 min and normalized using Bradford assay (Bradford, 1976). The normalized lysate was loaded onto 25 µL of GFP-trap beads which were equilibrated with IP-Buffer, following incubation for 25 min at 4 °C. Afterwards, the beads were washed three times with IP-Buffer and then washed three times with 1 x PBS.

For MS/MS experiments beads were stored at – 80 °C until further usage (see section 3.4.14.).

For subsequent SDS-PAGE and Western blot analysis protein were eluted from the beads by adding 50 µL 1x Laemmli buffer and boiling for 10 min.

3.3.9. Sample preparation for whole proteome analysis

For the preparation of total, supernatant and pellet protein fractions from yeast, R1158 TetO7-SGT1 cells were grown to log phase at 30°C in the presence (*sgt1* depletion) or absence of 10 µg/mL doxycycline. Cells were harvested at 3000 x g for 1 min at 4 °C. Subsequent, cells were washed once (5000 x g, 30 s, 4°C) with 1 mL of chilled S_O-buffer (120 mM KCl, 2 mM EDTA, 20 mM HEPES-KOH, pH 7.4). The cell pellets were resuspended in 150 µL buffer S (S_0-buffer + 0.5mM DTT, 1:100 protease inhibitor MixFY (Serva), 1mM PMSF). This resuspension was divided in half and 75 µL were used for the total fraction (T). To the protein sample T 500 µL of buffer T (20mM HEPES-NaOH, pH7.4, 150 mM NaCl, 3% SDS, 5 mM EDTA, 2 mM DTT, 10 µM PMSF, 1:1000 protease inhibitor MixFY) were added. Next, cells were lysed by boiling for 20 min at 95 °C. The lysate was centrifuged for 1min at 5500 x g. The remaining supernatant (sample T) was flash frozen and stored at -80 °C until further usage. The remaining half of the resuspension (75 µL) was lysed by bead disruption using 9 mm stainless stell balls for 90 s at 30 Hz. Afterwards, 400 µL cooled buffer S was added and the lysate was cleared by centrifugation at 3000 x g for 30 s. The supernatant was transferred into a 1.5 mL ultracentrifuge tube and span down at 100000 x g for 20 min at 4 °C. The aqueous fraction was designated as supernatant fraction (S). The pellet was washed once with 500 µL buffer S (100000 x g, 20 min, 4°C). The pellet was resuspended in buffer P (8 M urea, 20 mM HEPES-NaOH, pH7.4, 150 mM NaCl, 2% SDS, 2 mM EDTA, 2 mM DTT, 10 µM PMSF, 1:1000 protease inhibitor MixFY) and centrifuged at 20000 x g at room temperature for 5 min. The supernatant was deignated as the pellet fraction (P). Until further usage samples were flash frozen and stored at -80 °C. Protein concentration was determined by BCA assay according to the manufacturer's instruction (Pierce BCA Protein Assay, ThermoFischer, USA).

3.3.10. Cycloheximide chase

The fungicide cycloheximide inhibits protein synthesis by blocking translation elongation. Hence, it is used to stop synthesis of new proteins and allows monitoring protein degradation *in vivo*. For chase experiments, yeast cells were grown to log phase in liquid culture (OD_{600}=0.6-0.8). The chase was

started by adding 100 µg/mL cycloheximide. 1 OD_{600} unit was harvested at indicated time points starting with sample time zero. Preparations of protein extracts were performed as described in section 3.3.11.

Additional to address the dependence of protein stability on Hsp90, yeast cultures were grown supplemented with 25 µM radicicol.

3.3.11. Post-alkaline extraction

The preparation of extracts of yeast proteins was performed as described by Kushnirov (Kushnirov, 2000). Briefly, 1 OD_{600} unit of yeast culture was harvested and resuspended in 200 µL 0.1 M NaOH. After 5 min incubation at room temperature cells were pelleted and resuspended in 50 µL 1 x Laemmli buffer, subsequently boiled for 3 min and again pelleted. 6-10 µL were used for SDS-PAGE analysis.

3.3.12. Isolation of yeast genomic DNA

The isolation of genomic DNA for colony PCRs and cloning was performed as described by Harju *et al.* (Harju et al., 2004). In brief, a yeast overnight culture was pelleted and resuspended in 200 µL lysis buffer (2 % Triton X-100, 1 % SDS, 100 mM NaCl, 10 mM Tris-HCl pH 8.0, 1 mM EDTA). Lysis was obtained after two freeze-thaw cycles. Next, 200 µL of chloroform/phenol (1:1) was added and the samples were vortexed. After centrifugation at 14,000 x g for 10 min, the aqueous phase was transferred into 400 µL ice-cold 100 % ethanol. The precipitate was washed once with 70 % ethanol followed by drying. The isolated genomic DNA was resuspended in nuclease free water.

3.3.13. Plasmid shuffling

For the characterization of essential genes, the well describe method of 5-FOA plasmid shuffling was used (Boeke et al., 1987). In sum, the *sgt1Δ* [p416-GPD-SGT1] strain was used for plasmid shuffling containing the knockout of the genomic copy of SGT1, only harboring the wild-type gene on a plasmid containing the URA3-marker. The URA3 gene encodes orotidine-5'-phosphate decarboxylase which converts 5'-FOA to the cell toxic 5'-fluorouracil allowing counter-selection. After 5-FOA treatment *sgt1Δ* survival depends on prior transformed plasmids containing *sgt1* mutants.

3.4. Protein expression, purification and analytical methods

3.4.1. Protein expression

Proteins were expressed in *E.coli* BL21-Codon Plus (DE3)-RIL or Rosetta BL21 cell, if the construct was not codon optimized. For expression in *E.coli,* the pET28 expression system or the thereof derived pET-SUMO system was used. Standard protein expression was carried out in LB-medium + 50 µg/mL kanamycin; 2YT-medium + 50 µg/mL kanamycin was used for the expression of Hsp82. If Rosetta BL21 was used, 50 µg/mL chloramphenicol were additionally added to the medium. Expression of the recombinant protein was induced with 1 mM IPTG when the culture reached an OD_{600}=0.8. Depending on the protein requirements expression took place between 3-4 h at 30 °C or 37 °C.

In case of the expression of isotope labeled protein for NMR (nuclear magnetic resonance) spectroscopy, *E.coli* was cultivated in M9 minimal media which was supplemented with ^{15}N enriched ammonium chloride and/or ^{13}C enriched glucose.

3.4.2. Cell harvest and disruption

E.coli cells were harvested by centrifugation at 10,000 x g, 4 °C for 10 min. The cell pellets were washed once with NiNTA-A buffer (40 mM K_2HPO_4/KH_2PO_4, 300 mM KCl, 20 mM imidazole, pH 7.5) supplemented with protease inhibitor mix HP. For storage cell pellets were shock frozen in liquid nitrogen and stored at -20 °C until further usage.

Cell disruption was performed either by a cell disruption system at 1.8 kbar at 8 °C or by sonication (5 x 45 s, 50 % duty cycle, 50 % output). Before cell disruption DnaseI, protease inhibitor mix G and 2 mM PMSF were added to the cell suspension. Cell lysate was cleared at 100,000 x g, 4 °C for 45 min.

3.4.3. Protein purification

Protein purification steps were performed at 4 °C. In the case of proteins carrying only an N-terminal fused His_6 tag (e.g. Hsp82) following strategy was used for purification. After cell disruption and lysate clearance, the lysate was loaded on a His-Trap FF column, which was equilibrated in NiNTA-A buffer (40 mM K_2HPO_4/KH_2PO_4, 300 mM KCl, 20 mM imidazole, pH 7.5). Subsequently, the column was washed with 8 column volumes (CV) of 2 % NiNTA-B buffer (40 mM K_2HPO_4/KH_2PO_4, 300 mM KCl, 500 mM imidazole, pH 7.5). Elution from the nickel affinity column took place with 100 % NiNTA-B buffer.

Elution fraction containing protein were pooled and diluted to approximately 150 mL with ResQ-A buffer (40 mM HEPES, 20 mM KCl, 1 mM EDTA, pH 7.8) to dilute the salt concentration of the protein

fractions to ensure protein binding to the following ion exchange column. Next, the diluted protein was loaded onto a ResQ column equilibrated in ResQ-A buffer, washed with 8 CV of ResQ-A buffer and subsequently protein elution took place over a gradient ranging from 0-50 % ResQ-B buffer (40 mM HEPES, 1 M KCl, 1 mM EDTA, pH 7.8). The protein containing fractions again were pooled and concentrated to approximately 5 mL using Amicon ultracentrifugal filter units with the required molecular weight cut-off.

The concentrate was loaded on a Superdex 16/60 200 pg column, which was equilibrated in SEC-buffer (40 mM HEPES, 150 mM KCl, 5 mM $MgCl_2$, pH 7.5). Protein purity was checked by SDS-PAGE (section 3.4.4.). Protein concentration was determined as described in section 3.4.6. and the protein was frozen in liquid nitrogen and stored at – 80 °C.

For SUMO-/TEV-tagged proteins, a buffer exchange was performed after the nickel affinity chromatography. For that reason, the elution fractions containing protein were loaded onto a HiPrep 26/10 Desalting column equilibrated with SEC-buffer. After tag cleavage, which was carried out overnight at 4 °C by adding SUMO protease or TEV protease, the protein was run again over a His-Trap FF column equilibrated with NiNTA-A buffer. The flow-through was collected, concentrated and subsequently loaded onto a Superdex 16/60 200 pg. Protein purity was checked by SDS-PAGE (section 3.4.4.). Protein concentration was determined as described in section 3.4.6. and the protein was frozen in liquid nitrogen and stored at – 80 °C.

If the size of the desired protein was in the range of 8-20 kDa, a Superdex 16/60 75pg was used instead of the 200 pg column. For purification of cysteine containing proteins, 1 mM DTT was added to all buffers.

3.4.4. SDS-PAGE (sodium dodecyl sulfate polyacrylamide gel electrophoresis)

For protein separation, SDS-PAGE was performed as previously described by Laemmli (Laemmli, 1970). To analyze the protein purity of purifications, self-made gels were used (gel recipe shown in table 20). If subsequent Western Blot analysis were planned, commercially available gradient gels (4-20 % Serva TG Prime) were used.

Samples were mixed with Laemmli buffer and boiled for 5 min at 95 °C, loaded onto the gel. Triple Color Protein Standard III was loaded as standard and the gel was run at constant amperage of 35 mA for self-made gels or 50 mA for pre-cast gels.

Table 20: SDS-gel protocol

Ingredient	Stacking gel 5 %	Separation gel 12.5 %
40 % Acrylamide	0.625 mL	3.125 mL
4 x separation gel buffer	-	2.5 mL
2 x stacking gel buffer	2.5 mL	-
H_2O	1.875 mL	4.375 mL
APS	125 µL	125 µL
TEMED	6.6 µL	6.6 µL

Protein purification gels were stained according to Fairbanks *et al.* (Fairbanks et al., 1971). Gels were stained with pre-warmed Fairbanks A solution and destained with pre-warmed Fairbanks D solution.

3.4.5. Western blotting

After SDS-PAGE, gels were blotted on methanol-activated PVDF membranes in a semi-dry blotting apparatus at constant amperage of 72 mA for 2 h. Afterwards, the membrane was blocked by incubation overnight at 4 °C or 1 h at room temperature in 3 % milk powder in 1 x TBS-T. Subsequent, the membrane was incubated with primary antibodies diluted in 1 % milk powder in 1 x TBS-T for 1 h at room temperature, followed by three times washing with 1 x TBS-T and another 1 h incubation with the secondary antibody (Peroxidase (POD)-conjugate). The blot was again washed three times with TBS-T and bands were detected using Western Bright ECL spray and ImageQuant LAS4000 following manufacturer's instructions.

3.4.6. Determination of protein concentration and degree of labeling

The protein concentration was determined according to the Lambert-Beer law.

$$A = \varepsilon \, x \, c \, x \, d$$

With A = absorbance at 280 nm, ε = extinction coefficient of the protein at 280 nm [M^{-1} x cm^{-1}], c = concentration [M] and d = layer thickness [cm].

The absorbance was determined using a Varian Cary 50/100 Bio UV-Vis spectrophotometer. Molar extinction coefficients were determined using the ProtParam online tool.

In the case of labeled proteins protein concentration and degree of labeling was determined according to following equation.

$$c_{prot} = \frac{A_{280} - A_{max} \, x \, CF_{280}}{\varepsilon_{prot} \, x \, d}$$

With c_{prot}= concentration of the protein, A_{280}=Absorbance at 280 nm, A_{max}= Absorbance at the absorption maximum of the dye, CF_{280}= correction factor for the dye at 280 nm, ε_{prot}= extinction coefficient of the protein at 280 nm [M^{-1} x cm^{-1}] and d= layer thickness [cm].

$$DOL = \frac{A_{max}\ x\ \varepsilon_{prot}}{\varepsilon_{max}\ x\ (A_{280} - A_{max}\ x\ CF_{280})}$$

With DOL= degree of labeling, A_{280}=Absorbance at 280 nm, A_{max}= Absorbance at the absorption maximum of the dye, CF_{280}= correction factor for the dye at 280 nm, ε_{prot}= extinction coefficient of the protein at 280 nm [M^{-1} x cm^{-1}] and ε_{max}= extinction coefficient of the dye at its maximum absorbance wavelength.

3.4.7. Protein labeling

Labeling of proteins was performed for analytical ultracentrifugation experiments. The label was introduced at native or mutational introduced cysteine residues with maleimide chemistry. Before labeling, the buffer of the protein was exchanged from the SEC-buffer containing DTT to SEC buffer without DTT using a PD-10 column according to the manufacturer's protocol. The fluorescent dye was afterwards added in a 2-fold molar excess over the protein and the reaction was incubated in the dark for 1 h at room temperature. The labeling reaction was quenched by addition of 5 mM DTT and subsequently unreacted fluorescent dye was separated from the labeled protein by running the sample over a PD-10 column equilibrated in SEC buffer. Concentration and DOL were determined as described in Section 3.4.6.

3.4.8. CD spectroscopy

Far-UV circular dichroism spectroscopy is a technique based on the characteristics of optically active (chiral) molecules to differentially absorb circular polarized light. The peptide bond is one of the optical active elements in proteins with an absorbance between 170-260 nm. In this spectrum range information about the secondary structure of the peptide can be gained by Far-UV CD. α-helical proteins show two minima at 208 nm and 222 nm, whereas β-sheets display a single minimum at 218 nm, and a minimum at 195 nm indicates an unstructured protein.

The ellipticity θ [°] is the quantity for CD. The molar ellipticity is the correlation of the ellipticity, the amino acid composition and the molecular weight of a protein as is determined as displayed in the following equation.

$$\theta_{MRW} = \frac{\theta\ x\ 100\ x\ M}{c\ x\ d\ N_{Aa}}$$

With θ_{MRW}= molar ellipticity, θ= measured ellipticity [mdeg], M= molecular weight of the protein [kDa], c= protein concentration [mg/mL], d= layer thickness [cm], N_{Aa}= count of amino acids of the protein.

Spectra were recorded with a Chirascan V100 CD spectrometer. Protein samples were dialysis into 1 x PBS before measurements were carried out with the following settings:

Table 21: CD spectrometer settings

parameter	setting
Start	260 nm
End	190 nm
Resolution	0.1 nm
Accumulations	30
Scanning Speed	20 nm/min
Layer thickness	0.1 cm
temperature	20 °C

Recorded CD-data was further analyzed using Origin 9.1 software.

3.4.9. Analytical ultracentrifugation (AUC)

AUC was performed to follow complex formation of a given fluorescently-labeled protein species. The interaction studies were carried out as sedimentation velocity experiments. The experiments were performed using a Beckman XL-A centrifuge equipped with an AVIV fluorescence detection system and an eight-hole Beckman-Coulter AN-50 Ti rotor. All samples were prepared in AUC buffer (40 mM HEPES, 50 mM KCl, 5 mM $MgCl_2$), if not stated otherwise. Fluorescently-labeled protein was used at a concentration of 500 nM. All other proteins had a concentration of 2.5 µM or as indicated.

ATTO488-labeled proteins were excited at a wavelength of 488 nm and the emission of the fluorescent dye was recorded with a band pass filter from 505-565 nm. The samples were loaded into assembled cell with 12-mm path length charcoal-filled epon double sector centerpieces and quartz windows. Rotation rate was set to 42 000 rpm. Partial specific volume, density and viscosity were calculated using SEDNTERP (Laue TM, 1992). Analysis of the data was performed using SedView (Hayes and Stafford, 2010), SedFit (Brown et al., 2009) and Origin 9.1.

3.4.10. Fluorescence anisotropy

Fluorescence anisotropy measurements were performed on a Jasco Fluorescence Spectrometer FP-8500 equipped with polarizers. Anisotropy of ATTO488-labeled proteins were monitored in a quartz cuvette using HKM buffer (40 mM HEPES, 150 mM KCl, 5 mM $MgCl_2$). Excitation wavelength was set to 490 nm and emission to 520 nm. Temperature was set to 30 °C. Analysis of the data was performed using Origin 9.1.

3.4.11. Förster resonance energy transfer (FRET) measurements

Förster resonance energy transfer measurements were carried out using a Horiba Fluoromax 4 fluorescence spectrometer. The previously described Hsp90-FRET system was used consisting of the Hsp82 D61C mutant (Hessling et al., 2009). The measurements were conducted at 30 °C in a quartz cuvette with the excitation wavelength set to 490 nm. Emission was monitored at 520 nm and

575 nm. The Hsp82 D61C mutant was fluorescently labeled with either ATTO488 or ATTO550. Donor and acceptor were used at a concentration of 200 nM. Closing of Hsp90 was induced with 2 mM AMP-PNP or ATPγS, respectively. For data analysis and processing Origin 9.1 was used.

3.4.12. Hydrogen/deuterium exchange-mass spectrometry (HDX-MS)

Hydrogen/deuterium exchange experiments were performed using an automated system equipped with a Leap robot (HTS PAL), a Waters ACQUITY M-Class UPLC, a HDX manager and a Synapt G2-S mass spectrometer as described previously (Kazman et al., 2020). In brief, the protein samples were diluted in a ration of 1:20 with D_2O containing SEC buffer (40 mM HEPES, 150 mM KCl, 5 mM $MgCl_2$, 1 mM TCEP, pH 7.5) and data points were acquired at 0 s, 10 s, 60 s, 1800 s, and 7200 s at 20 °C. At each time point of the kinetic 3 µL were extracted from the protein samples, which were composed of Sgt1 or mutants at a concentration of 30 µM and additional in complex with Hsp82 with a concentration of 90 µM, and quenched by a 1:1 dilution with quenching buffer (400 mM Na_2HPO_4/NaH_2PO_4, 250 mM TCEP, 3 M GdmCl, pH 2.2) at 1 °C. Subsequently, the proteins were digested on a Waters Enzymate BEH Pepsin Column 2.1 x 30 mm at 20°C. Next, peptides were separated using a H_2O/acetonitrile gradient containing 0.1 % formic acid (v/v) at 0 °C on a Waters AQUITY UPLC BEH C18 column. Finally, peptides were subjected to a Synapt TOF mass spectrometer by electronspray ionization. Waters Protein Lynx Global Server PLGs and DynamX software were used for data processing. HDX experiments were operated by Florian Ruhrnößl (Technische Universität München).

3.4.13. NMR spectroscopy

NMR experiments and data processing were performed by Dr. Abraham Lopez (Lehrstuhl für Biomolekulare NMR-Spektroskopie, Technische Universität München) at the chair of Prof. Dr. Michael Sattler.

For NMR studies of WT Sgt1 SGS domain (residues 312-395) two samples were employed: U-15N and U-15N, 13C labeled samples, with approximate concentrations of 1000 and 700 uM, respectively. Samples were buffer exchanged to Hsp90 NMR buffer (20 mM NaPhos pH 6.5, 100 mM NaCl, 5 mM MgCl2, 0.02% sodium azide). All experiments were performed at 500 and 600 MHz fields in Bruker instruments (Bruker biospin, Karlsruhe, Germany) using room temperature (600 MHz) or cryogenically cooled (500 MHz) probes. ^{1}H-^{15}N HSQC experiments with watergate flip-back water suppression scheme were performed with the ^{15}N-labeled sample, consisting of 2048 x 380 data points. The spectral width was adjusted to 27 ppm for the ^{15}N dimension. For backbone resonance assignment, a set of HNCACB/CBCACONH and HNCO/HNCACO pairs of experiments were recorded on the double labeled sample, using the same water suppression sequence. Experiments comprised

2048 x 60 x 120 and 2048 x 60 x 50 points, for each respective pair. Non-uniform sampling (NUS) was used in 3D experiments, with 60 and 25% of the increments sampled, respectively. In addition, a ^{15}N-edited NOESY experiment was recorded to support the assignment, with 2048 x 60 x 110 points and using a 50% NUS.

To obtain HA assignments, we employed 3D HNHA experiments (Vuister et al., 1993), recorded on double labeled sample. In addition, $^{3}J_{HN\text{-}HA}$ coupling constants were extracted from the intensity ratio between the diagonal and cross-peaks using a 111% of relaxation correction. With this set-up, $_{3JHN\text{-}HA}$ values of 4.8 and 8.5 Hz report on α-helix and β-strand, respectively.

To analyze structural flexibility in the sub-nanosecond time scale, we performed ^{1}H-^{15}N heteronuclear NOE experiments (Farrow et al., 1994). In this set-up, two sets of ^{1}H-^{15}N correlation spectra were recorded in an interleaved manner, with and without ^{1}H saturation prior to the starting of the pulse scheme. After splitting of the dataset, ^{1}H-^{15}N heteronuclear NOE values were extracted from the ratio of the peak intensities. Typically, values around 0.7-0.8 are obtained for structured regions, and deviations from the average heteronuclear NOE values indicate increased flexibility.

All spectra were processed with NMRpipe (Delaglio et al., 1995), using SMILE reconstruction for NUS-acquired data. In addition, 2x zero filling and SMILE extrapolation was used in all 3D spectra. Data analysis was performed with Ccpnmr Analysis software V2.4.2 (Vranken et al., 2005).

3.4.14. MS/MS

Sample preparation, measurements and data processing was performed by Moritz Mühlhofer (Technische Universität München).

3.4.14.1. On bead digest and desalting

Protein digest was performed in a similar manner as described previously (Keilhauer et al., 2015). In brief, GFP-trap beads were resuspended in 25 µL digestion (50 mM Tris-HCl, 5 ng/µL Trypsin, 2 M Urea, 1 mM DTT, pH 7.5) and incubated at room temperature for 2 h. Afterwards the peptides were alkylated by adding 100 µL alkylation buffer (50 mM Tris-HCl, 2 M Urea, 5 mM 2-Iodoacetamide (IAA)) and incubation at 37 °C overnight. Next, the digest was stopped by the addition of 1.5 µL formic acid. Self-packed stage tips with a double C18 layer, which were equilibrated wit 70 µL methanol and washed three times with 70 µL 0.5 % formic acid, were used to desalt the peptides (Rappsilber et al., 2007). Beads were separated by centrifugation for 1 min at 16900 x g. The peptides were loaded on the column, washed three times with 70 µL 0.5 % formic acid and eluted with two times 30 µL 80 % acetonitrile containing 0.5 % formic acid. Lastly, samples were dried in a speed vacuum concentrator and sored at -80 °C.

3.4.14.2. Filtering peptide solutions for MS measurements

After the digestion and desalting peptides were dissolved in 23 µL 0.1 % formic acid and incubated for 15 min in an ultrasonic bath at room temperature. Next, the solution was transferred onto centrifugal filters (0.22 µM) and filtered by centrifugation at 10,000 x g for 2 min. The filtered solution was carried over into Chromacol vials with Chromacol closures.

3.4.14.3. MS/MS measurement of pull-down experiments

Measurements were performed on a Q Excative Plus instrument coupled to an Ultimate3000 Nano-HPCL via an electrospray easy source. The peptides were loaded on a 2 cm PepMap RSLC C18 trap column (particles 3 µm, 100 A, inner diameter 75 µm) with 0.1 % triflouric acid and separated on a 50 cm PepMap RSLC C18 column (particles 2 µm, 100 A, inner diameter 75 µm) at 40 °C. The gradient was run at a flow rate of 400 nL/min from 5-35 % acetonitrile + 0.1 % formic acid during 42 min (7 min 5 % acetonitrile, 30 min up to 28 %, 5 min to 35 %, washed with 90 % for 10 min, re-equilibrated with 5 % for 10 min).

Survey scans (m/z 300-1500) were acquired with a resolution of 70,000 and the maximum injection time set to 50 ms. Data dependent HCD fragmentation cans of the 12 most intense ions of the survey scans were acquired with a resolution of 17,500, maximum injection time of 50 ms. Isolation window was set to 1.6 m/z. Unassigned, single charged ions were excluded, and the dynamic exclusion of peptides enabled for 60 s. For real-time mass calibration the lock-mass ion 455.12002 from ambient air was used. Data were acquired using Xcalibur 3.1sp3 software.

3.4.14.4. Data analysis

Analysis of the raw data was performed using MaxQuant 1.6.2.6. (Cox et al., 2014a, Cox and Mann, 2008b). Raw files were searched against reviewed *Saccharomyces cerevisiae* (taxon identifier: 559292) proteome database downloaded from UniprotDB. All files were assigned to the same fraction with default settings. Tryptic cleavage sites before proline were included, two missed cleavage site were allowed and a peptide tolerance of 4.5 ppm. Methionine oxidation as well as N-terminal acetylation were selected as variable modifications, carbamidomethylation as fixed one. Maximal 5 modifications per peptide were allowed. Minimal ration count for label free quantification was set to 1. The peptide length had to be between 7 and 25 amino acids. Match between runs was applied (match time window 0.7 min, align window 20 min). The proteins were identified with a FDR of 1 %. Unique and razor peptides were included with a minimal ratio count of 1. For the statistical validation of the results, the peptides were searched against a reverse decoy database.

The processed MS data were further evaluated by Perseus 1.6.2.1 (Tyanova et al., 2016). After filtering the protein groups file by potential contaminant hits, hits from the reverse database and hits

only identified by site, the LFQ intensities were log_2 transformed, grouped into replicates and the rows filtered on 3 valid values in at least one replicate group. Missing values were calculated from the Gaussian distribution (width: 0.3, downshift: 1.8) and volcano plots with a two-sided t-test (FDR: 0.05; S_0= 0.1) were plotted (Hochberg, 1995)

3.4.14.5. Di(N-succinimidyl) glutarate (DSG) crosslink

For crosslink experiments disuccinimidyl glutarate as amine reactive homo-bifunctional crosslinker was used at a final concentration of 3 mM. Samples were compiled in HKM buffer (40 mM HEPES, 150 mM KCl, 5 mM $MgCl_2$). Sgt1 was used at a concentration of 15 µM, Hsp90 at 50 µM. After addition of DSG the samples were incubated for 45 min at room temperature. The reaction was quenched by the addition of 100 mM tris(hydroxymethyl) aminomethane. Samples were further process for MS/MS measurements.

3.4.14.6. Wessel-Flügge-precipitation

The crosslink approach was filled with MS grade water to 160 µL. The proteins were precipitated according to Wessel and Flügge (Wessel and Flugge, 1984). In brief, 600 µL methanol (Sigma) were added, the emulsion was vortexed and centrifuged for 10 s at 16,200 x g and RT. This procedure was repeated with 225 µL chloroform (Sigma). Then, 450 µl H_2O were added, it was vortexed again, incubated for 7 min in an ultrasonic bath (VWR) and centrifuged for 10 s at 16,200 x g. The upper phase was taken off until the precipitated proteins in the interphase were reached. Then, 450 µL methanol were added, the suspension was vortexed and centrifuged at 16,200 x g for 20 min at RT. Finally, the supernatant was discarded and the pellets were air-dried. The proteins were dissolved in 25 µL digestion buffer (50 mM Tris/HCl, pH 7.5, 2 M urea, 1 mM DTT, 5 ng/µL Trypsin) and the further sample preparation was performed as described for the on bead digest.

3.4.14.7. MS/MS measurement of crosslink samples

MS/MS measurements were performed on an Orbitrap Fusion instrument coupled to an Ultimate3000 Nano-HPLC via an electrospray easy source (ThermoFisher Scientific). After loading the peptides on a 2 cm PepMap RSLC C18 trap column (particles 3 µm, 100 A, inner diameter 75 µm, ThermoFisher Scientific) with 0.1 % TFA, they were separated on a 50 cm PepMap RSLC C18 column (particles 2 µm, 100 A, inner diameter 75 µm, ThermoFisher Scientific) constantly held at 40 °C. The peptides were eluted with a gradient from 5 to 35 % ACN, 0.1 % FA during 35 min at a flow rate of 0.4 µL/min (7 min 5 % ACN, 30 min to 28 % ACN, 5 min to 35 % ACN, 0.1 min to 90 % ACN, 10 min wash at 90 % ACN, 10 min equilibration at 5 % ACN).

Survey scans (m/z 300 - 1,500) with a resolution of 120,000 were acquired. The automatic gain control (AGC) target value was set to 2.0*e5 with a maximum injection time of 80 ms. For HCD

fragmentation, the most intense ions of charge states 2-12 were selected. The collision energy was set to 30 %. In the ion trap, the maximum injection time was set to 100 ms and the AGC target value was reduced to 5.0*e4. Inject ions for all available parallelizable time was allowed. Dynamic exclusion of sequenced peptides was set to 60 s. Internally generated fluoroanthene ions were used for real-time mass calibration. Data were acquired using Xcalibur software version 3.0sp2 (ThermoFisher Scientific).

3.4.14.8. Sample preparation for whole proteome MS/MS measurements

Samples from section 3.3.9. were further processed as following described. 250 µg protein were precipitated according to section 3.4.14.6. (Wessel and Flugge, 1984). The air-dried proteins were dissolved in 8 M urea, 50 mM Tris (pH 7.5), 4 mM DTT. 20 µg protein were transferred into a 1.5 mL tube and diluted with 50 mM Tris to a final volume of 25 µL. Protein digestion was carried out with sequencing grade Trypsin (5 ng/µL; Promega) for 2 h at RT. The peptides were alkylated (50 mM Tris/HCl, pH 7.5, 2 M urea, 5 mM IAA) overnight in the dark at RT at 500 rpm in a thermomixer. The digest was quenched with 1.5 µL formic acid (FA). The samples were desalted with double C18 layer stage tips (Rappsilber et al., 2007). Therefore, the tips were equilibrated with 70 µL methanol and washed three times with 70 µL 0.5 % FA. The peptides were loaded onto the tips, washed three times with 70 µL 0.5 % FA and eluted with two times 30 µL 80 % ACN, 0.5 % FA (960 x g). The samples were dried in a speed vacuum concentrator (Eppendorf). Prior to MS/MS measurement, the peptides were dissolved in 23 µL 1 % (v/v) FA and incubated for 15 min in an ultrasonic bath at RT. The peptide solutions were filtered with centrifugal filters (0.22 µM; Merck; 2 min at 10,000 x g) and transferred into Chromacol vials (ThermoFisher Scientific).

3.4.14.9. MS/MS measurement of whole proteome analysis

MS/MS measurements were performed on an Orbitrap Fusion coupled to an Ultimate3000 Nano-HPLC via an electrospray easy source (ThermoFisher Scientific). After loading the peptides on a 2 cm PepMap RSLC C18 trap column (particles 3 µm, 100 Å, inner diameter 75 µm, ThermoFisher Scientific) with 0.1 % TFA, they were separated on a 50 cm PepMap RSLC C18 column (particles 2 µm, 100 Å, inner diameter 75 µm, ThermoFisher Scientific) at 40 °C. The peptides were eluted with a gradient from 5 to 32 % ACN, 0.1 % FA during 152 min at a flow rate of 0.3 µL/min (7 min 5 % ACN, 105 min to 22 % ACN, 10 min to 32 % ACN, 10 min to 90 % ACN, 10 min wash at 90 % ACN, 10 min equilibration at 5 % ACN). Survey scans (m/z 300 - 1,500) with a resolution of 120,000 were acquired. The automatic gain control (AGC) target value was set to 2.0*e5 with a maximum injection time of 50 ms. For fragmentation with high-energy collisional dissociation, the most intense ions of charge states 2-7 were selected. The collision energy was set to 30 %. In the ion trap, the maximum injection time was also set to 50 ms and the AGC target value was reduced to 1.0*e4. Inject ions for all

available parallelizable time was allowed. Dynamic exclusion of sequenced peptides was set to 60 s. Internally generated fluoroanthene ions were used for real-time mass calibration. Data were acquired using Xcalibur software version 3.0sp2 (ThermoFisher Scientific).

3.4.14.10. MS/MS data analysis for whole proteome analysis

The MS data were analyzed with MaxQuant (version 1.6.2.6) (Cox et al., 2014b, Cox and Mann, 2008a). The S. cerevisiae proteome database downloaded from UniprotDB was used for protein identification. The same fraction was set for all files of one experimental setup. Only tryptic peptides were searched and cleavage sites before proline were included. Peptides with up to two missed cleavage sites were included in the analysis and a peptide tolerance of 4.5 ppm was applied. As fixed modification, carbamidomethylation was selected. N-terminal acetylation and methionine oxidation were selected as variable modifications. Maximum five modifications per peptide were allowed. For the primary search in MaxQuant the min. ratio count was set to 1 and Label min. ratio count was also set to 1. Furthermore, unique + razor peptides were taken into account. Otherwise, the default orbitrap instrument settings of MaxQuant were applied. The minimal peptide length was set to 7 amino acids, the maximal length was 25 amino acids. Match between runs was applied (match time window: 0.7 min; align window: 20 min). The identification parameters were left preset with a protein false discovery rate (FDR) of 1 %. The peptides were also searched against a decoy database (reverse database) generated by MaxQuant. The protein groups table that was generated by MaxQuant was further evaluated in Perseus (version 1.6.2.1) (Tyanova et al., 2016). First, the table was filtered by potential contaminant hits, hits from the reverse (decoy) database and hits that were only identified by side. After log2 transformation of the LFQ intensities, the associated replicates were grouped into categories. For the supernatant and total proteome measurements, the rows were filtered on three valid values in each group, for the pellet measurement they were filtered on three valid values in at least one group. The missing values were calculated from the Gaussian distribution (width: 0.3; downshift: 1.8). To analyze the fold changes, Volcano plots were plotted and a two-sided t-test was applied (Benjamini and Hochberg, 1995) in Perseus. A protein was considered to be significantly up- or downregulated if $|\log2\ fc| > 1$ and p-value < 5 %.

4. Results

4.1. Identification of the essential Sgt1 domain

In *S. cerevisiae* the Hsp90 machinery contains twelve co-chaperones, of which three are essential for viability under standard growth conditions. Cdc37 is crucial for the recruitment of kinases to the Hsp90 system (Breter et al., 1983, Brugge et al., 1981).The essential Cns1 was reported to be involved in the chaperoning of the elongation factor 2 (Schopf et al., 2019). Sgt1 is mainly associated with kinetochore assembly and SCF E3-ligases (Kitagawa et al., 1999). For Sgt1 different functions were ascribed to the three domains (TPR-CS-SGS), the TPR domain mediates Skp1 binding and homo-dimerization, the CS domain facilitates interaction with Hsp90 and the SGS domain is the putative binding site for Hsp70 and LRR-containing proteins (Bansal et al., 2004, Catlett and Kaplan, 2006, Willhoft et al., 2017, Spiechowicz et al., 2007, Stuttmann et al., 2008). Research on the plant homologue of Sgt1 showed that a TPR deletion mutant is sufficient to provide the intrinsic function of Sgt1 (Azevedo et al., 2006). Additionally, the nematode Sgt1 lacks the TPR domain (Eckl et al., 2014). However, the structural element providing the essential function of Sgt1 was so far not defined.

For the purpose of defining the essential part of Sgt1, *in vivo* plasmid shuffling was carried out. To this end, the yeast strain *sgt1Δ* [SGT1] was generated, which harbors the wild-type SGT1 gene under the control of the constitutively active GPD-promoter on a CEN-plasmid selectable for uracil auxotrophy (p416-GPD-Sgt1) and a chromosomal deletion of the SGT1 gene. The selection marker URA3 can be counter-selected by the addition of 5-fluoroorotic acid (5-FOA) due to the enzymatic conversion of 5-FOA to 5-FU (5-fluoro uracil), a cell toxin, by the gene product of URA3 (Boeke et al., 1987). The selection pressure leads to the loss of the p416-GPD-Sgt1 plasmid and allows probing yeast viability depending on the gene product of a previously transformed plasmid carrying a *sgt1* mutant. To define the essential domain of Sgt1, single domain and double domain constructs with the domain boundaries depicted in figure 13 were cloned in the p415-GPD vector and transformed into the *sgt1Δ* [SGT1] shuffling strain. In case of the non-native double domain construct TPR-L-SGS, a flexible glycine-serine linker was introduced between the two single domains.

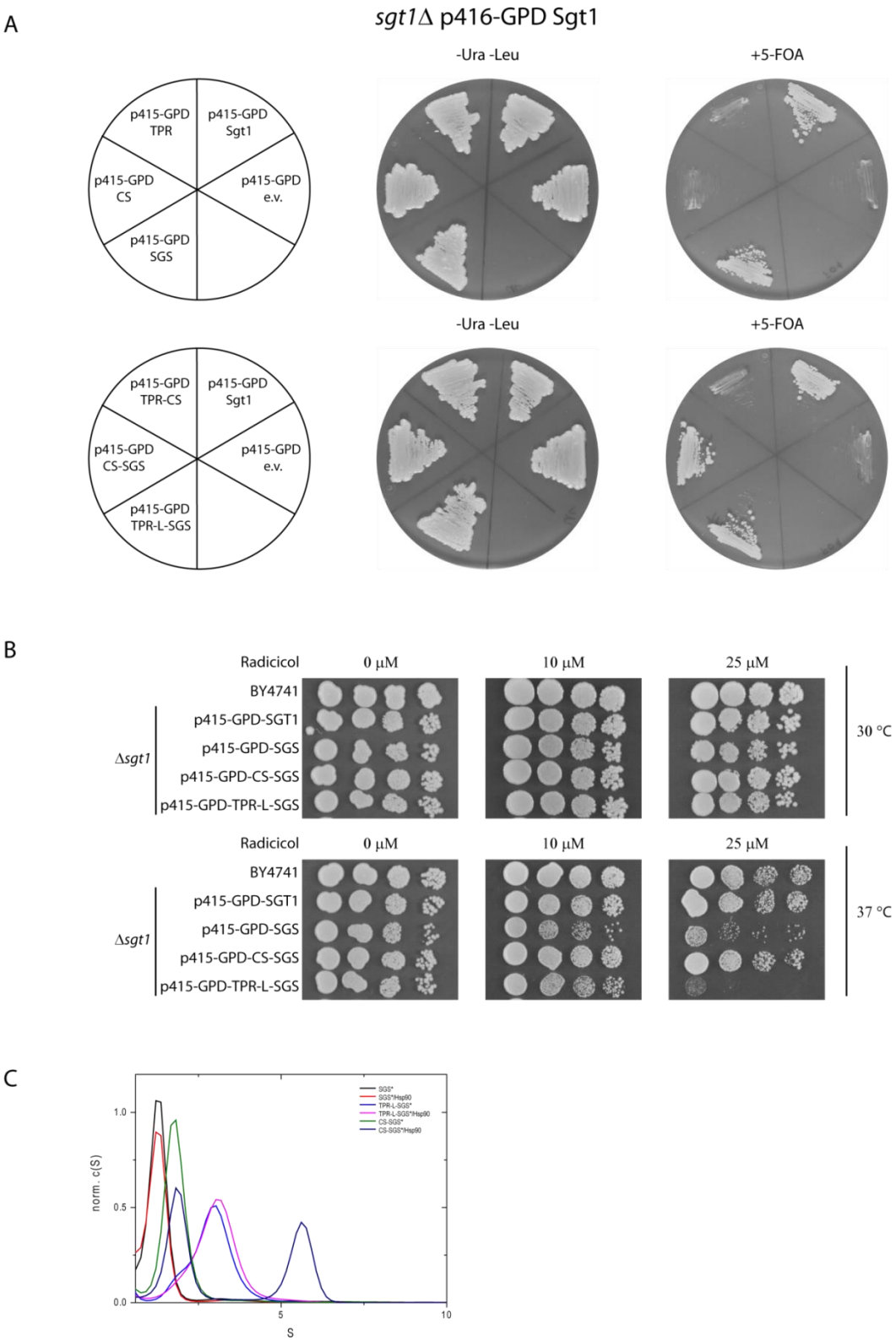

Figure 13: The essential domain of Sgt1. (A) Plasmid shuffling using the *sgt1Δ* [SGT1] strain transformed with p415-GPD plasmids containing Sgt1 domain constructs or empty vector as indicated in the left panel. Strains were grown on SD media without (middle panel) or with 200 µg/mL 5-flourortic acid (right panel) at 30 °C for 3 days. Representative picture of three independent experiments. (B) Radicicol sensitivity assay. Ten-fold serial dilutions of indicated strains with the starting OD_{600} of 1 were spotted onto YPD plates containing the indicated radicicol concentration. Yeast growth was monitored after three days of incubation at 30 °C or 37 °C as indicated. Representative picture of independent triplicates. (C) Analysis of complex formation between Sgt1 domain constructs and Hsp90 by analytical ultracentrifugation sedimentation velocity experiments using 500 nM of the Atto488-labeled species (indicated by an asterisk) and 5 µM Hsp90. Normalized c(S) distributions were plotted against the apparent sedimentation coefficient S.

As expected, the vector harboring Sgt1^{WT} as positive control supported growth on 5-FOA whereas the empty vector, negative control, did not provide yeast growth (Fig 13A). Strikingly, yeast viability only depended on the C-terminal SGS domain of Sgt1. The strain expressing the SGS domain showed wild-type like growth indicating that the last 83 amino acids of Sgt1 are sufficient to fulfill the essential function *in vivo*. Notably, all fusion constructs which comprise the SGS domain provided yeast viability, too. Inversely, the TPR and the CS domain are dispensable for cell viability.

Since the SGS domain is the putative site of client recognition and Hsp70 interaction (Spiechowicz et al., 2007, Stuttmann et al., 2008), the plasmid shuffling experiment suggests that the essential *in vivo* function of Sgt1 is linked to the Hsp70 chaperone network. Hsp90-dependence of the essential function was probed by serial dilution spot assay in presence of the Hsp90 inhibitor radicicol. The *sgt1Δ* strains harboring constructs which were viable in the prior shuffling and a wild-type strain (BY4741) were analyzed regarding their sensitivity towards increasing concentrations of radicicol (Fig 13B). All tested strains grew wild-type like in the absence of radicicol. Also, lower concentrations of radicicol (10 µM) did not lead to a visible growth defect at 30 °C. Yet, at the highest concentration tested (25 µM) a slight reduction in growth was observed for the strain expressing the SGS domain or the fusion construct TPR-L-SGS as only copy of Sgt1. To amplify those growth defects additional mild heat stress was applied by incubation at 37 °C. Also, at higher temperature all strains behaved wild-type like in the absence of radicicol. However, the previously slight growth defect of the *sgt1Δ* [SGS] and *sgt1Δ* [TPR-L-SGS] strain was now severe even at 10 µM radicicol. Since the SGS domain and the TPR domain were reported to be not involved in Hsp90 binding, the radicicol assay suggests that a stable Hsp90 interaction is crucial to fulfil Sgt1's essential function, if Hsp90 function is impaired.

To test the interaction of the Sgt1 constructs with Hsp90 *in vitro*, analytical ultracentrifugation experiments were carried out monitoring the sedimentation of the fluorescently labeled Sgt1 domain construct. Complex formation could be observed by the shifting of the peak of the labeled construct alone to higher Svedberg values upon addition of Hsp90 (Fig 13C). In line with the literature only the construct containing the CS domain was able to form a complex with Hsp90 (Lee et al., 2004b), as shown by the occurrence of an additional peak at around 6 S, if Hsp90 was added to the labeled CS-SGS construct.

In summary, yeast strains expressing constructs of Sgt1 which lack the CS domain lack direct Hsp90 interaction and are sensitive to the inhibition of Hsp90 by radicicol. As a consequence thereof, interaction with Hsp90 is crucial for the essential function of Sgt1 *in vivo*.

4.2. Mutational analysis of Sgt1-related thermo-sensitive mutants

Sgt1 was initially discovered as a suppressor of the thermo-sensitive phenotype of the *skp1-4* strain (Kitagawa et al., 1999). Analysis of the rescue of thermo-sensitive (ts) phenotypes allows drawing conclusions about the involvement in a certain pathway or interaction which was assigned to the ts-phenotype. The involvement of Sgt1 domains in the rescue of Sgt1-related thermo-sensitive strains was examined to gain further insights into the function of the different domains. Therefore, single domain, double domain and mutant constructs, which were previously reported in the literature, were cloned in a vector (p413) under the control of a galactose-inducible promoter (GAL1). The plasmids were transformed in the different ts-strains (*skp1-3, skp1-4, cdc35-1, sgt1-3, sgt1-5)* and rescue events were monitored after shifting the strains to the non-permissive temperature and onto medium containing galactose as the carbon source inducing the overexpression of the vector product.

Table 22: Characteristics of the Sgt1-related thermo-sensitive strains (Kitagawa et al., 1999, Connelly and Hieter, 1996, Dubacq et al., 2002).

ts-strain	Mutation	Cell cycle arrest	Rescue by Sgt1	Reported impairment
skp1-3	I172N	G_1/S	-	N/A
skp1-4	L146S	G_2	+	Kinetochore function
cdc35-1	L901H	N/A	+	Cyr1 regulation
sgt1-3	L31P, F99L, N213L	G_2	+	Skp1 binding, sectoring
sgt1-5	D220V, E364K	G_1	+	N/A

The thermo-sensitive strains *skp1-3* and *skp1-4* were discovered by Connelly and Hieter (Connelly and Hieter, 1996), both harbor a single point mutation, isoleucine at position 172 exchanged to asparagine and leucine at position 146 exchanged to serine, respectively. *skp1-4* displays chromosomal missegregation at non-permissive temperature and arrests in the G_2 phase of the cell cycle, whereas *skp1-3* arrests at G_1/S-phase transition. The thermo-sensitive phenotype of s*kp1-4* is associated with an impaired kinetochore function, while the arrest of s*kp1-3* suggest an distinct yet unknown function during cell cycle progression (Connelly and Hieter, 1996). *cdc35-1* carries a single point mutation in the adenylate cyclase Cyr1 replacing leucine at position 901 with a histidine residue (Dubacq et al., 2002). The mutation is located in the leucine-rich-repeat (LRR) of Cyr1 substituting one of the conserved leucine residues, thereby destabilizing the fold. The LRR-motif is the putative site of Sgt1 interaction (Dubacq et al., 2002, Stuttmann et al., 2008). The mutation alters also the responsiveness to regulatory stimulation by G proteins, like Ras2, and leads to an arrest in the G_1 phase at non-permissive temperatures (Dubacq et al., 2002, Suzuki et al., 1990, Sy and Tamai,

1986). *sgt1-3* and *sgt1-5* were generated during the initial discovery of Sgt1 (Kitagawa et al., 1999). Both strains express a *sgt1* mutant with a few point mutations (*sgt1-3*: L31P, F99L, N213I; *sgt1-5*: D220V, E364K). Regardless, the critical point mutation of *sgt1-3* is the substitution of leucine 31 to a proline residue leading to a conformational alteration of the TPR domain of Sgt1 impairing the binding to Skp1. *sgt1-3* displays chromosomal missegregation and arrests in the G_2 phase. (Kitagawa et al., 1999, Lingelbach and Kaplan, 2004, Bansal et al., 2004, Willhoft et al., 2017). In contrast, *sgt1-5* arrests in the G_1 phase at non-permissive temperature. The mutation of the glutamic acid at position 364 to a lysine is responsible for the thermo-sensitive growth (Kitagawa et al., 1999, Lingelbach and Kaplan, 2004).

Besides the wild-type domains of Sgt1, two mutants were tested for suppression of the thermo-sensitive growth, the dimerization incompetent H59A (histidine to alanine) TPR-mutant described by Willhoft *et al.* (Willhoft et al., 2017) and the Y190R/F201R (tyrosine to arginine/phenylalanine to arginine) CS-mutant which displays impaired Hsp90 interaction previously described by Zhang *et al.* (Zhang et al., 2008).

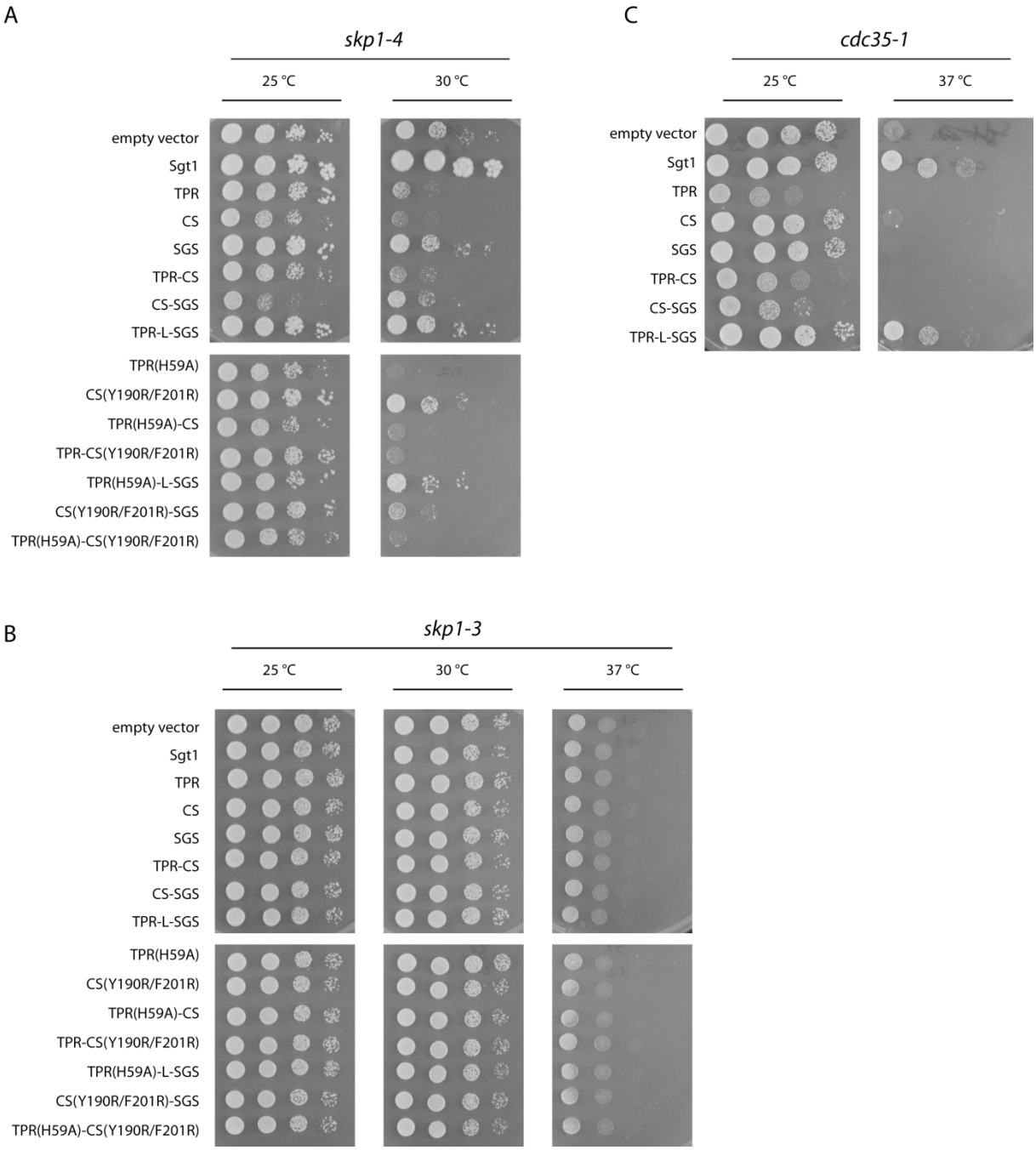

Figure 14: Analysis of Sgt1-related thermo-sensitive strains. (A) The ts-strain *skp1-4* was transformed with p413-GAL1 plasmids carrying the indicated domain construct of Sgt1 or empty vector. Ten-fold serial dilutions starting with an OD_{600} of 1 were spotted onto the respective SD medium containing 2% galactose as carbon source. Plates were incubated at indicated temperature for 72 h. Representative picture of three independent experiments. (B) Procedure according to A using the ts-strain *skp1-3*. (C) Same experiments as described for A using *cdc35-1* instead of *skp1-4*.

In the case of *skp1-4* (Fig 14A), overexpression of Sgt1 was able to reconstitute growth at 30 °C, in line with the initially discovery of Sgt1 as a suppressor of this phenotype (Kitagawa et al., 1999). Notably, the overexpression of Sgt1 increased the growth of *skp1-4* even at the permissive temperature of 25 °C as indicated by the increased colony size compared to the empty vector control. The tested domain constructs of Sgt1 could not restore growth compared to the control. In fact, overexpression of the TPR domain, CS domain and fusion constructs of these domains, except

TPR-L-SGS, decreased the growth rate. The essential SGS domain alone was not able to rescue or to interfere with the thermo-sensitive growth. Solely full length Sgt1 was able to rescue the phenotype indicating that a cooperative action of all three domains of Sgt1 is necessary to overcome the cell cycle stalling induced by the *skp1-4* mutant. The cell toxic effect of the overexpression of the TPR and CS domain is most likely due to the competition of the domain constructs for the binding to Skp1, in case of the TPR domain, and Hsp90 for the CS domain, respectively, suggesting that a complex comprised of Skp1, Sgt1 and Hsp90 is necessary to counteract the ts-phenotype. These findings coincide with previous studies which suggest that the functional kinetochore assembly relies on the interplay of Skp1, Sgt1 and Hsp90. As well as that, the *skp1-4* phenotype is due to an impairment of the kinetochore assembly (Connelly and Hieter, 1996, Lingelbach and Kaplan, 2004).

In accordance with the literature, the growth defect of *skp1-3* could not be rescued by Sgt1 overexpression or any tested construct (Fig 14B) (Kitagawa et al., 1999) suggesting that the cell cycle arrest induced by the *skp1-3* mutation displays a Sgt1-independent function.

The growth defect of *cdc35-1* at non-permissive temperatures could be rescued by overexpressing Sgt1 in agreement with Dubacq *et al.* (Dubacq et al., 2002) (Fig 14C). Interestingly, also the construct comprising the TPR domain fused to the SGS domain was able to restore growth at 37 °C indicating that the cooperative action of these two domains is sufficient to attenuate the growth defect induced by the mutant adenylate cyclase Cyr1/Cdc35. Notably, overexpression of the TPR domain decreased the growth rate at permissive temperature again most likely by blocking or competing for binding of a necessary interaction partner. Because the mutation L901H of Cyr1 is located in the putative binding motif for Sgt1's SGS domain (Dubacq et al., 2002), the overexpression of the SGS domain highly probable antagonizes the weakened interaction. The additionally required TPR domain might recruit certain interaction partner to restore full functionality of Cyr1 (Sy and Tamai, 1986, Suzuki et al., 1990).

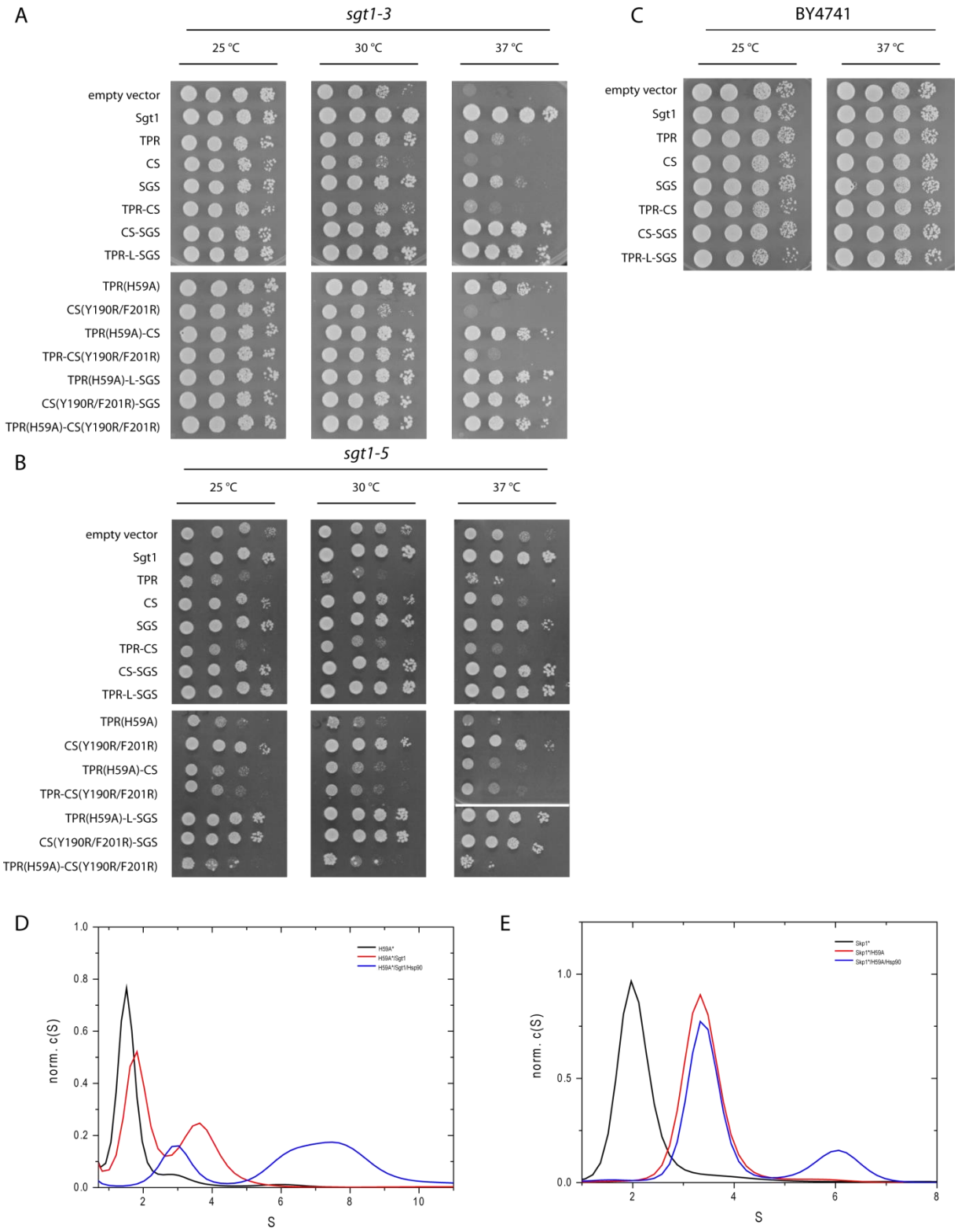

Figure 15: Analysis of thermo-sensitive Sgt1 strains. (A) The ts-strain *sgt1-3* was transformed with p413-GAL1 plasmids carrying the indicated domain construct of Sgt1 or empty vector. Ten-fold serial dilutions starting with an OD_{600} of 1 were spotted onto the respective SD medium containing 2% galactose as carbon source. Plates were incubated at the indicated temperature for 72 h. Representative picture of three independent experiments. (B) Same experimental set up as described in A, albeit the *sgt1-5* strain was used. (C) Experimental set up according to A using the wild-type strain BY4741. (D) Complex formation of H59A analyzed by analytical ultracentrifugation experiments (500 nM Atto488-labeled Sgt1-H59A, 5 µM Hsp90, 5 µM Sgt1). Normalized c(S) distributions were plotted against the apparent sedimentation coefficient S. (E) Analysis of complex formation of Skp1 by analytical ultracentrifugation sedimentation velocity experiments using 500 nM of the Atto488-labeled species (indicated by asterisk) and each other protein indicated at 5 µM. Normalized c(S) distributions were plotted against the apparent sedimentation coefficient S.

Expression of wild-type Sgt1 from the plasmid could, as expected, complement the chromosomal *sgt1-3* mutant allele (Fig 15A). The essential SGS domain and all derived constructs as well rescued the thermo-sensitive phenotype as anticipated since the SGS domain alone is sufficient to provide yeast viability and the overexpression of the constructs ensures the competitive advantage over the endogenous expressed mutant protein. The CS domain and derived mutants had no impact on the growth of *sgt1-3.* Interestingly, also the dimerization-incompetent TPR domain (TPR(H59A)) and fusion construct of this mutant could rescue *sgt1-3*. A possible explanation for this rescue event could be the restoration of the Sgt1-Skp1 interaction which is abrogated by the L31P mutation of *sgt1-3*. Even though H59A does not dimerize with itself or to a negligible degree only (Willhoft et al., 2017), the mutant could dimerize with wild-type Sgt1 as demonstrated by analytical ultracentrifugation (Fig 15D). The mutant TPR domain also interacted with Skp1 (Fig 15E) suggesting that TPR(H59A) supports *sgt1-3* interaction with Skp1, thereby restoring cell cycle progression. In contrast, overexpression of the wildtype TPR domain did not reconstitute *sgt1-3*'s viability at 37°C to the same extend as the mutant TPR(H59A) domain, which could be explained by an alternate binding affinity towards Skp1 and *sgt1-3,* either leading to a steric blocking or incomplete restoration of the Skp1-Sgt1 complex, respectively.

Alike *sgt1-3*, the overexpression of the essential SGS domain could bypass the growth defect of *sgt1-5* (Fig 15B). In the case of *sgt1-5*, the thermo-sensitivity is caused by the E364K mutation located in the SGS domain (Lingelbach and Kaplan, 2004). The same study suggested that the thermo-sensitivity of *sgt1-5* depends on an imbalance in the dwell time of an Hsp90-Sgt1-Skp1 complex. Noteworthy, the additional D220V mutation was reported to be necessary to alter the binding (Lingelbach and Kaplan, 2004). Again, as seen by *skp1-4* and *cdc35-1*, the overexpression of the TPR domain was toxic. Since the TPR domain mediates interaction with Skp1, the overexpression might alter the dwell time of the complex leading to a toxic dysregulation. The CS domain and derived mutants did not show any effect on the growth rate of *sgt1*-5. Notably, overexpression of any Sgt1 domain in a wild-type yeast strain did not cause any observable growth defect (Fig 15C).

In sum, the cooperative action of Sgt1's domains is necessary to overcome the thermo-sensitive phenotype of *skp1-4 and cdc35-1*. Since the SGS domain solely is capable to fulfill the essential *in vivo* function, it is not surprising, that overexpression of the SGS domain rescued the *sgt1* thermo-sensitive strains.

4.3. Conservation of the essential domain

Among the three domains of Sgt1, the essential SGS domain displays the highest degree of conservation (Fig 14). In human, two isoforms of Sgt1 exist, Sugt1B and the splicing variant Sugt1A (Niikura and Kitagawa, 2003). Sugt1A lacks residues 110-142 which are located at the very end of the TPR domain and partly reach into the linker region to the CS domain.

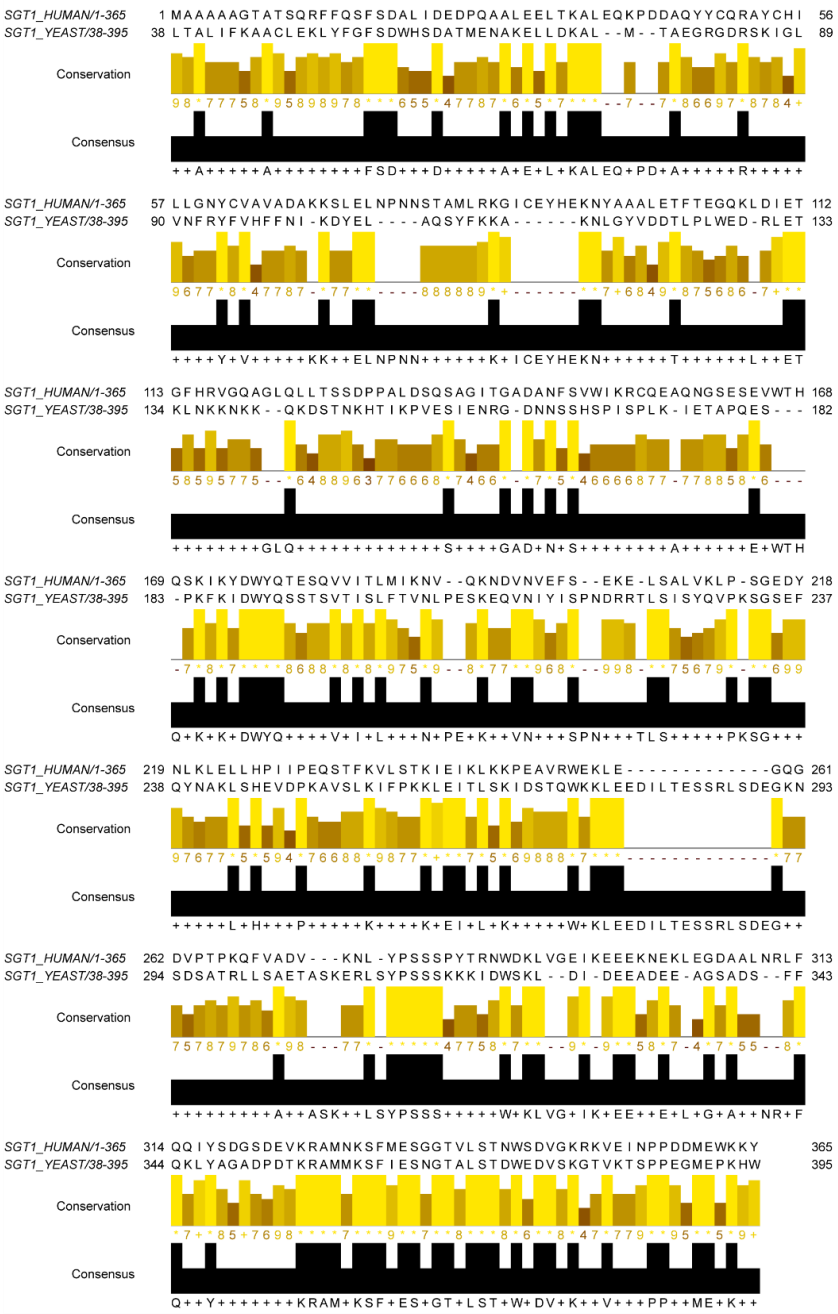

*Figure 16: Sequence alignment of yeast Sgt1 and human Sugt1.*The alignment was generated using Jalview depicting additional the degree of conservation and the consensus sequence. Domain boundaries of yeast Sgt1: TPR 1-144; CS 184-277; SGS 312-395; human Sugt1B: TPR 1-112; CS 169-258; SGS 276-365.

It was reported that the human homologue of Sgt1, Sugt1, was sufficient to support yeast viability in a *Δsgt1* strain (Kitagawa et al., 1999). To further dissect the functional conservation a plasmid shuffling on a single domain resolution was carried out (Fig 17).

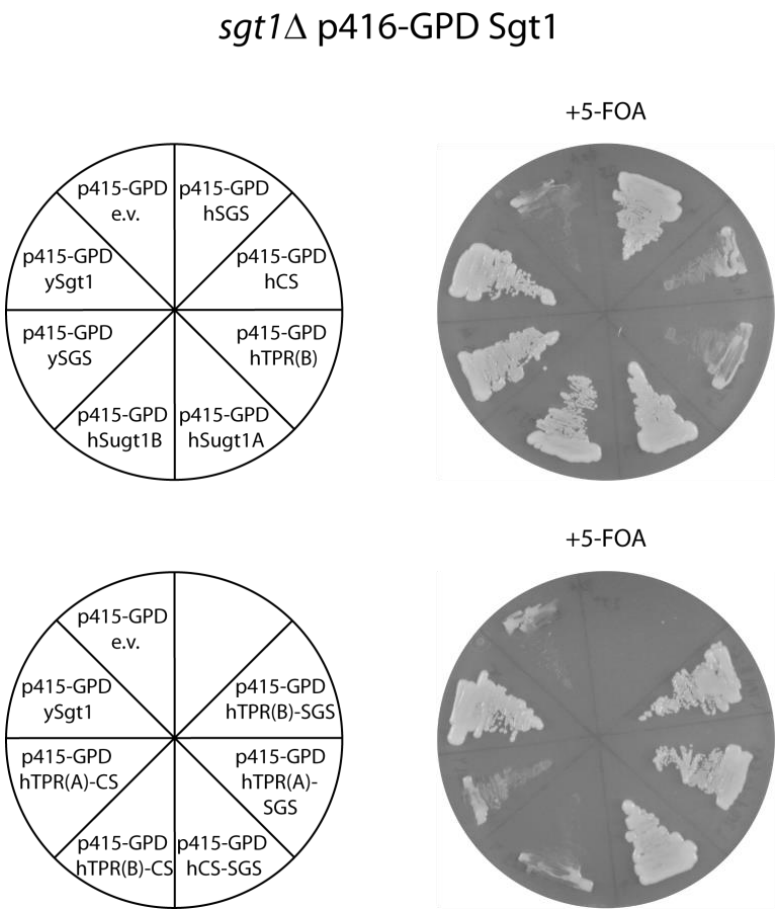

Figure 17: Substitution of yeast Sgt1 by its human homologue. Plasmid shuffling using the *sgt1Δ* [SGT1] strain transformed with p415-GPD plasmids containing Sgt1 domain constructs (y=yeast; h=human) or empty vector as indicated in the left panel. Strains were grown on SD media with 200 µg/mL 5-flourortic acid (right panel) at 30 °C for 3 days. Representative picture of three independent experiments.

Like the results obtained for the plasmid shuffling with yeast Sgt1 domains, the human domain constructs containing the SGS domain were able to provide yeast viability. Remarkably, the human SGS domain comprising residue 276-365 of the human Sugt1B could complement the lack of yeast Sgt1 indicating that not only the sequence but also the function is conserved from yeast to man.

4.4. Structure of the essential SGS domain

In recent studies, the crystal structure of the TPR domain of *S.cerevisiae* Sgt1 in complex with the BTB domain of Skp1 was revealed (Willhoft et al., 2017). Previously, the crystal structure of the *Arabidopsis thaliana* CS domain in complex with the NTD of Hsp90 was obtained (Zhang et al., 2008). Additionally, the NMR structure of the CS domain of the human homologue was solved (Lee et al., 2004b). However, structural information about the essential SGS domain is limited to a single NMR experiment and CD spectra indicating some helical propensity (Lee et al., 2004b). To gain further insight into the structure of the SGS domain NMR experiments using the yeast SGS domain were performed (Fig 18).

A

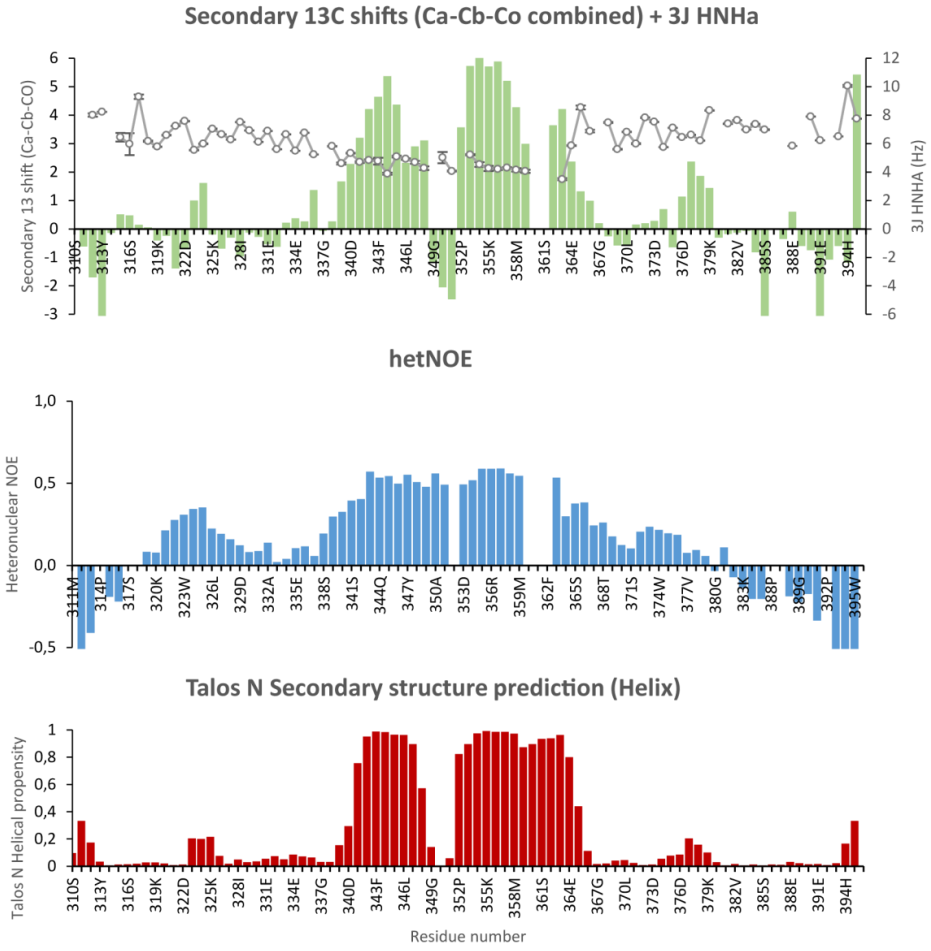

B

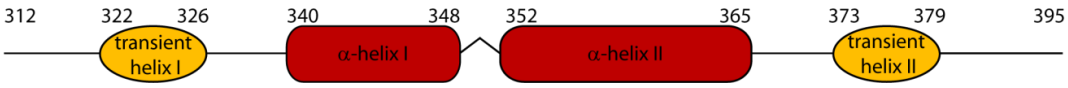

Figure 18: Structure of the essential SGS domain. (A) Top panel: Secondary ^{13}C chemical shifts (left axis) and $^{3}J_{HNHA}$ coupling (right axis) are shown for the SGS domain. High positive ^{13}C chemical shift values indicate helical propensity. Additionally, $^{3}J_{HNHA}$ coupling constants around 4.8 indicate α-helices. Middle panel: Heteronuclear NOEs are depicted for the SGS domain. hetNOEs above 0.7 indicate a rigid structural element. Bottom panel: Talos-N secondary structure prediction for helical propensities was applied to the SGS domain. NMR experiments were performed by Abraham Lopez at Michael Sattlers chair. (B) Schematic model of the structure of the SGS domain of Sgt1. Numbers indicate residue position according to the numbering of yeast Sgt1.

The backbone of the SGS domain could be assigned to 96 % of the non-proline residues. The secondary ^{13}C chemical shifts, $^{3}J_{HNHA}$ coupling constants and the heteronuclear NOEs suggest a stable helical structure between residue 340 and 365 (residues numbers according to the yeast full length Sgt1) (Fig 18A). Residues 349 to 351 form a putative turn dividing the helical propensity into two α-helices (helix I: 340-348; helix II: 352-365). Additionally, there might be two transient helices present, one ranging from residues 322 to 326 and the other from 373 to 379. Noteworthy, the residue serine 361 in helix two could not be assigned due to severe line broadening indicating conformational dynamics at this position. This serine was previously reported to be the target of phosphorylation and the phospho-mimic mutant S361D is lethal (Bansal et al., 2009a). It is tempting to speculate about a conformational switch regulated by phosphorylation. Figure 18B presents the current model of the domain architecture of the essential SGS domain as determined by NMR experiments.

4.5. Determination of the minimal structural element carrying the essential *in vivo* function

Based on the NMR results the SGS domain was further broken up to determine the structural element necessary for yeast viability. A set of truncation mutants of Sgt1 and point mutations disturbing structural features of the SGS domain was tested for yeast viability using plasmid shuffling (Fig 19 and Fig 20).

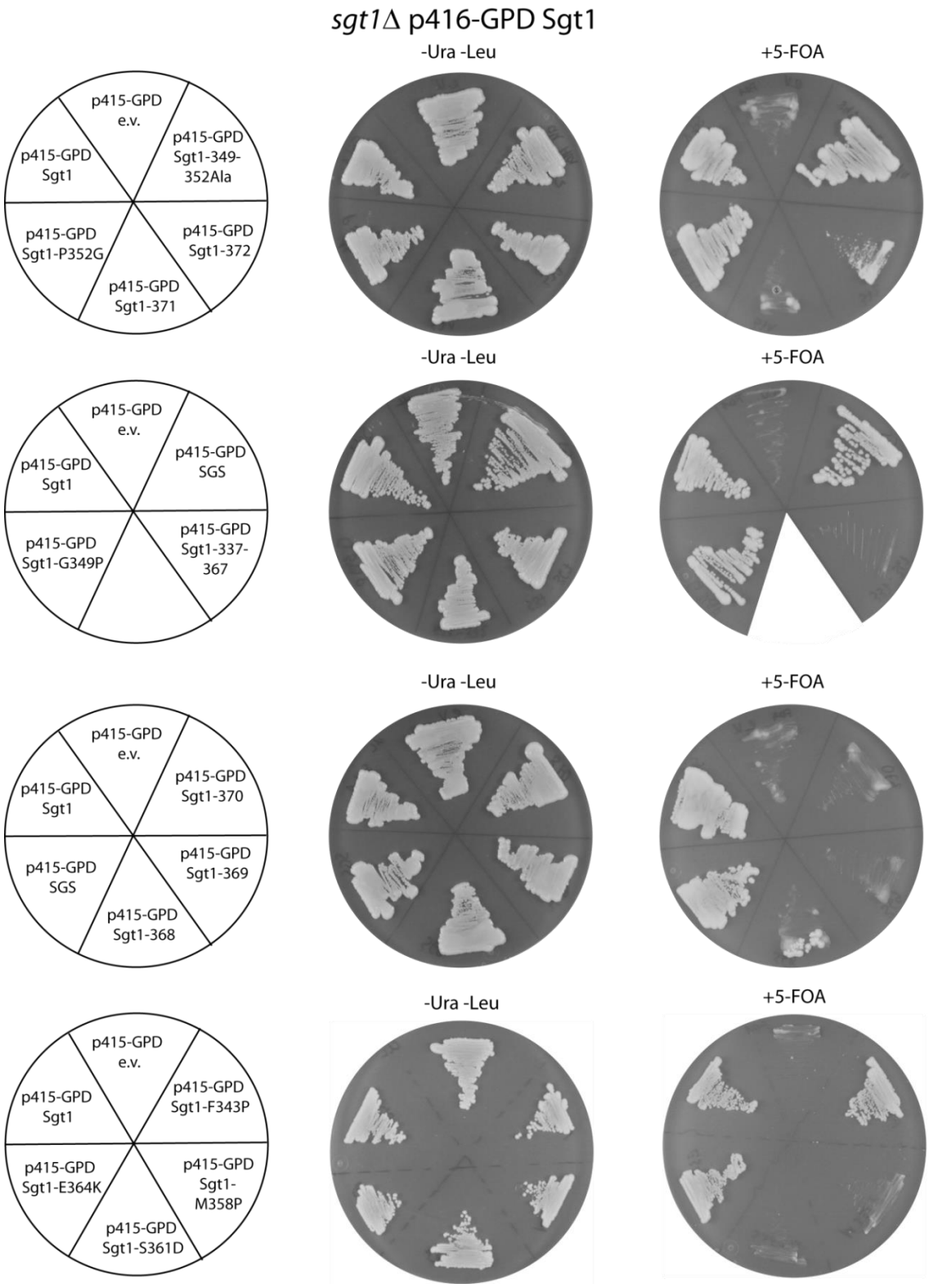

Figure 19: Determination of the essential structural element. Plasmid shuffling was carried out using the *sgt1Δ* [SGT1] strain transformed with p415-GPD plasmids containing Sgt1 domain constructs or empty vector as indicated in the left panel. Strains were grown on SD media without (middle panel) or with 200 µg/mL 5-flourortic acid (right panel) at 30 °C for 3 days.

The plasmid shuffling showed that truncations of the C-terminal region still supported viability until residue 372. Further C-terminal truncation of the SGS domain led to cell death. Even the Sgt1-372 mutant displayed a severe growth defect. However, the putative transient helix spanning from

residue 373 to 379 and the following unstructured tail are dispensable for the essential function of Sgt1 (Fig 19).

Point mutations addressing the structural integrity of the helix I-turn-helix II motif showed different behavior (Fig 19). Mutations in the turn region between the two stable helices disrupting their potential rigid arrangement like the exchange of glycine 349 to proline or the substitution of proline 352 to glycine did not show any growth defect indicating that a specific fixed conformational arrangement of the two helices is not necessary for the function. Additionally, substitution of all amino acids involved in the turn to alanine also showed no effect further suggesting that the conformational arrangement of the two helices should be flexible. Disruption of the architecture of helix I by exchanging phenylalanine 343 to proline also had no effect on yeast growth. In contrast, breaking helix II by the substitution of methionine 358 to proline was lethal indicating that the structural integrity is crucial. Notably, as the lethal phospho-mimic S361D might also break the architecture of helix II like the M358P mutation, it is tempting to speculate that the dynamic of the putative conformational switch is essential.

Since the SGS domain alone was able to provide the essential Sgt1 function *in vivo* and C-terminal truncation of Sgt1's SGS domain were tolerated until residue 372, further minimal constructs consisting only of structural parts of the SGS domain were tested for yeast viability. The construct 337-372, which only comprises the two stable helices, was not able to fulfill the essential function. The addition of the first putative helix (construct 321-372) could also not restore yeast viability (Fig 17). Surprisingly, mutants consisting of the truncated SGS domain and either CS or TPR domain were also lethal indicating that upon loss of the C-terminal 23 amino acids both the CS and TPR domain are necessary to provide the essential function (Fig 20). Interestingly, the Sgt1-372 mutant displayed thermo-sensitive growth leading to cell death at 37 °C (Fig 20). The thermo-sensitivity might be due to a lowered structural stability of the essential helix II, if the C-terminal extension is missing.

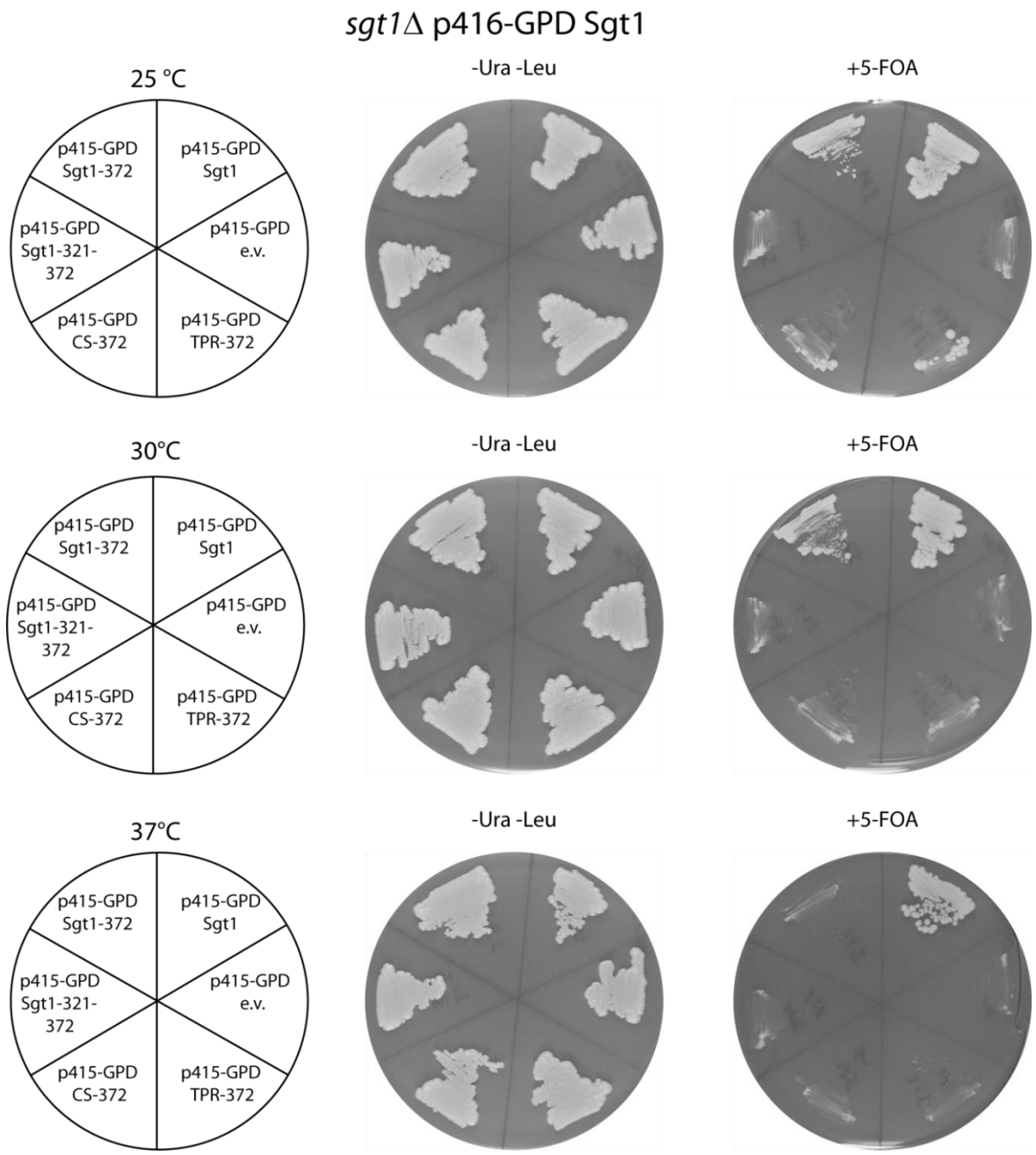

Figure 20: C-terminal truncated Sgt1 requires the TPR and CS domain for yeast viability. Plasmid shuffling was carried out using the *sgt1Δ* [SGT1] strain transformed with p415-GPD plasmids containing Sgt1 domain constructs or empty vector as indicated in the left panel. Strains were grown on SD media without (middle panel) or with 200 µg/mL 5-flourortic acid (right panel) at 25 °C (top), 30 °C (middle) or 37 °C (bottom) for 3 days.

Taken together, further dissection of the SGS domain *in vivo* demonstrated the importance of the helical structural features determined by NMR. The most vulnerable element seems to be the stable helix II, since structural perturbation led to cell death. Notably, C-terminal truncation was tolerable up to residue 372, but only if the full-length N-terminal part of Sgt1 was present. In figure 21 selected *sgt1* mutants are schematically depicted.

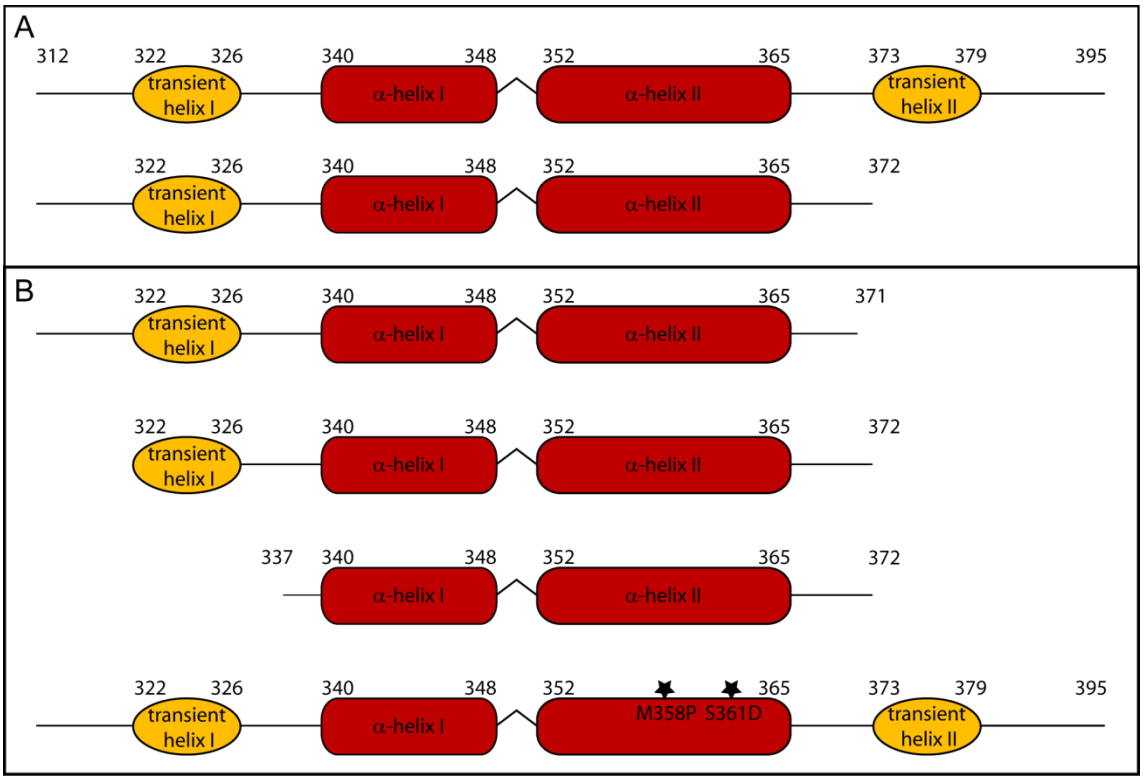

Figure 21: Schematic model of selected sgt1 mutants. Structural features of the essential SGS domain are depicted. Numbers indicate residue position according to the numbering of yeast Sgt1. The lack of an N-terminal number indicates full-length mutants (A) Viable mutants: SGS domain, $Sgt1^{1-372}$ (B) Lethal mutants: $Sgt1^{1-371}$ (and further truncation), $Sgt1^{321-372}$, $Sgt1^{337-372}$, Sgt1 point mutants S361D and M358P.

4.6. Dissection of the interaction between Sgt1 and Hsp90

Early work on Sgt1 suggested that the TPR domain of Sgt1 mediates the interaction with Hsp90 (Bansal et al., 2004). NMR studies and finally a crystal structure established that the CS domain of Sgt1 interacts with the NTD of Hsp90 (Lee et al., 2004b, Zhang et al., 2008). To extend the knowledge about the interaction of Sgt1 and Hsp90, sedimentation velocity experiments with recombinant proteins were set up.

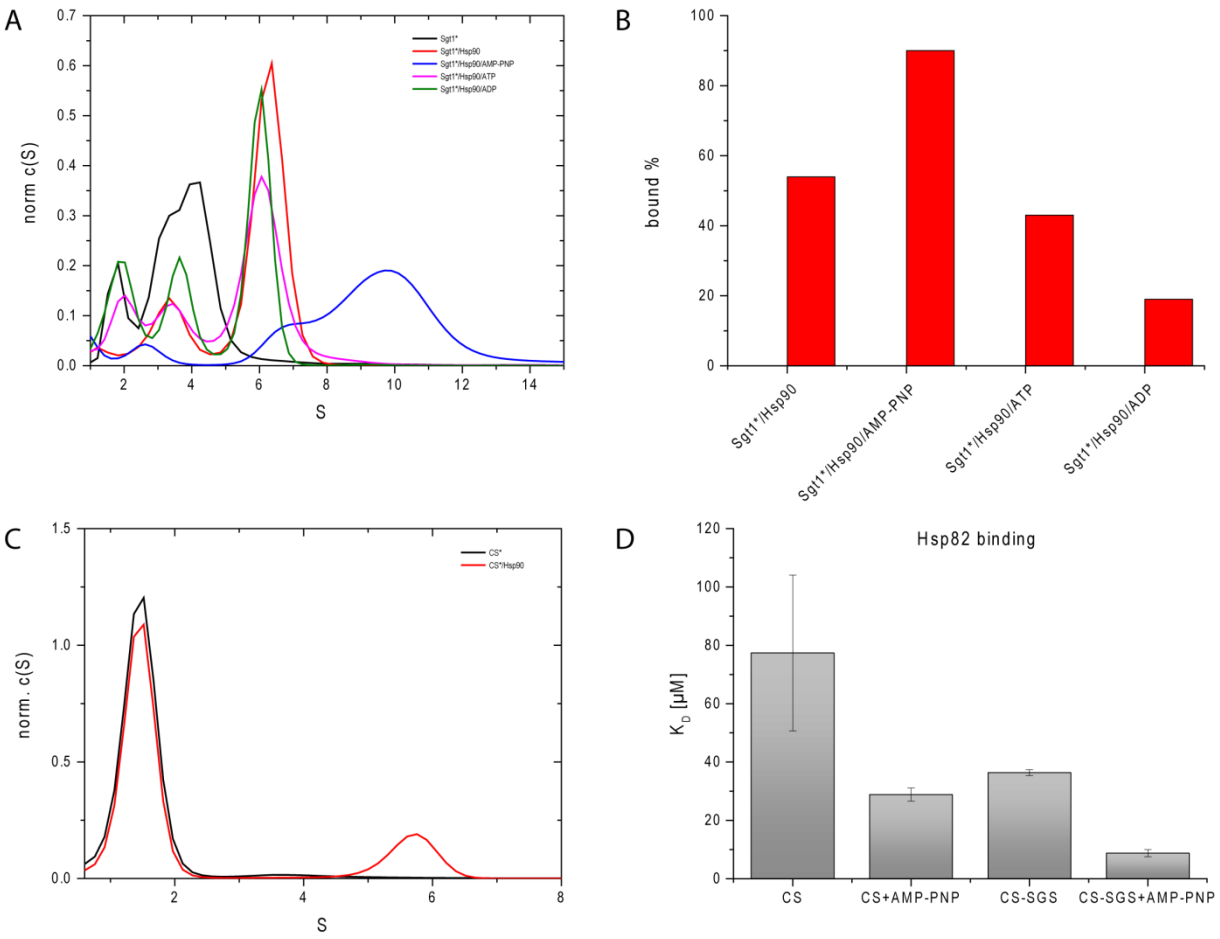

Figure 22: Interaction of Sgt1 with Hsp90. (A) Analysis of complex formation of Sgt1 with Hsp90 by analytical ultracentrifugation sedimentation velocity (AUC) experiments using 500 nM of the Atto488-labeled species (indicated by asterisk) and Hsp90 at 5 µM. Additional indicated nucleotides were present at 2 mM. Normalized c(S) distributions were plotted against the apparent sedimentation coefficient S. (B) Determination of bound fraction of Sgt1 to Hsp90 by integrative analysis of free Sgt1 species of (A) at the different nucleotide states. (C) Binding of the single CS-domain of Sgt1 to Hsp90 analyzed by AUC (500 nM Atto488-labeled CS, 5 µM Hsp90). Normalized c(S) distributions were plotted against the apparent sedimentation coefficient S. (D) K_D of indicated Sgt1 domains to Hsp90 with or without 2 mM AMP-PNP present. Affinity values were determined by fluorescence anisotropy experiments using 500 nM of the Atto488-labeled indicated Sgt1 domain and a titration of Hsp90 up to 50 µM. Means with error bars for three independent experiments are shown.

AUC experiments were performed monitoring the sedimentation of a fluorescently labeled protein. To this end, in Sgt1 and its domain constructs prior to the experiments a serine residue was mutated to cysteine to introduce the fluorescence label via thiol-maleimide chemistry (Sgt1-S233C, CS-S233C, TPR-S109C, SGS-S312C). Sgt1 alone displayed peaks at around 2 S and around 4 S representing the monomer and dimer species, respectively (Fig 22A, black curve). The fitting algorithm resulted in variations in the distributions of monomers and dimers; sometimes only a single peak for Sgt1 was detected. Upon addition of Hsp90 peak shifting towards Svedberg values around 6 indicated the complex formation of Sgt1 with Hsp90 (Fig 22A). The interaction was also probed in the presence of different nucleotides to address conformation-specific binding to Hsp90. By comparison of the integral of the peak of free, labeled Sgt1, bound fractions were determined displaying a clear preference of Sgt1 binding to Hsp90 in the presence of the non-hydrolysable ATP analogue adenylyl-

imidodiphosphate (AMP-PNP) (Fig 22B). Contrary to previously results which suggested that the apo form of Hsp90 is favored by Sgt1 (Catlett and Kaplan, 2006). However, in the presence of AMP-PNP, which induces the closed conformation of Hsp90, peak broadening occurred. The broadening might not only be due to increased Sgt1 binding but could also display different conformational binding modes of Sgt1 to Hsp90, which would vary the overall shape of the complex leading ultimately to different sedimentation profiles (Fig 22A, blue curve). The concept that Sgt1 binds to different interfaces of Hsp90 was previously suggested by Eckl *et al.* (Eckl et al., 2014).

In line with the literature, the labeled single domain construct of the CS domain was sufficient to bind to Hsp90 as probed by AUC (Fig 22C). To further validate the preference of Sgt1 towards the AMP-PNP bound form of Hsp90, fluorescence anisotropy experiments were carried out and the K_D of the CS domain and a CS-SGS construct for Hsp90 were determined (Fig 22D). The CS domain alone showed a weak interaction with Hsp90 (K_D ≈ 78 µM). However, the presence of AMP-PNP significantly increased the affinity by more than two-fold (K_D ≈ 29 µM). Notably, the CS-SGS construct consisting of the CS domain, the CS-SGS-interdomain linker and the SGS domain exhibited also an increased affinity (K_D ≈ 36 µM) compared to the CS domain alone. The addition of AMP-PNP in this case further increased the binding (K_D ≈ 8 µM), nearly about 10-fold compared to the CS domain alone without AMP-PNP.

To confirm the NTD of Hsp90 as the interaction site for Sgt1, complex formation of Sgt1 with Hsp90 domain constructs was analyzed by AUC (Fig 23A). As expected, the deletion of the C-terminal MEEVD motif of Hsp90 did not disrupt binding, since Sgt1 does not utilizes the TPR domain for binding to this motif. Interestingly, Sgt1 was able to form complexes with constructs consisting of the NTD and MD (shift from 4 S to 5 S since the NM-construct occurs as monomer) as well as MD and CTD, indicating that at least a further domain of Hsp90 provides a substantial binding site for Sgt1. In agreement with previous suggestions (Eckl et al., 2014), the extended binding interface might be explained by a second interaction mode. Because interactors, which bind to the NTD of Hsp90, might modify the N-N-closing kinetics of Hsp90, Förster resonance energy transfer (FRET) experiments were carried out using a well described set up, in which Hsp90 protomers are fluorescently labeled with either Atto488 or Atto550 at position 61 (Hessling et al., 2009). N-terminal dimerization of Hsp90 was induced by AMP-PNP or adenosine 5'-(3-thiotriphosphate) (ATPγS), respectively. The kinetic in the presence of Sgt1 and without Sgt1 showed no significant change in closing for the ATPγS-induced closing and only a hardly significant decrease in the closing kinetic in case of AMP-PNP-induced N-N-closing (Fig 23B+C).

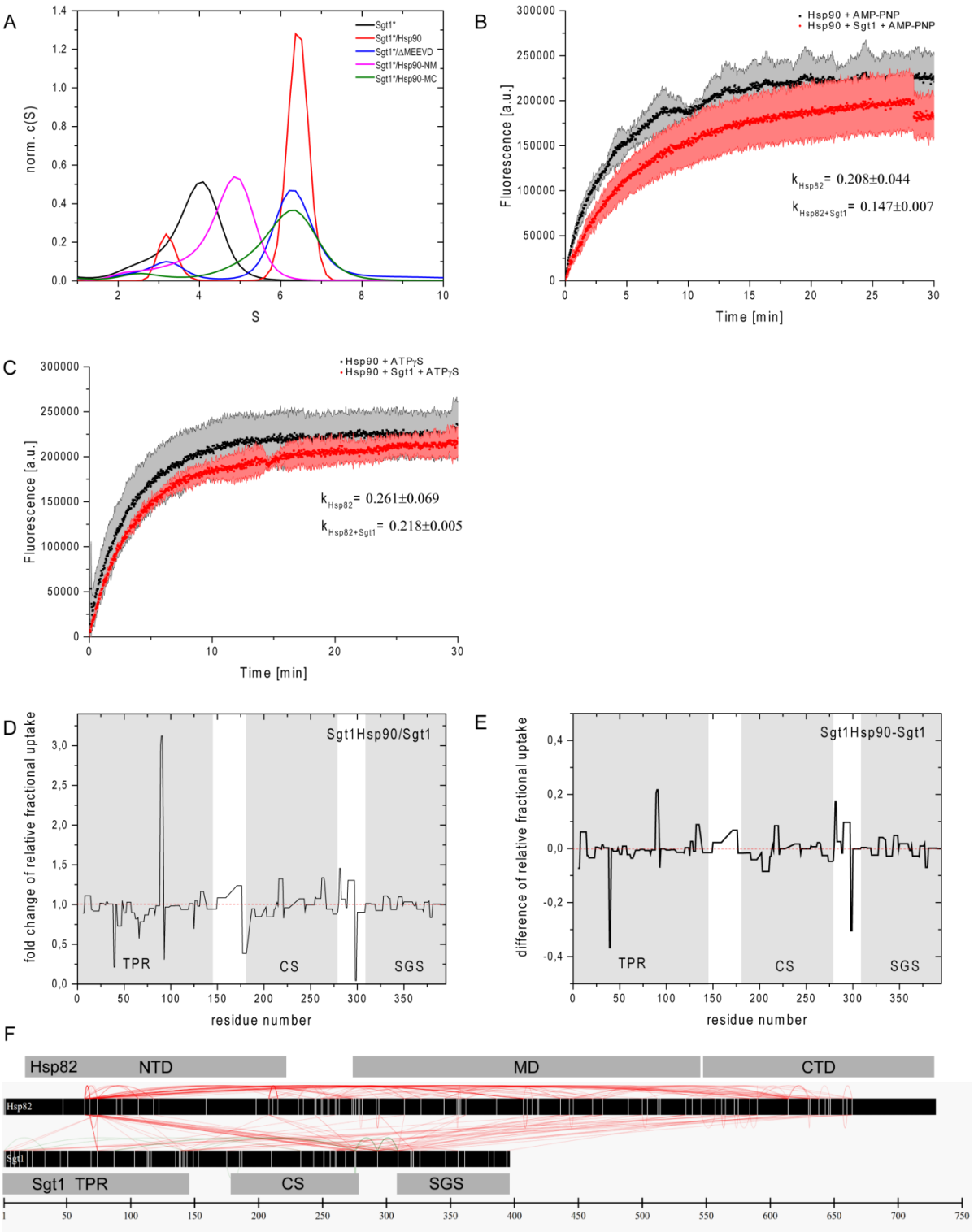

Figure 23: Impact of the binding between Sgt1 and Hsp90. (A) Complex formation of Sgt1 with Hsp90 domain constructs using AUC. Atto488-labeld Sgt1 was used at 500 nM, while all indicated other proteins had a concentration of 5 µM. Normalized c(S) distributions were plotted against the apparent sedimentation coefficient S. (B) Determination of Hsp90 closing kinetics by FRET experiments using Hsp82 fluorescently labeled at position 61 with Atto488 as donor and Atto550 as acceptor dye. (Hessling et al., 2009). Closing of Hsp82 was induced by the addition of 2 mM AMP-PNP in the presence (red) or absence (black) of 5 µM Sgt1 showing means and error areas of triplicates. (C) Experimental set up as described for (B), but closing was induced by adding 2 mM ATPγS. (D) Fold change of the relative fractional deuterium uptake +(E) Difference in H/D exchange of Sgt1 in complex with Hsp90 and Sgt1 alone at time point 600 s plotted against the residue number of Sgt1. Grey areas indicate the position of the three Sgt1 domains. (F) DSG-crosslinks between Sgt1 and Hsp82. Sgt1 (15 µM) was crosslinked with Hsp82 (50 µM) utilizing 3 mM disuccinimidyl glutarate. Inter- (red) and intra- (green) molecular crosslinked pepetides were analyzed by mass spectrometry. Bottom axis indicates residue numbers of the proteins. Gray boxes display the indicated domains of Hsp82 or Sgt1, respectively.

The impact of Hsp90 binding to Sgt1 was further investigated using hydrogen/deuterium exchange coupled to mass spectrometry. The relative fractional uptake of Sgt1 alone and Sgt1 in complex with Hsp90 was monitored (Fig 23D+E). The segment ranging from residue 185 to 215 showed higher uptake in case of sole Sgt1 indicating a decreased accessibility of these residues in the Hsp90-Sgt1 complex most likely due to direct interaction. That this segment might be the interaction site of Sgt1 with Hsp90 is supported by previously described key residues for Hsp90 interaction, tyrosine 190 and phenylalanine 201 which reside in this area (Zhang et al., 2008). The interdomain linker regions of Sgt1 displayed both protected and deprotected regions if in complex with Hsp90. This might indicate an overall conformational rearrangement of the three Sgt1 domains upon Hsp90 binding. Additional alterations in deuterium uptake could be observed also in the TPR and only slightly in the SGS domain. However, both domains were not reported to be involved in Hsp90 binding and it was demonstrated that both are dispensable for binding. Yet, the alteration might be due to overall domain rearrangements. Moreover, binding to Hsp90 could shift the oligomeric state of Sgt1 and with that changes in the TPR domain would be expected. Since, the TPR domain is the site of dimerization. The overall variation of H/D exchange rates throughout Sgt1 could indicate conformational rearrangements of the domains as well as within the domains to provide binding. Furthermore, this pattern might be due to different binding modes of Sgt1 (Eckl et al., 2014) which overlay in the measurement also explaining the in total low H/D uptake differences.

The complex formation of Sgt1 with Hsp90 was additionally probed by disuccinimidyl glutarate (DSG) crosslink coupled to mass spectrometry. Disuccinimidyl glutarate is used to crosslink primary amines like ε-amino group of lysines and the N-terminus. The crosslink profile of Sgt1 with Hsp90 is shown in figure 23F. The red connections display inter-protein crosslinks, while the green ones indicate intra-protein crosslinks. The crosslink profile revealed three crosslink hotspots of Sgt1. Namely, the lysine residue 73, which resides in the TPR domain and shows extensive crosslinks to the NTD of Hsp90. The lysine residues K137/138/140/141/143, which are located at the very end of the TPR domain, display interactions all over Hsp90. The crosslinking site of Sgt1 displaying the most crosslinks consists of K274/275/292/308. The two latter ones reside in the interdomain linker between the CS domain and the SGS domain, while the first two are located at the end of the CS domain. From this hotspot crosslinks to the MD, CTD and NTD of Hsp90 occurred. Notably, the lysine residues K54/58/64 of Hsp90's NTD were the main location of crosslink events showing connections to K73 and the K274/275/292/308 hotspot of Sgt1. However, crosslinks between Sgt1 and Hsp90 occurred all over both proteins including every domain. The spacer length of 7.7 Å for DSG might be one explanation for the appearance of crosslinks between all domains, even those which should not directly participate in binding like the CTD of Hsp90 or TPR of Sgt1. However, the extensive crosslinking between the CS-SGS-interdomain linker and Hsp90 fits to the increased binding affinity of the CS-SGS

construct compared to the CS domain alone as determined by fluorescence anisotropy implying a direct involvement of this region in Hsp90 binding.

In sum, the interaction studies between Sgt1 and Hsp90 revealed, contrary to previous publications, that Sgt1 favors the AMP-PNP-induced close state of Hsp90. Additionally, an extended binding interface between Sgt1 and Hsp90 was shown including the CS-SGS-interdomain linker of Sgt1 and the MD of Hsp90 in binding.

4.7. Integration of Sgt1 into the Hsp90 co-chaperone cycle

The Hsp90 chaperone cycle is tuned by co-chaperones; Some acting sequential, other concomitant to ensure client maturation (Schopf et al., 2017). Sgt1 can interact with Hsp90 in any nucleotide state. However, it displays species-specific preferences (Catlett and Kaplan, 2006, Lee et al., 2004b, Eckl et al., 2014). Even though Sgt1 was suggested to be an adaptor protein linking Skp1 and its putative LRR-motif containing clients to the Hsp90 machinery (Stuttmann et al., 2008, Bansal et al., 2004), Sgt1 was also reported to play a comprehensive role in the Hsp90 cycle affecting client maturation in general (Sahasrabudhe et al., 2017). To further address the integration of Sgt1 within the Hsp90 co-chaperone cycle, a synthetic genetic array analysis (SGA) (Tong and Boone, 2006) aiming to reveal genetic interactions between Sgt1 and other Hsp90 co-chaperones was carried out. Genetic interaction analyses score the fitness of a combination of two mutations in comparison to the single mutants, in this case the down regulation of Sgt1 combined with an additional depletion of another co-chaperone. Genetic interactions allow to draw conclusions about the buffering or impinging effects of the tested gene products (Tong and Boone, 2006). Since Sgt1 is essential for yeast viability, a strain harboring SGT1 under the control of a doxycycline-repressible promoter system was constructed (Y8205 tetO7-SGT1) (Mnaimneh et al., 2004). Upon addition of doxycycline to the medium, SGT1 expression was down-regulated leading to the depletion of the protein (Fig 24B). The double mutant strains were derived from Y8205 tetO7-SGT1 and combined with a gene knock-out in the case of the non-essential co-chaperones or for the essential ones, decreased abundance by mRNA perturbation (DAmP) (Breslow et al., 2008). The fitness of the single and double mutant strains was assessed by serial dilution spot assays onto medium with and without doxycycline (Fig 24A).

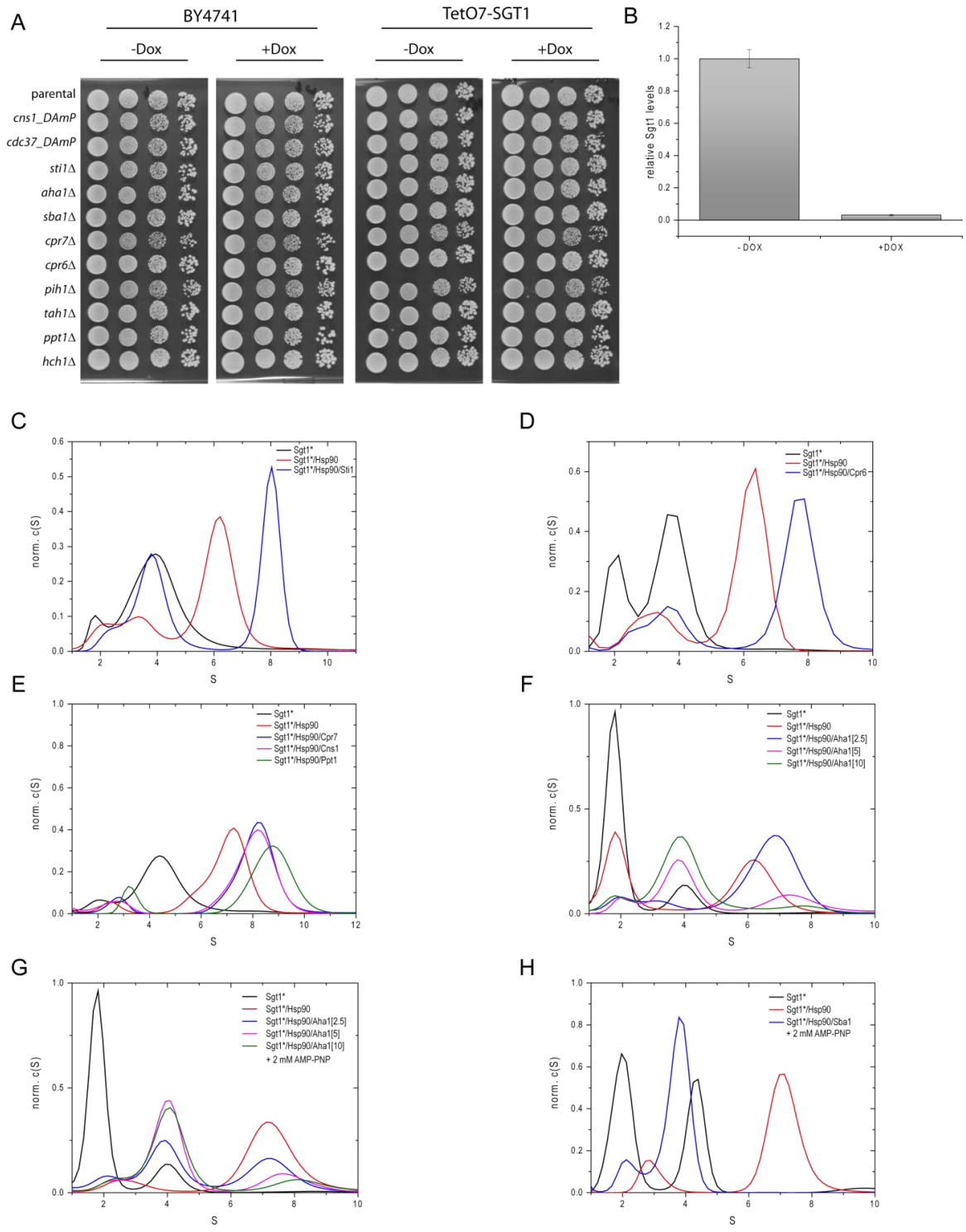

Figure 24: Sgt1 in the Hsp90 co-chaperone machinery. (A) Synthetic genetic array analysis using TetO7-SGT1 in the Y8205 background. Double mutant strains harboring SGT1 under the control of the doxycycline repressible promoter (TetO7)were generated according to (Tong and Boone, 2006). The additional gene deletion or depletion by perturbation of the 3'UTR (DAmP) is indicated on the left. Single depletion mutants (left panel) and double depletion mutants (right panel) were spotted onto YPD plates with or without 10 µg/mL doxycycline as indicated. Photos were taken after three days of incubation at 30 °C. Representative picture of three independent experiments. (B) Densiometric analysis of Sgt1 levels from Westernblots from TetO7-SGT1 grown in presence (+DOX) or absence (-DOX) of 10 µg/mL doxycycline. Sgt1 levels were detected with a polyclonal antibody against Sgt1 and normalized to GAPDH levels. Graph displays the mean of three independent experiments (C)-(H) Analysis of complex formation of Sgt1 with Hsp90 and additional co-chaperones by AUC. Atto488-labeled Sgt1 was used at 500 nM, while all other indicated proteins had a concentration of 5 µM, if not otherwise indicated. The nucleotide analogue AMP-PNP was supplemented at 2 mM if indicated. Normalized c(S) distributions were plotted against the apparent sedimentation coefficient S.

The comparison of the single mutants with the double mutants showed no alteration in fitness. The strains harboring the CPR7 or PIH1 knock-out exhibited reduced growth rates as previously reported (Duina et al., 1996, Paci et al., 2012, Sahasrabudhe et al., 2017). The combination of Sgt1 downregulation and additional co-chaperone depletions did not display any genetic interaction under standard growth conditions. The lack of genetic interaction between Sgt1 and other Hsp90 co-chaperones suggests no functional overlap or synergistic action important for cell viability. Noteworthy, Johnson and colleagues described dosage growth defects for a thermo-sensitive *sgt1* mutant K360E, if certain Hsp90 co-chaperones were overexpressed (Johnson et al., 2014). However, the growth defects could be tracked back to competitive binding to Hsp90 between the tested co-chaperones and the *sgt1* mutant disrupting the Sgt1-Hsp90 axis (Johnson et al., 2014, Flom et al., 2012).

Regardless missing genetic interactions between Sgt1 and other Hsp90 co-chaperones, cooperative action of the co-chaperone machinery might be present. To analyze synergies or competition with other co-chaperones during the Hsp90 cycle, *in vitro* complex formation was probed using analytical ultracentrifugation (Fig 24C-H). Sedimentation velocity experiments monitoring the sedimentation of fluorescently labeled Sgt1 were carried out. Sgt1 alone displayed peaks at around 2 S and around 4 S representing the monomer and dimer species, respectively. Interaction of Sgt1 with Hsp90 was observed by the shifting of the peak to around 6 S. If the non-hydrolysable ATP analogue AMP-PNP was present the Sgt1-Hsp90 complex shifted to higher Svedberg values due to the nucleotide-induced change of the Hsp90 conformation (Lorenz et al., 2014). The common Hsp90 co-chaperone cycle starts with the open conformation of Hsp90 and the client transfer facilitated by Sti1 (Biebl and Buchner, 2019). At this step of the cycle Sgt1 could join as indicated by the additional shift of the Sgt1-Hsp90 complex to 8.5 S (Fig 24C). Even though a trimeric complex between Sgt1-Hsp90-Sti1 was possible, the increased signal at around 4 S suggested that Sti1 disrupts binding of Sgt1 to Hsp90 to some degree most likely due to steric hindrance. Sti1 binds to the MEEVD motif of the CTD of Hsp90, however additional contacts to the MD of Hsp90 were reported (Schmid et al., 2012). These contacts might overlap with Sgt1's abovementioned extended interaction site despite its reported binding to the NTD (Zhang et al., 2008). Other TPR-containing co-chaperone like Cpr6, Cpr7 and Ppt1, which bind to the MEEVD motif, did not interfere with Sgt1 binding (Fig 24D+E). In contrast, the addition of Aha1, which binds to the MD and NTD of Hsp90 (Meyer et al., 2004), abolished Sgt1 binding in a concentration-dependent manner indicating overlapping binding site of these two co-chaperones. Remarkably, low concentrations of Aha1 seem to trigger the formation of the trimeric Sgt1-Hsp90-Aha1 complex in the absence of nucleotides (Fig 24F). Interestingly, in the presence of AMP-PNP this effect could not be observed. However, trimeric complex formation was also observed. Notably, above a certain concentration of Aha1 no more competition with Sgt1 for binding was noticed (Fig

24G). This could be an indication that Sgt1 has an additional conformation-specific interaction sites as suggested by Eckl *et al.* (Eckl et al., 2014). The late stage acting co-chaperone Sba1/p23 only binds to Hsp90 in the closed state mediated by its CS domain (Ali et al., 2006). Despite Sba1 and Sgt1 utilizing their CS domain for Hsp90 interaction, different binding site has been observed (Zhang et al., 2008). Nevertheless, addition of Sba1 in the presence of AMP-PNP, which induces the closed state of Hsp90, disrupted the Sgt1-Hsp90 complex (Fig 24H). This is in line with the hypothesis that Sgt1 might interact with a different Hsp90 interface in the closed state (Eckl et al., 2014) while the findings by Zhang *et al.* (Zhang et al., 2008) represent the binding to the open conformation of Hsp90.

Table 23: Summary of Sgt1's interplay with other co-chaperones.

	Sti1	**Cpr6**	**Cpr7**	**Cns1**	**Ppt1**	**Aha1**	**Sba1**	**Hch1**	**Pih1**	**Tah1**	**Cdc37**
Genetic interaction	-	-	-	-	-	-	-	-	-	-	-
Trimeric complex formation	+	+	+	+	+	+	-	N/A	N/A	N/A	N/A
Competitive binding to Hsp90	+	-	-	-	-	+	+	N/A	N/A	N/A	N/A

Taken together, Sgt1 is able to participate throughout the Hsp90 co-chaperone cycle forming trimeric complexes except for the late stage acting Sba1, which competes for binding to Hsp90. Yet, this conformational state of Hsp90 is favored by Sgt1 tempting to speculate about a Sba1-alike function within the cycle.

4.8. Sgt1 interacts with the Hsp40-Hsp70 system

Earlier studies demonstrated that Sgt1 can not only interact with the Hsp90 system but also with Hsp70 (Noel et al., 2007, Spiechowicz et al., 2007). Interestingly, a Sgt1 construct lacking the C-terminal SGS domain was not able to interact with Hsp70, which in turn led to the conclusion that the SGS domain mediates the Hsp70 interaction (Spiechowicz et al., 2007). To gain further insights into the interaction of Hsp70 and Sgt1, AUC experiments with recombinant purified proteins were carried out monitoring the fluorescently labeled species (Fig 25A-C).

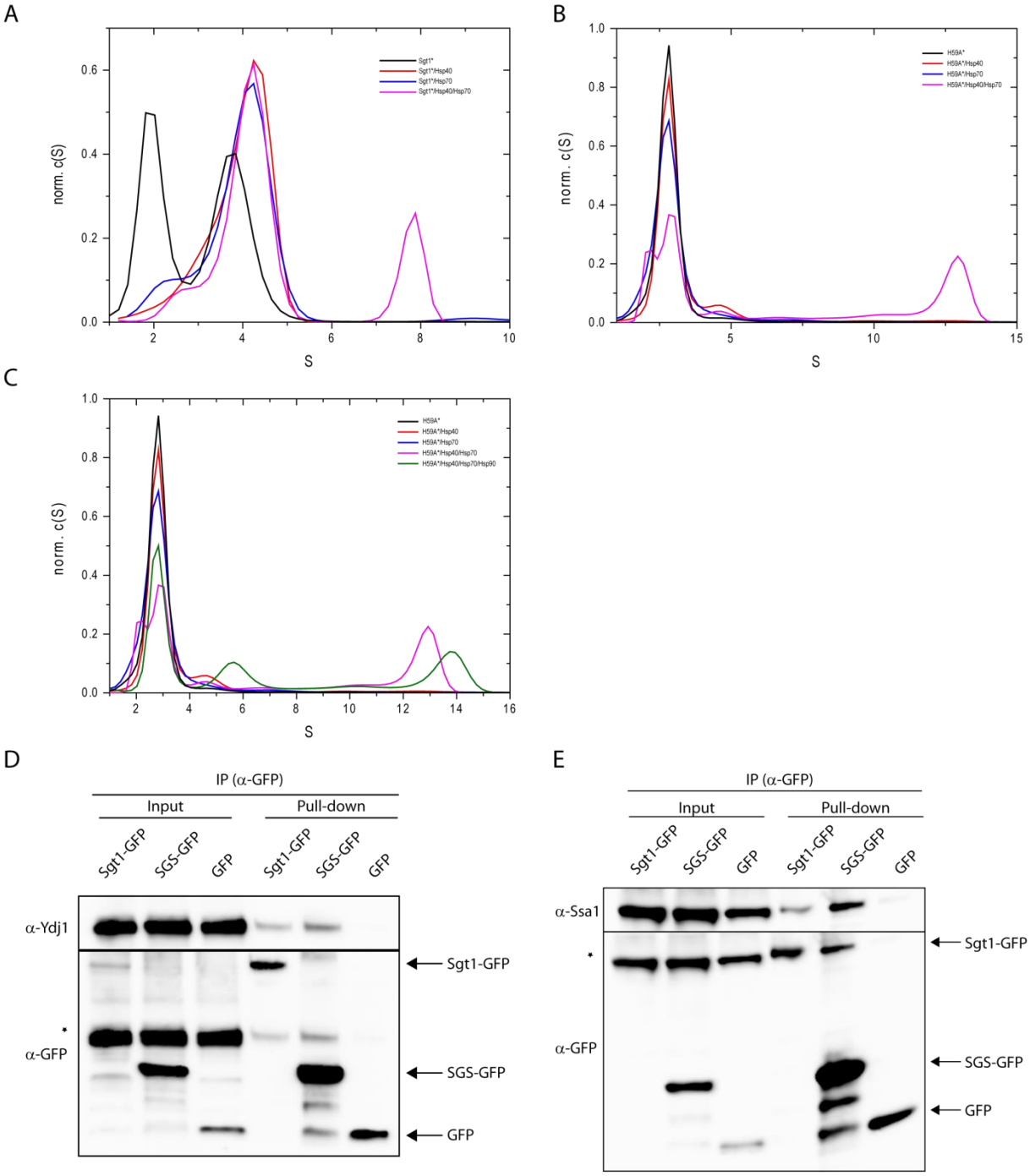

Figure 25: Sgt1's interplay with the Hsp40-Hsp70 system. (A)-(C) Analysis of complex formation of Sgt1 or mutant with the Hsp40-Hsp70 system by AUC sedimentation velocity experiments using 500 nM of the Atto488-labeled species (indicated by asterisk) and all other proteins at 5 µM. Additionally, ATP was present at 2 mM in all samples. Normalized c(S) distributions were plotted against the apparent sedimentation coefficient S. (D)+(E) GFP-pull-down from yeast expressing either Sgt1-GFP, SGS-GFP or GFP from a p415-GPD plasmid. Westernblot analysis of input and pull-down fractions with antibodies as indicated. The different GFP-constructs were detected using an α-GFP antibody. Arrows indicate the different constructs. The asterisk indicates bands from the beforehand used antibody either α-Ydj1 (D) or α-Ssa1. Picture of an independent triplicate.

Like previous AUC experiments, Sgt1 sedimented as a monomer-dimer distribution (peaks at 2 S and 4 S). The addition of Hsp70 to the labeled Sgt1 shifted the monomer-dimer distribution of Sgt1. However, a direct interaction of these two proteins is unlikely since higher Svedberg values would be expected for a Sgt1-Hsp70 complex. A similar picture was depicted if Hsp40 was added to Sgt1, yet a

complex of monomeric Sgt1 and Hsp40 might be in the range of four Svedberg. Interestingly, if Hsp40 and Hsp70 were added a peak at eight Svedberg occurred pointing to a trimeric complex of Sgt1, Hsp40 and Hsp70 (Fig 25A). To bypass the resolution issues due to the dynamic oligomerization of Sgt1, the dimerization incompetent H59A mutant of Sgt1 was used in AUC experiments. In the case of the addition of Hsp40, a small shoulder at the H59A peak occurred (Fig 25B). This shoulder could indicate a direct interaction of the monomeric Sgt1 with Hsp40, yet highly unfavorable under the *in vitro* conditions. Hsp70 did not shift the H59A peak indicating no direct interaction between Sgt1 and Hsp70. Again, the combined addition of Hsp40 and Hsp70 led to a peak at higher Svedberg values. Noteworthy, the peak occurred at around 12 Svedberg suggesting that the monomeric Sgt1 displays multiple binding sites for the Hsp40-Hsp70 system. Dimeric Sgt1 might hinder multiple binding due to steric restrictions or by occupying the binding site due to the homo-dimer interactions. Remarkably, if further Hsp90 was added to the Sgt1-Hsp40-Hsp70 complex, a shift to an even higher Svedberg value was observable demonstrating that a quaternary complex is possible (Fig 25C). The formation of a complex between the Hsp40-Hsp70 system and Hsp90 linked by Sgt1 tempts to speculate that Sgt1 facilitates client transfer likewise the co-chaperone Sti1 (Chen and Smith, 1998, Kirschke et al., 2014).

The *in vitro* reconstitution of the suggested interaction between the SGS domain of Sgt1 and Hsp70 failed. No single domain or double domain construct of Sgt1 bound to Hsp40 or Hsp70, respectively. To verify the interaction of the SGS domain and Hsp70 *in vivo* pull-down experiments were performed. Prior to the co-immunoprecipitation wild-type *Saccharomyces cerevisiae* (BY4741) was transformed with a plasmid (p415-GPD) expressing GFP, Sgt1-GFP or SGS-GFP, respectively. The GFP-trap system consisting of immobilized high affinity GFP antibodies was used to pull-down GFP or the fusion protein constructs from crude extract. Subsequent Western blot analysis revealed that Ydj1, the most common yeast Hsp40, and Ssa1, the main cytosolic Hsp70 isoform, were co-immunoprecipitated with Sgt1 as well as the SGS domain confirming previous suggestions (Spiechowicz et al., 2007) (Fig 25 D+E).

In brief, the interaction of Sgt1 with the Hsp70 system could be confirmed. I*n vitro* analyses suggest that Sgt1 directly interacts with Hsp40, which further mediates trimeric complex formation with Hsp70. Still, the interaction to the Hsp40-Hsp70 system is mediated by the SGS domain of Sgt1 as suggested by *in vivo* pull-down experiments.

4.9. Integration of Skp1 into the chaperone network

The link to the two most extensively studied pathways in which Sgt1 is involved, SCF-E3-ligase assembly and kinetochore assembly, is Skp1 (Kitagawa et al., 1999). The interaction of Sgt1 with Skp1 is mediated by the TPR domain (Willhoft et al., 2017, Catlett and Kaplan, 2006). Sgt1 was thought to be the adaptor protein linking Skp1 to Hsp90. However, cooperative action of the three proteins was reported to be important for kinetochore assembly (Catlett and Kaplan, 2006, Bansal et al., 2004, Steensgaard et al., 2004). To further analyze Skp1's effect on the interplay of the chaperones *in vitro,* complex formation was monitored using analytical ultracentrifugation. For that, Skp1 was recombinant expressed, purified and labeled with Atto488 via maleimide-thiol chemistry.

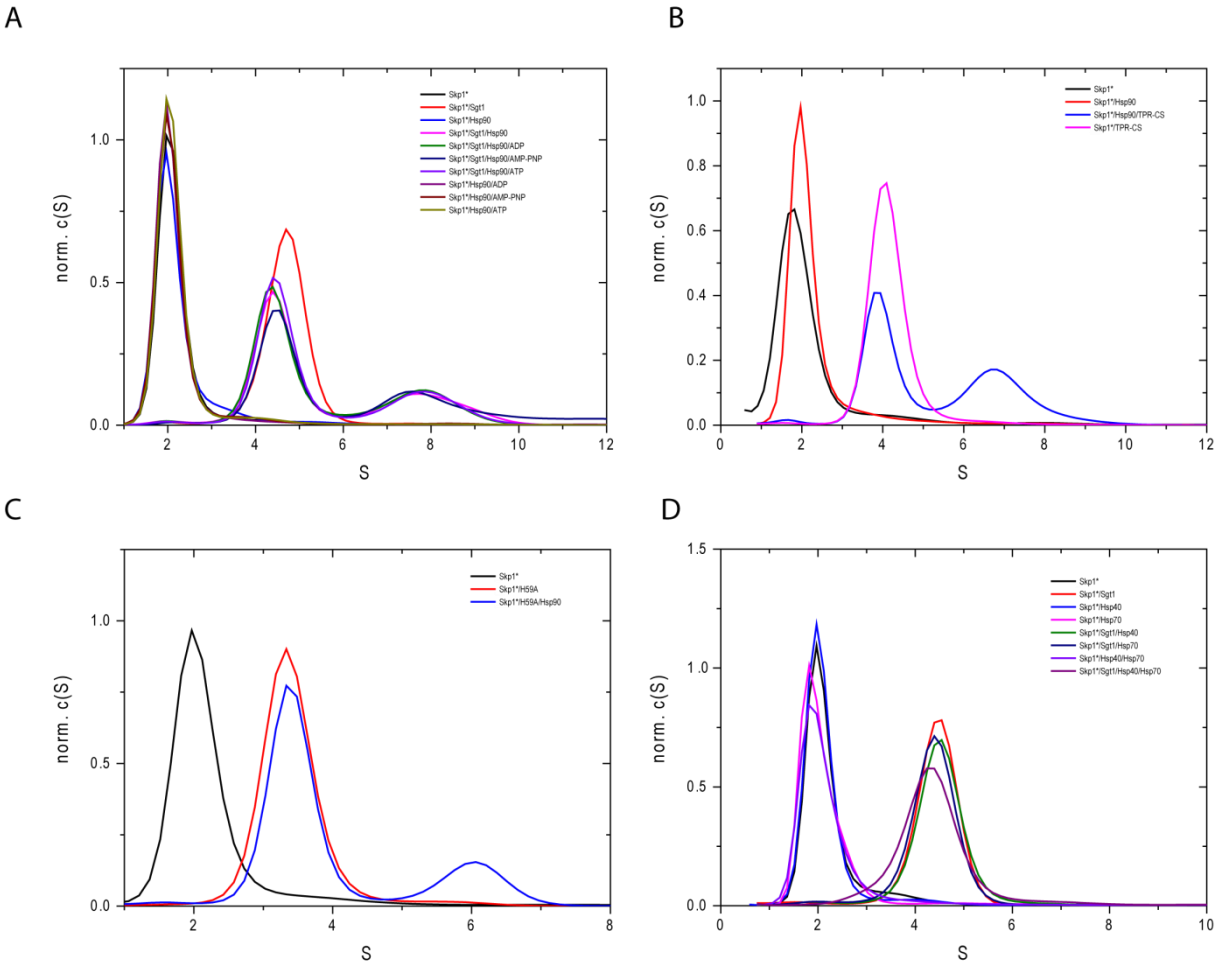

Figure 26: Interplay of Skp1 with chaperone systems. (A)-(D) Analysis of complex formation of Skp1 by AUC. Atto488-labeled Skp1 was used at 500 nM, while all other indicated proteins had a concentration of 2.5 µM (H59A corresponds to the dimerization incompetent Sgt1 mutant; TPR-CS to the double domain construct of Sgt1's TPR and CS domain). The nucleotides were supplemented at 2 mM. Normalized c(S) distributions were plotted against the apparent sedimentation coefficient S.

The fluorescently labeled Skp1 sedimented at 2 S, what could be expected for a 22 kDa, monomeric protein (Fig 26A). The interaction of Skp1 with Sgt1 could be reconstituted as shown by the shift of the peak for labeled Skp1 to around 4.5 S upon addition of Sgt1. A further peak at higher Svedberg values (6-8 S) was observed when Hsp90 was supplemented demonstrating the formation of the

trimeric complex consisting of Skp1, Sgt1 and Hsp90. The formation of the trimeric complex was also observed in the presences of different nucleotides (ATP, ADP, AMP-PNP) indicating that Skp1 can be linked to Hsp90 by Sgt1 during all phases of the ATPase cycle of Hsp90 (Fig 26A). Notably, a direct interaction between Skp1 and Hsp90 could not be observed in line with previous results (Bansal et al., 2004, Lingelbach and Kaplan, 2004) (Fig 26A). Complex formation between Skp1 and Hsp90 was also observed if Sgt1 was substituted by the TPR-CS domain construct suggesting that the SGS domain is dispensable for association of the three proteins (Fig 26B). Additionally, the use of the dimerization-incompetent Sgt1 mutant H59A demonstrated that a Sgt1 monomer is sufficient to bind both Skp1 and Hsp90 (Fig 26C).

Strikingly, even though the putative Hsp70 interaction site of Sgt1 is not engaged in Skp1 binding, complex formation between Skp1, Sgt1 and the Hsp40-Hsp70 system failed (Fig 26D, 25 A). This indicates that Skp1-related complex assembly depends on the Sgt1-Hsp90 axis (Fig 26A).

Collectively, Skp1 interaction with Sgt1 and the Hsp90-bridging property of Sgt1 could be demonstrated *in vitro*. The cooperative action of the TPR- and CS-domain of Sgt1 are is sufficient to establish the Skp1-Hsp90 axis. Noteworthy, Skp1 did not enter into the Hsp40-Hsp70 system together with Sgt1.

4.10. The phospho-mimic mutant S361D of Sgt1

Among post-translational modifications, phosphorylation is the most abundant one (Kruger et al., 2006). Protein phosphorylation can alter, *inter alia*, biological activity, subcellular localization and complex formation of target protein (Cohen, 2002, Cohen, 2000). Sgt1 was also reported to be the target of phosphorylation throughout different species (Bansal et al., 2009a, Prus et al., 2011, Martins et al., 2009, Liu et al., 2012). In yeast serine 361 was identified to be phosphorylated by casein kinase 2 (CK2), while the human orthologue Sugt1 was reported to be targeted by polo-like kinase 1 (Plk1) at serine 331, which corresponds to yeast serine 361 displaying a conserved phosphorylation site from yeast to man (Liu et al., 2012, Bansal et al., 2009a). Permanent phosphorylation of Sgt1 as represented by the phospho-mimic mutant S361D was shown to be lethal (Bansal et al., 2009a). The phosphorylation site resides in the essential SGS domain of Sgt1 and the substitution of serine 361, which showed a dynamic conformation in our NMR studies, to aspartate is lethal (Fig 18A, 19).

Bansal and colleagues reported the inability of homo-dimerization of the phospho-mimic (Bansal et al., 2009a). To validate the published *in vivo* data, which display decreased association of *sgt1*-S361D with itself, analytical ultracentrifugation experiments were carried out using recombinant purified S361D. The Atto-488 labeled S361D exhibited a peak at 2 and 4 S like Sgt1 wild-type (Fig 27A) indicating that the phospho-mimic variant is capable of homo-dimerization in contrast to the literature. Furthermore, upon addition of unlabeled S361D, the peak shifted to even higher Svedberg values depicting a shift in the oligomerization equilibrium to larger species. In addition, hydrogen-deuterium exchange experiments coupled to mass spectroscopy were performed monitoring the conformational dynamic and protection of the phospho-mimic mutant, Sgt1-WT and the dimerization incompetent H59A mutant of Sgt1 (Willhoft et al., 2017). In comparison to the wild-type Sgt1 deuterium uptake was increased in the TPR domain of H59A for several peptides (Fig 27B). Peptides between residue 40 to 100 of Sgt1 showed three- to five-fold increase in deuteration indicating an elevated solvent exposure. Since the TPR-domain is the site of homo-dimerization (Willhoft et al., 2017, Nyarko et al., 2007), the loss of the mutual shielding by dimerizing TPR domains could explain the increased deuterium exchange in the TPR domain of the H59A mutant. If S361D is incapable of dimerization, a similar deuteration profile would be expected. However, the relative fractional uptake of deuterium by S361D in comparison to Sgt1-WT did not display the monomer-like profile in agreement with the AUC data (Fig 27A-C). Moreover, the difference in relative fractional uptake (Fig 27D) did not change between S361D and Sgt1 except for the peptides ranging around the amino acid substitution suggesting that the putative conformational switching through the insertion of aspartate is locally restricted.

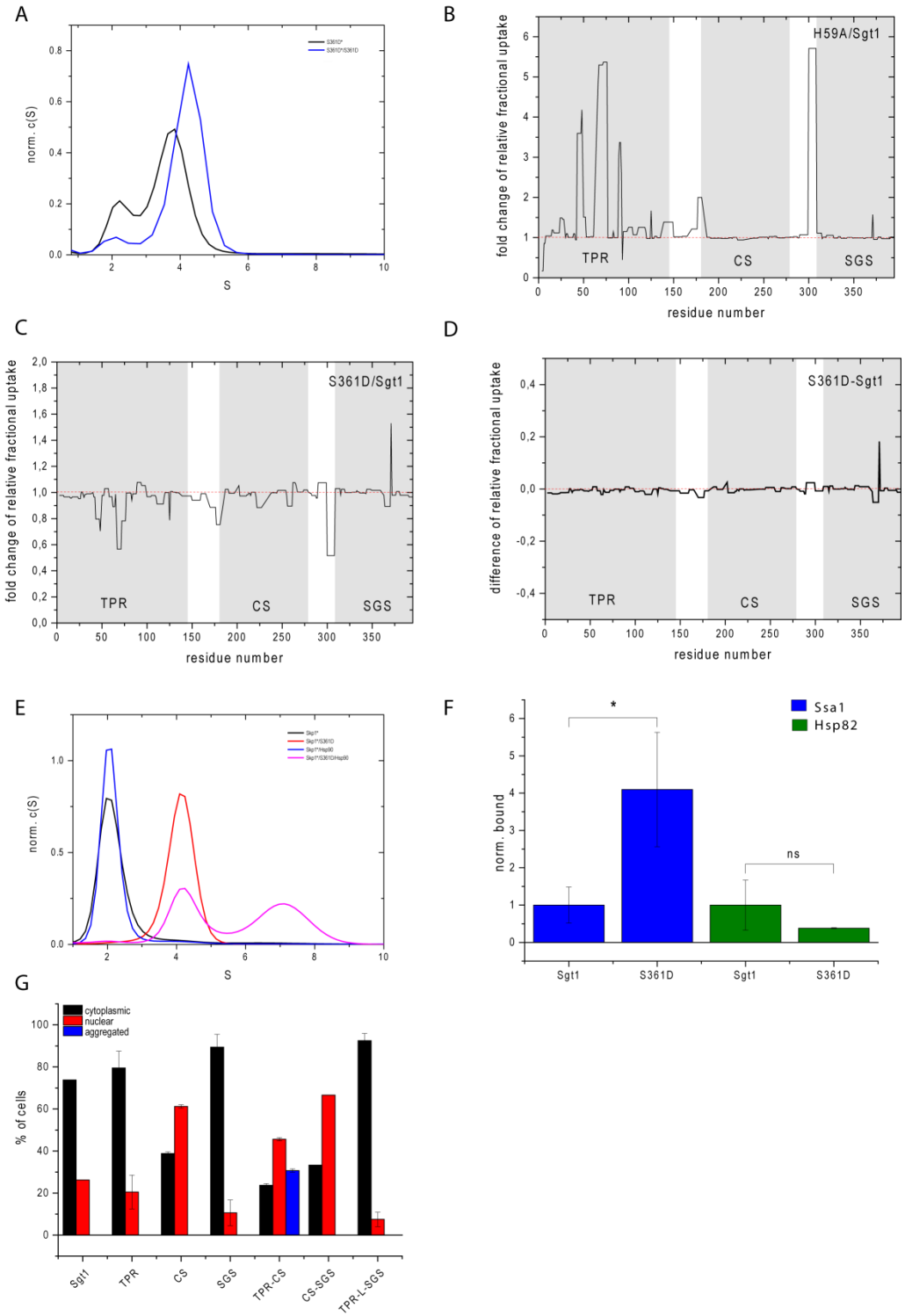

Figure 27: Analysis of the phospho-mimic S361D variant. (A) Complex formation of S361D with itself analyzed by AUC experiments (500 nM Atto488-labeled S361D, 5 µM S361D). Normalized c(S) distributions were plotted against the apparent sedimentation coefficient S. (B) Fold change of relative fractional deuterium uptake of the monomeric Sgt1 mutant H59A compared to wild-type Sgt1. HDX fold changes at 10 s were plotted against the residue number of Sgt1. Grey areas indicate the three defined Sgt1 domains. (C) HDX fold changes of the phospho-mimic mutant S361D compared with wild-type Sgt1 at 10 s time point. Grey areas indicate the three defined Sgt1 domains. X axis displays residue numbers of Sgt1. (D) Difference in H/D exchange between Sgt1 and S361D at 10 s. Deuteration differences were plotted against the residue number of Sgt1. Grey areas indicate the three defined Sgt1 domains. (E) Complex formation between Skp1, S361D and Hsp90 analyzed by analytical ultracentrifugation sedimentation velocity experiments using 500 nM of the Atto488-labeled species (indicated by an asterisk), 2.5 µM S361D and 5 µM Hsp90. Normalized c(S) distributions were plotted against the apparent sedimentation coefficient S.

Furthermore, Bansal and colleagues stated that the phospho-mimic Sgt1 variant did not bind to Skp1, thereby disrupting the assembly of the CBF3 complex (Bansal et al., 2009a). To verify this suggestion again AUC experiments using fluorescently labeled Skp1 were performed (Fig 27E). Labeled Skp1 displayed a peak around 2 S. Similar to previous experiments with Skp1, the addition of S361D shifted the peak to 4 S indicating direct binding of Skp1 to the phospho-mimic mutant. Moreover, the interaction between Skp1 and Hsp90 could be bridged by S361D as shown by the further peak shift to 7 S in the presence of the three components.

Since the phosphorylation of Sgt1 resides in the SGS domain, the putative interaction site for Hsp70 (Spiechowicz et al., 2007), and since both suggested effects on the binding of the S361D mutant could not be confirmed (Bansal et al., 2009a), differences in Hsp70 interaction between Sgt1 and S361D were probed. As the *in vitro* analysis of the complex formation between S361D and the Hsp70 system failed, *in vivo* pull-down experiments were carried out. For that purpose, Sgt1 and S361D were expressed as GFP fusion proteins from a p415 plasmid with a constitutive active GPD promoter in TetO7-SGT1. Because S361D can dimerize with endogenous wild-type Sgt1, yeast was cultivated in the presence of doxycycline to knock-down endogenous Sgt1 levels. Using the GFP-trap system, the fusion proteins and GFP as a control were pulled down from crude extract. Subsequent Western blot analysis using antibodies directed against the cytosolic Hsp70 isoform Ssa1 and Hsp82 confirmed the binding of both chaperones to Sgt1 or the phospho-mimic S361D (Fig 27F). Surprisingly, the densitometric analysis revealed that S361D showed strongly increased Hsp70 binding (4-fold), while the binding to Hsp90 is not significantly altered compared to the wild-type Sgt1. This suggests that the phosphorylation of Sgt1 alters its preference for a certain chaperone system.

Notably, phosphorylation of Sgt1 was also reported to impair the nuclear distribution of Sgt1 (Prus et al., 2011). Since the phospho-mimic mutant is lethal, this raises the question if Sgt1's essential function is in the nucleus. To probe this hypothesis, fluorescence microscopy experiments were performed. To this end, p415 plasmids expressing C-terminal GFP-tagged Sgt1 domain constructs were transformed into BY4741 wild-type yeast and their localization was detected by fluorescence microscopy with a view to determine the cytosolic and nuclear localization. At least 50 yeast cells were classified per strain. In the case of the SGS domain, which provides the essential function, only a small portion of cells displayed a nuclear GFP signal (Fig 27G). In contrast to the hypothesis this

Figure 28: Analysis of the phospho-mimic S361D variant. (F) Densitometric analysis of Westernblots of a GFP-pull-down from yeast expressing either Sgt1-GFP, S361D-GFP from a p415-GPD plasmid. Binding of Ssa1 and Hsp82 was detected by immunostaining with an α-Ssa1 or α-Hsp82 antibody and normalized against the amount of GFP construct present. Bars display the mean of three independent experiments. (G) Localization of GFP-tagged Sgt1 and domain constructs. BY4741 strains expressing the GFP-fusion protein from a p415-GPD plasmid were analyzed by microscopy. Using ImageJ Cell Counter cells displaying nuclear or cytoplasmic localization of the GFP signal were quantified. Percentage of total cells classified in the indicated category for the indicated Sgt1 constructs were plotted showing the mean of three independent experiments.

implies that the essential function of Sgt1 is not restricted to the nucleus. Interestingly, constructs harboring the CS domain showed the highest tendency for nuclear localization proposing a critical role for the CS domain in Sgt1's cellular distribution, which might be due to CS interaction with Hsp90. The TPR domain showed similar behavior as the full-length Sgt1 displaying around 80 % cytosolic and 20 % nuclear fractions. Notably, the TPR-CS construct tended to form foci which were classified as aggregates.

In sum, previously published aspects regarding the phospho-mimic mutant S361D like the dimerization incompetence or the Skp1 binding impairment were disproven. Importantly, an increased propensity of phosphorylated Sgt1 towards Hsp70 binding could be shown.

4.11. Physical interactome analysis of Sgt1

Early interaction studies put Sgt1 within the Hsp90 chaperone network as well as in the assembly of the inner kinetochore and SCF-E3-ligases (Kitagawa et al., 1999, Bansal et al., 2004, Catlett and Kaplan, 2006). Further high-throughput studies on the protein-protein interaction network of *Saccharomyces cerevisiae* corroborated previous findings and also added information on Sgt1's interactome (Ho et al., 2002, Uetz et al., 2000, Willmund et al., 2013, Gong et al., 2009). However, the understanding of the biological role of Sgt1 remains partly. To further expand the physical interactome of Sgt1 and with that the classification within certain pathways, pull-down experiments coupled to mass spectrometry were carried out. For that purpose, wild-type yeast BY4741 was transformed with p415-GPD-plasmids expressing either GFP or C-terminal GFP-tagged Sgt1. After pulling down GFP or the GFP-tagged Sgt1 via the GFP-trap system from crude extract, mass spectrometry analyses were performed. Additionally, samples, which were prior to the pull-down crosslinked using formaldehyde to preserve weak transient interactors, were analyzed.

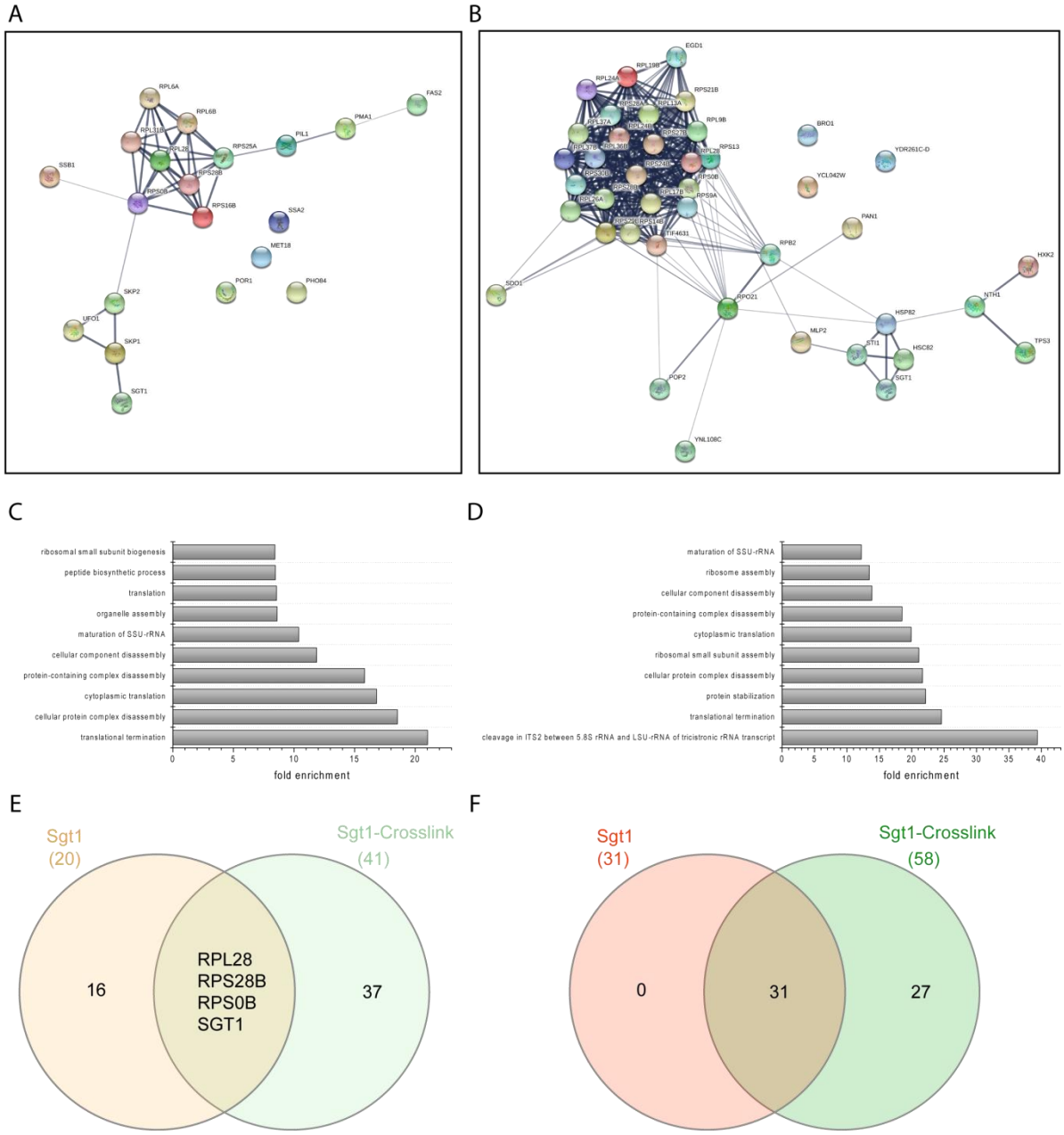

Figure 29: Physical interactome analysis of Sgt1. (A) STRING database network analysis of the significant enriched interactors of Sgt1 without crosslink (including Sgt1). Displayed proteins were enriched in all three analyzed sets. STRING clusters interactions including information from direct and indirect high- and low-throughput data, computational prediction, knowledge transfer between organisms and textmining (Szklarczyk et al., 2019, Szklarczyk et al., 2017). Increase in line width correlates with the number of evidences for that interaction. (B) STRING database network analysis of the significant enriched interactors of Sgt1 with formaldehyde crosslink (including Sgt1). Displayed proteins were enriched in all three analyzed sets. Increase in line width correlates with the number of evidences for that interaction. (C) Gene ontology analysis of statistical overrepresented biological process within the enriched interactors of Sgt1 without crosslink generated by the use of PANTHER (Thomas et al., 2003, Mi et al., 2013). Displaying the ten most enriched GO biological processes. (D) Gene ontology analysis of statistical overrepresented biological process within the enriched interactors of Sgt1 with crosslink generated by the use of PANTHER. Displaying the ten most enriched GO biological processes. (E) Overlap of the enriched proteins between the two sets, Sgt1 (yellow) and Sgt1 with formaldehyde crosslink (green). Venn diagram was generated using *InteractiVenn* (Heberle et al., 2015). (F) Overlap of the statistical overrepresented biological process of the two sets (Sgt1, red, Sgt1 with formaldehyde crosslink, green).

The enriched proteins which were pulled down together with Sgt1 are listed in table 24. Proteins listed are enriched in each replicate of the recorded triplicate compared to the GFP control (threshold for enrichment: 2-fold). Enrichment of Sgt1 is an inherent control for the success of the pull down. In figure 28A, an interaction network based on STRING analysis of the Sgt1 interactors is shown (Szklarczyk et al., 2019, von Mering et al., 2003). A broader connecting line correlates with the number of evidences for that interaction. Among the Sgt1 interactors two distinct clusters occurred, one consisting of ribosomal proteins and the other one of Sgt1, Skp1, Skp2 and Ufo1. Interestingly, two Hsp70 isoforms, Ssa2 and Ssb1, were among the interactors in line with previous analysis (Willmund et al., 2013, Gong et al., 2009). Also, the interaction with Skp1 was in agreement with earlier studies (Kitagawa et al., 1999, Catlett and Kaplan, 2006). Notably, two F-box proteins Skp2 and Ufo1, which participate in SCF-E3-ligases, were pulled down with Sgt1. Most likely these interactions were linked by Skp1 as reasoned by Catlett and Kaplan (Catlett and Kaplan, 2006). Gene ontology (GO) analyses were performed using PANTHER to extract biological processes which are statistically overrepresented among the enriched proteins (Thomas et al., 2003, Mi et al., 2013). The ten most enriched GO biological processes are presented in figure 28C; all are listed in table 25. The putative Sgt1 interactors are involved in processes ranging from translation to protein complex disassembly. Noteworthy, the fold enrichment of these biological processes can be ascribed to the ribosomal proteins found in the Sgt1 pull-down.

Table 24: Enriched proteins of the Sgt1 pull-down.

Sgt1									
RPL28	POR1	PMA1	RPL6B	RPS25A	RPS28B	RPL31B	RPS16B	SSA2	SSB1
FAS2	PHO84	RPS0B	MET18	SKP2	SKP1	PIL1	RPL6A	UFO1	SGT1

Table 25: Geneontology (GO) statistically overrepresented biological processes of the Sgt1 pull-down

Sgt1			
GO biological process	Fold enrichment	GO biological process	Fold enrichment
translational termination	21,03	protein-containing complex subunit organization	5,48
cellular protein complex disassembly	18,54	ribonucleoprotein complex biogenesis	5,03
cytoplasmic translation	16,82	ncRNA processing	4,81
protein-containing complex disassembly	15,83	organonitrogen compound biosynthetic process	3,59
cellular component disassembly	11,87	cellular nitrogen compound biosynthetic process	3,31
maturation of SSU-rRNA	10,39	cellular macromolecule biosynthetic process	3,28
organelle assembly	8,61	cellular protein metabolic process	3,28
translation	8,56	macromolecule biosynthetic process	3,23

peptide biosynthetic process	8,47	protein metabolic process	3,14
ribosomal small subunit biogenesis	8,43	cellular component biogenesis	3,14
peptide metabolic process	7,78	gene expression	2,81
amide biosynthetic process	7,46	organonitrogen compound metabolic process	2,29
rRNA processing	6,86	cellular component organization	2,26
rRNA metabolic process	6,45	cellular macromolecule metabolic process	2,16
cellular amide metabolic process	6,37	cellular component organization or biogenesis	2,02
ribosome biogenesis	6,09		

The mass spectrometry data of the crosslinked set was analyzed in the same way as the non-crosslinked one (Fig 28B+D; table 26+27). In this case again a large amount of ribosomal proteins were enriched (53% of all hits). However, the cluster with Skp1 was lost due to the crosslink. Yet, Sgt1 clustered with the two Hsp90 isoforms and the Hsp90 co-chaperone Sti1. Additionally, two minor clusters defined by strong evidence of their interactions occurred. One composed of Rpb2, Rpo21 and Pop2, which are part of the RNA polymerase, and the other one consisting of Hxk2, Nth1 and Tps3, which are involved in trehalose metabolism.

Nevertheless, determination of the overlap of enriched proteins between Sgt1 pull-down with (41 hits) and without (20 hits) crosslink showed that only three ribosomal proteins (Rpl28, Rps28b, Rps0b) besides Sgt1 itself were found to be enriched in both sets. Albeit, all 31 enriched GO biological processes identified for Sgt1 without formaldehyde crosslink were also determined for the crosslinked set indicating that even though the interacting proteins varied a lot, the overall functional relation has been in common (Fig 28E+F). Noteworthy, no leucine-rich-repeat (LRR) motif containing protein was enriched in the sets contrary to previous suggestions that LRR-containing proteins are specific clients of Sgt1 (Dubacq et al., 2002, Stuttmann et al., 2008).

Table 26: Enriched proteins of the Sgt1 pull-down with formaldehyde crosslink.

Sgt1-crosslinked									
RPS9A	RPL36B	RPL28	HSP82	RPO21	RPL24A	HXK2	RPL9B	RPL26A	RPS13
RPB2	RPS21B	RPS28B	TY1B-DR4	RPS24B	RPS30B	RPL19B	HSC82	STI1	RPL24B
YCL042W	NTH1	PAN1	RPS27B	TPS3	POP2	RPS14B	TIF4631	MLP2	RPS29B
RPS0B	RPL17B	BRO1	RPL37A	RPL37B	YNL108C	EGD1	SDO1	SGT1	RPL13A
RPS28A									

Table 27: Geneontology (GO) statistically overrepresented biological processes of the Sgt1 pull-down with formaldehyde crosslink

Sgt1-crosslinked			
GO biological process	Fold enrichment	GO biological process	Fold enrichment
cleavage in ITS2 between 5.8S rRNA and LSU-rRNA of tricistronic rRNA transcript	39,39	protein-containing complex subunit organization	5,87
translational termination	24,58	RNA phosphodiester bond hydrolysis	4,85
protein stabilization	22,15	cellular nitrogen compound biosynthetic process	4,49
cellular protein complex disassembly	21,67	cellular macromolecule biosynthetic process	4,46
ribosomal small subunit assembly	21,1	ncRNA processing	4,42
cytoplasmic translation	19,92	macromolecule biosynthetic process	4,39
protein-containing complex disassembly	18,5	organonitrogen compound biosynthetic process	4,33
cellular component disassembly	13,87	nucleic acid phosphodiester bond hydrolysis	3,87
ribosome assembly	13,46	ncRNA metabolic process	3,84
maturation of SSU-rRNA	12,22	gene expression	3,64
endonucleolytic cleavage of tricistronic rRNA transcript	12,22	cellular protein metabolic process	3,12
endonucleolytic cleavage involved in rRNA processing	12,22	RNA processing	3,1
maturation of SSU-rRNA from tricistronic rRNA transcript	11,36	protein metabolic process	2,99
translation	10,33	cellular biosynthetic process	2,97
peptide biosynthetic process	10,22	organic substance biosynthetic process	2,88
ribosomal small subunit biogenesis	9,92	cellular component biogenesis	2,87
ribosomal large subunit biogenesis	9,53	biosynthetic process	2,85
peptide metabolic process	9,38	cellular component organization	2,45
amide biosynthetic process	9	cellular nitrogen compound metabolic process	2,43
cleavage involved in rRNA processing	8,65	RNA metabolic process	2,38
organelle assembly	7,74	cellular macromolecule metabolic process	2,29
cellular amide metabolic process	7,68	organonitrogen compound metabolic process	2,24
ribonucleoprotein complex assembly	6,95	cellular component organization or biogenesis	2,18
ribosome biogenesis	6,86	macromolecule metabolic process	1,99
ribonucleoprotein complex subunit organization	6,68	nitrogen compound metabolic process	1,71

rRNA processing	6,31	primary metabolic process	1,67
ribonucleoprotein complex biogenesis	6,17	organic substance metabolic process	1,61
rRNA metabolic process	5,93	cellular metabolic process	1,58
RNA phosphodiester bond hydrolysis, endonucleolytic	5,91	metabolic process	1,55

Since the analysis of the pull-downs displayed a hazy insight into processes Sgt1 might be involved in, pull-down experiments using only the essential SGS domain of Sgt1 were performed. The experimental procedure was set up as described above. SGS with a C-terminal GFP-tagged was expressed from a p415-GPD-plasmid in BY4741 wild-type yeast. Additionally, since Sgt1 might play a role in cell cycling, pull-downs with cell cycle-specific arrested cells were carried out. For the arrest at specific cycle steps, well described protocols like α-factor for the arrest in G_1-phase, hydroxyurea for the synchronization in the early S-phase and nocodazole for arresting cells at the G_2/M transition were used (Rosebrock, 2017). Because the experimental procedure without formaldehyde crosslink did not yield a significant amount of enriched proteins, all SGS-pull downs shown were performed with crosslinking.

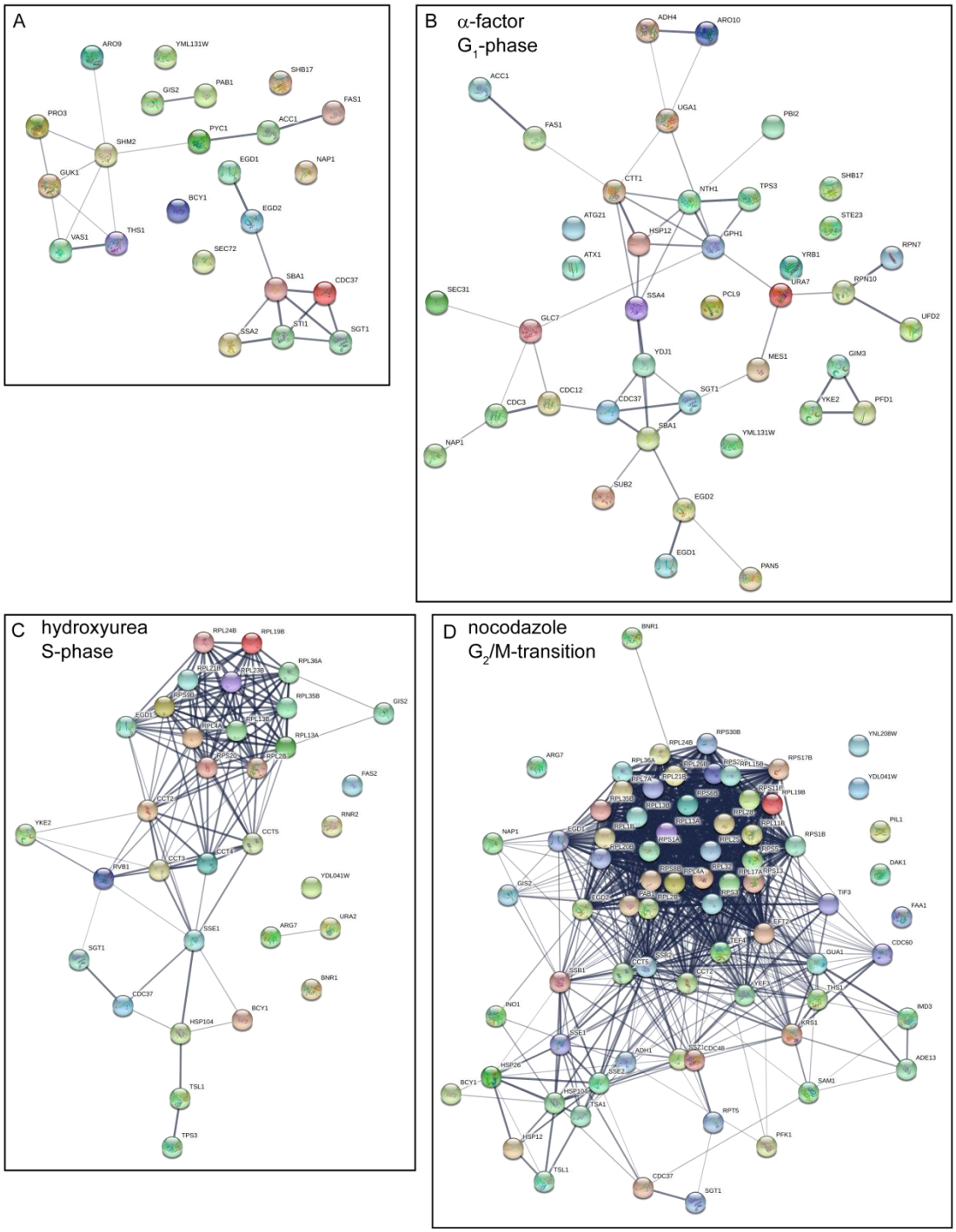

Figure 30: Physical interactome analysis of the essential SGS domain at different cell cycle states. (A) STRING database network analysis of the significant enriched interactors of the SGS domain with formaldehyde crosslink. Displayed proteins were enriched in all three analyzed sets. STRING clusters interactions including information from direct and indirect high- and low-throughput data, computational prediction, knowledge transfer between organisms and textmining (Szklarczyk et al., 2019, Szklarczyk et al., 2017). Line width increase correlates with the number of evidences for certain interaction. (B)-(D) STRING networks of the enriched physical interactors of the SGS domain during cell cycle arrest at a specific phase. Yeast cells were prior to the pull-down experiments arrested at the indicated cell cycle point with the indicated chemical as described elsewhere (Rosebrock, 2017).

In figure 29A, the STRING network of the SGS pull-down from asynchronous yeast cells is shown. The enriched proteins as well as the overrepresented biological processes are listed in table 28-34 for all SGS pull-downs. Interestingly, in the case of the SGS-pulldown without synchronization no gene ontology annotation was possible. In line with that, the enriched proteins only display a weak interacting network based on published data. However, one cluster of chaperones stands out consisting of three Hsp90 co-chaperones Sgt1, Sba1 and Cdc37, a cytosolic Hsp70 isoform Ssa2 and the two components of the nascent polypeptide-associated complex (NAC), Egd1 and Egd2.

Table 28: Enriched proteins of the SGS pull-down from asynchronous cells.

SGS									
PAB1	THS1	CDC37	FAS1	BCY1	VAS1	SSA2	PYC1	GUK1	STI1
NAP1	SBA1	PRO3	SHB17	SHM2	ARO9	EGD2	SEC72	GIS2	ACC1
EGD1	YML131W	SGT1							

Table 29: Enriched proteins of the SGS pull-down from cells arrested by α-factor.

SGS-α-factor									
MES1	CDC37	CTT1	GPH1	FAS1	PBI2	ADH4	UGA1	SSA4	HSP12
NAP1	YDJ1	URA7	SBA1	NTH1	CDC3	CDC12	GLC7	SHB17	TPS3
ATX1	PAN5	EGD2	RPN10	SEC31	YRB1	PFD1	YKE2	GIM3	UFD2
ACC1	EGD1	ATG21	YML131W	STE23	RPN7	ARO10	SUB2	SGT1	PCL9

Table 30: Enriched proteins of the SGS pull-down from cells arrested by hydroxyurea.

SGS-hydroxyurea									
RPL36A	RPL24B	RPS9B	CDC37	URA2	BCY1	RNR2	RPL23B	RPL2B	RPL19B
RPL35B	RPL4A	FAS2	HSP104	SSE1	TPS3	TSL1	RPS20	CCT2	CCT3
CCT4	RPL13B	CCT5	BNR1	YKE2	GIS2	EGD1	RPL21B	RVB1	ARG7
SGT1	YDL041W	RPL13A							

Table 31: Enriched proteins of the SGS pull-down from cells arrested by nocodazole

SGS-nocodazole									
RPL36A	ADH1	RPL28	RPS17B	PAB1	RPL24B	RPL25	THS1	RPL7A	RPL17A
RPL15B	RPS3	RPS13	CDC37	BCY1	RPL11B	RPL20B	RPS30B	RPS6B	RPS8B
RPL1B	RPL2B	RPS11B	RPL19B	RPL35B	SAM1	RPL4A	SSB1	INO1	KRS1
HSP26	YEF3	PFK1	HSP12	RPS1B	NAP1	CDC48	CDC60	RPS5	FAA1
HSP104	EFT1/2	SSE1	SSE2	RPT5	RPS1A	TIF3	TSA1	TEF4	RPL32
TSL1	GUA1	SSZ1	EGD2	CCT2	SSB2	YNL208W	RPL13B	CCT5	BNR1
RPS29B	IMD3	RPL26B	PIL1	GIS2	DAK1	EGD1	RPL21B	ARG7	ADE13
SGT1	YDL041W	RPL13A							

The pull-downs from synchronized cultures yielded an increased number of enriched proteins enabling GO annotation. The STRING network for the SGS-interactors of the α-factor synchronized cells is presented in figure 29B. Three biological processes could be annotated to this set of enriched proteins, protein folding, ER targeting and ´establishment of protein localization to endoplasmic reticulum` (Fig 30B). These GO annotations mainly arise from the presence of the two NAC components, Egd1 and Egd2, the cytosolic Hsp40 Ydj1, the cytosolic Hsp70 Ssa4 and parts of the hetero-hexameric prefoldin complex, Gim3, Pfd1 and Yke2 (table 29). Additional to these chaperones the Hsp90 co-chaperones Sba1 and Cdc37 were enriched. Interestingly, Ste23 a part of the mating cascade was also enriched tempting to speculate that Sgt1 in cooperation with the other chaperone systems acts on the triggered pathway.

In the presence of hydroxyurea, which induces cell arrest in the early S-phase, again an appreciable network of chaperones was enriched (Fig 29C). Besides parts of the prefoldin and NAC complex, this time also components of the TRiC/CCT complex occurred to be enriched with SGS (table 30). Furthermore, the Hsp70 nucleotide exchange factor Sse1, a chaperone of the Hsp110 class, and the disaggregase Hsp104 belong to the chaperones co-precipitated with the SGS domain. Noteworthy, a cohort of ribosomal proteins was again enriched leading to a statistical overrepresentation of biological processes like protein complex disassembly (Fig 30A). Markedly, ´trehalose metabolic process` was the most enriched biological process in this set due to the occurrence of Tsl1, Tps3 and Hsp104, which participate in the stress protective pathway (Eleutherio et al., 2015). Strikingly, Rnr2 a part of the ribonucleotide reductase complex, which is the target of hydroxyurea (Singh and Xu, 2016), was also found to be enriched again tempting to speculate about a directed stress response.

Yet, in the case of the nocodazole-arrested cells, no direct relation to the stress factor was found. Nocodazole acts on the polymerization of tubulin (Thelestam and Gross, 1990) thereby arresting cells in the G_2/M transition. However, again an extended network of chaperones was enriched including NAC, TRiC/CCT, Prefoldin, Hsp70s and also Ssz1 the specific Hsp70 isoform of the ribosome-associated complex (RAC) (Fig 29D + table 31). In addition, a number of ribosomal proteins and even translational factors were present in the SGS pull-down. Hence, again the overrepresentation of biological processes like protein complex disassembly was determined (Fig 30C). Interestingly, due to the appearance of Ssz1, Egd1/2 and Ssb1, the ribosome-associated cytosolic Hsp70 isoform, processes as *de novo* co-translational and posttranslational protein folding and chaperone mediated protein folding were significant enriched.

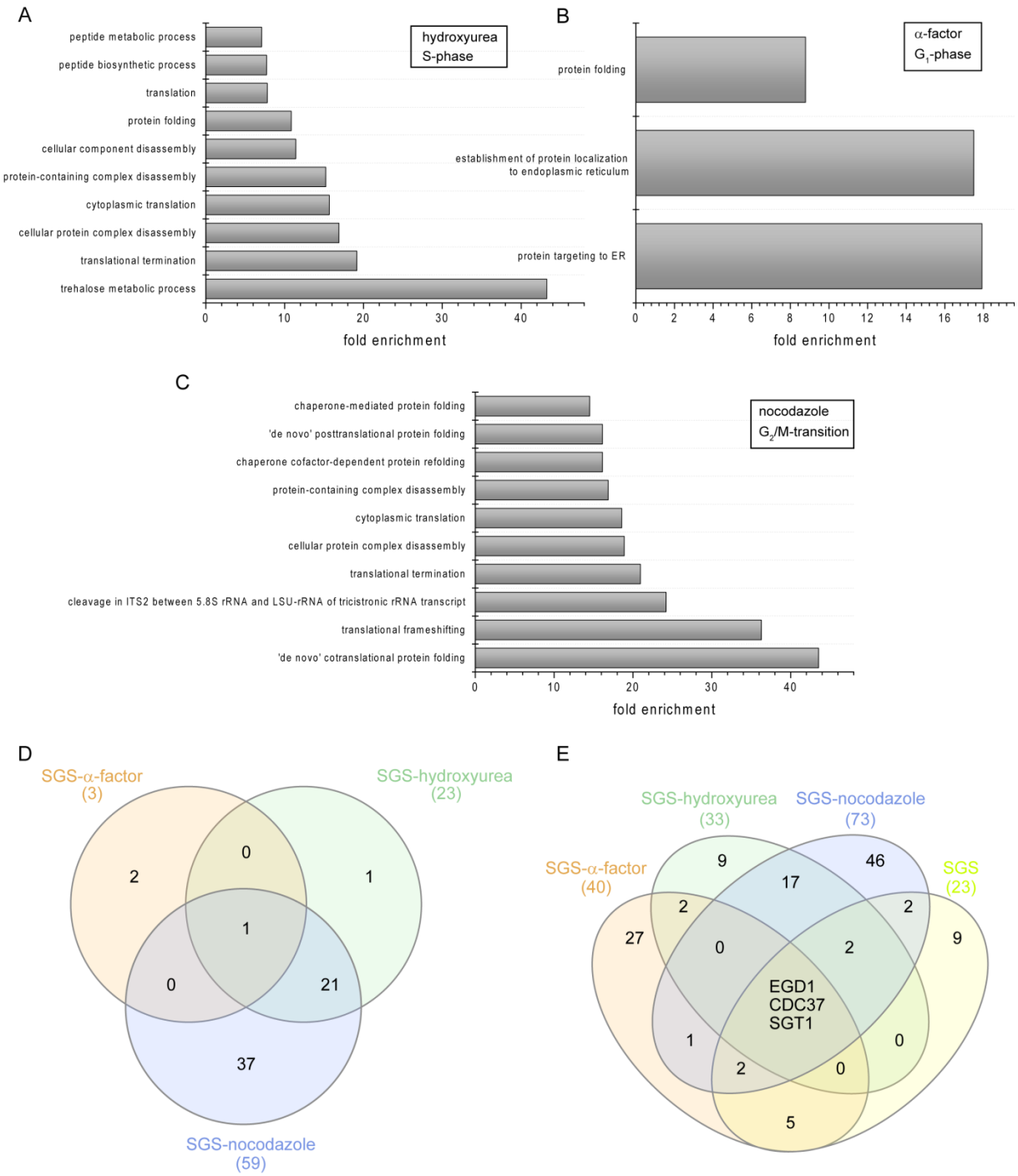

Figure 31: Gene ontology analysis of the SGS domain interactome. (A)-(C) Gene ontology analysis of statistical overrepresented biological process within the enriched interactors of the SGS domain during indicated arrest generated by the use of PANTHER (Thomas et al., 2003, Mi et al., 2013). Displaying the ten most enriched GO biological processes. (D) Overlap of the statistical overrepresented biological process (SGS arrested with α-factor, orange, SGS arrested with hydroxyurea, green, SGS arrested with nocodazole, blue). Venn diagrams were generated using *InteractiVenn* (Heberle et al., 2015). (F) Overlap of the enriched proteins of the four SGS sets (SGS arrested with α-factor, orange, SGS arrested with hydroxyurea, green, SGS arrested with nocodazole, blue, SGS pull-down from asynchronous cells, yellow). Venn diagram was generated using *InteractiVenn* (Heberle et al., 2015).

When the GO annotations of the three cell cycle arrested pull-down sets were compared only protein folding was found in common (Fig 30D). However, the nocodazole set, which displayed 59 GO annotations, encompassed nearly all GOs of the hydroxyurea set. Overall this indicates a consistent biological function of the SGS domain troughout the cell cycle. The SGS is most likely involved in

protein folding, and taking the co-enrichment of NAC into account, in the early onset of protein folding. Egd1, one of the NAC components is, besides Cdc37, the only protein enriched in all SGS-pull-down sets (Fig 30E). The presence of another Hsp90 co-chaperone might point to a unique functional module formed by Sgt1 and Cdc37. Nevertheless, also using only the putative client interactor domain, no LRR-containing protein was enriched.

Table 32: Geneontology (GO) statistically overrepresented biological processes of the SGS pull-down from cells arrested by α-factor.

SGS-α-factor	
GO biological process	Fold enrichment
protein targeting to ER	17,92
establishment of protein localization to endoplasmic reticulum	17,5
protein folding	8,79

Table 33: Geneontology (GO) statistically overrepresented biological processes of the SGS pull-down from cells arrested by hydroxyurea.

SGS-hydroxyurea			
GO biological process	Fold enrichment	GO biological process	Fold enrichment
trehalose metabolic process	43,25	protein-containing complex subunit organization	4,96
translational termination	19,16	organonitrogen compound biosynthetic process	3,63
cellular protein complex disassembly	16,89	cellular nitrogen compound biosynthetic process	3,35
cytoplasmic translation	15,67	cellular macromolecule biosynthetic process	3,16
protein-containing complex disassembly	15,22	macromolecule biosynthetic process	3,11
cellular component disassembly	11,41	cellular protein metabolic process	2,66
protein folding	10,84	cellular biosynthetic process	2,59
translation	7,8	organic substance biosynthetic process	2,51
peptide biosynthetic process	7,71	biosynthetic process	2,48
peptide metabolic process	7,08	protein metabolic process	2,41
amide biosynthetic process	6,8	gene expression	2,38
cellular amide metabolic process	5,8		

Table 34: Geneontology (GO) statistically overrepresented biological processes of the SGS pull-down from cells arrested by nocodazole

SGS-nocodazole			
GO biological process	Fold enrichment	GO biological process	Fold enrichment
'de novo' cotranslational protein folding	43,56	ribonucleoprotein complex biogenesis	4,24
translational frameshifting	36,3	ribonucleoprotein complex subunit organization	4,1
cleavage in ITS2 between 5.8S rRNA and LSU-rRNA of tricistronic rRNA transcript	24,2	cellular nitrogen compound biosynthetic process	3,98
translational termination	20,95	cellular macromolecule biosynthetic process	3,81
cellular protein complex disassembly	18,9	macromolecule biosynthetic process	3,74
cytoplasmic translation	18,57	ncRNA metabolic process	3,31
protein-containing complex disassembly	16,87	cellular protein metabolic process	3,13
chaperone cofactor-dependent protein refolding	16,13	ncRNA processing	3,08
'de novo' posttranslational protein folding	16,13	gene expression	3,03
chaperone-mediated protein folding	14,52	protein metabolic process	2,84
protein refolding	13,44	cellular biosynthetic process	2,81
cellular component disassembly	12,65	organic substance biosynthetic process	2,77
translational elongation	12,1	biosynthetic process	2,74
regulation of translational fidelity	11,71	organonitrogen compound metabolic process	2,38
translation	9,72	cellular nitrogen compound metabolic process	2,18
peptide biosynthetic process	9,61	cellular component biogenesis	2,14
peptide metabolic process	8,83	cellular macromolecule metabolic process	1,98
maturation of LSU-rRNA	8,61	cellular component organization	1,97
amide biosynthetic process	8,47	cellular component organization or biogenesis	1,79
ribosomal large subunit assembly	8,44	macromolecule metabolic process	1,67
ribosomal large subunit biogenesis	7,61	nitrogen compound metabolic process	1,64
cellular amide metabolic process	7,38	primary metabolic process	1,62
ribosome assembly	7,35	cellular metabolic process	1,53
protein folding	6,83	organic substance metabolic process	1,53
protein-containing complex subunit organization	5,16	metabolic process	1,43
ribosome biogenesis	4,95	cellular process	1,17

ribosomal small subunit biogenesis	4,57	protein modification process	0,1
organonitrogen compound biosynthetic process	4,41	cellular protein modification process	0,1
rRNA processing	4,39	macromolecule modification	0,08
rRNA metabolic process	4,37		

Taken together, the pull-down experiments did not yield a specific set of previously defined clients. However, the results point to a cooperative functional role of Sgt1 with a broad spectrum of chaperone systems in protein folding and more specific in the onset of protein folding at the ribosome. Even though, the overlap of enriched proteins was limited between the sets, the overlap of biological process indicates that Sgt1 and especially the SGS domain function are coherent.

4.12. Impact of Sgt1 down-regulation on the proteome

The SGS domain of Sgt1 is the putative site of interaction for client proteins, which contain a LRR-motif (Stuttmann et al., 2008). Yet, the physical interaction studies did not yield such client proteins. To address if the homeostasis of a specific set of proteins depends on the presence of Sgt1, whole proteome analysis were carried out in the presence and absence of Sgt1. To this end, the R1158 TetO7-SGT1 yeast strain, which harbors SGT1 under the control of a doxycycline-repressible promoter system, was grown to log-phase in the presence or absence of doxycycline. The total, supernatant and pellet fraction were analyzed by mass spectrometry (Fig 31).

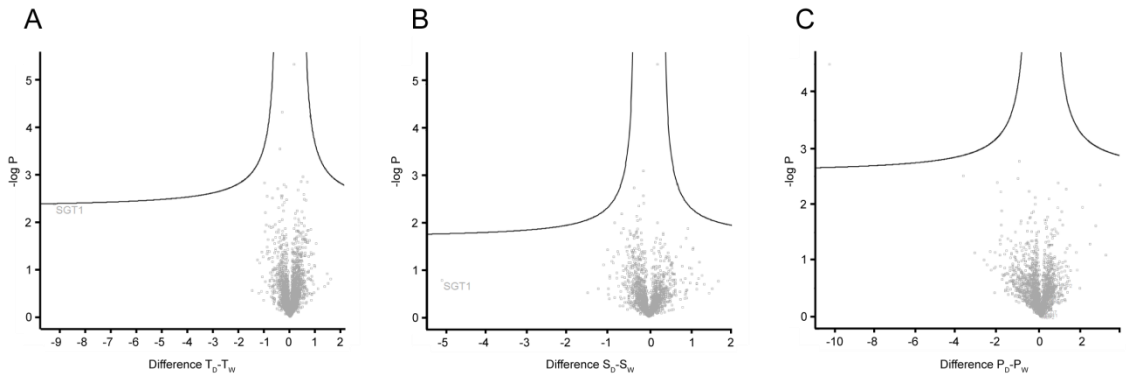

Figure 32: Impact of sgt1 depletion on the proteome. Volcano plots display up- and down-regulation of the proteome for the total protein fraction (A), the supernatant fraction (B) and the pellet fraction (C). A protein is considered to be significantly up- or downregulated if $|\text{Difference } (X_D\text{-}X_W)| > 1$ and p-value < 5 %. –logP values are plotted against the difference(S_D-S_W).For the total- and supernatant fraction proteins were selected if three valid values were present in each group, for the pellet measurement they were filtered on three valid values in at least one group.

The comparison of the protein abundance between the *sgt1* depleted cells and the untreated cells is shown in figure 31. The total fraction and the supernatant fraction (Fig 31A+B) exhibit a strongly decreased abundance of Sgt1, thereby confirming the depletion of Sgt1 by the addition of doxycycline. However, no further significant change in the protein levels could be observed. Moreover, the pellet fraction does, likewise, not display any changes comparing the *sgt1* depletion with the untreated samples indicating that in the absence of Sgt1 putative client proteins have not an increased tendency to aggregate. Additionally, the unchanged overall levels indicated that also the homeostasis of the putative clients of Sgt1 is unaffected by *sgt1* depletion.

In brief, *sgt1* depletion did not affect the whole proteome levels. Furthermore, no specific set of proteins depends on the presence of Sgt1 regarding their stability. This raises the question if sgt1 specific clients require a chaperoning action of Sgt1.

4.13. Sgt1's genetic interaction among chaperones

Large scale studies by Constanzo *et al*. (Costanzo et al., 2016) using the thermo-sensitive *sgt1-3* and *sgt1-5* mutant demonstrated negative genetic interaction between Sgt1 and the cytosolic Hsp70 Ssa1, the Hsp40 Ydj1, the Hsp110 Sse2 and the RAC component Zuo1. Additionally, positive genetic interactions between Sgt1 and parts of the prefoldin and TRiC/CCT complex were reported in this study. Genetic interactions allow drawing conclusions about the buffering or impinging effects of the tested gene products (Tong and Boone, 2006). Since the physical interactome analyses showed interaction of Sgt1 with several chaperones including prefoldin, TRiC/CCT, Hsp70s, Hsp110 and Hsp40s as well as RAC and NAC a synthetic genetic screen probing for genetic interactions with Sgt1 was carried out. Because the thermo-sensitive *sgt1*-mutants might accumulate diverse defects due to their aforementioned chromosomal instability, a strain harboring SGT1 under the control of a doxycycline repressible promoter system was used (Y8205 tetO7-SGT1) (Mnaimneh et al., 2004). From this query strain, all double mutants were generated by mating with single knock-out strains in case of non-essential genes or DAmP strains for essential genes (Breslow et al., 2008). After sporulation of the diploids, haploid double mutants were obtained by several steps of selection (Tong and Boone, 2006). Genetic interaction was probed by serial dilution spot assays onto YPD-plates with or without doxycycline and scoring the viability of the double mutants in comparison to the individual single depletion. Notably, some combinations had to be excluded from the analyses, because the diploid strains refused to sporulate. Figure 32 represents one of the biological triplicates after two days incubation at 30 °C. In figure 33 incubation was carried out at 37 °C for two days. Strains which refused to sporulate can be identified by strong growth with and without doxycycline,

e.g. *Δydj1*. However, most tested double mutants did not show an alteration in growth if doxycycline was present indicating no genetic interaction with Sgt1. So, several genetic interactions of the previous published large-scale study could not be confirmed (Costanzo et al., 2016). Only two chaperone deletions lead to a visible reduction in growth, namely Ssz1 and Zuo1. The growth defect of TetO7-SGT1 *ssz1Δ* and TetO7-SGT1 *zuo1.Δ* in the presence of doxycycline was even increased by additional mild heat stress at 37 °C. Each, ZUO1 and SSZ1, encode for one component of the ribosome-associated complex (RAC). Synthetic sick interactions like these ones suggest a buffering role of the gene products and an impact in the same pathway (Tong and Boone, 2006). This would point to an involvement of Sgt1 in ribosome-associated protein folding. Although previously reported genetic interactions could not be confirmed, the occurrence of a negative genetic interaction of Sgt1 with the RAC matches the physical interactome analyses, both suggesting an involvement of Sgt1 in *de novo* protein folding.

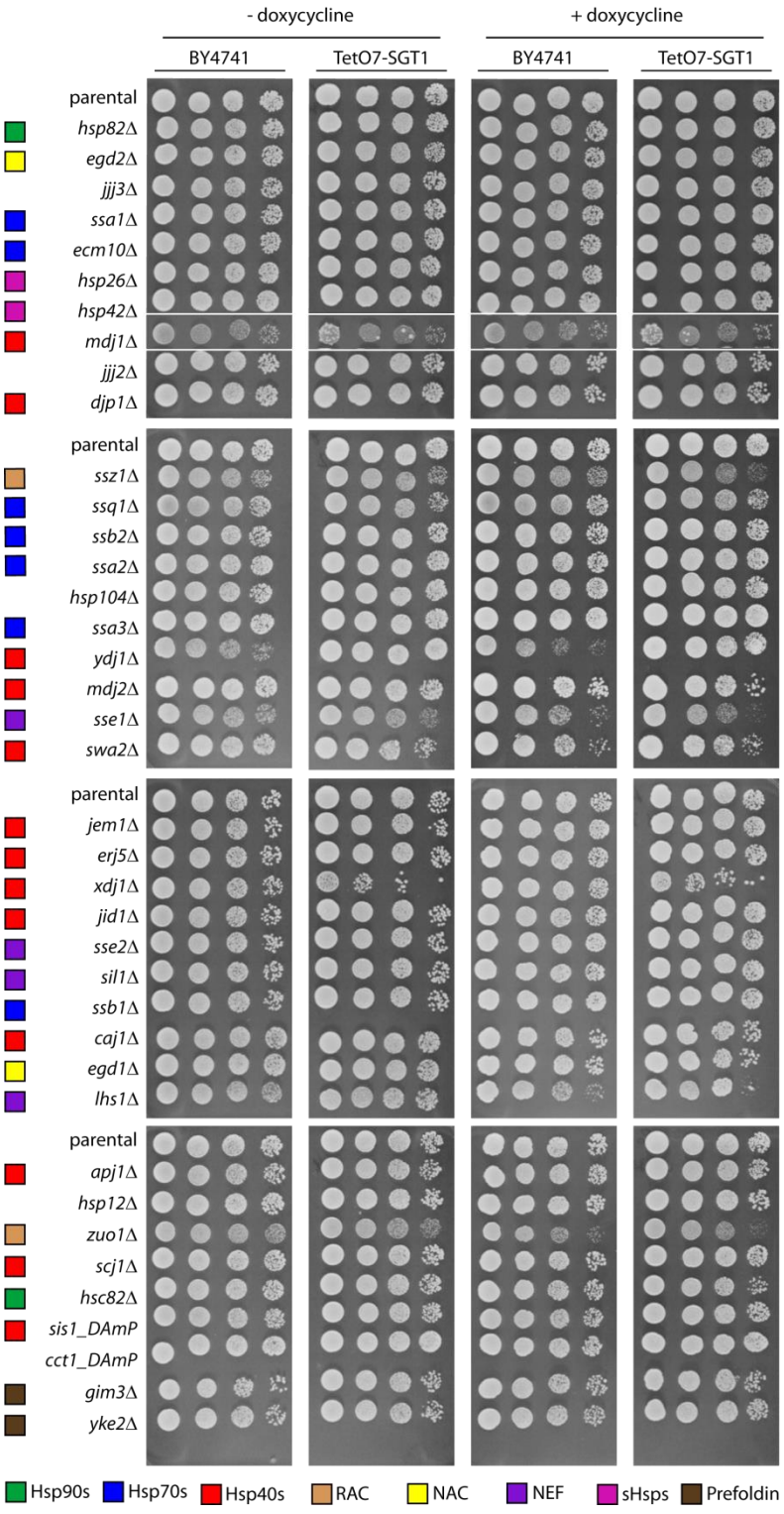

Figure 33: SGA of Sgt1 among other chaperones at 30°C. Synthetic genetic array analysis using TetO7-SGT1 in the Y8205 background. Double mutant strains harboring SGT1 under the control of the doxycycline repressible promoter (TetO7)were generated according to (Tong and Boone, 2006). The additional gene deletion or depletion by perturbation of the 3'UTR (DAmP) is indicated on the left. Single depletion mutants (left panel and central right panel) and double depletion mutants (central left panel and right panel) were spotted onto YPD plates with or without 10 µg/mL doxycycline as indicated. Photos were taken after two days of incubation at 30 °C. Representative picture of three independent experiments. Color code on the left displays the chaperone classification of certain genes as given by the legend at the bottom.

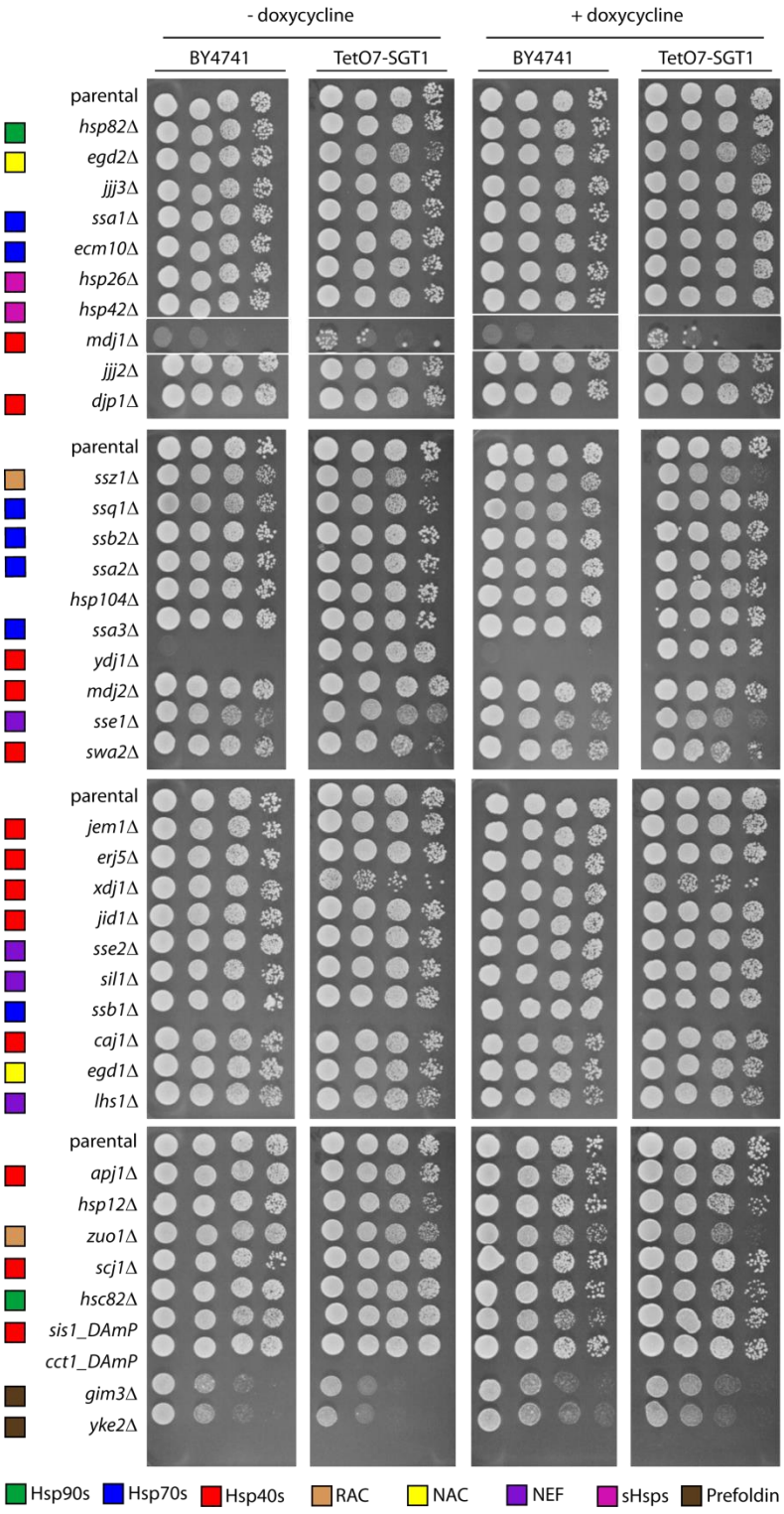

Figure 34: SGA of Sgt1 among chaperones at 37°C. Synthetic genetic array analysis using TetO7-SGT1 in the Y8205 background. Double mutant strains harboring SGT1 under the control of the doxycycline repressible promoter (TetO7)were generated according to (Tong and Boone, 2006). The additional gene deletion or depletion by perturbation of the 3'UTR (DAmP) is indicated on the left. Single depletion mutants (left panel and central right panel) and double depletion mutants (central left panel and right panel) were spotted onto YPD plates with or without 10 µg/mL doxycycline as indicated. Photos were taken after two days of incubation at 37 °C. Representative picture of three independent experiments. Color code on the left displays the chaperone classification of certain genes as given by the legend at the bottom.

5. Discussion

5.1. Characterization of the essential domain

Research on Sgt1 during the last decades assigned distinct functions to its three single domains. The TPR domain was reported to be the site of homo-dimerization and Skp1 interaction (Bansal et al., 2004, Catlett and Kaplan, 2006, Bansal et al., 2009b), while the CS domain mediates the interaction with Hsp90 (Lee et al., 2004b, Zhang et al., 2008). The SGS domain was thought to be the interaction site for Hsp70 and the putative LRR-motif containing clients (Stuttmann et al., 2008, Dubacq et al., 2002, Spiechowicz et al., 2007). However, the essential character of Sgt1 was never ascribed to a specific structural element. In this study, 5-FOA shuffling was used to identify the essential part of Sgt1. Surprisingly, yeast viability was solely dependent on the presence of the SGS domain. The overexpression of these last 83 amino acids restored growth of a *sgt1Δ* strain to wild-type levels. Fusion domain constructs harboring the SGS domain were also capable to compensate for the loss of endogenous Sgt1.

The finding that only the SGS domain is sufficient to provide viability suggests a link of the essential function towards its interactor Hsp70. Yet, previously published literature on thermo-sensitive *sgt1* mutants demonstrated a geldanamycin-sensitivity indicating an Hsp90 dependence of these mutants (Bansal et al., 2004). Therefore, the Hsp90 dependence of the viable domain constructs in a *sgt1Δ* background were probed by Hsp90 inhibition using radicicol. Remarkably, the constructs lacking the CS domain (TPR-L-SGS, SGS) were sensitive to Hsp90 inhibition, especially if mild heat stress was applied. Conversely, only if interaction with Hsp90 was mediated by the CS domain, inhibition of Hsp90 was tolerable, strongly suggesting a connection between the essential function of Sgt1 and Hsp90.

The human orthologue Sugt1 was previously shown to be able to substitute Sgt1 in yeast (Kitagawa et al., 1999). Sequence alignments of the yeast and human protein showed that the SGS domain has the highest degree of conservation. Conducting 5-FOA shuffling with domain constructs of the human orthologue Sugt1 revealed that also the human SGS domain alone was sufficient to provide yeast viability. Hence, the essential function residing in the SGS domain is conserved from yeast to man.

Since structural information about the essential SGS domain was lacking NMR experiments were carried out to gain insights about the domain architecture. The experiments revealed two stable helical structures ranging from residue 340 to 365 (numbering according to full length Sgt1). These two helices were separated by a short turn comprising residue 349 to 351. Additional two transient

helices were identified ranging from residue 322 to 326 and from 373 to 379, respectively. Noteworthy, serine 361 which resides in the second stable helix showed severe peak broadening indicating conformational dynamics around this position.

Using the new insights into the architecture of the SGS domain, a further dissection of Sgt1 concerning the essential element was addressed by plasmid shuffling. C-terminal truncations of Sgt1 until residues 372 lacking the second transient helical region were sufficient to provide viability in a *sgt1Δ* strain. Yet, cells depending on $Sgt1^{1-372}$ showed a severe growth defect. This suggests that the second transient helix of the SGS domain is dispensable for yeast growth. Mutational analysis addressing the integrity of the helix I-turn- helix II motif revealed that the orientation of the two helices is not important since glycine and proline substitutions within the turn did not influence the viability. Also the introduction of a proline in helix I did not affect cell growth. However, breaking the helical character of helix II by the introduction of a proline was lethal demonstrating the essential nature of this structural element. Notably, the helix-turn-helix motif alone was not able to provide the essential function of Sgt1. Moreover, C-terminal truncation until residue 372 was only tolerable in combination with the entire N-terminal part of Sgt1. Since the integrity of helix II seemingly is crucial for the essential function, these results suggest that if either the C-terminal tail or the N-terminal part is missing, the inherent stability of this helix is reduced leading ultimately to a lethal phenotype. In agreement with that *sgt1Δ* [$Sgt1^{1-372}$] exhibits a thermo-sensitive phenotype.

In summary, this study assigned the essential function of Sgt1 solely to the SGS domain. Furthermore, missing structural data on the SGS domain were gained revealing a crucial helix-turn-helix-motif. Further dissection of the SGS domain suggests that the helix ranging from residue 351 to 365 harbors the vital element. Additionally, the conservation of the essential nature of the SGS domain from yeast to man was demonstrated.

5.2. Sgt1's domain function in the suppression of Sgt1-related thermo-sensitive strains

First, Kitagawa and colleagues reported SGT1 as a multicopy-suppressor of the ts-phenotype of *skp1-4* (Kitagawa et al., 1999). Additionally, Sgt1 was reported to rescue the growth defect of *cdc35-1* at non-permissive temperature (Dubacq et al., 2002). Moreover, early work on Sgt1 was based on the thermo-sensitive Sgt1 strains, *sgt1-3 and sgt1-5* (Kitagawa et al., 1999, Bansal et al., 2004, Lingelbach and Kaplan, 2004). Characteristics of the strains are depicted in table 22. Dissection of the functionality of Sgt1's domains was carried out by analyzing the suppression of certain thermo-sensitive phenotypes.

The overexpression of the SGS domain could rescue the growth defects of the *sgt1* mutant strains, which is not surprising since the SGS domain supports growth of a *sgt1Δ* strain. Interestingly, the SGS domain alone was not able to rescue the ts-phenotypes of the two Sgt1-related ts-strains, *skp1-4* and *cdc35-1.* The suppression of the thermo-sensitivity of *skp1-4* depended on the presence of full-length Sgt1 suggesting a cooperative action of all three domains. The growth defect of *skp1-4* is due to an impairment of the kinetochore assembly and a functional Skp1-Sgt1-Hsp90-axis was reported to be crucial for it (Connelly and Hieter, 1996, Lingelbach and Kaplan, 2004). Thus, most likely the overexpression of Sgt1 restores the interaction between the mutant *skp1-4* and Hsp90. For that, the TPR domain mediates the binding to Skp1 and the CS domain mediates complex formation with Hsp90. However, those two domains alone were not able to overcome the growth defect of *skp1-4* suggesting that the SGS domain introduces a critical component to the axis. The disruption of the endogenous weakened *skp1-4*-Sgt1-Hsp90 axis by the overexpression of the TPR or CS domain is highly probable the reason for the cytotoxic effect of their overexpression.

The thermo-sensitivity of *cdc35-1* is most likely due to a defective response of Cyr1 to its regulatory mechanism (Dubacq et al., 2002). Additionally, the interaction with Sgt1 is impaired since the mutation of Cyr1 resides in the LRR-motif, which is thought to be critical for interaction (Dubacq et al., 2002). Notably, the ts-phenotype of *cdc35-1* could be rescued by the TPR-L-SGS fusion construct as well as full-length Sgt1 indicating cooperative function of at least the TPR and SGS domain to circumvent the defect. Overexpression of the SGS domain might restore the stable interaction with Cyr1, since the SGS domain is the putative LRR-motif recognition site (Stuttmann et al., 2008). Due to the fact that the growth defect of *cdc35-1* results from a dysregulation of Cyr1, the TPR domain is probably involved in the recruitment of certain regulators. Therefore, both domains together suppress the temperature sensitivity of *cdc35-1* (Fig 34A). Noteworthy, the dispensability of the CS domain for that function suggest an Hsp90-independent action of Sgt1.

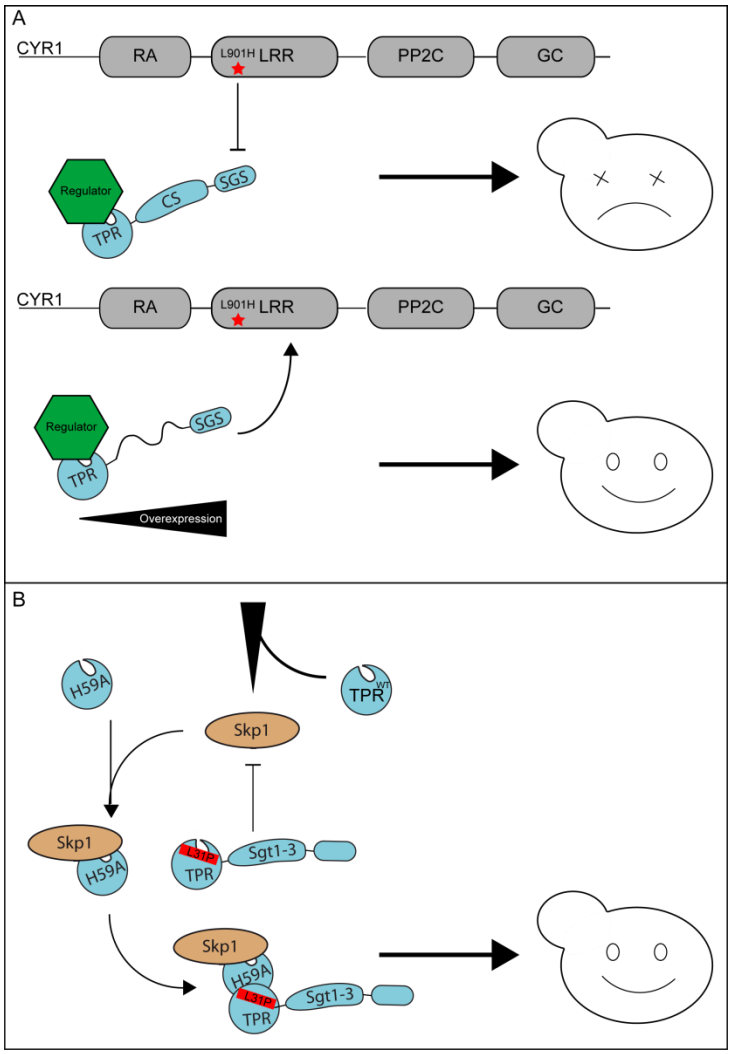

Figure 35: Model of the thermo-sensitivity rescue of cdc35-1 and sgt1-3. (A) Rescue of *cdc35-1.* The mutant *cyr1* does not interact with Sgt1 thereby escaping regulation by the regulator ultimately leading to cell growth arrest. Overexpression of the TPR-L-SGS construct restores the interaction and regulation of *cyr1* leading to cell cycle progression. Cyr1 (grey) consists of 4 domains RA (Ras-associating domain), LRR (leucine-rich repeat motif), PP2C (protein phosphatase 2 C) and GC (guanylate cyclase). Sgt1 depicted in blue. Happy yeast indicates cell cycle progression; dead yeast cell cycle arrest. (B) Rescue of *sgt1-3* by the TPR(H59A). *sgt1-3* does not interact with Skp1 (brown). The wild-type TPR domain extracts Skp1 thereby further disrupting the Skp1-Sgt1-axis. The mutant H59A restores the interaction between *sgt1-3* and Skp1 by binding to both ultimately leading to cell cycle progression.

The rescue of the growth defect of *sgt1-3* and *sgt1-5* by the overexpression of the SGS domain was expected. However, in the case of *sgt1-3* also the dimerization-incompetent TPR domain mutant H59A was able to restore growth. The mutant phenotype of *sgt1-3* is due to an impairment in Skp1 binding (Lingelbach and Kaplan, 2004, Kitagawa et al., 1999). Hence, the mutant TPR domain seems to be able to provide a Skp1-*sgt1-3* interaction. This study could demonstrate that H59A can bind to Skp1 as well as to wild-type TPR domains but not to another H59A mutant (Fig. 15). For that reason, TPR(H59A) most likely recruits endogenous Skp1 to *sgt1-3* by homo-dimerization with the TPR domain of *sgt1-3*. Interestingly, the wild-type TPR domain was not capable to restore growth of *sgt1-3* in comparison to TPR(H59A). This could be due to an increased tendency of wild-type TPR to oligomerize, thereby not supporting the restoration of the Skp1-*sgt1-3* axis. Additionally, the

overexpression of the TPR domain might extract Skp1 from the endogenous weakened interaction with *sgt1-3* according to a titration model (Fig34B).

Notably, the overexpression of the TPR domain was cytotoxic in *sgt1-5*. The thermo-sensitive phenotype of *sgt1-5* remains mostly enigmatic. However, an impairment in the activity of the SCF-E3-ligase apparatus during cell cycle progression was hypothesized (Kitagawa et al., 1999). If so, again the adverse impact of the TPR domain could be explained by a disruption of the Sgt1-Skp1-axis, which is critical for the formation of SCF-E3-ligase complexes (Kitagawa et al., 1999, Gray et al., 2003).

Taken together, the Sgt1-related thermo-sensitive phenotypes could be rescued by the cooperative action of the three domains of Sgt1. The three domains together ensure stable complex formation and provide the critical platform for function. In these analyses, the TPR domain occupies an important role by regulating complex formation. However, the essential SGS domain has to be always present to restore function. It is tempting to speculate about a distinct action of the SGS domain, which is diversified by the complex regulatory function of the TPR domain and also of the CS domain.

5.3. Dissection of the interaction between Sgt1 and Hsp90

The discovery of structural similarity of Sgt1 domains with Hsp90 co-chaperones by sequence alignments provided the first evidence that Sgt1 might be a co-chaperone of Hsp90 (Dubacq et al., 2002). Initially, TPR domain was thought to mediate the interplay (Bansal et al., 2004). However, subsequent work led to the commonly accepted model that Sgt1 binds via its CS domain to Hsp90 (Lingelbach and Kaplan, 2004, Lee et al., 2004b, Zhang et al., 2008). Since plasmid shuffling experiments in combination with Hsp90 inhibition assays provided evidence for a connection between the essential function of Sgt1 and Hsp90, the interplay of these to proteins was further dissected.

Sgt1 was able to bind to Hsp90 independent of the nucleotide state as probed by AUC. In contrast to the literature, Sgt1 preferred the AMP-PNP-induced closed state of Hsp90 *in vitro* (Catlett and Kaplan, 2006). This preference was further supported by fluorescence anisotropy measurements which displayed a two-fold increase in the binding affinity of the CS domain to Hsp90 if AMP-PNP was present. In line with previous reports the CS domain was sufficient to bind to Hsp90 (Lee et al., 2004b, Zhang et al., 2008). However, the affinity to Hsp90 was further increased if the CS-SGS-inter-domain linker and the SGS domain were present suggesting an additional involvement of these

regions in the binding of Hsp90. Crosslinking experiments coupled to mass spectrometry added evidence that the inter-domain linker is involved in binding to Hsp90. Moreover, the crosslink experiments revealed contacts to all domains of Hsp90 suggesting an extended binding interface contrary to Zhang *et al.* (Zhang et al., 2008), whereby only the NTD of Hsp90 contacts Sgt1. Additionally, AUC experiments using domain constructs of Hsp90 showed that Sgt1 was able to bind also to a MD-CTD construct indicating that at least one more domain of Hsp90 is involved in binding. Studies on the nematode orthologue of Sgt1 D1054.3 led to the hypothesis that Sgt1 binds to two distinct binding interfaces of Hsp90 in an ATPase cycle-dependent manner (Eckl et al., 2014). The alteration in binding of Sgt1 during the conformational cycle of Hsp90 could explain why Sgt1 has hardly an impact on the N-N-closing kinetic of Hsp90 as determined by FRET experiments. Due to the changing binding site of Sgt1, possible steric hindrance during the closing of the Hsp90 might be circumvented.

In brief, the dissection of the Sgt1-Hsp90 interaction provided evidence that the interaction is not exclusively mediated through the CS domain of Sgt1 and the NTD of Hsp90. The CS-SGS-inter-domain linker seems to be involved in binding, and on the Hsp90 side the extended binding interface may include at least the MD. Moreover, this study demonstrated that Sgt1 favors the AMP-PNP-induced closed state of Hsp90 for binding.

5.4. Integration of Sgt1 in the Hsp90 co-chaperone cycle

Hsp90 co-chaperones fine tune the Hsp90 cycle to optimize the maturation of clients. Sgt1 was shown to interact with any conformational state of Hsp90 allowing action throughout the cycle. However, the integration of Sgt1 in the Hsp90 co-chaperone cycle or the elucidation of a unique co-chaperone cycle of Sgt1 is enigmatic. Monitoring complex formation between Sgt1, Hsp90 and further co-chaperones by AUC was used to reveal the possible order of action. The commonly accepted Hsp90 co-chaperone cycle starts with the client transfer facilitated by Sti1. Hsp90 is kept in an open conformation by the TPR-containing co-chaperone (Prodromou et al., 1999, Richter et al., 2003). At this stage of the cycle, Sgt1 was able to form trimeric complexes suggesting the capability to act on early Hsp90-related processes. The simultaneous binding of Sgt1 with Sti1 was previously reported (Catlett and Kaplan, 2006). Notably, Sti1 addition to a Sgt1-Hsp90 complex led to a partial release of Sgt1 indicating overlapping binding sites supporting the assumption that Sgt1 does not exclusively bind to the NTD of Hsp90. Following, the cycle is joined by other TPR-containing co-chaperones like Cpr6, Cpr7, Cns1 or Ppt1. Trimeric complex formation with any of these co-chaperones was observed allowing cooperative action. Next, the closing of Hsp90 is accelerated by

Aha1 (Li et al., 2013). On the one hand Aha1 was capable to compete for binding to Hsp90 and on the other hand Aha1 joined an Hsp90-Sgt1 complex. Increasing amounts of Aha1 could completely disrupt the Sgt1-Hsp90 complex in the nucleotide-free state, while in the presence of AMP-PNP competition was saturated. The complex competition pattern of Sgt1 and Aha1 for Hsp90 binding could not be finally resolved. However, the presence of Aha1 might force Sgt1 to alter its binding mode. Finally, Sba1 binds to the closed state of Hsp90 (Ali et al., 2006, Li et al., 2011, Richter et al., 2004). The CS-domain containing co-chaperone was not able to bind simultaneously with Sgt1 to Hsp90, but did disrupt the Hsp90-Sgt1 complex in a concentration-dependent manner. The crystal structure of the plant Sgt1 CS domain with the Hsp90 NTD suggested a different binding interfaces in comparison to Sba1 (Zhang et al., 2008), yet Eckl *et al.* reasoned that the crystal structure might display the binding to the open conformation of Hsp90 (Eckl et al., 2014). The competition of Sgt1 and Sba1 further supports the idea of conformation-specific binding interfaces for Sgt1. Moreover, the preference of Sgt1 to bind to the closed state of Hsp90 and the concomitant competition with Sba1 tempt to speculate about a Sba1-like function of Sgt1 within the co-chaperone cycle. Noteworthy, the ability of Sgt1 to form a quaternary complex consisting of Sgt1, Hsp90, Hsp70 and Hsp40 suggests a client transfer function between those two chaperone systems like Sti1. This allows speculating about a unique client entrance point at the close state of Hsp90.

Taken together, Sgt1 is able to act during the early Hsp90 co-chaperone cycle also in cooperation with TPR-containing co-chaperones. The conformational rearrangement of Hsp90 accelerated by Aha1 most likely drives the conformation-specific binding of Sgt1 to the closed state. In the late stage a unique role of Sgt1 is implemented. Conceivably, Sgt1 could introduce a client protein in the closed state. Furthermore, Sgt1 might delay the action of Sba1, thereby tuning the dwell-time of client proteins. It could be also conceivable, that Sgt1 extracts a client protein before a Sba1-Hsp90 complex is formed. This gives the possibility to speculate about a Sgt1-specific Hsp90-cycle entrance or exit.

5.5. Sgt1's interplay with the Hsp70 system

Sgt1 was previously reported to interact not only with Hsp90 but also with Hsp70 (Noel et al., 2007, Spiechowicz et al., 2007). The interaction with Hsp70 was thought to be mediated by the essential SGS domain of Sgt1. *In vitro* complex formation monitored by AUC could not confirm a direct interaction between Sgt1 and Hsp70 nor between the SGS domain and Hsp70. However, *in vivo* pull-down experiments reinforced the binding between the SGS domain and the Hsp70 system. The analysis of the interplay of the monomeric Sgt1 mutant H59A with the Hsp70 system suggested that Sgt1 binds to Hsp40. Thus, the formation of the trimeric Sgt1-Hsp40-Hsp70 complex is mediated by the initial interaction of Sgt1 with Hsp40. Notably; Hsp40 was pulled down together with the SGS domain *in vivo* suggesting that the essential domain of Sgt1 provides the binding site.

Strikingly, the phospho-mimic mutant S361D of Sgt1 showed an increased preference for interaction with the Hsp70 system *in vivo.* The serine to aspartate substitution at position 361 is lethal for yeast. Interestingly, the structure determination of the SGS domain by NMR revealed a dynamic conformation around serine 361 suggesting a conformational switch. Hence, phosphorylation of serine 361 might decide the fate of a certain client protein by dictating treatment by a defined chaperone system. However, locking the system in the phospho-state as mimicked by the aspartate substitution drives cell death. It is tempting to speculate that the dysregulation of a distinct client (set) is accountable for cell death or a global disorder of the chaperone systems. Noteworthy, previously published changes in the binding pattern regarding the phospho-mimic mutant S361D, like the dimerization incompetence or the Skp1 binding impairment, were disproven (Bansal et al., 2009a).

Briefly, the essential SGS domain of Sgt1 mediates the integration into the Hsp70 chaperone system by interacting with Hsp40. The conformational switch residing in the crucial stable helix II of the SGS domain dictates chaperone system specificity for Sgt1 favoring the Hsp70 system if phosphorylated.

5.6. Physical and genetic interaction analysis of Sgt1

The discovery of Sgt1 dates back to a genetic interaction with the thermo-sensitive *skp1-4* strain (Kitagawa et al., 1999). Subsequent interaction studies on Sgt1 assigned a role in the assembly of the inner kinetochore complex as well as SCF-E3-ligase complexes (Bansal et al., 2004, Catlett and Kaplan, 2006, Willhoft et al., 2017). Additionally, high-throughput studies on the protein interaction networks and genetic interaction networks of *Saccharomyces cerevisiae* could support initial findings and further extended the view on Sgt1 (Uetz et al., 2000, Ho et al., 2002, Gong et al., 2009, Costanzo et al., 2016). However, the biological role of Sgt1 is still enigmatic. In this study the analysis of the physical interactome of Sgt1 by pull-down experiments coupled to mass spectrometry and a small-scale synthetic genetic array (SGA) using the Sgt1-depletable TetO7-SGT1 strain were carried out to enhance the understanding of Sgt1's biological role. Further the essential role of Sgt1 was addressed by determining the physical interactome of the SGS domain at different cell cycle states.

The physical interactome analysis of Sgt1 yielded previously identified interactors like Skp1, Hsp90 and Hsp70s (Kitagawa et al., 1999, Lingelbach and Kaplan, 2004, Willmund et al., 2013). Moreover, a broad network of ribosomal proteins was detected. So far, genetic interactions between Sgt1 and some ribosomal proteins were reported (Costanzo et al., 2016). Determination of the statistical overrepresented biological processes points to a role of Sgt1 in the disassembly of protein complexes as well as the organization of these. Mostly, the enrichment of those processes can be assigned to the presence of several ribosomal proteins. Hence, also processes like ribosome biogenesis were enriched. Interestingly, chaperones known to act at the ribosome could be detected, like Ssb1 and the NAC component, Egd1. Furthermore, the SGA analysis displayed negative genetic interaction between Sgt1 and the ribosome-associated complex (RAC), namely Zuo1 and Ssz1, additionally supporting a role of Sgt1 in ribosome-associated processes, especially in *de novo* protein folding. The genetic interaction with Zuo1 was also reported by Costanzo *et al.* (Costanzo et al., 2016). The importance of ribosome-associated processes was further underlined by the occurrence of RAC and NAC components among the SGS interactors. The essential domain of Sgt1 showed an even broader network of chaperone interactions compared to full-length Sgt1 consisting of parts of the Prefoldin complex and TRiC, Hsp70s, Hsp110s, RAC and NAC. Additionally, a large number of ribosomal proteins were among the interactors in the hydroxyurea and the nocodazole set. The arrest in the G_1 phase via α-factor did not show any ribosomal proteins, which in turn might indicate a cell cycle-specific function of Sgt1. However, again ribosome-associated chaperones were co-precipitated with the SGS domain. Even though, the enriched proteins varied between the different cell cycle states, the determination of overrepresented biological processes did show a significant overlap indicating an overall consistent function of the essential domain during the cell cycle. However, open questions

remain, such as whether the SGS domain directly interacts with a broad spectrum of chaperones or the cooperative action on a specific client leads to the enrichment.

In sum, the interaction studies on Sgt1 suggest the involvement in ribosome-associated processes ranging from ribosome biogenesis to ribosome-associated folding. Additionally, the physical interactome indicates the coordinated action of Sgt1 with a broad range of different chaperone systems. Notably, the essential SGS domain is seemingly also involved in those processes and interactions.

5.7. The chaperone cycle of Sgt1

Hitherto, Sgt1 was linked via its CS domain to the Hsp90 chaperone machinery and via its SGS domain to Hsp70 (Lee et al., 2004b, Catlett and Kaplan, 2006, Spiechowicz et al., 2007). This study provides further insights into the integration of Sgt1 in both chaperone systems, in fact it allows the connection of both mediated by Sgt1. Additionally, the conducted interactome studies on Sgt1 further suggest that Sgt1 interacts with an even broader network of chaperones. In the following a potential chaperone cycle of Sgt1 is depicted (Fig 35).

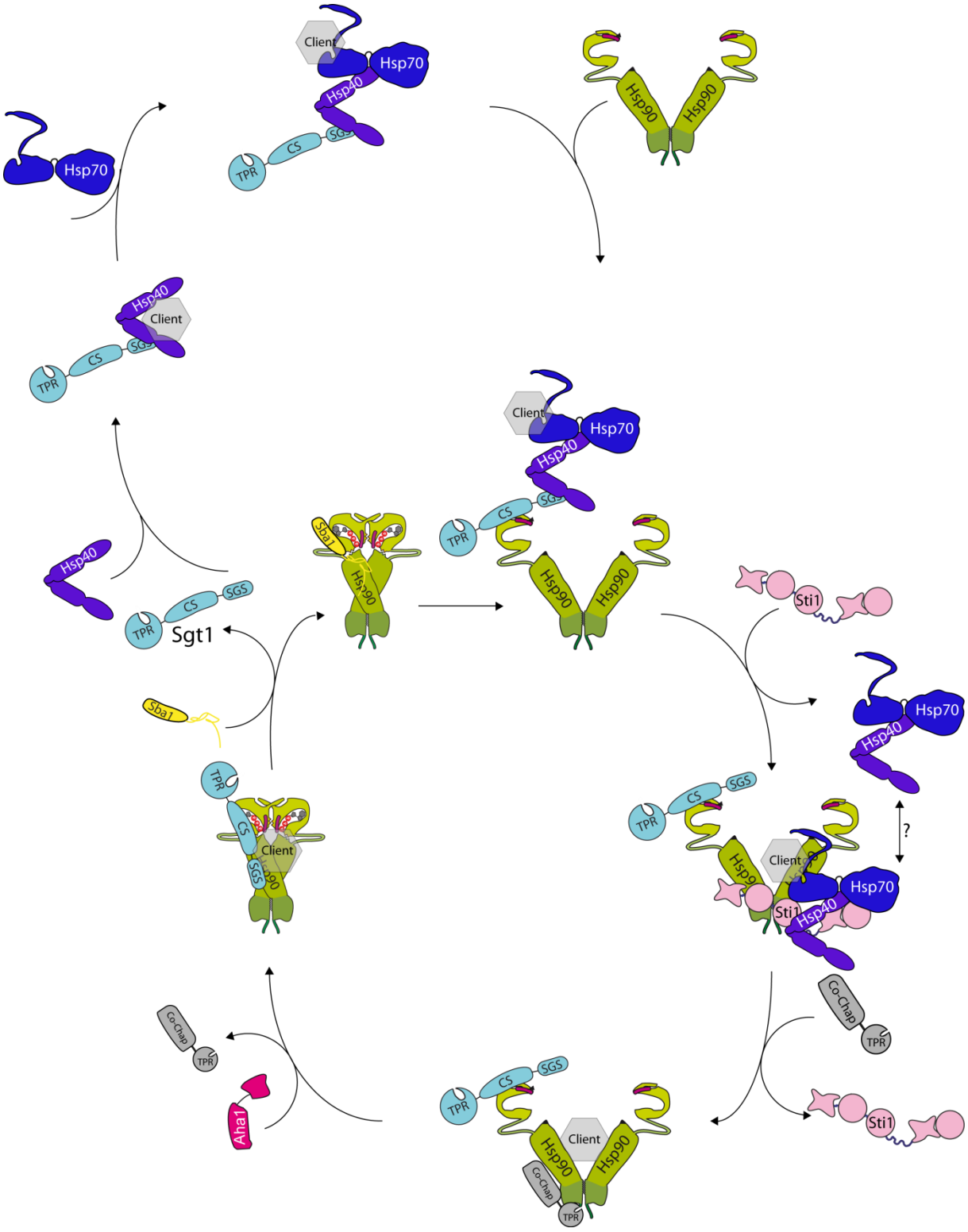

Figure 36: Chaperone cycle of Sgt1. Sgt1 enters the Hsp70 system by interacting with Hsp40. By facilitating a bridging complex between Hsp90 and Hsp40/Hsp70, Sgt1 traverses to the Hsp90 machinery. Trimeric complex formation with TPR-containing co-chaperones allows simultaneous action. Acceleration of the conformational cycle of Hsp90 by Aha1 drives the conformation-specific binding of Sgt1. Ultimately, Sba1 compete for binding to the closed Hsp90 releasing Sgt1.

Initially, Sgt1 interacts via the essential SGS domain with Hsp40, which allows the entering into the Hsp70 machinery. Whether client recruitment is accomplished by Sgt1 or Hsp40 remains an open question. Additionally, Sgt1 might modulate the client specifity of Hsp40 or *vice versa*. Subsequently, trimeric complex formation with Hsp70 occurs. Phosphorylation of Sgt1 enhances the interplay with the Hsp70 machinery. The Sgt1-Hsp40-Hsp70 complex might prime a specific client for the transfer to Hsp90. Next, Hsp90 joins into this putative "priming complex" by interacting with the CS domain of Sgt1. This bridging complex forms the entrance to the Hsp90 machinery. Within the Hsp90 co-chaperone cycle, Sti1 can act concomitant with Sgt1. If Sti1 simultaneously with Sgt1 bridges the Hsp70- with the Hsp90-machinery remains enigmatic. Subsequent, TPR-containing Hsp90 co-chaperones, which bind to the MEEVD motif of Hsp90, can enter the Sgt1-Hsp90 complex for cooperative action. The acceleration of the closing of Hsp90 by Aha1 drives Sgt1's conformation-specific binding alteration. Finally, Sgt1 binds to the closed state of Hsp90, which is the favored conformational state of Hsp90 for Sgt1 interaction. Ultimately, Sba1 can compete for binding to Hsp90 releasing Sgt1 from the complex. If Sgt1 provides a unique entrance into the Hsp90 machinery at the closed state is unresolved. Additionally, an open question remains if Sgt1 exits the Hsp90 machinery bound to a client or the client reached a final state. Besides, the interactome studies suggest that Sgt1's action might already begin upstream of the Hsp70- and Hsp90-machinery collaborating with ribosome-associated chaperones and early acting chaperones.

6. Perspective

In this thesis the essential Hsp90 co-chaperone Sgt1 was dissected by the combination of *in vivo* and *in vitro* methods. This study provides an extended understanding of the essential part of Sgt1 as well as the interplay of Sgt1 with the chaperone network. However, several questions remain unresolved.

The analysis of the essential part of Sgt1 revealed that the SGS domain solely harbors the *in vivo* relevant function. NMR studies could reveal the architecture of the essential domain. Since a structural model of the SGS domain is still lacking, extended NMR experiments could be applied to determine the structure of the essential domain. Further dissection of the SGS domain demonstrated that the stable helix II is the most crucial for function. The combination of NMR data and the previously reported lethal phospho-mimic mutant S361D suggests a conformational switch, which resides in this helix. To resolve the mechanistic details of the putative conformational switch, NMR studies on the phospho-mimic mutant would be helpful. In addition, to understand the *in vivo* relevance of the switching, physical interactome studies using the S361D mutant would be suitable. To this end, an alteration in the preference for Hsp70 could be reported for S361D *in vivo*. Further *in vitro* dissection of the complex formation will be needed to understand the mechanism.

Sgt1's interaction with Hsp90 was further analyzed in this thesis indicating an extended binding interface of Hsp90 and probably also different interaction modes depending on the conformational state of Hsp90. Again, with the help of NMR, the interaction between Sgt1 and Hsp90 could be resolved in the future at single residue level to elucidate the still enigmatic interaction.

The integration of Sgt1 into the Hsp70 system suggested that Sgt1 initially interacts with Hsp40. Further *in vitro* analysis will have to address the order of interaction during trimeric complex formation of Sgt1, Hsp70 and Hsp40. Additionally, the mechanistic insight of the interaction could be resolved.

The integration of Sgt1 into the Hsp90 co-chaperone cycle in combination with the Hsp70 system analysis allowed hypothesizing about a Sgt1-driven interplay of the two chaperone machineries. The progression order and relevance of certain complexes needs to be further confirmed by *in vitro* and *in vivo* analysis. However, the current model also leaves questions open. The most important one would be the integration of a client protein. For that, a model client could be used to determine possible and critical complexes for maturation. Moreover, the identification of a Sgt1-specific client and its integration would ultimately be crucial for confirmation. The pull-down experiments further suggest an interaction between Sgt1 and Cdc37. This interplay of two essential Hsp90 co-chaperones should be further dissected by genetic analysis as well as *in vitro* interaction studies to elucidate the nature of this module.

The interactome studies on Sgt1 imply a biological role in early protein folding and probably ribosome homeostasis. The impact of Sgt1 on protein biosynthesis should be further addressed by monitoring *de novo* protein synthesis using isotope-labeling. Moreover, ribosome biogenesis and homeostasis could be studied by ribosome fractionation.

In short, the chaperone cycle of Sgt1 should be further elucidated, in particular the interaction of Sgt1 with Hsp90 and Hsp40 should be resolved at single amino acid level. The started exploration of Sgt1's essential biological role should be extended focusing on ribosome-associated protein homeostasis.

7. List of abbreviations

For amino acids the one and three letter code was used.

5-FOA	5-Fluoroorotic acid
ACD	α-crystallin domain
ADP	Adenosine diphosphate
ALP	Autophagy-lysosomal pathway
AMP-PNP	Adenylyl-imidodiphosphate
ATP	Adenosine triphosphate
ATPγS	Adenosine 5'-(3-thiotriphosphate)
AUC	Analytical ultracentrifugation
cAMP	Cyclic adenosine monophosphate
CASA	chaperone-assisted selective autophagy
CD	Circular dichroism
CMA	chaperone-mediated autophagy
CS	Chord-containing proteins and Sgt1
CTD	C-terminal domain
CTR	C-terminal region
DNA	Deoxyribonucleic acid
dNTP	Deoxynucleotide
E.coli	*Escherichia coli*
ER	Endoplasmic reticulum
FRET	Förster resonance energy transfer
GFP	Green fluorescent protein
GO	Gene ontology
GPD	Glyceraldehyde 3-phosphate dehydrogenase
HDX	Hydrogen/deuterium exchange
Hsp100	Heat shock protein 100 kDa
Hsp110	Heat shock protein 110 kDa
Hsp40	Heat shock protein 40 kDa
Hsp60	Heat shock protein 60 kDa
Hsp70	Heat shock protein 70 kDa
Hsp90	Heat shock protein 90 kDa
IP	Immunoprecipitation
JDP	J-domain containing protein
K_D	Dissociation constant
LB	Lysogeny broth
LRR	leucine rich repeat
MD	Middle domain
MS	Mass spectrometry
NAC	Nascent polypeptide-associated complex
NBD	nucleotide binding domain
NEF	nucleotide exchange factor
NMR	Nuclear magnetic resonance
NTD	N-terminal domain
NTR	N-terminal region
OD	Optical density
PCR	Polymerase chain reaction
pH	*potentia Hydrogenii*
P_i	Inorganic phosphate
PN	Proteostasis network

PTM	Posttranslational modification
RAC	Ribosome-associated complex
SBD	Substrate binding domain
SCF	Skp1-Cullin-F-box
SGA	Synthetic genetic array
SGS	Sgt1 specific
sHsps	Small heat shock protein
TF	Trigger factor
TPR	tetratricopepetide repeat
TRiC/CCT	TCP-1 ring complex
UPS	Ubiquitin-proteasome system
URA	Uracil

8. List of Figures

9. List of Tables

10. References

ABU-FARHA, M., LANOUETTE, S., ELISMA, F., TREMBLAY, V., BUTSON, J., FIGEYS, D. & COUTURE, J. F. 2011. Proteomic analyses of the SMYD family interactomes identify HSP90 as a novel target for SMYD2. *J Mol Cell Biol,* 3**,** 301-8.

ALI, M. M. U., MARK ROE, S., VAUGHAN, C. K., MEYER, P., PANARETOU, B., PIPER, P. W., PRODROMOU, C. & PEARL, L. H. 2006. Crystal structure of an Hsp90-nucleotide-p23/Sba1 closed chaperone complex. *Nature,* 440**,** 1013-1017.

ANDERSSON, V., HANZEN, S., LIU, B., MOLIN, M. & NYSTROM, T. 2013. Enhancing protein disaggregation restores proteasome activity in aged cells. *Aging (Albany NY),* 5**,** 802-12.

ANFINSEN, C. B. 1973. Principles that govern the folding of protein chains. *Science,* 181**,** 223-30.

AOYAGI, S. & ARCHER, T. K. 2005. Modulating molecular chaperone Hsp90 functions through reversible acetylation. *Trends Cell Biol,* 15**,** 565-7.

ARNDT, V., DICK, N., TAWO, R., DREISEIDLER, M., WENZEL, D., HESSE, M., FURST, D. O., SAFTIG, P., SAINT, R., FLEISCHMANN, B. K., HOCH, M. & HOHFELD, J. 2010. Chaperone-assisted selective autophagy is essential for muscle maintenance. *Curr Biol,* 20**,** 143-8.

ASSIMON, V. A., SOUTHWORTH, D. R. & GESTWICKI, J. E. 2015. Specific Binding of Tetratricopeptide Repeat Proteins to Heat Shock Protein 70 (Hsp70) and Heat Shock Protein 90 (Hsp90) Is Regulated by Affinity and Phosphorylation. *Biochemistry,* 54**,** 7120-31.

AZEVEDO, C., BETSUYAKU, S., PEART, J., TAKAHASHI, A., NOEL, L., SADANANDOM, A., CASAIS, C., PARKER, J. & SHIRASU, K. 2006. Role of SGT1 in resistance protein accumulation in plant immunity. *EMBO J,* 25**,** 2007-16.

BACKE, S. J., SAGER, R. A., WOODFORD, M. R., MAKEDON, A. M. & MOLLAPOUR, M. 2020. Post-translational modifications of Hsp90 and translating the chaperone code. *J Biol Chem,* 295**,** 11099-11117.

BAKER, J. D., SHELTON, L. B., ZHENG, D., FAVRETTO, F., NORDHUES, B. A., DARLING, A., SULLIVAN, L. E., SUN, Z., SOLANKI, P. K., MARTIN, M. D., SUNTHARALINGAM, A., SABBAGH, J. J., BECKER, S., MANDELKOW, E., UVERSKY, V. N., ZWECKSTETTER, M., DICKEY, C. A., KOREN, J., III & BLAIR, L. J. 2017. Human cyclophilin 40 unravels neurotoxic amyloids. *PLoS Biology,* 15.

BALCHIN, D., HAYER-HARTL, M. & HARTL, F. U. 2016. In vivo aspects of protein folding and quality control. *Science,* 353**,** aac4354.

BALCHIN, D., HAYER-HARTL, M. & HARTL, F. U. 2020. Recent advances in understanding catalysis of protein folding by molecular chaperones. *FEBS Lett*.

BALI, P., PRANPAT, M., BRADNER, J., BALASIS, M., FISKUS, W., GUO, F., ROCHA, K., KUMARASWAMY, S., BOYAPALLE, S., ATADJA, P., SETO, E. & BHALLA, K. 2005. Inhibition of histone deacetylase 6 acetylates and disrupts the chaperone function of heat shock protein 90: A novel basis for antileukemia activity of histone deacetylase inhibitors. *Journal of Biological Chemistry,* 280**,** 26729-26734.

BALLINGER, C. A. 1999. Identification of CHIP, a novel tetratricopeptide repeat-containing protein that interacts with heat shock proteins and negatively regulates chaperone functions. *Mol. Cell. Biol.,* 19.

BANSAL, P. K., ABDULLE, R. & KITAGAWA, K. 2004. Sgt1 associates with Hsp90: an initial step of assembly of the core kinetochore complex. *Mol Cell Biol,* 24**,** 8069-79.

BANSAL, P. K., MISHRA, A., HIGH, A. A., ABDULLE, R. & KITAGAWA, K. 2009a. Sgt1 dimerization is negatively regulated by protein kinase CK2-mediated phosphorylation at Ser361. *J Biol Chem,* 284**,** 18692-8.

BANSAL, P. K., NOURSE, A., ABDULLE, R. & KITAGAWA, K. 2009b. Sgt1 dimerization is required for yeast kinetochore assembly. *J Biol Chem,* 284**,** 3586-92.

BARDWELL, J. C. & CRAIG, E. A. 1988. Ancient heat shock gene is dispensable. *Journal of bacteriology,* 170**,** 2977-2983.

BEKKER-JENSEN, D. B., KELSTRUP, C. D., BATTH, T. S., LARSEN, S. C., HALDRUP, C., BRAMSEN, J. B., SORENSEN, K. D., HOYER, S., ORNTOFT, T. F., ANDERSEN, C. L., NIELSEN, M. L. & OLSEN, J. V. 2017. An Optimized Shotgun Strategy for the Rapid Generation of Comprehensive Human Proteomes. *Cell Syst,* 4**,** 587-599 e4.

BENJAMINI, Y. & HOCHBERG, Y. 1995. Controlling the False Discovery Rate: A Practical and Powerful Approach to Multiple Testing. 57**,** 289-300.

BHATTACHARYYA, S., YU, H., MIM, C. & MATOUSCHEK, A. 2014. Regulated protein turnover: snapshots of the proteasome in action. *Nat Rev Mol Cell Biol,* 15**,** 122-33.

BIEBL, M. M. & BUCHNER, J. 2019. Structure, Function, and Regulation of the Hsp90 Machinery. *Cold Spring Harb Perspect Biol,* 11.

BIEBL, M. M., RIEDL, M. & BUCHNER, J. 2020. Hsp90 Co-chaperones Form Plastic Genetic Networks Adapted to Client Maturation. *Cell Rep,* 32**,** 108063.

BLAGOSKLONNY, M. V., TORETSKY, J., BOHEN, S. & NECKERS, L. 1996. Mutant conformation of p53 translated in vitro or in vivo requires functional HSP90. *Proceedings of the National Academy of Sciences of the United States of America,* 93**,** 8379-8383.

BLOEMENDAL, H. 1977. The vertebrate eye lens. *Science,* 197**,** 127-38.

BOCZEK, E. E., REEFSCHLÄGER, L. G., DEHLING, M., STRULLER, T. J., HÄUSLER, E., SEIDL, A., KAILA, V. R. I. & BUCHNER, J. 2015. Conformational processing of oncogenic v-Src kinase by the molecular chaperone Hsp90. *Proceedings of the National Academy of Sciences of the United States of America,* 112**,** E3189-E3198.

BOEKE, J. D., TRUEHEART, J., NATSOULIS, G. & FINK, G. R. 1987. 5-Fluoroorotic acid as a selective agent in yeast molecular genetics. *Methods Enzymol,* 154**,** 164-75.

BOHEN, S. P. & YAMAMOTO, K. R. 1993. Isolation of Hsp90 mutants by screening for decreased steroid receptor function. *Proceedings of the National Academy of Sciences of the United States of America,* 90**,** 11424-11428.

BORGESE, N., MOK, W., KREIBICH, G. & SABATINI, D. D. 1974. Ribosomal-membrane interaction: in vitro binding of ribosomes to microsomal membranes. *J Mol Biol,* 88**,** 559-80.

BORKOVICH, K. A., FARRELLY, F. W., FINKELSTEIN, D. B., TAULIEN, J. & LINDQUIST, S. 1989. hsp82 Is an essential protein that is required in higher concentrations for growth of cells at higher temperatures. *Molecular and Cellular Biology,* 9**,** 3919-3930.

BOSE, S., WEIKL, T., BÜGL, H. & BUCHNER, J. 1996. Chaperone function of Hsp90-associated proteins. *Science,* 274**,** 1715-1717.

BRADFORD, M. M. 1976. A rapid and sensitive method for the quantitation of microgram quantities of protein utilizing the principle of protein-dye binding. *Anal Biochem,* 72**,** 248-54.

BRAUN, N., ZACHARIAS, M., PESCHEK, J., KASTENMULLER, A., ZOU, J., HANZLIK, M., HASLBECK, M., RAPPSILBER, J., BUCHNER, J. & WEINKAUF, S. 2011. Multiple molecular architectures of the eye lens chaperone alphaB-crystallin elucidated by a triple hybrid approach. *Proc Natl Acad Sci U S A,* 108**,** 20491-6.

BREHME, M., VOISINE, C., ROLLAND, T., WACHI, S., SOPER, J. H., ZHU, Y., ORTON, K., VILLELLA, A., GARZA, D., VIDAL, M., GE, H. & MORIMOTO, R. I. 2014. A chaperome subnetwork safeguards proteostasis in aging and neurodegenerative disease. *Cell Reports,* 9**,** 1135-1150.

BREHMER, D. 2001. Tuning of chaperone activity of Hsp70 proteins by modulation of nucleotide exchange. *Nat. Struct. Biol.,* 8.

BRESLOW, D. K., CAMERON, D. M., COLLINS, S. R., SCHULDINER, M., STEWART-ORNSTEIN, J., NEWMAN, H. W., BRAUN, S., MADHANI, H. D., KROGAN, N. J. & WEISSMAN, J. S. 2008. A comprehensive strategy enabling high-resolution functional analysis of the yeast genome. *Nat Methods,* 5**,** 711-8.

BRETER, H. J., FERGUSON, J., PETERSON, T. A. & REED, S. I. 1983. Isolation and transcriptional characterization of three genes which function at start, the controlling event of the Saccharomyces cerevisiae cell division cycle: CDC36, CDC37, and CDC39. *Mol Cell Biol,* 3**,** 881-91.

BRINKER, A., SCHEUFLER, C., VON DER MÜLBE, F., FLECKENSTEIN, B., HERRMANN, C., JUNG, G., MOAREFI, I. & ULRICH HARTL, F. 2002. Ligand discrimination by TPR domains. Relevance and selectivity of EEVD-recognition in Hsp70·Hop·Hsp90 complexes. *Journal of Biological Chemistry,* 277**,** 19265-19275.

BROCKWELL, D. J. & RADFORD, S. E. 2007. Intermediates: ubiquitous species on folding energy landscapes? *Curr Opin Struct Biol,* 17**,** 30-7.

BROWN, P. H., BALBO, A. & SCHUCK, P. 2009. On the analysis of sedimentation velocity in the study of protein complexes. *Eur Biophys J,* 38**,** 1079-99.

BRUGGE, J. S., ERIKSON, E. & ERIKSON, R. L. 1981. The specific interaction of the Rous sarcoma virus transforming protein, pp60src, with two cellular proteins. *Cell,* 25**,** 363-372.

BUCZYNSKI, G., SLEPENKOV, S. V., SEHORN, M. G. & WITT, S. N. 2001. Characterization of a lidless form of the molecular chaperone DnaK: deletion of the lid increases peptide on- and off-rate constants. *J. Biol. Chem.,* 276.

CALDERWOOD, S. K. & GONG, J. 2016. Heat Shock Proteins Promote Cancer: It's a Protection Racket. *Trends in Biochemical Sciences,* 41**,** 311-323.

CALDERWOOD, S. K., KHALEQUE, M. A., SAWYER, D. B. & CIOCCA, D. R. 2006. Heat shock proteins in cancer: Chaperones of tumorigenesis. *Trends in Biochemical Sciences,* 31**,** 164-172.

CARRA, S., SEGUIN, S. J., LAMBERT, H. & LANDRY, J. 2008. HspB8 chaperone activity toward poly(Q)-containing proteins depends on its association with Bag3, a stimulator of macroautophagy. *J Biol Chem,* 283**,** 1437-44.

CASPERS, G. J., LEUNISSEN, J. A. & DE JONG, W. W. 1995. The expanding small heat-shock protein family, and structure predictions of the conserved "alpha-crystallin domain". *J Mol Evol,* 40**,** 238-48.

CATLETT, M. G. & KAPLAN, K. B. 2006. Sgt1p is a unique co-chaperone that acts as a client adaptor to link Hsp90 to Skp1p. *Journal of Biological Chemistry,* 281**,** 33739-33748.

CHEETHAM, M. E. & CAPLAN, A. J. 1998. Structure, function and evolution of DnaJ: conservation and adaptation of chaperone function. *Cell Stress Chaperones,* 3.

CHEN, B., ZHONG, D. & MONTEIRO, A. 2006. Comparative genomics and evolution of the HSP90 family of genes across all kingdoms of organisms. *BMC Genomics,* 7.

CHEN, K. C., QU, S., CHOWDHURY, S., NOXON, I. C., SCHONHOFT, J. D., PLATE, L., POWERS, E. T., KELLY, J. W., LANDER, G. C. & WISEMAN, R. L. 2017. The endoplasmic reticulum HSP40 co-chaperone ERdj3/DNAJB11 assembles and functions as a tetramer. *EMBO J,* 36**,** 2296-2309.

CHEN, S. & SMITH, D. F. 1998. Hop as an adaptor in the heat shock protein 70 (Hsp70) and Hsp90 chaperone machinery. *Journal of Biological Chemistry,* 273**,** 35194-35200.

CHEN, S., SULLIVAN, W. P., TOFT, D. O. & SMITH, D. F. 1998. Differential interactions of p23 and the TPR-containing proteins Hop, Cyp40, FKBP52 and FKBP51 with Hsp90 mutants. *Cell Stress and Chaperones,* 3**,** 118-129.

CHEN, Y., WANG, B., LIU, D., LI, J. J., XUE, Y., SAKATA, K., ZHU, L. Q., HELDT, S. A., XU, H. & LIAO, F. F. 2014. Hsp90 chaperone inhibitor 17-AAG Attenuates Aβ-induced synaptic toxicity and memory impairment. *Journal of Neuroscience,* 34**,** 2464-2470.

CHIOSIS, G., LUCAS, B., SHTIL, A., HUEZO, H. & ROSEN, N. 2002. Development of a purine-scaffold novel class of hsp90 binders that inhibit the proliferation of cancer cells and induce the degradation of Her2 tyrosine kinase. *Bioorganic and Medicinal Chemistry,* 10**,** 3555-3564.

CHITI, F. & DOBSON, C. M. 2006. Protein misfolding, functional amyloid, and human disease. *Annu Rev Biochem,* 75**,** 333-66.

CLARE, D. K., VASISHTAN, D., STAGG, S., QUISPE, J., FARR, G. W., TOPF, M., HORWICH, A. L. & SAIBIL, H. R. 2012. ATP-triggered conformational changes delineate substrate-binding and -folding mechanics of the GroEL chaperonin. *Cell,* 149**,** 113-23.

CLERICO, E. M., TILITSKY, J. M., MENG, W. & GIERASCH, L. M. 2015. How Hsp70 molecular machines interact with their substrates to mediate diverse physiological functions. *J. Mol. Biol.,* 427.

COHEN-KAPLAN, V., LIVNEH, I., AVNI, N., COHEN-ROSENZWEIG, C. & CIECHANOVER, A. 2016. The ubiquitin-proteasome system and autophagy: Coordinated and independent activities. *Int J Biochem Cell Biol,* 79**,** 403-418.

COHEN, P. 2000. The regulation of protein function by multisite phosphorylation--a 25 year update. *Trends Biochem Sci,* 25**,** 596-601.

COHEN, P. 2002. The origins of protein phosphorylation. *Nat Cell Biol,* 4**,** E127-30.

COHEN, T. & YAO, T. P. 2004. AcK-knowledge reversible acetylation. *Sci STKE,* 2004**,** pe42.

CONNELL, P. 2001. The co-chaperone CHIP regulates protein triage decisions mediated by heat-shock proteins. *Nat. Cell Biol.,* 3.

CONNELLY, C. & HIETER, P. 1996. Budding yeast SKP1 encodes an evolutionarily conserved kinetochore protein required for cell cycle progression. *Cell,* 86**,** 275-85.

COSTANZO, M., VANDERSLUIS, B., KOCH, E. N., BARYSHNIKOVA, A., PONS, C., TAN, G., WANG, W., USAJ, M., HANCHARD, J., LEE, S. D., PELECHANO, V., STYLES, E. B., BILLMANN, M., VAN LEEUWEN, J., VAN DYK, N., LIN, Z. Y., KUZMIN, E., NELSON, J., PIOTROWSKI, J. S., SRIKUMAR, T., BAHR, S., CHEN, Y., DESHPANDE, R., KURAT, C. F., LI, S. C., LI, Z., USAJ, M. M., OKADA, H., PASCOE, N., LUIS, B. J. S., SHARIFPOOR, S., SHUTERIQI, E., SIMPKINS, S. W., SNIDER, J., SURESH, H. G., TAN, Y., ZHU, H., MALOD-DOGNIN, N., JANJIC, V., PRZULJ, N., TROYANSKAYA, O. G., STAGLJAR, I., XIA, T., OHYA, Y., GINGRAS, A. C., RAUGHT, B., BOUTROS, M., STEINMETZ, L. M., MOORE, C. L., ROSEBROCK, A. P., CAUDY, A. A., MYERS, C. L., ANDREWS, B. & BOONE, C. 2016. A global genetic interaction network maps a wiring diagram of cellular function. *Science,* 353.

COX, D., SELIG, E., GRIFFIN, M. D., CARVER, J. A. & ECROYD, H. 2016. Small Heat-shock Proteins Prevent alpha-Synuclein Aggregation via Transient Interactions and Their Efficacy Is Affected by the Rate of Aggregation. *J Biol Chem,* 291**,** 22618-22629.

COX, D., WHITEN, D. R., BROWN, J. W. P., HORROCKS, M. H., SAN GIL, R., DOBSON, C. M., KLENERMAN, D., VAN OIJEN, A. M. & ECROYD, H. 2018. The small heat shock protein Hsp27 binds alpha-synuclein fibrils, preventing elongation and cytotoxicity. *J Biol Chem,* 293**,** 4486-4497.

COX, J., HEIN, M. Y., LUBER, C. A., PARON, I., NAGARAJ, N. & MANN, M. 2014a. Accurate proteome-wide label-free quantification by delayed normalization and maximal peptide ratio extraction, termed MaxLFQ. *Mol Cell Proteomics,* 13**,** 2513-26.

COX, J., HEIN, M. Y., LUBER, C. A., PARON, I., NAGARAJ, N. & MANN, M. 2014b. Accurate proteome-wide label-free quantification by delayed normalization and maximal peptide ratio extraction, termed MaxLFQ. *Molecular & cellular proteomics : MCP,* 13**,** 2513-2526.

COX, J. & MANN, M. 2008a. MaxQuant enables high peptide identification rates, individualized p.p.b.-range mass accuracies and proteome-wide protein quantification. *Nature Biotechnology,* 26**,** 1367.

COX, J. & MANN, M. 2008b. MaxQuant enables high peptide identification rates, individualized p.p.b.-range mass accuracies and proteome-wide protein quantification. *Nat Biotechnol,* 26**,** 1367-72.

CRAIG, E. A. 2018. Hsp70 at the membrane: driving protein translocation. *BMC Biol.,* 16.

CRAIG, E. A., HUANG, P., ARON, R. & ANDREW, A. 2006. The diverse roles of J-proteins, the obligate Hsp70 co-chaperone. *Rev Physiol Biochem Pharmacol,* 156**,** 1-21.

CRAIG, E. A. & MARSZALEK, J. 2017. How Do J-Proteins Get Hsp70 to Do So Many Different Things? *Trends Biochem Sci,* 42**,** 355-368.

CRIADO-MARRERO, M., REIN, T., BINDER, E. B., PORTER, J. T., KOREN, J., III & BLAIR, L. J. 2018. Hsp90 and FKBP51: Complex regulators of psychiatric diseases. *Philosophical Transactions of the Royal Society B: Biological Sciences,* 373.

CUNNINGHAM, C. N., KRUKENBERG, K. A. & AGARD, D. A. 2008. Intra- and intermonomer interactions are required to synergistically facilitate ATP hydrolysis in Hsp90. *Journal of Biological Chemistry,* 283**,** 21170-21178.

CUNNINGHAM, C. N., SOUTHWORTH, D. R., KRUKENBERG, K. A. & AGARD, D. A. 2012. The conserved arginine 380 of Hsp90 is not a catalytic residue, but stabilizes the closed conformation required for ATP hydrolysis. *Protein Science,* 21**,** 1162-1171.

CYR, D. M., LU, X. & DOUGLAS, M. G. 1992. Regulation of Hsp70 function by a eukaryotic DnaJ homolog. *J Biol Chem,* 267**,** 20927-31.

DA SILVA CORREIA, J., MIRANDA, Y., LEONARD, N. & ULEVITCH, R. 2007. SGT1 is essential for Nod1 activation. *Proc Natl Acad Sci U S A,* 104**,** 6764-9.

DAHIYA, V., AGAM, G., LAWATSCHECK, J., RUTZ, D. A., LAMB, D. C. & BUCHNER, J. 2019. Coordinated Conformational Processing of the Tumor Suppressor Protein p53 by the Hsp70 and Hsp90 Chaperone Machineries. *Mol Cell,* 74**,** 816-830 e7.

DATURPALLI, S., WAUDBY, C. A., MEEHAN, S. & JACKSON, S. E. 2013. Hsp90 inhibits α-synuclein aggregation by interacting with soluble oligomers. *Journal of Molecular Biology,* 425**,** 4614-4628.

DAVIES, A. E. & KAPLAN, K. B. 2010. Hsp90-Sgt1 and Skp1 target human Mis12 complexes to ensure efficient formation of kinetochore-microtubule binding sites. *J Cell Biol,* 189**,** 261-74.

DEL ALAMO, M., HOGAN, D. J., PECHMANN, S., ALBANESE, V., BROWN, P. O. & FRYDMAN, J. 2011. Defining the specificity of cotranslationally acting chaperones by systematic analysis of mRNAs associated with ribosome-nascent chain complexes. *PLoS Biol,* 9**,** e1001100.

DELAGLIO, F., GRZESIEK, S., VUISTER, G. W., ZHU, G., PFEIFER, J. & BAX, A. 1995. NMRPipe: a multidimensional spectral processing system based on UNIX pipes. *J Biomol NMR,* 6**,** 277-93.

DELBECQ, S. P., ROSENBAUM, J. C. & KLEVIT, R. E. 2015. A Mechanism of Subunit Recruitment in Human Small Heat Shock Protein Oligomers. *Biochemistry,* 54**,** 4276-84.

DEMAND, J., ALBERTI, S., PATTERSON, C. & HOHFELD, J. 2001. Cooperation of a ubiquitin domain protein and an E3 ubiquitin ligase during chaperone/proteasome coupling. *Curr Biol,* 11**,** 1569-77.

DESANTIS, M. E., LEUNG, E. H., SWEENY, E. A., JACKREL, M. E., CUSHMAN-NICK, M., NEUHAUS-FOLLINI, A., VASHIST, S., SOCHOR, M. A., KNIGHT, M. N. & SHORTER, J. 2012. Operational plasticity enables hsp104 to disaggregate diverse amyloid and nonamyloid clients. *Cell,* 151**,** 778-793.

DESANTIS, M. E. & SHORTER, J. 2012. Hsp104 drives "protein-only" positive selection of Sup35 prion strains encoding strong [PSI(+)]. *Chem Biol,* 19**,** 1400-10.

DEUERLING, E., SCHULZE-SPECKING, A., TOMOYASU, T., MOGK, A. & BUKAU, B. 1999. Trigger factor and DnaK cooperate in folding of newly synthesized proteins. *Nature,* 400**,** 693-6.

DEUERLING, E. G., M.; KREFT, S.G. 2019. Chaperone Interactions at the Ribosome. *Cold Spring Harb Perspect Biol.,* 1.

DICKEY, C. A., DUNMORE, J., LU, B., WANG, J. W., LEE, W. C., KAMAL, A., BURROWS, F., ECKMAN, C., HUTTON, M. & PETRUCELLI, L. 2006. HSP induction mediates selective clearance of tau phosphorylated at proline-directed Ser/Thr sites but not KXGS (MARK) sites. *FASEB Journal,* 20**,** 753-755.

DICKEY, C. A., KAMAL, A., LUNDGREN, K., KLOSAK, N., BAILEY, R. M., DUNMORE, J., ASH, P., SHORAKA, S., ZLATKOVIC, J., ECKMAN, C. B., PATTERSON, C., DICKSON, D. W., NAHMAN JR, N. S., HUTTON, M., BURROWS, F. & PETRUCELLI, L. 2007. The high-affinity HSP90-CHIP complex recognizes and selectively degrades phosphorylated tau client proteins. *Journal of Clinical Investigation,* 117**,** 648-658.

DIKIC, I. 2017. Proteasomal and Autophagic Degradation Systems. *Annu Rev Biochem,* 86**,** 193-224.

DILL, K. A. & MACCALLUM, J. L. 2012. The protein-folding problem, 50 years on. *Science,* 338**,** 1042-6.

DIMAS, D. T. H., PERLEPE, C. D., SERGENTANIS, T. N., MISITZIS, I., KONTZOGLOU, K., PATSOURIS, E., KOURAKLIS, G., PSALTOPOULOU, T. & NONNI, A. 2018. The prognostic significance of hsp70/hsp90 expression in breast cancer: A systematic review and meta-analysis. *Anticancer Research,* 38**,** 1551-1562.

DINGWALL, C. & LASKEY, R. A. 1990. Nucleoplasmin: the archetypal molecular chaperone. *Semin Cell Biol,* 1**,** 11-7.

DINNER, A. R., SALI, A., SMITH, L. J., DOBSON, C. M. & KARPLUS, M. 2000. Understanding protein folding via free-energy surfaces from theory and experiment. *Trends Biochem Sci,* 25**,** 331-9.
DITZEL, L., LOWE, J., STOCK, D., STETTER, K. O., HUBER, H., HUBER, R. & STEINBACHER, S. 1998. Crystal structure of the thermosome, the archaeal chaperonin and homolog of CCT. *Cell,* 93**,** 125-38.
DOBSON, C. M. 2003. Protein folding and misfolding. *Nature,* 426**,** 884-90.
DOBSON, C. M. & KARPLUS, M. 1999. The fundamentals of protein folding: bringing together theory and experiment. *Curr Opin Struct Biol,* 9**,** 92-101.
DOLINSKI, K. J., CARDENAS, M. E. & HEITMAN, J. 1998. CNS1 encodes an essential p60/Sti1 homolog in Saccharomyces cerevisiae that suppresses cyclophilin 40 mutations and interacts with Hsp90. *Mol Cell Biol,* 18**,** 7344-52.
DOLLINS, D. E., WARREN, J. J., IMMORMINO, R. M. & GEWIRTH, D. T. 2007. Structures of GRP94-Nucleotide Complexes Reveal Mechanistic Differences between the hsp90 Chaperones. *Molecular Cell,* 28**,** 41-56.
DONG, Y., ZHANG, S., WU, Z., LI, X., WANG, W. L., ZHU, Y., STOILOVA-MCPHIE, S., LU, Y., FINLEY, D. & MAO, Y. 2019. Cryo-EM structures and dynamics of substrate-engaged human 26S proteasome. *Nature,* 565**,** 49-55.
DONLIN, L. T., ANDRESEN, C., JUST, S., RUDENSKY, E., PAPPAS, C. T., KRUGER, M., JACOBS, E. Y., UNGER, A., ZIESENISS, A., DOBENECKER, M. W., VOELKEL, T., CHAIT, B. T., GREGORIO, C. C., ROTTBAUER, W., TARAKHOVSKY, A. & LINKE, W. A. 2012. Smyd2 controls cytoplasmic lysine methylation of Hsp90 and myofilament organization. *Genes Dev,* 26**,** 114-9.
DORING, K., AHMED, N., RIEMER, T., SURESH, H. G., VAINSHTEIN, Y., HABICH, M., RIEMER, J., MAYER, M. P., O'BRIEN, E. P., KRAMER, G. & BUKAU, B. 2017. Profiling Ssb-Nascent Chain Interactions Reveals Principles of Hsp70-Assisted Folding. *Cell,* 170**,** 298-311 e20.
DOUGHERTY, J. J., PURI, R. K. & TOFT, D. O. 1984. Polypeptide components of two 8 S forms of chicken oviduct progesterone receptor. *Journal of Biological Chemistry,* 259**,** 8004-8009.
DOUGLAS, N. R., REISSMANN, S., ZHANG, J., CHEN, B., JAKANA, J., KUMAR, R., CHIU, W. & FRYDMAN, J. 2011. Dual action of ATP hydrolysis couples lid closure to substrate release into the group II chaperonin chamber. *Cell,* 144**,** 240-52.
DUBACQ, C., GUEROIS, R., COURBEYRETTE, R., KITAGAWA, K. & MANN, C. 2002. Sgt1p contributes to cyclic AMP pathway activity and physically interacts with the adenylyl cyclase Cyr1p/Cdc35p in budding yeast. *Eukaryot Cell,* 1**,** 568-82.
DUBINSKA-MAGIERA, M., JABLONSKA, J., SACZKO, J., KULBACKA, J., JAGLA, T. & DACZEWSKA, M. 2014. Contribution of small heat shock proteins to muscle development and function. *FEBS Lett,* 588**,** 517-30.
DUINA, A. A., MARSH, J. A. & GABER, R. F. 1996. Identification of two CyP-40-like cyclophilins in Saccharomyces cerevisiae, one of which is required for normal growth. *Yeast,* 12**,** 943-952.
DUINA, A. A., MARSH, J. A., KURTZ, R. B., CHANG, H. C. J., LINDQUIST, S. & GABER, R. F. 1998. The peptidyl-prolyl isomerase domain of the CyP-40 cyclophilin homolog Cpr7 is not required to support growth or glucocorticoid receptor activity in Saccharomyces cerevisiae. *Journal of Biological Chemistry,* 273**,** 10819-10822.
DUNKER, A. K., OLDFIELD, C. J., MENG, J., ROMERO, P., YANG, J. Y., CHEN, J. W., VACIC, V., OBRADOVIC, Z. & UVERSKY, V. N. 2008. The unfoldomics decade: an update on intrinsically disordered proteins. *BMC Genomics,* 9 Suppl 2**,** S1.
DURAN, E. C., WEAVER, C. L. & LUCIUS, A. L. 2017. Comparative Analysis of the Structure and Function of AAA+ Motors ClpA, ClpB, and Hsp104: Common Threads and Disparate Functions. *Front Mol Biosci,* 4**,** 54.
DUTTA, R. & INOUYE, M. 2000. GHKL, an emergent ATPase/kinase superfamily. *Trends in Biochemical Sciences,* 25**,** 24-28.
DUTTLER, S., PECHMANN, S. & FRYDMAN, J. 2013. Principles of cotranslational ubiquitination and quality control at the ribosome. *Mol Cell,* 50**,** 379-93.

ECHEVERRÍA, P. C., BERNTHALER, A., DUPUIS, P., MAYER, B. & PICARD, D. 2011. An interaction network predicted from public data as a discovery tool: Application to the Hsp90 molecular chaperone machine. *PLoS ONE,* 6.

ECHTENKAMP, F., ZELIN, E., OXELMARK, E., WOO, J., ANDREWS, B., GARABEDIAN, M. & FREEMAN, B. 2011. Global Functional Map of the p23 Molecular Chaperone Reveals an Extensive Cellular Network. *Molecular Cell,* 43**,** 229-241.

ECHTENKAMP, F. J., GVOZDENOV, Z., ADKINS, N. L., ZHANG, Y., LYNCH-DAY, M., WATANABE, S., PETERSON, C. L. & FREEMAN, B. C. 2016. Hsp90 and p23 Molecular Chaperones Control Chromatin Architecture by Maintaining the Functional Pool of the RSC Chromatin Remodeler. *Molecular Cell,* 64**,** 888-899.

ECKL, J. M., DAAKE, M., SCHWARTZ, S. & RICHTER, K. 2016. Nucleotide-Free sB-Raf is Preferentially Bound by Hsp90 and Cdc37 In Vitro. *Journal of Molecular Biology,* 428**,** 4185-4196.

ECKL, J. M., DRAZIC, A., RUTZ, D. A. & RICHTER, K. 2014. Nematode Sgt1-homologue D1054.3 binds open and closed conformations of Hsp90 via distinct binding sites. *Biochemistry,* 53**,** 2505-14.

ECKL, J. M., RUTZ, D. A., HASLBECK, V., ZIERER, B. K., REINSTEIN, J. & RICHTER, K. 2013. Cdc37 (cell division cycle 37) restricts Hsp90 (heat shock protein 90) motility by interaction with N-terminal and middle domain binding sites. *Journal of Biological Chemistry,* 288**,** 16032-16042.

ECKL, J. M., SCHERR, M. J., FREIBURGER, L., DAAKE, M. A., SATTLER, M. & RICHTER, K. 2015. Hsp90.Cdc37 complexes with protein kinases form cooperatively with multiple distinct interaction sites. *Journal of Biological Chemistry,* 290**,** 30843-30854.

ELEUTHERIO, E., PANEK, A., DE MESQUITA, J. F., TREVISOL, E. & MAGALHAES, R. 2015. Revisiting yeast trehalose metabolism. *Curr Genet,* 61**,** 263-74.

ELLIS, R. J. 1990. The molecular chaperone concept. *Semin Cell Biol,* 1**,** 1-9.

ELLIS, R. J. 2006. Molecular chaperones: assisting assembly in addition to folding. *Trends Biochem Sci,* 31**,** 395-401.

ELLIS, R. J. & MINTON, A. P. 2006. Protein aggregation in crowded environments. *Biol Chem,* 387**,** 485-97.

ERIVES, A. J. & FASSLER, J. S. 2015. Metabolic and chaperone gene loss marks the origin of animals: evidence for Hsp104 and Hsp78 chaperones sharing mitochondrial enzymes as clients. *PLoS One,* 10**,** e0117192.

ERZBERGER, J. P. & BERGER, J. M. 2006. Evolutionary relationships and structural mechanisms of AAA+ proteins. *Annu Rev Biophys Biomol Struct,* 35**,** 93-114.

ESSER, C., ALBERTI, S. & HOHFELD, J. 2004. Cooperation of molecular chaperones with the ubiquitin/proteasome system. *Biochim Biophys Acta,* 1695**,** 171-88.

EVANS, C. G., WISÉN, S. & GESTWICKI, J. E. 2006. Heat shock proteins 70 and 90 inhibit early stages of amyloid β-(1-42) aggregation in vitro. *Journal of Biological Chemistry,* 281**,** 33182-33191.

FAIRBANKS, G., STECK, T. L. & WALLACH, D. F. 1971. Electrophoretic analysis of the major polypeptides of the human erythrocyte membrane. *Biochemistry,* 10**,** 2606-17.

FALSONE, S. F., KUNGL, A. J., REK, A., CAPPAI, R. & ZANGGER, K. 2009. The molecular chaperone Hsp90 modulates intermediate steps of amyloid assembly of the Parkinson-related protein α-synuclein. *Journal of Biological Chemistry,* 284**,** 31190-31199.

FARROW, N. A., MUHANDIRAM, R., SINGER, A. U., PASCAL, S. M., KAY, C. M., GISH, G., SHOELSON, S. E., PAWSON, T., FORMAN-KAY, J. D. & KAY, L. E. 1994. Backbone dynamics of a free and phosphopeptide-complexed Src homology 2 domain studied by 15N NMR relaxation. *Biochemistry,* 33**,** 5984-6003.

FEIFEL, B., SCHONFELD, H. J. & CHRISTEN, P. 1998. d-Peptide ligands for the co-chaperone DnaJ. *J. Biol. Chem.,* 273.

FEIGE, M. J. & HENDERSHOT, L. M. 2011. Disulfide bonds in ER protein folding and homeostasis. *Curr Opin Cell Biol,* 23**,** 167-75.

FERSHT, A. R. 2000. Transition-state structure as a unifying basis in protein-folding mechanisms: contact order, chain topology, stability, and the extended nucleus mechanism. *Proc Natl Acad Sci U S A,* 97**,** 1525-9.

FILIPEK, A. & LESNIAK, W. 2018. Current view on cellular function of S100A6 and its ligands, CacyBP/SIP and Sgt1. *Postepy Biochem,* 64**,** 242-252.
FINLEY, D. 2009. Recognition and processing of ubiquitin-protein conjugates by the proteasome. *Annu Rev Biochem,* 78**,** 477-513.
FLAHERTY, K. M., DELUCA-FLAHERTY, C. & MCKAY, D. B. 1990. Three-dimensional structure of the ATPase fragment of a 70K heat-shock cognate protein. *Nature,* 346.
FLECKENSTEIN, T., KASTENMULLER, A., STEIN, M. L., PETERS, C., DAAKE, M., KRAUSE, M., WEINFURTNER, D., HASLBECK, M., WEINKAUF, S., GROLL, M. & BUCHNER, J. 2015. The Chaperone Activity of the Developmental Small Heat Shock Protein Sip1 Is Regulated by pH-Dependent Conformational Changes. *Mol Cell,* 58**,** 1067-78.
FLOM, G., BEHAL, R. H., ROSEN, L., COLE, D. G. & JOHNSON, J. L. 2007. Definition of the minimal fragments of Sti1 required for dimerization, interaction with Hsp70 and Hsp90 and in vivo functions. *Biochemical Journal,* 404**,** 159-167.
FLOM, G. A., LANGNER, E. & JOHNSON, J. L. 2012. Identification of an Hsp90 mutation that selectively disrupts cAMP/PKA signaling in Saccharomyces cerevisiae. *Current Genetics,* 58**,** 149-163.
FORSTER, F., UNVERDORBEN, P., SLEDZ, P. & BAUMEISTER, W. 2013. Unveiling the long-held secrets of the 26S proteasome. *Structure,* 21**,** 1551-62.
FREEMAN, B. C., FELTS, S. J., TOFT, D. O. & YAMAMOTO, K. R. 2000. The p23 molecular chaperones act at a late step in intracellular receptor action to differentially affect ligand efficacies. *Genes and Development,* 14**,** 422-434.
FREEMAN, B. C., TOFT, D. O. & MORIMOTO, R. I. 1996. Molecular chaperone machines: Chaperone activities of the cyclophilin Cyp-40 and the steroid aporeceptor-associated protein p23. *Science,* 274**,** 1718-1720.
GALLUZZI, L., BAEHRECKE, E. H., BALLABIO, A., BOYA, P., BRAVO-SAN PEDRO, J. M., CECCONI, F., CHOI, A. M., CHU, C. T., CODOGNO, P., COLOMBO, M. I., CUERVO, A. M., DEBNATH, J., DERETIC, V., DIKIC, I., ESKELINEN, E. L., FIMIA, G. M., FULDA, S., GEWIRTZ, D. A., GREEN, D. R., HANSEN, M., HARPER, J. W., JAATTELA, M., JOHANSEN, T., JUHASZ, G., KIMMELMAN, A. C., KRAFT, C., KTISTAKIS, N. T., KUMAR, S., LEVINE, B., LOPEZ-OTIN, C., MADEO, F., MARTENS, S., MARTINEZ, J., MELENDEZ, A., MIZUSHIMA, N., MUNZ, C., MURPHY, L. O., PENNINGER, J. M., PIACENTINI, M., REGGIORI, F., RUBINSZTEIN, D. C., RYAN, K. M., SANTAMBROGIO, L., SCORRANO, L., SIMON, A. K., SIMON, H. U., SIMONSEN, A., TAVERNARAKIS, N., TOOZE, S. A., YOSHIMORI, T., YUAN, J., YUE, Z., ZHONG, Q. & KROEMER, G. 2017. Molecular definitions of autophagy and related processes. *EMBO J,* 36**,** 1811-1836.
GAMERDINGER, M. 2009. Protein quality control during aging involves recruitment of the macroautophagy pathway by BAG3. *EMBO J.,* 28.
GAMERDINGER, M. 2016. Protein quality control at the ribosome: focus on RAC, NAC and RQC. *Essays Biochem,* 60**,** 203-212.
GAMERDINGER, M., HAJIEVA, P., KAYA, A. M., WOLFRUM, U., HARTL, F. U. & BEHL, C. 2009. Protein quality control during aging involves recruitment of the macroautophagy pathway by BAG3. *EMBO J,* 28**,** 889-901.
GAMERDINGER, M., HANEBUTH, M. A., FRICKEY, T. & DEUERLING, E. 2015. The principle of antagonism ensures protein targeting specificity at the endoplasmic reticulum. *Science,* 348**,** 201-7.
GAO, G., KUN, T., SHENG, Y., QIAN, M., KONG, F., LIU, X., YU, Z., ZHANG, H., ZHANG, Q., GU, J. & ZHANG, X. 2013. SGT1 regulates Akt signaling by promoting beta-TrCP-dependent PHLPP1 degradation in gastric cancer cells. *Mol Biol Rep,* 40**,** 2947-53.
GAO, X. 2015. Human Hsp70 disaggregase reverses Parkinson's-linked α-synuclein amyloid fibrils. *Mol. Cell,* 59.
GARCIA-CARBONERO, R., CARNERO, A. & PAZ-ARES, L. 2013. Inhibition of HSP90 molecular chaperones: moving into the clinic. *Lancet Oncol,* 14**,** e358-69.

GASSLER, C. S., WIEDERKEHR, T., BREHMER, D., BUKAU, B. & MAYER, M. P. 2001. Bag-1M accelerates nucleotide release for human Hsc70 and Hsp70 and can act concentration-dependent as positive and negative cofactor. *J. Biol. Chem.,* 276.

GATES, S. N., YOKOM, A. L., LIN, J., JACKREL, M. E., RIZO, A. N., KENDSERSKY, N. M., BUELL, C. E., SWEENY, E. A., MACK, K. L., CHUANG, E., TORRENTE, M. P., SU, M., SHORTER, J. & SOUTHWORTH, D. R. 2017. Ratchet-like polypeptide translocation mechanism of the AAA+ disaggregase Hsp104. *Science,* 357**,** 273-279.

GELLER, R., ANDINO, R. & FRYDMAN, J. 2013. Hsp90 Inhibitors Exhibit Resistance-Free Antiviral Activity against Respiratory Syncytial Virus. *PLoS ONE,* 8.

GELLER, R., TAGUWA, S. & FRYDMAN, J. 2012. Broad action of Hsp90 as a host chaperone required for viral replication. *Biochimica et Biophysica Acta - Molecular Cell Research,* 1823**,** 698-706.

GENEST, O., HOSKINS, J. R., KRAVATS, A. N., DOYLE, S. M. & WICKNER, S. 2015. Hsp70 and Hsp90 of E. coli Directly Interact for Collaboration in Protein Remodeling. *Journal of Molecular Biology,* 427**,** 3877-3889.

GESTAUT, D., ROH, S. H., MA, B., PINTILIE, G., JOACHIMIAK, L. A., LEITNER, A., WALZTHOENI, T., AEBERSOLD, R., CHIU, W. & FRYDMAN, J. 2019. The Chaperonin TRiC/CCT Associates with Prefoldin through a Conserved Electrostatic Interface Essential for Cellular Proteostasis. *Cell,* 177**,** 751-765 e15.

GHOSH, A., CHAWLA-SARKAR, M. & STUEHR, D. J. 2011. Hsp90 interacts with inducible NO synthase client protein in its heme-free state and then drives heme insertion by an ATP-dependent process. *FASEB Journal,* 25**,** 2049-2060.

GHOSH, A., GAREE, G., SWEENY, E. A., NAKAMURA, Y. & STUEHR, D. J. 2018. Hsp90 chaperones hemoglobin maturation in erythroid and nonerythroid cells. *Proceedings of the National Academy of Sciences of the United States of America,* 115**,** E1117-E1126.

GHOSH, A. & STUEHR, D. J. 2012. Soluble guanylyl cyclase requires heat shock protein 90 for heme insertion during maturation of the NO-active enzyme. *Proceedings of the National Academy of Sciences of the United States of America,* 109**,** 12998-13003.

GIETZ, R. D. & WOODS, R. A. 2002. Transformation of yeast by lithium acetate/single-stranded carrier DNA/polyethylene glycol method. *Methods Enzymol,* 350**,** 87-96.

GIRSTMAIR, H., TIPPEL, F., LOPEZ, A., TYCH, K., STEIN, F., HABERKANT, P., SCHMID, P. W. N., HELM, D., RIEF, M., SATTLER, M. & BUCHNER, J. 2019. The Hsp90 isoforms from S. cerevisiae differ in structure, function and client range. *Nat Commun,* 10**,** 3626.

GLOVER, J. R. & LINDQUIST, S. 1998. Hsp104, Hsp70, and Hsp40: a novel chaperone system that rescues previously aggregated proteins. *Cell,* 94**,** 73-82.

GOLOUBINOFF, P. & RIOS, D. E. L. O. S. 2007. P. The mechanism of Hsp70 chaperones: (entropic) pulling the models together. *Trends Biochem. Sci.,* 32.

GONG, C. X., LIU, F., WU, G., ROSSIE, S., WEGIEL, J., LI, L., GRUNDKE-IQBAL, I. & IQBAL, K. 2004. Dephosphorylation of microtubule-associated protein tau by protein phosphatase 5. *Journal of Neurochemistry,* 88**,** 298-310.

GONG, Y., KAKIHARA, Y., KROGAN, N., GREENBLATT, J., EMILI, A., ZHANG, Z. & HOURY, W. A. 2009. An atlas of chaperone-protein interactions in Saccharomyces cerevisiae: implications to protein folding pathways in the cell. *Mol Syst Biol,* 5**,** 275.

GOWDA, N. K. C. 2018. Nucleotide exchange factors Fes1 and HspBP1 mimic substrate to release misfolded proteins from Hsp70. *Nat. Struct. Mol. Biol.,* 25.

GRAF, C., STANKIEWICZ, M., KRAMER, G. & MAYER, M. P. 2009. Spatially and kinetically resolved changes in the conformational dynamics of the Hsp90 chaperone machine. *EMBO Journal,* 28**,** 602-613.

GRAGEROV, A. & GOTTESMAN, M. E. 1994. Different peptide binding specificities of hsp70 family members. *J. Mol. Biol.,* 241.

GRAMMATIKAKIS, N., LIN, J. H., GRAMMATIKAKIS, A., TSICHLIS, P. N. & COCHRAN, B. H. 1999. p50(cdc37) acting in concert with Hsp90 is required for Raf-1 function. *Molecular and Cellular Biology,* 19**,** 1661-1672.

GRAY, W. M., MUSKETT, P. R., CHUANG, H. W. & PARKER, J. E. 2003. Arabidopsis SGT1b is required for SCF(TIR1)-mediated auxin response. *Plant Cell,* 15**,** 1310-9.
GRUBER, R. & HOROVITZ, A. 2016. Allosteric Mechanisms in Chaperonin Machines. *Chem Rev,* 116**,** 6588-606.
GUPTA, A. J., HALDAR, S., MILICIC, G., HARTL, F. U. & HAYER-HARTL, M. 2014. Active cage mechanism of chaperonin-assisted protein folding demonstrated at single-molecule level. *J Mol Biol,* 426**,** 2739-54.
GUPTA, R. S. 1995. Phylogenetic analysis of the 90 kD heat shock family of protein sequences and an examination of the relationship among animals, plants, and fungi species. *Molecular Biology and Evolution,* 12**,** 1063-1073.
HAGN, F., LAGLEDER, S., RETZLAFF, M., ROHRBERG, J., DEMMER, O., RICHTER, K., BUCHNER, J. & KESSLER, H. 2010. Structural analysis of the interaction between Hsp90 and the tumor suppressor protein p53. *Nature Structural and Molecular Biology,* 18**,** 1086-1093.
HAINZL, O., LAPINA, M. C., BUCHNER, J. & RICHTER, K. 2009. The charged linker region is an important regulator of Hsp90 function. *Journal of Biological Chemistry,* 284**,** 22559-22567.
HANAHAN, D. & MESELSON, M. 1983. Plasmid screening at high colony density. *Methods Enzymol,* 100**,** 333-42.
HANAHAN, D. & WEINBERG, R. A. 2011. Hallmarks of cancer: The next generation. *Cell,* 144**,** 646-674.
HANZEN, S., VIELFORT, K., YANG, J., ROGER, F., ANDERSSON, V., ZAMARBIDE-FORES, S., ANDERSSON, R., MALM, L., PALAIS, G., BITEAU, B., LIU, B., TOLEDANO, M. B., MOLIN, M. & NYSTROM, T. 2016. Lifespan Control by Redox-Dependent Recruitment of Chaperones to Misfolded Proteins. *Cell,* 166**,** 140-51.
HARJU, S., FEDOSYUK, H. & PETERSON, K. R. 2004. Rapid isolation of yeast genomic DNA: Bust n' Grab. *BMC Biotechnol,* 4**,** 8.
HARRIS, S. F., SHIAU, A. K. & AGARD, D. A. 2004. The crystal structure of the carboxy-terminal dimerization domain of htpG, the Escherichia coli Hsp90, reveals a potential substrate binding site. *Structure,* 12**,** 1087-1097.
HARRISON, C. J., HAYER-HARTL, M., LIBERTO, M., HARTL, F. & KURIYAN, J. 1997. Crystal structure of the nucleotide exchange factor GrpE bound to the ATPase domain of the molecular chaperone DnaK. *Science,* 276.
HARTL, F. U., BRACHER, A. & HAYER-HARTL, M. 2011. Molecular chaperones in protein folding and proteostasis. *Nature,* 475**,** 324-332.
HARTL, F. U. & HAYER-HARTL, M. 2009. Converging concepts of protein folding in vitro and in vivo. *Nat Struct Mol Biol,* 16**,** 574-81.
HASLBECK, M., FRANZMANN, T., WEINFURTNER, D. & BUCHNER, J. 2005. Some like it hot: the structure and function of small heat-shock proteins. *Nat Struct Mol Biol,* 12**,** 842-6.
HASLBECK, M., PESCHEK, J., BUCHNER, J. & WEINKAUF, S. 2016. Structure and function of alpha-crystallins: Traversing from in vitro to in vivo. *Biochim Biophys Acta,* 1860**,** 149-66.
HASLBECK, M. & VIERLING, E. 2015. A first line of stress defense: small heat shock proteins and their function in protein homeostasis. *J Mol Biol,* 427**,** 1537-48.
HASLBECK, M., WALKE, S., STROMER, T., EHRNSPERGER, M., WHITE, H. E., CHEN, S., SAIBIL, H. R. & BUCHNER, J. 1999. Hsp26: a temperature-regulated chaperone. *EMBO J,* 18**,** 6744-51.
HASLBECK, M., WEINKAUF, S. & BUCHNER, J. 2019. Small heat shock proteins: Simplicity meets complexity. *J Biol Chem,* 294**,** 2121-2132.
HASLBECK, V., ECKL, J. M., KAISER, C. J., PAPSDORF, K., HESSLING, M. & RICHTER, K. 2013. Chaperone-interacting TPR proteins in Caenorhabditis elegans. *J Mol Biol,* 425**,** 2922-39.
HAYER-HARTL, M., BRACHER, A. & HARTL, F. U. 2016. The GroEL-GroES Chaperonin Machine: A Nano-Cage for Protein Folding. *Trends Biochem Sci,* 41**,** 62-76.
HAYES, D. B. & STAFFORD, W. F. 2010. SEDVIEW, real-time sedimentation analysis. *Macromol Biosci,* 10**,** 731-5.
HEBERLE, H., MEIRELLES, G. V., DA SILVA, F. R., TELLES, G. P. & MINGHIM, R. 2015. InteractiVenn: a web-based tool for the analysis of sets through Venn diagrams. *BMC Bioinformatics,* 16**,** 169.

HESKE, C. M., MENDOZA, A., EDESSA, L. D., BAUMGART, J. T., LEE, S., TREPEL, J., PROIA, D. A., NECKERS, L. & HELMAN, L. J. 2016. STA-8666, a novel HSP90 inhibitor/SN-38 drug conjugate, causes complete tumor regression in preclinical mouse models of pediatric sarcoma. *Oncotarget,* 7**,** 65540-65552.

HESSLING, M., RICHTER, K. & BUCHNER, J. 2009. Dissection of the ATP-induced conformational cycle of the molecular chaperone Hsp90. *Nature Structural and Molecular Biology,* 16**,** 287-293.

HETZ, C., CHEVET, E. & OAKES, S. A. 2015. Proteostasis control by the unfolded protein response. *Nat Cell Biol,* 17**,** 829-38.

HIGUCHI-SANABRIA, R., FRANKINO, P. A., PAUL, J. W., 3RD, TRONNES, S. U. & DILLIN, A. 2018. A Futile Battle? Protein Quality Control and the Stress of Aging. *Dev Cell,* 44**,** 139-163.

HO, Y., GRUHLER, A., HEILBUT, A., BADER, G. D., MOORE, L., ADAMS, S. L., MILLAR, A., TAYLOR, P., BENNETT, K., BOUTILIER, K., YANG, L., WOLTING, C., DONALDSON, I., SCHANDORFF, S., SHEWNARANE, J., VO, M., TAGGART, J., GOUDREAULT, M., MUSKAT, B., ALFARANO, C., DEWAR, D., LIN, Z., MICHALICKOVA, K., WILLEMS, A. R., SASSI, H., NIELSEN, P. A., RASMUSSEN, K. J., ANDERSEN, J. R., JOHANSEN, L. E., HANSEN, L. H., JESPERSEN, H., PODTELEJNIKOV, A., NIELSEN, E., CRAWFORD, J., POULSEN, V., SORENSEN, B. D., MATTHIESEN, J., HENDRICKSON, R. C., GLEESON, F., PAWSON, T., MORAN, M. F., DUROCHER, D., MANN, M., HOGUE, C. W., FIGEYS, D. & TYERS, M. 2002. Systematic identification of protein complexes in Saccharomyces cerevisiae by mass spectrometry. *Nature,* 415**,** 180-3.

HO YEONG, S., DUNBAR, J. D., YUAN XIN, Z., GUO, D. & DONNER, D. B. 1995. Identification of a protein with homology to hsp90 that binds the type 1 tumor necrosis factor receptor. *Journal of Biological Chemistry,* 270**,** 3574-3581.

HOCHBERG, B. 1995. Controlling the False Discovery Rate: A Practical and Powerful Approach to Multiple Testing. *Journal of the Royal Statistical Society,* 57.

HOHFELD, J., CYR, D. M. & PATTERSON, C. 2001. From the cradle to the grave: molecular chaperones that may choose between folding and degradation. *EMBO Rep.,* 2.

HOLTKAMP, W., KOKIC, G., JAGER, M., MITTELSTAET, J., KOMAR, A. A. & RODNINA, M. V. 2015. Cotranslational protein folding on the ribosome monitored in real time. *Science,* 350**,** 1104-7.

HOMBACH, A., OMMEN, G., SATTLER, V. & CLOS, J. 2015. Leishmania donovani P23 protects parasites against HSP90 inhibitor-mediated growth arrest. *Cell Stress and Chaperones,* 20**,** 673-685.

HORWICH, A. L. & WILLISON, K. R. 1993. Protein folding in the cell: functions of two families of molecular chaperone, hsp 60 and TF55-TCP1. *Philos Trans R Soc Lond B Biol Sci,* 339**,** 313-25; discussion 325-6.

HORWITZ, J. 2003. Alpha-crystallin. *Exp Eye Res,* 76**,** 145-53.

HUNTER, T. & POON, R. Y. 1997. Cdc37: a protein kinase chaperone? *Trends Cell Biol,* 7**,** 157-61.

HUTCHISON, K. A., SCHERRER, L. C., CZAR, M. J., NING, Y., SANCHEZ, E., LEACH, K. L., DEIBEL, M. R., JR. & PRATT, W. B. 1993. FK506 Binding to the 56-Kilodalton Immunophilin (Hsp56) in the Glucocorticoid Receptor Heterocomplex Has No Effect on Receptor Folding or Function. *Biochemistry,* 32**,** 3953-3957.

IM, C. N. 2016. Past, present, and emerging roles of mitochondrial heat shock protein TRAP1 in the metabolism and regulation of cancer stem cells. *Cell Stress and Chaperones,* 21**,** 553-562.

INOUE, H., LI, M. & SCHNELL, D. J. 2013. An essential role for chloroplast heat shock protein 90 (Hsp90C) in protein import into chloroplasts. *Proceedings of the National Academy of Sciences of the United States of America,* 110**,** 3173-3178.

JAHN, M., REHN, A., PELZ, B., HELLENKAMP, B., RICHTER, K., RIEFA, M., BUCHNER, J. & HUGEL, T. 2014. The charged linker of the molecular chaperone Hsp90 modulates domain contacts and biological function. *Proceedings of the National Academy of Sciences of the United States of America,* 111**,** 17881-17886.

JAISWAL, H., CONZ, C., OTTO, H., WOLFLE, T., FITZKE, E., MAYER, M. P. & ROSPERT, S. 2011. The chaperone network connected to human ribosome-associated complex. *Mol Cell Biol,* 31**,** 1160-73.

JANKE, C., MAGIERA, M. M., RATHFELDER, N., TAXIS, C., REBER, S., MAEKAWA, H., MORENO-BORCHART, A., DOENGES, G., SCHWOB, E., SCHIEBEL, E. & KNOP, M. 2004. A versatile toolbox for PCR-based tagging of yeast genes: new fluorescent proteins, more markers and promoter substitution cassettes. *Yeast,* 21**,** 947-62.

JAYARAJ, G. G., HIPP, M. S. & HARTL, F. U. 2020. Functional Modules of the Proteostasis Network. *Cold Spring Harb Perspect Biol,* 12.

JEHLE, S., VOLLMAR, B. S., BARDIAUX, B., DOVE, K. K., RAJAGOPAL, P., GONEN, T., OSCHKINAT, H. & KLEVIT, R. E. 2011. N-terminal domain of alphaB-crystallin provides a conformational switch for multimerization and structural heterogeneity. *Proc Natl Acad Sci U S A,* 108**,** 6409-14.

JEONG, J. Y., YIM, H. S., RYU, J. Y., LEE, H. S., LEE, J. H., SEEN, D. S. & KANG, S. G. 2012. One-step sequence- and ligation-independent cloning as a rapid and versatile cloning method for functional genomics studies. *Appl Environ Microbiol,* 78**,** 5440-3.

JIANG, J., PRASAD, K., LAFER, E. M. & SOUSA, R. 2005. Structural basis of interdomain communication in the Hsc70 chaperone. *Mol. Cell,* 20.

JIANG, Y., ROSSI, P. & KALODIMOS, C. G. 2019. Structural basis for client recognition and activity of Hsp40 chaperones. *Science,* 365**,** 1313-1319.

JINWAL, U. K., KOREN III, J. & DICKEY, C. A. 2013. Reconstructing the Hsp90/Tau machine. *Current Enzyme Inhibition,* 9**,** 41-45.

JOACHIMIAK, L. A., WALZTHOENI, T., LIU, C. W., AEBERSOLD, R. & FRYDMAN, J. 2014. The structural basis of substrate recognition by the eukaryotic chaperonin TRiC/CCT. *Cell,* 159**,** 1042-1055.

JOHNSON, B. D., SCHUMACHER, R. J., ROSS, E. D. & TOFT, D. O. 1998. Hop modulates hsp70/hsp90 interactions in protein folding. *Journal of Biological Chemistry,* 273**,** 3679-3686.

JOHNSON, J. L. 2012. Evolution and function of diverse Hsp90 homologs and cochaperone proteins. *Biochimica et Biophysica Acta - Molecular Cell Research,* 1823**,** 607-613.

JOHNSON, J. L., ZUEHLKE, A. D., TENGE, V. R. & LANGWORTHY, J. C. 2014. Mutation of essential Hsp90 co-chaperones SGT1 or CNS1 renders yeast hypersensitive to overexpression of other co-chaperones. *Curr Genet,* 60**,** 265-76.

JOVCEVSKI, B., KELLY, M. A., ROTE, A. P., BERG, T., GASTALL, H. Y., BENESCH, J. L., AQUILINA, J. A. & ECROYD, H. 2015. Phosphomimics destabilize Hsp27 oligomeric assemblies and enhance chaperone activity. *Chem Biol,* 22**,** 186-95.

JUNGNICKEL, B. & RAPOPORT, T. A. 1995. A posttargeting signal sequence recognition event in the endoplasmic reticulum membrane. *Cell,* 82**,** 261-70.

KADOTA, Y., AMIGUES, B., DUCASSOU, L., MADAOUI, H., OCHSENBEIN, F., GUEROIS, R. & SHIRASU, K. 2008. Structural and functional analysis of SGT1-HSP90 core complex required for innate immunity in plants. *EMBO Rep,* 9**,** 1209-15.

KADOTA, Y., SHIRASU, K. & GUEROIS, R. 2010. NLR sensors meet at the SGT1-HSP90 crossroad. *Trends Biochem Sci,* 35**,** 199-207.

KAIMAL, J. M., KANDASAMY, G., GASSER, F. & ANDREASSON, C. 2017. Coordinated Hsp110 and Hsp104 Activities Power Protein Disaggregation in Saccharomyces cerevisiae. *Mol Cell Biol,* 37.

KAISER, C. J. O., PETERS, C., SCHMID, P. W. N., STAVROPOULOU, M., ZOU, J., DAHIYA, V., MYMRIKOV, E. V., ROCKEL, B., ASAMI, S., HASLBECK, M., RAPPSILBER, J., REIF, B., ZACHARIAS, M., BUCHNER, J. & WEINKAUF, S. 2019. The structure and oxidation of the eye lens chaperone alphaA-crystallin. *Nat Struct Mol Biol,* 26**,** 1141-1150.

KAKIHARA, Y. & HOURY, W. A. 2012. The R2TP complex: Discovery and functions. *Biochimica et Biophysica Acta - Molecular Cell Research,* 1823**,** 101-107.

KALISMAN, N., ADAMS, C. M. & LEVITT, M. 2012. Subunit order of eukaryotic TRiC/CCT chaperonin by cross-linking, mass spectrometry, and combinatorial homology modeling. *Proc Natl Acad Sci U S A,* 109**,** 2884-9.

KAMPINGA, H. H. & CRAIG, E. A. 2010. The HSP70 chaperone machinery: J proteins as drivers of functional specificity. *Nat. Rev. Mol. Cell Biol.,* 11.

KARAGOZ, G. E. 2014. Hsp90-Tau complex reveals molecular basis for specificity in chaperone action. *Cell,* 156.

KARMAKAR, S. & DAS, K. P. 2011. Stabilization of oligomeric structure of alpha-crystallin by Zn+(2) through intersubunit bridging. *Biopolymers,* 95**,** 105-16.

KAUSHIK, S. & CUERVO, A. M. 2018. The coming of age of chaperone-mediated autophagy. *Nat Rev Mol Cell Biol,* 19**,** 365-381.

KAZMAN, P., VIELBERG, M. T., PULIDO CENDALES, M. D., HUNZIGER, L., WEBER, B., HEGENBART, U., ZACHARIAS, M., KOHLER, R., SCHONLAND, S., GROLL, M. & BUCHNER, J. 2020. Fatal amyloid formation in a patient's antibody light chain is caused by a single point mutation. *Elife,* 9.

KEILHAUER, E. C., HEIN, M. Y. & MANN, M. 2015. Accurate protein complex retrieval by affinity enrichment mass spectrometry (AE-MS) rather than affinity purification mass spectrometry (AP-MS). *Mol Cell Proteomics,* 14**,** 120-35.

KIRSCHKE, E., GOSWAMI, D., SOUTHWORTH, D., GRIFFIN, P. R. & AGARD, D. A. 2014. Glucocorticoid receptor function regulated by coordinated action of the Hsp90 and Hsp70 chaperone cycles. *Cell,* 157**,** 1685-1697.

KITAGAWA, K., SKOWYRA, D., ELLEDGE, S. J., HARPER, J. W. & HIETER, P. 1999. SGT1 encodes an essential component of the yeast kinetochore assembly pathway and a novel subunit of the SCF ubiquitin ligase complex. *Mol Cell,* 4**,** 21-33.

KITYK, R., KOPP, J. & MAYER, M. P. 2018. Molecular mechanism of J-domain-triggered ATP hydrolysis by Hsp70 chaperones. *Mol. Cell,* 69.

KITYK, R., KOPP, J., SINNING, I. & MAYER, M. P. 2012. Structure and dynamics of the ATP-bound open conformation of Hsp70 chaperones. *Mol. Cell,* 48.

KITYK, R., VOGEL, M., SCHLECHT, R., BUKAU, B. & MAYER, M. P. 2015. Pathways of allosteric regulation in Hsp70 chaperones. *Nat. Commun.,* 6.

KLAIPS, C. L., HOCHSTRASSER, M. L., LANGLOIS, C. R. & SERIO, T. R. 2014. Spatial quality control bypasses cell-based limitations on proteostasis to promote prion curing. *Elife,* 3.

KLUMPP, M., BAUMEISTER, W. & ESSEN, L. O. 1997. Structure of the substrate binding domain of the thermosome, an archaeal group II chaperonin. *Cell,* 91**,** 263-70.

KOULOV, A. V., LAPOINTE, P., LU, B., RAZVI, A., COPPINGER, J., DONG, M. Q., MATTESON, J., LAISTER, R., ARROWSMITH, C., YATES III, J. R. & BALCH, W. E. 2010. Biological and structural basis for Aha1 regulation of Hsp90 ATPase activity in maintaining proteostasis in the human disease cystic fibrosis. *Molecular Biology of the Cell,* 21**,** 871-884.

KRAMER, G., SHIBER, A. & BUKAU, B. 2019. Mechanisms of Cotranslational Maturation of Newly Synthesized Proteins. *Annu Rev Biochem,* 88**,** 337-364.

KRAVATS, A. N., HOSKINS, J. R., REIDY, M., JOHNSON, J. L., DOYLE, S. M., GENEST, O., MASISON, D. C. & WICKNER, S. 2018. Functional and physical interaction between yeast Hsp90 and Hsp70. *Proceedings of the National Academy of Sciences of the United States of America,* 115**,** E2210-E2219.

KROSCHWALD, S., MAHARANA, S., MATEJU, D., MALINOVSKA, L., NUSKE, E., POSER, I., RICHTER, D. & ALBERTI, S. 2015. Promiscuous interactions and protein disaggregases determine the material state of stress-inducible RNP granules. *Elife,* 4**,** e06807.

KRUGER, R., KUBLER, D., PALLISSE, R., BURKOVSKI, A. & LEHMANN, W. D. 2006. Protein and proteome phosphorylation stoichiometry analysis by element mass spectrometry. *Anal Chem,* 78**,** 1987-94.

KULAK, N. A., GEYER, P. E. & MANN, M. 2017. Loss-less Nano-fractionator for High Sensitivity, High Coverage Proteomics. *Mol Cell Proteomics,* 16**,** 694-705.

KUSHNIROV, V. V. 2000. Rapid and reliable protein extraction from yeast. *Yeast,* 16**,** 857-60.

LABBADIA, J. & MORIMOTO, R. I. 2015. The biology of proteostasis in aging and disease. *Annu Rev Biochem,* 84**,** 435-64.

LACKIE, R. E., MACIEJEWSKI, A., OSTAPCHENKO, V. G., MARQUES-LOPES, J., CHOY, W. Y., DUENNWALD, M. L., PRADO, V. F. & PRADO, M. A. M. 2017. The Hsp70/Hsp90 chaperone machinery in neurodegenerative diseases. *Frontiers in Neuroscience,* 11.

LAEMMLI, U. K. 1970. Cleavage of structural proteins during the assembly of the head of bacteriophage T4. *Nature,* 227**,** 680-5.
LANE, D. P. 1992. Cancer. p53, guardian of the genome. *Nature,* 358**,** 15-6.
LAUE TM, S. B., RIDGEWAY TM, PELLETIER SL. 1992. Computer-aided interpretation of analytical sedimentation data for proteins. . *Analytical Ultracentrifugation in Biochemistry and Polymer Science. Royal Society of Chemistry***,** 90-125.
LEE, D. H. & GOLDBERG, A. L. 2010. Hsp104 is essential for the selective degradation in yeast of polyglutamine expanded ataxin-1 but not most misfolded proteins generally. *Biochem Biophys Res Commun,* 391**,** 1056-61.
LEE, P., SHABBIR, A., CARDOZO, C. & CAPLAN, A. J. 2004a. Sti1 and Cdc37 Can Stabilize Hsp90 in Chaperone Complexes with a Protein Kinase. *Molecular Biology of the Cell,* 15**,** 1785-1792.
LEE, S., FAN, C. Y., YOUNGER, J. M., REN, H. & CYR, D. M. 2002. Identification of essential residues in the type II Hsp40 Sis1 that function in polypeptide binding. *J. Biol. Chem.,* 277.
LEE, S., HISAYOSHI, M., YOSHIDA, M. & TSAI, F. T. 2003. Crystallization and preliminary X-ray crystallographic analysis of the Hsp100 chaperone ClpB from Thermus thermophilus. *Acta Crystallogr D Biol Crystallogr,* 59**,** 2334-6.
LEE, Y. T., JACOB, J., MICHOWSKI, W., NOWOTNY, M., KUZNICKI, J. & CHAZIN, W. J. 2004b. Human Sgt1 binds HSP90 through the CHORD-Sgt1 domain and not the tetratricopeptide repeat domain. *J Biol Chem,* 279**,** 16511-7.
LEVINTHAL, C. 1968. Are there pathways for protein foldin? *Journal de Chimie Physique,* 65**,** 44-45.
LI, J., RICHTER, K. & BUCHNER, J. 2011. Mixed Hsp90-cochaperone complexes are important for the progression of the reaction cycle. *Nature Structural and Molecular Biology,* 18**,** 61-67.
LI, J., RICHTER, K., REINSTEIN, J. & BUCHNER, J. 2013. Integration of the accelerator Aha1 in the Hsp90 co-chaperone cycle. *Nature Structural and Molecular Biology,* 20**,** 326-331.
LI, J. & SHA, B. 2003. Preliminary X-ray crystallographic studies of yeast Hsp40 Ydj1 complexed with its peptide substrate. *Acta Crystallogr. D,* 59.
LI, J., SOROKA, J. & BUCHNER, J. 2012. The Hsp90 chaperone machinery: Conformational dynamics and regulation by co-chaperones. *Biochimica et Biophysica Acta - Molecular Cell Research,* 1823**,** 624-635.
LI, J., WU, Y., QIAN, X. & SHA, B. 2006. Crystal structure of yeast Sis1 peptide-binding fragment and Hsp70 Ssa1 C-terminal complex. *Biochem J,* 398**,** 353-60.
LIBEREK, K., MARSZALEK, J., ANG, D., GEORGOPOULOS, C. & ZYLICZ, M. 1991. Escherichia coli DnaJ and GrpE heat shock proteins jointly stimulate ATPase activity of DnaK. *Proc Natl Acad Sci U S A,* 88**,** 2874-8.
LIN, Y. & CHENG, C. L. 1997. A chlorate-resistant mutant defective in the regulation of nitrate reductase gene expression in arabidopsis defines a new HY locus. *Plant Cell,* 9**,** 21-35.
LIN, Z., MADAN, D. & RYE, H. S. 2008. GroEL stimulates protein folding through forced unfolding. *Nat Struct Mol Biol,* 15**,** 303-11.
LINGELBACH, L. B. & KAPLAN, K. B. 2004. The interaction between Sgt1p and Skp1p is regulated by HSP90 chaperones and is required for proper CBF3 assembly. *Mol Cell Biol,* 24**,** 8938-50.
LIU, B., YANG, Y., QIU, Z., STARON, M., HONG, F., LI, Y., WU, S., LI, Y., HAO, B., BONA, R., HAN, D. & LI, Z. 2010. Folding of Toll-like receptors by the HSP90 paralogue gp96 requires a substrate-specific cochaperone. *Nature Communications,* 1.
LIU, X. S., SONG, B., TANG, J., LIU, W., KUANG, S. & LIU, X. 2012. Plk1 phosphorylates Sgt1 at the kinetochores to promote timely kinetochore-microtubule attachment. *Mol Cell Biol,* 32**,** 4053-67.
LO BIANCO, C., SHORTER, J., REGULIER, E., LASHUEL, H., IWATSUBO, T., LINDQUIST, S. & AEBISCHER, P. 2008. Hsp104 antagonizes alpha-synuclein aggregation and reduces dopaminergic degeneration in a rat model of Parkinson disease. *J Clin Invest,* 118**,** 3087-97.
LOO, M. A., JENSEN, T. J., CUI, L., HOU, Y. X., CHANG, X. B. & RIORDAN, J. R. 1998. Perturbation of Hsp90 interaction with nascent CFTR prevents its maturation and accelerates its degradation by the proteasome. *EMBO Journal,* 17**,** 6879-6887.

LOPEZ, T., DALTON, K. & FRYDMAN, J. 2015. The Mechanism and Function of Group II Chaperonins. *J Mol Biol,* 427**,** 2919-30.
LORENZ, O. R., FREIBURGER, L., RUTZ, D. A., KRAUSE, M., ZIERER, B. K., ALVIRA, S., CUÉLLAR, J., VALPUESTA, J., MADL, T., SATTLER, M. & BUCHNER, J. 2014. Modulation of the Hsp90 chaperone cycle by a stringent client protein. *Molecular Cell,* 53**,** 941-953.
LOS RIOS, P. & BARDUCCI, A. 2014. Hsp70 chaperones are non-equilibrium machines that achieve ultra-affinity by energy consumption. *eLife,* 3.
LU, X. A., WANG, X., ZHUO, W., JIA, L., JIANG, Y., FU, Y. & LUO, Y. 2014. The regulatory mechanism of a client kinase controlling its own release from Hsp90 chaperone machinery through phosphorylation. *Biochem J,* 457**,** 171-83.
LUDERS, J., DEMAND, J., PAPP, O. & HOHFELD, J. 2000. Distinct isoforms of the cofactor BAG-1 differentially affect Hsc70 chaperone function. *J. Biol. Chem.,* 275.
MAINZ, A., BARDIAUX, B., KUPPLER, F., MULTHAUP, G., FELLI, I. C., PIERATTELLI, R. & REIF, B. 2012. Structural and mechanistic implications of metal binding in the small heat-shock protein alphaB-crystallin. *J Biol Chem,* 287**,** 1128-38.
MAINZ, A., PESCHEK, J., STAVROPOULOU, M., BACK, K. C., BARDIAUX, B., ASAMI, S., PRADE, E., PETERS, C., WEINKAUF, S., BUCHNER, J. & REIF, B. 2015. The chaperone alphaB-crystallin uses different interfaces to capture an amorphous and an amyloid client. *Nat Struct Mol Biol,* 22**,** 898-905.
MARTÍNEZ-RUIZ, A., VILLANUEVA, L., DE ORDUÑA, C. G., LÓPEZ-FERRER, D., ÁNGELES HIGUERAS, M., TARÍN, C., RODRÍGUEZ-CRESPO, I., VÁZQUEZ, J. & LAMAS, S. 2005. S-nitrosylation of Hsp90 promotes the inhibition of its ATPase and endothelial nitric oxide synthase regulatory activities. *Proceedings of the National Academy of Sciences of the United States of America,* 102**,** 8525-8530.
MARTINS, T., MAIA, A. F., STEFFENSEN, S. & SUNKEL, C. E. 2009. Sgt1, a co-chaperone of Hsp90 stabilizes Polo and is required for centrosome organization. *EMBO J,* 28**,** 234-47.
MARTINS, T. & SUNKEL, C. E. 2009. Sgt1 plays polo during cell division. *Cell Cycle,* 8**,** 1110-1.
MARZEC, M., ELETTO, D. & ARGON, Y. 2012. GRP94: An HSP90-like protein specialized for protein folding and quality control in the endoplasmic reticulum. *Biochimica et Biophysica Acta - Molecular Cell Research,* 1823**,** 774-787.
MAYER, M. & LE BRETON, L. 2015. Hsp90: Breaking the symmetry. *Molecular Cell,* 58**,** 8-20.
MAYER, M. P. 2000. Multistep mechanism of substrate binding determines chaperone activity of Hsp70. *Nat. Struct. Biol.,* 7.
MAYER, M. P. & BUKAU, B. 2005. Hsp70 chaperones: cellular functions and molecular mechanism. *Cell. Mol. Life Sci.,* 62.
MAYER, M. P., RUDIGER, S. & BUKAU, B. 2000. Molecular basis for interactions of the DnaK chaperone with substrates. *Biol. Chem.,* 381.
MAYOR, A., MARTINON, F., DE SMEDT, T., PETRILLI, V. & TSCHOPP, J. 2007. A crucial function of SGT1 and HSP90 in inflammasome activity links mammalian and plant innate immune responses. *Nat Immunol,* 8**,** 497-503.
MAYR, C., RICHTER, K., LILIE, H. & BUCHNER, J. 2000. Cpr6 and Cpr7, two closely related Hsp90-associated immunophilins from Saccharomyces cerevisiae, differ in their functional properties. *Journal of Biological Chemistry,* 275**,** 34140-34146.
MCCLELLAN, A. J., XIA, Y., DEUTSCHBAUER, A. M., DAVIS, R. W., GERSTEIN, M. & FRYDMAN, J. 2007. Diverse cellular functions of the Hsp90 molecular chaperone uncovered using systems approaches. *Cell,* 131**,** 121-35.
MCLAUGHLIN, S. H., SMITH, H. W. & JACKSON, S. E. 2002. Stimulation of the weak ATPase activity of human Hsp90 by a client protein. *Journal of Molecular Biology,* 315**,** 787-798.
MCLAUGHLIN, S. H., SOBOTT, F., YAO, Z. P., ZHANG, W., NIELSEN, P. R., GROSSMANN, J. G., LAUE, E. D., ROBINSON, C. V. & JACKSON, S. E. 2006. The co-chaperone p23 arrests the Hsp90 ATPase cycle to trap client proteins. *Journal of Molecular Biology,* 356**,** 746-758.

MELDAU, S., BALDWIN, I. T. & WU, J. 2011. For security and stability: SGT1 in plant defense and development. *Plant Signal Behav,* 6**,** 1479-82.

MEYER, P., PRODROMOU, C., HU, B., VAUGHAN, C., ROE, S. M., PANARETOU, B., PIPER, P. W. & PEARL, L. H. 2003. Structural and functional analysis of the middle segment of Hsp90: Implications for ATP hydrolysis and client protein and cochaperone interactions. *Molecular Cell,* 11**,** 647-658.

MEYER, P., PRODROMOU, C., LIAO, C., HU, B., ROE, S. M., VAUGHAN, C. K., VLASIC, I., PANARETOU, B., PIPER, P. W. & PEAR, L. H. 2004. Structural basis for recruitment of the ATPase activator Aha1 to the Hsp90 chaperone machinery. *EMBO Journal,* 23**,** 511-519.

MI, H., MURUGANUJAN, A. & THOMAS, P. D. 2013. PANTHER in 2013: modeling the evolution of gene function, and other gene attributes, in the context of phylogenetic trees. *Nucleic Acids Res,* 41**,** D377-86.

MICKLER, M., HESSLING, M., RATZKE, C., BUCHNER, J. & HUGEL, T. 2009. The large conformational changes of Hsp90 are only weakly coupled to ATP hydrolysis. *Nature Structural and Molecular Biology,* 16**,** 281-286.

MIJNDERS, M., KLEIZEN, B. & BRAAKMAN, I. 2017. Correcting CFTR folding defects by small-molecule correctors to cure cystic fibrosis. *Curr Opin Pharmacol,* 34**,** 83-90.

MILLSON, S. H., TRUMAN, A. W., RÁCZ, A., HU, B., PANARETOU, B., NUTTALL, J., MOLLAPOUR, M., SÖTI, C. & PIPER, P. W. 2007. Expressed as the sole Hsp90 of yeast, the α and β isoforms of human Hsp90 differ with regard to their capacities for activation of certain client proteins, whereas only Hsp90β generates sensitivity to the Hsp90 inhibitor radicicol. *FEBS Journal,* 274**,** 4453-4463.

MINOIA, M. 2014. BAG3 induces the sequestration of proteasomal clients into cytoplasmic puncta: implications for a proteasome-to-autophagy switch. *Autophagy,* 10.

MIYATA, Y., NAKAMOTO, H. & NECKERS, L. 2013. The therapeutic target Hsp90 and cancer hallmarks. *Current Pharmaceutical Design,* 19**,** 347-365.

MNAIMNEH, S., DAVIERWALA, A. P., HAYNES, J., MOFFAT, J., PENG, W. T., ZHANG, W., YANG, X., POOTOOLAL, J., CHUA, G., LOPEZ, A., TROCHESSET, M., MORSE, D., KROGAN, N. J., HILEY, S. L., LI, Z., MORRIS, Q., GRIGULL, J., MITSAKAKIS, N., ROBERTS, C. J., GREENBLATT, J. F., BOONE, C., KAISER, C. A., ANDREWS, B. J. & HUGHES, T. R. 2004. Exploration of essential gene functions via titratable promoter alleles. *Cell,* 118**,** 31-44.

MOEHLE, E. A., SHEN, K. & DILLIN, A. 2019. Mitochondrial proteostasis in the context of cellular and organismal health and aging. *J Biol Chem,* 294**,** 5396-5407.

MOLLAPOUR, M., BOURBOULIA, D., BEEBE, K., WOODFORD, M. R., POLIER, S., HOANG, A., CHELLURI, R., LI, Y., GUO, A., LEE, M. J., FOTOOH-ABADI, E., KHAN, S., PRINCE, T., MIYAJIMA, N., YOSHIDA, S., TSUTSUMI, S., XU, W., PANARETOU, B., STETLER-STEVENSON, W. G., BRATSLAVSKY, G., TREPEL, J. B., PRODROMOU, C. & NECKERS, L. 2014. Asymmetric Hsp90 N Domain SUMOylation Recruits Aha1 and ATP-Competitive Inhibitors. *Molecular Cell,* 53**,** 317-329.

MOLLAPOUR, M. & NECKERS, L. 2012. Post-translational modifications of Hsp90 and their contributions to chaperone regulation. *Biochimica et Biophysica Acta - Molecular Cell Research,* 1823**,** 648-655.

MOLLAPOUR, M., TSUTSUMI, S., TRUMAN, A., XU, W., VAUGHAN, C., BEEBE, K., KONSTANTINOVA, A., VOURGANTI, S., PANARETOU, B., PIPER, P., TREPEL, J., PRODROMOU, C., PEARL, L. & NECKERS, L. 2011. Threonine 22 Phosphorylation Attenuates Hsp90 Interaction with Cochaperones and Affects Its Chaperone Activity. *Molecular Cell,* 41**,** 672-681.

MOLLER, I., BEATRIX, B., KREIBICH, G., SAKAI, H., LAURING, B. & WIEDMANN, M. 1998. Unregulated exposure of the ribosomal M-site caused by NAC depletion results in delivery of non-secretory polypeptides to the Sec61 complex. *FEBS Lett,* 441**,** 1-5.

MORANO, K. A., SANTORO, N., KOCH, K. A. & THIELE, D. J. 1999. A trans-activation domain in yeast heat shock transcription factor is essential for cell cycle progression during stress. *Molecular and Cellular Biology,* 19**,** 402-411.

MORRA, G., VERKHIVKER, G. & COLOMBO, G. 2009. Modeling signal propagation mechanisms and ligand-based conformational dynamics of the Hsp90 molecular chaperone full-length dimer. *PLoS Computational Biology,* 5.

MORSHAUSER, R. C. 1999. High-resolution solution structure of the 18 kDa substrate-binding domain of the mammalian chaperone protein Hsc70. *J. Mol. Biol.,* 289.

MULLER, P., RUCKOVA, E., HALADA, P., COATES, P. J., HRSTKA, R., LANE, D. P. & VOJTESEK, B. 2013. C-terminal phosphorylation of Hsp70 and Hsp90 regulates alternate binding to co-chaperones CHIP and HOP to determine cellular protein folding/degradation balances. *Oncogene,* 32**,** 3101-10.

MURPHY, P. J., MORISHIMA, Y., KOVACS, J. J., YAO, T. P. & PRATT, W. B. 2005. Regulation of the dynamics of hsp90 action on the glucocorticoid receptor by acetylation/deacetylation of the chaperone. *J Biol Chem,* 280**,** 33792-9.

MUSKETT, P. & PARKER, J. 2003. Role of SGT1 in the regulation of plant R gene signalling. *Microbes Infect,* 5**,** 969-76.

MYMRIKOV, E. V., DAAKE, M., RICHTER, B., HASLBECK, M. & BUCHNER, J. 2017. The Chaperone Activity and Substrate Spectrum of Human Small Heat Shock Proteins. *J Biol Chem,* 292**,** 672-684.

MYMRIKOV, E. V., RIEDL, M., PETERS, C., WEINKAUF, S., HASLBECK, M. & BUCHNER, J. 2020. Regulation of small heat-shock proteins by hetero-oligomer formation. *J Biol Chem,* 295**,** 158-169.

NAGATA, Y., ANAN, T., YOSHIDA, T., MIZUKAMI, T., TAYA, Y., FUJIWARA, T., KATO, H., SAYA, H. & NAKAO, M. 1999. The stabilization mechanism of mutant-type p53 by impaired ubiquitination: The loss of wild-type p53 function and the hsp90 association. *Oncogene,* 18**,** 6037-6049.

NATHAN, D. F. & LINDQUIST, S. 1995. Mutational analysis of Hsp90 function: Interactions with a steroid receptor and a protein kinase. *Molecular and Cellular Biology,* 15**,** 3917-3925.

NGUYEN, M. T. N., KNIESS, R. A., DATURPALLI, S., LE BRETON, L., KE, X., CHEN, X. & MAYER, M. P. 2017. Isoform-Specific Phosphorylation in Human Hsp90beta Affects Interaction with Clients and the Cochaperone Cdc37. *J Mol Biol,* 429**,** 732-752.

NIIKURA, Y. & KITAGAWA, K. 2003. Identification of a novel splice variant: human SGT1B (SUGT1B). *DNA Seq,* 14**,** 436-41.

NILLEGODA, N. B. 2015. Crucial HSP70 co-chaperone complex unlocks metazoan protein disaggregation. *Nature,* 524.

NILSSON, O. B., HEDMAN, R., MARINO, J., WICKLES, S., BISCHOFF, L., JOHANSSON, M., MULLER-LUCKS, A., TROVATO, F., PUGLISI, J. D., O'BRIEN, E. P., BECKMANN, R. & VON HEIJNE, G. 2015. Cotranslational Protein Folding inside the Ribosome Exit Tunnel. *Cell Rep,* 12**,** 1533-40.

NOEL, L. D., CAGNA, G., STUTTMANN, J., WIRTHMULLER, L., BETSUYAKU, S., WITTE, C. P., BHAT, R., POCHON, N., COLBY, T. & PARKER, J. E. 2007. Interaction between SGT1 and cytosolic/nuclear HSC70 chaperones regulates Arabidopsis immune responses. *Plant Cell,* 19**,** 4061-76.

NYARKO, A., MOSBAHI, K., ROWE, A. J., LEECH, A., BOTER, M., SHIRASU, K. & KLEANTHOUS, C. 2007. TPR-Mediated self-association of plant SGT1. *Biochemistry,* 46**,** 11331-41.

NYATHI, Y. & POOL, M. R. 2015. Analysis of the interplay of protein biogenesis factors at the ribosome exit site reveals new role for NAC. *J Cell Biol,* 210**,** 287-301.

OBERMANN, W. M. J., SONDERMANN, H., RUSSO, A. A., PAVLETICH, N. P. & HARTL, F. U. 1998. In vivo function of Hsp90 is dependent on ATP binding and ATP hydrolysis. *Journal of Cell Biology,* 143**,** 901-910.

OGI, H., SAKURABA, Y., KITAGAWA, R., XIAO, L., SHEN, C., CYNTHIA, M. A., OHTA, S., ARNOLD, M. A., RAMIREZ, N., HOUGHTON, P. J. & KITAGAWA, K. 2015. The oncogenic role of the cochaperone Sgt1. *Oncogenesis,* 4**,** e149.

OLZSCHA, H., SCHERMANN, S. M., WOERNER, A. C., PINKERT, S., HECHT, M. H., TARTAGLIA, G. G., VENDRUSCOLO, M., HAYER-HARTL, M., HARTL, F. U. & VABULAS, R. M. 2011. Amyloid-like

aggregates sequester numerous metastable proteins with essential cellular functions. *Cell,* 144**,** 67-78.
OTERO, J. H., LIZAK, B., FEIGE, M. J. & HENDERSHOT, L. M. 2014. Dissection of structural and functional requirements that underlie the interaction of ERdj3 protein with substrates in the endoplasmic reticulum. *J Biol Chem,* 289**,** 27504-12.
PACI, A., LIU, X. H., HUANG, H., LIM, A., HOURY, W. A. & ZHAO, R. 2012. The stability of the small nucleolar ribonucleoprotein (snoRNP) assembly protein Pih1 in Saccharomyces cerevisiae is modulated by its C terminus. *J Biol Chem,* 287**,** 43205-14.
PANARETOU, B., PRODROMOU, C., ROE, S. M., O'BRIEN, R., LADBURY, J. E., PIPER, P. W. & PEARL, L. H. 1998. ATP binding and hydrolysis are essential to the function of the Hsp90 molecular chaperone in vivo. *EMBO Journal,* 17**,** 4829-4836.
PANARETOU, B., SILIGARDI, G., MEYER, P., MALONEY, A., SULLIVAN, J. K., SINGH, S., MILLSON, S. H., CLARKE, P. A., NAABY-HANSEN, S., STEIN, R., CRAMER, R., MOLLAPOUR, M., WORKMAN, P., PIPER, P. W., PEARL, L. H. & PRODROMOU, C. 2002. Activation of the ATPase activity of Hsp90 by the stress-regulated cochaperone Aha1. *Molecular Cell,* 10**,** 1307-1318.
PARK, S. J., KOSTIC, M. & DYSON, H. J. 2011. Dynamic interaction of Hsp90 with its client protein p53. *Journal of Molecular Biology,* 411**,** 158-173.
PARSELL, D. A., KOWAL, A. S., SINGER, M. A. & LINDQUIST, S. 1994. Protein disaggregation mediated by heat-shock protein Hsp104. *Nature,* 372**,** 475-8.
PAUL, I. & GHOSH, M. K. 2014. The E3 ligase CHIP: insights into its structure and regulation. *Biomed Res Int,* 2014**,** 918183.
PECH, M., SPRETER, T., BECKMANN, R. & BEATRIX, B. 2010. Dual binding mode of the nascent polypeptide-associated complex reveals a novel universal adapter site on the ribosome. *J Biol Chem,* 285**,** 19679-87.
PELLECCHIA, M. 2000. Structural insights into substrate binding by the molecular chaperone DnaK. *Nat. Struct. Biol.,* 7.
PERALES-CALVO, J., MUGA, A. & MORO, F. 2010. Role of DnaJ G/F-rich domain in conformational recognition and binding of protein substrates. *J. Biol. Chem.,* 285.
PESCHEK, J., BRAUN, N., ROHRBERG, J., BACK, K. C., KRIEHUBER, T., KASTENMULLER, A., WEINKAUF, S. & BUCHNER, J. 2013. Regulated structural transitions unleash the chaperone activity of alphaB-crystallin. *Proc Natl Acad Sci U S A,* 110**,** E3780-9.
PICK, E., KLUGER, Y., GILTNANE, J. M., MOEDER, C., CAMP, R. L., RIMM, D. L. & KLUGER, H. M. 2007. High HSP90 expression is associated with decreased survival in breast cancer. *Cancer Research,* 67**,** 2932-2937.
PIRKL, F. & BUCHNER, J. 2001. Functional analysis of the Hsp90-associated human peptidyl prolyl cis/trans isomerases FKBP51, FKBP52 and Cyp40. *Journal of Molecular Biology,* 308**,** 795-806.
POLIER, S., DRAGOVIC, Z., HARTL, F. U. & BRACHER, A. 2008. Structural basis for the cooperation of Hsp70 and Hsp110 chaperones in protein folding. *Cell,* 133.
PRATT, W. B. & DITTMAR, K. D. 1998. Studies with purified chaperones advance the understanding of the mechanism of glucocorticoid receptor-hsp90 heterocomplex assembly. *Trends in Endocrinology and Metabolism,* 9**,** 244-252.
PREISSLER, S. & DEUERLING, E. 2012. Ribosome-associated chaperones as key players in proteostasis. *Trends Biochem Sci,* 37**,** 274-83.
PRESTON, G. M., GUERRIERO, C. J., METZGER, M. B., MICHAELIS, S. & BRODSKY, J. L. 2018. Substrate Insolubility Dictates Hsp104-Dependent Endoplasmic-Reticulum-Associated Degradation. *Mol Cell,* 70**,** 242-253 e6.
PREVILLE, X., SALVEMINI, F., GIRAUD, S., CHAUFOUR, S., PAUL, C., STEPIEN, G., URSINI, M. V. & ARRIGO, A. P. 1999. Mammalian small stress proteins protect against oxidative stress through their ability to increase glucose-6-phosphate dehydrogenase activity and by maintaining optimal cellular detoxifying machinery. *Exp Cell Res,* 247**,** 61-78.
PRODROMOU, C. 2016. REVIEW ARTICLE mechanisms of Hsp90 regulation. *Biochemical Journal,* 473**,** 2439-2452.

PRODROMOU, C., PANARETOU, B., CHOHAN, S., SILIGARDI, G., O'BRIEN, R., LADBURY, J. E., ROE, S. M., PIPER, P. W. & PEARL, L. H. 2000. The ATPase cycle of Hsp90 drives a molecular 'clamp' via transient dimerization of the hi-terminal domains. *EMBO Journal,* 19**,** 4383-4392.

PRODROMOU, C., ROE, S. M., O'BRIEN, R., LADBURY, J. E., PIPER, P. W. & PEARL, L. H. 1997. Identification and structural characterization of the ATP/ADP-binding site in the Hsp90 molecular chaperone. *Cell,* 90**,** 65-75.

PRODROMOU, C., SILIGARDI, G., O'BRIEN, R., WOOLFSON, D. N., REGAN, L., PANARETOU, B., LADBURY, J. E., PIPER, P. W. & PEARL, L. H. 1999. Regulation of Hsp90 ATPase activity by tetratricopeptide repeat (TPR)-domain co-chaperones. *EMBO Journal,* 18**,** 754-762.

PRUS, W., ZABKA, M., BIEGANOWSKI, P. & FILIPEK, A. 2011. Nuclear translocation of Sgt1 depends on its phosphorylation state. *Int J Biochem Cell Biol,* 43**,** 1747-53.

PUTCHA, P., DANZER, K. M., KRANICH, L. R., SCOTT, A., SILINSKI, M., MABBETT, S., HICKS, C. D., VEAL, J. M., STEED, P. M., HYMAN, B. T. & MCLEAN, P. J. 2010. Brain-permeable small-molecule inhibitors of Hsp90 prevent α-synuclein oligomer formation and rescue α-synuclein-induced toxicity. *Journal of Pharmacology and Experimental Therapeutics,* 332**,** 849-857.

RADLI, M. & RÜDIGER, S. G. D. 2018. Dancing with the Diva: Hsp90–Client Interactions. *Journal of Molecular Biology,* 430**,** 3029-3040.

RAJAGOPAL, P., TSE, E., BORST, A. J., DELBECQ, S. P., SHI, L., SOUTHWORTH, D. R. & KLEVIT, R. E. 2015. A conserved histidine modulates HSPB5 structure to trigger chaperone activity in response to stress-related acidosis. *Elife,* 4.

RAMOS, C. H., OLIVEIRA, C. L., FAN, C. Y., TORRIANI, I. L. & CYR, D. M. 2008. Conserved central domains control the quaternary structure of type I and type II Hsp40 molecular chaperones. *J Mol Biol,* 383**,** 155-66.

RAMSEY, A. J. & CHINKERS, M. 2002. Identification of potential physiological activators of protein phosphatase 5. *Biochemistry,* 41**,** 5625-5632.

RAPPSILBER, J., MANN, M. & ISHIHAMA, Y. 2007. Protocol for micro-purification, enrichment, pre-fractionation and storage of peptides for proteomics using StageTips. *Nat Protoc,* 2**,** 1896-906.

RATAJCZAK, T. & CARRELLO, A. 1996. Cyclophilin 40 (CyP-40), mapping of its hsp90 binding domain and evidence that FKBP52 competes with CyP-40 for hsp90 binding. *Journal of Biological Chemistry,* 271**,** 2961-2965.

RATZKE, C., NGUYEN, M. N. T., MAYER, M. P. & HUGEL, T. 2012. From a ratchet mechanism to random fluctuations evolution of Hsp90's mechanochemical cycle. *Journal of Molecular Biology,* 423**,** 462-471.

RAUCH, J. N., TSE, E., FREILICH, R., MOK, S. A., MAKLEY, L. N., SOUTHWORTH, D. R. & GESTWICKI, J. E. 2017. BAG3 Is a Modular, Scaffolding Protein that physically Links Heat Shock Protein 70 (Hsp70) to the Small Heat Shock Proteins. *J Mol Biol,* 429**,** 128-141.

RAUE, U., OELLERER, S. & ROSPERT, S. 2007. Association of protein biogenesis factors at the yeast ribosomal tunnel exit is affected by the translational status and nascent polypeptide sequence. *J Biol Chem,* 282**,** 7809-16.

REHN, A., LAWATSCHECK, J., JOKISCH, M. L., MADER, S. L., LUO, Q., TIPPEL, F., BLANK, B., RICHTER, K., LANG, K., KAILA, V. R. I. & BUCHNER, J. 2020. A methylated lysine is a switch point for conformational communication in the chaperone Hsp90. *Nat Commun,* 11**,** 1219.

RETZLAFF, M., HAGN, F., MITSCHKE, L., HESSLING, M., GUGEL, F., KESSLER, H., RICHTER, K. & BUCHNER, J. 2010. Asymmetric Activation of the Hsp90 Dimer by Its Cochaperone Aha1. *Molecular Cell,* 37**,** 344-354.

RETZLAFF, M., STAHL, M., EBERL, H. C., LAGLEDER, S., BECK, J., KESSLER, H. & BUCHNER, J. 2009. Hsp90 is regulated by a switch point in the C-terminal domain. *EMBO Reports,* 10**,** 1147-1153.

RICHTER, K., MUSCHLER, P., HAINZL, O., REINSTEIN, J. & BUCHNER, J. 2003. Sti1 is a non-competitive inhibitor of the Hsp90 ATPase. Binding prevents the N-terminal dimerization reaction during the ATPase cycle. *Journal of Biological Chemistry,* 278**,** 10328-10333.

RICHTER, K., WALTER, S. & BUCHNER, J. 2004. The co-chaperone Sba1 connects the ATPase reaction of Hsp90 to the progression of the chaperone cycle. *Journal of Molecular Biology,* 342**,** 1403-1413.

RIGGS, D. L., COX, M. B., CHEUNG-FLYNN, J., PRAPAPANICH, V., CARRIGAN, P. E. & SMITH, D. F. 2004. Functional specificity of co-chaperone interactions with Hsp90 client proteins. *Critical Reviews in Biochemistry and Molecular Biology,* 39**,** 279-295.

RITOSSA, F. 1962. A new puffing pattern induced by temperature shock and DNP in drosophila. *Experientia,* 18**,** 571-573.

RITOSSA, F. 1996. Discovery of the heat shock response. *Cell stress & chaperones,* 1**,** 97-98.

RIVENZON-SEGAL, D., WOLF, S. G., SHIMON, L., WILLISON, K. R. & HOROVITZ, A. 2005. Sequential ATP-induced allosteric transitions of the cytoplasmic chaperonin containing TCP-1 revealed by EM analysis. *Nat Struct Mol Biol,* 12**,** 233-7.

ROGALLA, T., EHRNSPERGER, M., PREVILLE, X., KOTLYAROV, A., LUTSCH, G., DUCASSE, C., PAUL, C., WIESKE, M., ARRIGO, A. P., BUCHNER, J. & GAESTEL, M. 1999. Regulation of Hsp27 oligomerization, chaperone function, and protective activity against oxidative stress/tumor necrosis factor alpha by phosphorylation. *J Biol Chem,* 274**,** 18947-56.

RÖHL, A., WENGLER, D., MADL, T., LAGLEDER, S., TIPPEL, F., HERRMANN, M., HENDRIX, J., RICHTER, K., HACK, G., SCHMID, A. B., KESSLER, H., LAMB, D. C. & BUCHNER, J. 2015. Hsp90 regulates the dynamics of its cochaperone Sti1 and the transfer of Hsp70 between modules. *Nature Communications,* 6.

ROSAM, M. 2018. Bap (Sil1) regulates the molecular chaperone BiP by coupling release of nucleotide and substrate. *Nat. Struct. Mol. Biol.,* 25.

ROSEBROCK, A. P. 2017. Synchronization and Arrest of the Budding Yeast Cell Cycle Using Chemical and Genetic Methods. *Cold Spring Harb Protoc,* 2017.

ROSENBAUM, M., ANDREANI, V., KAPOOR, T., HERP, S., FLACH, H., DUCHNIEWICZ, M. & GROSSCHEDL, R. 2014. MZB1 is a GRP94 cochaperone that enables proper immunoglobulin heavy chain biosynthesis upon ER stress. *Genes and Development,* 28**,** 1165-1178.

ROSENZWEIG, R., NILLEGODA, N. B., MAYER, M. P. & BUKAU, B. 2019. The Hsp70 chaperone network. *Nat Rev Mol Cell Biol,* 20**,** 665-680.

ROSENZWEIG, R., SEKHAR, A., NAGESH, J. & KAY, L. E. 2017. Promiscuous binding by Hsp70 results in conformational heterogeneity and fuzzy chaperone-substrate ensembles. *eLife,* 6.

ROTH, D. M., HUTT, D. M., TONG, J., BOUCHECAREILH, M., WANG, N., SEELEY, T., DEKKERS, J. F., BEEKMAN, J. M., GARZA, D., DREW, L., MASLIAH, E., MORIMOTO, R. I. & BALCH, W. E. 2014. Modulation of the maladaptive stress response to manage diseases of protein folding. *PLoS Biol,* 12**,** e1001998.

ROY, N., NAGESHAN, R. K., RANADE, S. & TATU, U. 2012. Heat shock protein 90 from neglected protozoan parasites. *Biochimica et Biophysica Acta - Molecular Cell Research,* 1823**,** 707-711.

RUAN, L., ZHOU, C., JIN, E., KUCHARAVY, A., ZHANG, Y., WEN, Z., FLORENS, L. & LI, R. 2017. Cytosolic proteostasis through importing of misfolded proteins into mitochondria. *Nature,* 543**,** 443-446.

RUDIGER, S., GERMEROTH, L., SCHNEIDER-MERGENER, J. & BUKAU, B. 1997. Substrate specificity of the DnaK chaperone determined by screening cellulose-bound peptide libraries. *EMBO J.,* 16.

RUDIGER, S., SCHNEIDER-MERGENER, J. & BUKAU, B. 2001. Its substrate specificity characterizes the DnaJ co-chaperone as a scanning factor for the DnaK chaperone. *EMBO J.,* 20.

RUSSMANN, F., STEMP, M. J., MONKEMEYER, L., ETCHELLS, S. A., BRACHER, A. & HARTL, F. U. 2012. Folding of large multidomain proteins by partial encapsulation in the chaperonin TRiC/CCT. *Proc Natl Acad Sci U S A,* 109**,** 21208-15.

RUTHERFORD, S. L. & LINDQUIST, S. 1998. Hsp90 as a capacitor for morphological evolution. *Nature,* 396**,** 336-342.

SAARIKANGAS, J. & BARRAL, Y. 2015. Protein aggregates are associated with replicative aging without compromising protein quality control. *Elife,* 4.

SAHASRABUDHE, P., ROHRBERG, J., BIEBL, M. M., RUTZ, D. A. & BUCHNER, J. 2017. The Plasticity of the Hsp90 Co-chaperone System. *Molecular Cell,* 67**,** 947-961.e5.
SAIBIL, H. R., FENTON, W. A., CLARE, D. K. & HORWICH, A. L. 2013. Structure and allostery of the chaperonin GroEL. *J Mol Biol,* 425**,** 1476-87.
SCHEIBEL, T., NEUHOFEN, S., WEIKL, T., MAYR, C., REINSTEIN, J., VOGEL, P. D. & BUCHNER, J. 1997. ATP-binding properties of human Hsp90. *Journal of Biological Chemistry,* 272**,** 18608-18613.
SCHEUFLER, C. 2000. Structure of TPR domain-peptide complexes: critical elements in the assembly of the Hsp70-Hsp90 multichaperone machine. *Cell,* 101.
SCHEUFLER, C., BRINKER, A., BOURENKOV, G., PEGORARO, S., MORODER, L., BARTUNIK, H., HARTL, F. U. & MOAREFI, I. 2000. Structure of TPR domain-peptide complexes: Critical elements in the assembly of the Hsp70-Hsp90 multichaperone machine. *Cell,* 101**,** 199-210.
SCHMID, A. B., LAGLEDER, S., GRÄWERT, M. A., RÖHL, A., HAGN, F., WANDINGER, S. K., COX, M. B., DEMMER, O., RICHTER, K., GROLL, M., KESSLER, H. & BUCHNER, J. 2012. The architecture of functional modules in the Hsp90 co-chaperone Sti1/Hop. *EMBO Journal,* 31**,** 1506-1517.
SCHOPF, F. H., BIEBL, M. M. & BUCHNER, J. 2017. The HSP90 chaperone machinery. *Nature Reviews Molecular Cell Biology,* 18**,** 345-360.
SCHOPF, F. H., HUBER, E. M., DODT, C., LOPEZ, A., BIEBL, M. M., RUTZ, D. A., MUHLHOFER, M., RICHTER, G., MADL, T., SATTLER, M., GROLL, M. & BUCHNER, J. 2019. The Co-chaperone Cns1 and the Recruiter Protein Hgh1 Link Hsp90 to Translation Elongation via Chaperoning Elongation Factor 2. *Mol Cell,* 74**,** 73-87 e8.
SCHUERMANN, J. P. 2008. Structure of the Hsp110:Hsc70 nucleotide exchange machine. *Mol. Cell,* 31.
SCHULZ-HEDDERGOTT, R. & MOLL, U. M. 2018. Gain-of-function (GOF) mutant p53 as actionable therapeutic target. *Cancers,* 10.
SCIOR, A. 2018. Complete suppression of Htt fibrilization and disaggregation of Htt fibrils by a trimeric chaperone complex. *EMBO J.,* 37.
SCROGGINS, B. T. & NECKERS, L. 2007. Post-translational modification of heat-shock protein 90: Impact on chaperone function. *Expert Opinion on Drug Discovery,* 2**,** 1403-1414.
SCROGGINS, B. T., ROBZYK, K., WANG, D., MARCU, M. G., TSUTSUMI, S., BEEBE, K., COTTER, R. J., FELTS, S., TOFT, D., KARNITZ, L., ROSEN, N. & NECKERS, L. 2007. An Acetylation Site in the Middle Domain of Hsp90 Regulates Chaperone Function. *Molecular Cell,* 25**,** 151-159.
SHAHHEYDARI, H., RAGAGNIN, A., WALKER, A. K., TOTH, R. P., VIDAL, M., JAGARAJ, C. J., PERRI, E. R., KONOPKA, A., SULTANA, J. M. & ATKIN, J. D. 2017. Protein Quality Control and the Amyotrophic Lateral Sclerosis/Frontotemporal Dementia Continuum. *Front Mol Neurosci,* 10**,** 119.
SHARMA, S., CHAKRABORTY, K., MULLER, B. K., ASTOLA, N., TANG, Y. C., LAMB, D. C., HAYER-HARTL, M. & HARTL, F. U. 2008. Monitoring protein conformation along the pathway of chaperonin-assisted folding. *Cell,* 133**,** 142-53.
SHELTON, L. B., BAKER, J. D., ZHENG, D., SULLIVAN, L. E., SOLANKI, P. K., WEBSTER, J. M., SUN, Z., SABBAGH, J. J., NORDHUES, B. A., KOREN, J., III, GHOSH, S., BLAGG, B. S. J., BLAIR, L. J. & DICKEY, C. A. 2017a. Hsp90 activator Aha1 drives production of pathological tau aggregates. *Proceedings of the National Academy of Sciences of the United States of America,* 114**,** 9707-9712.
SHELTON, L. B., KOREN, J., III & BLAIR, L. J. 2017b. Imbalances in the Hsp90 chaperone machinery: Implications for tauopathies. *Frontiers in Neuroscience,* 11.
SHIAU, A. K., HARRIS, S. F., SOUTHWORTH, D. R. & AGARD, D. A. 2006. Structural Analysis of E. coli hsp90 Reveals Dramatic Nucleotide-Dependent Conformational Rearrangements. *Cell,* 127**,** 329-340.
SHIRASU, K. 2009. The HSP90-SGT1 chaperone complex for NLR immune sensors. *Annu Rev Plant Biol,* 60**,** 139-64.
SHORTER, J. 2011. The mammalian disaggregase machinery: Hsp110 synergizes with Hsp70 and Hsp40 to catalyze protein disaggregation and reactivation in a cell-free system. *PLOS ONE,* 6.

SHORTER, J. & LINDQUIST, S. 2004. Hsp104 catalyzes formation and elimination of self-replicating Sup35 prion conformers. *Science,* 304**,** 1793-7.
SHORTER, J. & LINDQUIST, S. 2008. Hsp104, Hsp70 and Hsp40 interplay regulates formation, growth and elimination of Sup35 prions. *EMBO J,* 27**,** 2712-24.
SHORTER, J. & SOUTHWORTH, D. R. 2019. Spiraling in Control: Structures and Mechanisms of the Hsp104 Disaggregase. *Cold Spring Harbor perspectives in biology,* 11**,** a034033.
SIDERA, K. & PATSAVOUDI, E. 2014. HSP90 inhibitors: Current development and potential in cancer therapy. *Recent Patents on Anti-Cancer Drug Discovery,* 9**,** 1-20.
SIEGERT, R., LEROUX, M. R., SCHEUFLER, C., HARTL, F. U. & MOAREFI, I. 2000. Structure of the molecular chaperone prefoldin: unique interaction of multiple coiled coil tentacles with unfolded proteins. *Cell,* 103**,** 621-32.
SILIGARDI, G., PANARETOU, B., MEYERC, P., SINGH, S., WOOLFSON, D. N., PIPER, P. W., PEARL, L. H. & PRODROMOU, C. 2002. Regulation of Hsp90 ATPase activity by the Co-chaperone Cdc37p/p50 cdc37. *Journal of Biological Chemistry,* 277**,** 20151-20159.
SIMA, S. & RICHTER, K. 2018. Regulation of the Hsp90 system. *Biochimica et Biophysica Acta - Molecular Cell Research,* 1865**,** 889-897.
SINGH, A. & XU, Y. J. 2016. The Cell Killing Mechanisms of Hydroxyurea. *Genes (Basel),* 7.
SKJAERVEN, L., CUELLAR, J., MARTINEZ, A. & VALPUESTA, J. M. 2015. Dynamics, flexibility, and allostery in molecular chaperonins. *FEBS Lett,* 589**,** 2522-32.
SLUCHANKO, N. N., BEELEN, S., KULIKOVA, A. A., WEEKS, S. D., ANTSON, A. A., GUSEV, N. B. & STRELKOV, S. V. 2017. Structural Basis for the Interaction of a Human Small Heat Shock Protein with the 14-3-3 Universal Signaling Regulator. *Structure,* 25**,** 305-316.
SMITH, D. F., BAGGENSTOSS, B. A., MARION, T. N. & RIMERMAN, R. A. 1993. Two FKBP-related proteins are associated with progesterone receptor complexes. *Journal of Biological Chemistry,* 268**,** 18365-18371.
SMULDERS, R., CARVER, J. A., LINDNER, R. A., VAN BOEKEL, M. A., BLOEMENDAL, H. & DE JONG, W. W. 1996. Immobilization of the C-terminal extension of bovine alphaA-crystallin reduces chaperone-like activity. *J Biol Chem,* 271**,** 29060-6.
SONDERMANN, H. 2001. Structure of a Bag/Hsc70 complex: convergent functional evolution of Hsp70 nucleotide exchange factors. *Science,* 291.
SOROKA, J., WANDINGER, S. K., MÄUSBACHER, N., SCHREIBER, T., RICHTER, K., DAUB, H. & BUCHNER, J. 2012. Conformational Switching of the Molecular Chaperone Hsp90 via Regulated Phosphorylation. *Molecular Cell,* 45**,** 517-528.
SOTO, C. & PRITZKOW, S. 2018. Protein misfolding, aggregation, and conformational strains in neurodegenerative diseases. *Nat Neurosci,* 21**,** 1332-1340.
SOUSA, R. 2016. Clathrin-coat disassembly illuminates the mechanisms of Hsp70 force generation. *Nat. Struct. Mol. Biol.,* 23.
SOUSA, R. & LAFER, E. M. 2015. The role of molecular chaperones in clathrin mediated vesicular trafficking. *Front. Mol. Biosci.,* 2.
SOUTHWORTH, D. R. & AGARD, D. A. 2008. Species-Dependent Ensembles of Conserved Conformational States Define the Hsp90 Chaperone ATPase Cycle. *Molecular Cell,* 32**,** 631-640.
SPIECHOWICZ, M., BERNSTEIN, H. G., DOBROWOLNY, H., LESNIAK, W., MAWRIN, C., BOGERTS, B., KUZNICKI, J. & FILIPEK, A. 2006. Density of Sgt1-immunopositive neurons is decreased in the cerebral cortex of Alzheimer's disease brain. *Neurochem Int,* 49**,** 487-93.
SPIECHOWICZ, M., ZYLICZ, A., BIEGANOWSKI, P., KUZNICKI, J. & FILIPEK, A. 2007. Hsp70 is a new target of Sgt1--an interaction modulated by S100A6. *Biochem Biophys Res Commun,* 357**,** 1148-53.
STANKIEWICZ, M., NIKOLAY, R., RYBIN, V. & MAYER, M. P. 2010. CHIP participates in protein triage decisions by preferentially ubiquitinating Hsp70-bound substrates. *FEBS J.,* 277.

STEENSGAARD, P., GARRE, M., MURADORE, I., TRANSIDICO, P., NIGG, E. A., KITAGAWA, K., EARNSHAW, W. C., FARETTA, M. & MUSACCHIO, A. 2004. Sgt1 is required for human kinetochore assembly. *EMBO Rep,* 5**,** 626-31.

STEMMANN, O. & LECHNER, J. 1996. The Saccharomyces cerevisiae kinetochore contains a cyclin-CDK complexing homologue, as identified by in vitro reconstitution. *EMBO J,* 15**,** 3611-20.

STEPANOVA, L., LENG, X., PARKER, S. B. & HARPER, J. W. 1996. Mammalian p50Cdc37 is a protein kinase-targeting subunit of Hsp90 that binds and stabilizes Cdk4. *Genes Dev,* 10**,** 1491-502.

STIEGLER, S. C., RÜBBELKE, M., KOROTKOV, V. S., WEIWAD, M., JOHN, C., FISCHER, G., SIEBER, S. A., SATTLER, M. & BUCHNER, J. 2017. A chemical compound inhibiting the Aha1–Hsp90 chaperone complex. *Journal of Biological Chemistry,* 292**,** 17073-17083.

STUTTMANN, J., PARKER, J. E. & NOEL, L. D. 2008. Staying in the fold: The SGT1/chaperone machinery in maintenance and evolution of leucine-rich repeat proteins. *Plant Signal Behav,* 3**,** 283-5.

SUGIYAMA, Y., SUZUKI, A., KISHIKAWA, M., AKUTSU, R., HIROSE, T., WAYE, M. M., TSUI, S. K., YOSHIDA, S. & OHNO, S. 2000. Muscle develops a specific form of small heat shock protein complex composed of MKBP/HSPB2 and HSPB3 during myogenic differentiation. *J Biol Chem,* 275**,** 1095-104.

SUH, W. C., BURKHOLDER, W. F., LU, C. Z., ZHAO, X., GOTTESMAN, M. E. & GROSS, C. A. 1998. Interaction of the Hsp70 molecular chaperone, DnaK, with its cochaperone DnaJ. *Proc Natl Acad Sci U S A,* 95**,** 15223-8.

SUH, W. C., LU, C. Z. & GROSS, C. A. 1999. Structural features required for the interaction of the Hsp70 molecular chaperone DnaK with its cochaperone DnaJ. *J. Biol. Chem.,* 274.

SUURONEN, T., OJALA, J., HYTTINEN, J. M., KAARNIRANTA, K., THORNELL, A., KYRYLENKO, S. & SALMINEN, A. 2008. Regulation of ER alpha signaling pathway in neuronal HN10 cells: role of protein acetylation and Hsp90. *Neurochem Res,* 33**,** 1768-75.

SUZUKI, H., NOGUCHI, S., ARAKAWA, H., TOKIDA, T., HASHIMOTO, M. & SATOW, Y. 2010. Peptide-binding sites as revealed by the crystal structures of the human Hsp40 Hdj1 C-terminal domain in complex with the octapeptide from human Hsp70. *Biochemistry,* 49**,** 8577-84.

SUZUKI, N., CHOE, H. R., NISHIDA, Y., YAMAWAKI-KATAOKA, Y., OHNISHI, S., TAMAOKI, T. & KATAOKA, T. 1990. Leucine-rich repeats and carboxyl terminus are required for interaction of yeast adenylate cyclase with RAS proteins. *Proc Natl Acad Sci U S A,* 87**,** 8711-5.

SWEENY, E. A., JACKREL, M. E., GO, M. S., SOCHOR, M. A., RAZZO, B. M., DESANTIS, M. E., GUPTA, K. & SHORTER, J. 2015. The Hsp104 N-terminal domain enables disaggregase plasticity and potentiation. *Mol Cell,* 57**,** 836-849.

SWEENY, E. A. & SHORTER, J. 2016. Mechanistic and Structural Insights into the Prion-Disaggregase Activity of Hsp104. *J Mol Biol,* 428**,** 1870-85.

SY, J. & TAMAI, Y. 1986. An altered adenylate cyclase in cdc35-1 cell division cycle mutant of yeast. *Biochem Biophys Res Commun,* 140**,** 723-7.

SZKLARCZYK, D., GABLE, A. L., LYON, D., JUNGE, A., WYDER, S., HUERTA-CEPAS, J., SIMONOVIC, M., DONCHEVA, N. T., MORRIS, J. H., BORK, P., JENSEN, L. J. & MERING, C. V. 2019. STRING v11: protein-protein association networks with increased coverage, supporting functional discovery in genome-wide experimental datasets. *Nucleic Acids Res,* 47**,** D607-D613.

SZKLARCZYK, D., MORRIS, J. H., COOK, H., KUHN, M., WYDER, S., SIMONOVIC, M., SANTOS, A., DONCHEVA, N. T., ROTH, A., BORK, P., JENSEN, L. J. & VON MERING, C. 2017. The STRING database in 2017: quality-controlled protein-protein association networks, made broadly accessible. *Nucleic Acids Res,* 45**,** D362-D368.

TAGUCHI, H. 2015. Reaction Cycle of Chaperonin GroEL via Symmetric "Football" Intermediate. *J Mol Biol,* 427**,** 2912-8.

TAIPALE, M., JAROSZ, D. F. & LINDQUIST, S. 2010. HSP90 at the hub of protein homeostasis: Emerging mechanistic insights. *Nature Reviews Molecular Cell Biology,* 11**,** 515-528.

TAIPALE, M., KRYKBAEVA, I., KOEVA, M., KAYATEKIN, C., WESTOVER, K. D., KARRAS, G. I. & LINDQUIST, S. 2012. Quantitative analysis of Hsp90-client interactions reveals principles of substrate recognition. *Cell,* 150**,** 987-1001.

TAIPALE, M., TUCKER, G., PENG, J., KRYKBAEVA, I., LIN, Z. Y., LARSEN, B., CHOI, H., BERGER, B., GINGRAS, A. C. & LINDQUIST, S. 2014. A quantitative chaperone interaction network reveals the architecture of cellular protein homeostasis pathways. *Cell,* 158**,** 434-448.

TAKAYAMA, S., XIE, Z. & REED, J. C. 1999. An evolutionarily conserved family of Hsp70/Hsc70 molecular chaperone regulators. *J. Biol. Chem.,* 274.

TAYLOR, R. C. D., A. 2011. Aging as an event of proteostasis collapse. *Cold Spring Harb Perspect Biol. ,* 1.

TENGE, V. R., ZUEHLKE, A. D., SHRESTHA, N. & JOHNSON, J. L. 2015. The Hsp90 cochaperones Cpr6, Cpr7, and Cns1 interact with the intact ribosome. *Eukaryot Cell,* 14**,** 55-63.

TESIC, M., MARSH, J. A., CULLINAN, S. B. & GABER, R. F. 2003. Functional interactions between Hsp90 and the co-chaperones Cns1 and Cpr7 in Saccharomyces cerevisiae. *Journal of Biological Chemistry,* 278**,** 32692-32701.

TETER, S. A., HOURY, W. A., ANG, D., TRADLER, T., ROCKABRAND, D., FISCHER, G., BLUM, P., GEORGOPOULOS, C. & HARTL, F. U. 1999. Polypeptide flux through bacterial Hsp70: DnaK cooperates with trigger factor in chaperoning nascent chains. *Cell,* 97**,** 755-65.

THELESTAM, M. & GROSS, R. 1990. Toxins acting on the cytoskeleton. *Handbook of Toxinology***,** 423–492.

THOMAS, P. D., CAMPBELL, M. J., KEJARIWAL, A., MI, H., KARLAK, B., DAVERMAN, R., DIEMER, K., MURUGANUJAN, A. & NARECHANIA, A. 2003. PANTHER: a library of protein families and subfamilies indexed by function. *Genome Res,* 13**,** 2129-41.

TONG, A. H. & BOONE, C. 2006. Synthetic genetic array analysis in Saccharomyces cerevisiae. *Methods Mol Biol,* 313**,** 171-92.

TSUTSUMI, S., MOLLAPOUR, M., PRODROMOU, C., LEE, C. T., PANARETOU, B., YOSHIDA, S., MAYER, M. P. & NECKERS, L. M. 2012. Charged linker sequence modulates eukaryotic heat shock protein 90 (Hsp90) chaperone activity. *Proceedings of the National Academy of Sciences of the United States of America,* 109**,** 2937-2942.

TYANOVA, S., TEMU, T., SINITCYN, P., CARLSON, A., HEIN, M. Y., GEIGER, T., MANN, M. & COX, J. 2016. The Perseus computational platform for comprehensive analysis of (prote)omics data. *Nat Methods,* 13**,** 731-40.

UETZ, P., GIOT, L., CAGNEY, G., MANSFIELD, T. A., JUDSON, R. S., KNIGHT, J. R., LOCKSHON, D., NARAYAN, V., SRINIVASAN, M., POCHART, P., QURESHI-EMILI, A., LI, Y., GODWIN, B., CONOVER, D., KALBFLEISCH, T., VIJAYADAMODAR, G., YANG, M., JOHNSTON, M., FIELDS, S. & ROTHBERG, J. M. 2000. A comprehensive analysis of protein-protein interactions in Saccharomyces cerevisiae. *Nature,* 403**,** 623-7.

UNGEWICKELL, E. 1995. Role of auxilin in uncoating clathrin-coated vesicles. *Nature,* 378.

VACCHI, E., KAELIN-LANG, A. & MELLI, G. 2020. Tau and Alpha Synuclein Synergistic Effect in Neurodegenerative Diseases: When the Periphery Is the Core. *Int J Mol Sci,* 21.

VAN ANKEN, E., PENA, F., HAFKEMEIJER, N., CHRISTIS, C., ROMIJN, E. P., GRAUSCHOPF, U., OORSCHOT, V. M. J., PERTEL, T., ENGELS, S., ORA, A., LÁSTUN, V., GLOCKSHUBER, R., KLUMPERMAN, J., HECK, A. J. R., LUBAN, J. & BRAAKMAN, I. 2009. Efficient IgM assembly and secretion require the plasma cell induced endoplasmic reticulum protein pERp1. *Proceedings of the National Academy of Sciences of the United States of America,* 106**,** 17019-17024.

VARSHAVSKY, A. 2017. The Ubiquitin System, Autophagy, and Regulated Protein Degradation. *Annu Rev Biochem,* 86**,** 123-128.

VAUGHAN, C. K., MOLLAPOUR, M., SMITH, J. R., TRUMAN, A., HU, B., GOOD, V. M., PANARETOU, B., NECKERS, L., CLARKE, P. A., WORKMAN, P., PIPER, P. W., PRODROMOU, C. & PEARL, L. H. 2008. Hsp90-Dependent Activation of Protein Kinases Is Regulated by Chaperone-Targeted Dephosphorylation of Cdc37. *Molecular Cell,* 31**,** 886-895.

VERBA, K. A., WANG, R. Y. R., ARAKAWA, A., LIU, Y., SHIROUZU, M., YOKOYAMA, S. & AGARD, D. A. 2016. Atomic structure of Hsp90-Cdc37-Cdk4 reveals that Hsp90 traps and stabilizes an unfolded kinase. *Science,* 352**,** 1542-1547.

VON MERING, C., HUYNEN, M., JAEGGI, D., SCHMIDT, S., BORK, P. & SNEL, B. 2003. STRING: a database of predicted functional associations between proteins. *Nucleic Acids Res,* 31**,** 258-61.

VRANKEN, W. F., BOUCHER, W., STEVENS, T. J., FOGH, R. H., PAJON, A., LLINAS, M., ULRICH, E. L., MARKLEY, J. L., IONIDES, J. & LAUE, E. D. 2005. The CCPN data model for NMR spectroscopy: development of a software pipeline. *Proteins,* 59**,** 687-96.

VUISTER, G. W., DELAGLIO, F. & BAX, A. 1993. The use of 1JC alpha H alpha coupling constants as a probe for protein backbone conformation. *J Biomol NMR,* 3**,** 67-80.

WALDMANN, T., NIMMESGERN, E., NITSCH, M., PETERS, J., PFEIFER, G., MULLER, S., KELLERMANN, J., ENGEL, A., HARTL, F. U. & BAUMEISTER, W. 1995. The thermosome of Thermoplasma acidophilum and its relationship to the eukaryotic chaperonin TRiC. *Eur J Biochem,* 227**,** 848-56.

WALERYCH, D., KUDLA, G., GUTKOWSKA, M., WAWRZYNOW, B., MULLER, L., KING, F. W., HELWAK, A., BOROS, J., ZYLICZ, A. & ZYLICZ, M. 2004. Hsp90 chaperones wild-type p53 tumor suppressor protein. *Journal of Biological Chemistry,* 279**,** 48836-48845.

WALLACE, E. W., KEAR-SCOTT, J. L., PILIPENKO, E. V., SCHWARTZ, M. H., LASKOWSKI, P. R., ROJEK, A. E., KATANSKI, C. D., RIBACK, J. A., DION, M. F., FRANKS, A. M., AIROLDI, E. M., PAN, T., BUDNIK, B. A. & DRUMMOND, D. A. 2015. Reversible, Specific, Active Aggregates of Endogenous Proteins Assemble upon Heat Stress. *Cell,* 162**,** 1286-98.

WANDINGER, S. K., SUHRE, M. H., WEGELE, H. & BUCHNER, J. 2006. The phosphatase Ppt1 is a dedicated regulator of the molecular chaperone Hsp90. *EMBO Journal,* 25**,** 367-376.

WANG, X., VENABLE, J., LAPOINTE, P., HUTT, D. M., KOULOV, A. V., COPPINGER, J., GURKAN, C., KELLNER, W., MATTESON, J., PLUTNER, H., RIORDAN, J. R., KELLY, J. W., YATES III, J. R. & BALCH, W. E. 2006. Hsp90 Cochaperone Aha1 Downregulation Rescues Misfolding of CFTR in Cystic Fibrosis. *Cell,* 127**,** 803-815.

WAYNE, N. & BOLON, D. N. 2007. Dimerization of Hsp90 is required for in vivo function: Design and analysis of monomers and dimers. *Journal of Biological Chemistry,* 282**,** 35386-35395.

WEAVER, A. J., SULLIVAN, W. P., FELTS, S. J., OWEN, B. A. L. & TOFT, D. O. 2000. Crystal structure and activity of human p23, a heat shock protein 90 co-chaperone. *Journal of Biological Chemistry,* 275**,** 23045-23052.

WEGELE, H., WANDINGER, S. K., SCHMID, A. B., REINSTEIN, J. & BUCHNER, J. 2006. Substrate transfer from the chaperone Hsp70 to Hsp90. *Journal of Molecular Biology,* 356**,** 802-811.

WEGRZYN, R. D., HOFMANN, D., MERZ, F., NIKOLAY, R., RAUCH, T., GRAF, C. & DEUERLING, E. 2006. A conserved motif is prerequisite for the interaction of NAC with ribosomal protein L23 and nascent chains. *J Biol Chem,* 281**,** 2847-57.

WEIKL, T., ABELMANN, K. & BUCHNER, J. 1999. An unstructured C-terminal region of the Hsp90 co-chaperone p23 is important for its chaperone function. *Journal of Molecular Biology,* 293**,** 685-691.

WELCH, W. J. & FERAMISCO, J. R. 1982. Purification of the major mammalian heat shock proteins. *J Biol Chem,* 257**,** 14949-59.

WENDLER, P., SHORTER, J., SNEAD, D., PLISSON, C., CLARE, D. K., LINDQUIST, S. & SAIBIL, H. R. 2009. Motor mechanism for protein threading through Hsp104. *Mol Cell,* 34**,** 81-92.

WESSEL, D. & FLUGGE, U. I. 1984. A method for the quantitative recovery of protein in dilute solution in the presence of detergents and lipids. *Anal Biochem,* 138**,** 141-3.

WHITESELL, L. & LINDQUIST, S. L. 2005. HSP90 and the chaperoning of cancer. *Nature Reviews Cancer,* 5**,** 761-772.

WHITESELL, L., MIMNAUGH, E. G., DE COSTA, B., MYERS, C. E. & NECKERS, L. M. 1994. Inhibition of heat shock protein HSP90-pp60(v-src) heteroprotein complex formation by benzoquinone ansamycins: Essential role for stress proteins in oncogenic transformation. *Proceedings of the National Academy of Sciences of the United States of America,* 91**,** 8324-8328.

WHITESELL, L., SUTPHIN, P. D., PULCINI, E. J., MARTINEZ, J. D. & COOK, P. H. 1998. The physical association of multiple molecular chaperone proteins with mutant p53 is altered by geldanamycin, an hsp90-binding agent. *Molecular and Cellular Biology,* 18**,** 1517-1524.

WIEDMANN, B., SAKAI, H., DAVIS, T. A. & WIEDMANN, M. 1994. A protein complex required for signal-sequence-specific sorting and translocation. *Nature,* 370**,** 434-40.

WIESGIGL, M. & CLOS, J. 2001. Heat shock protein 90 homeostasis controls stage differentiation in Leishmania donovani. *Molecular Biology of the Cell,* 12**,** 3307-3316.

WILLHOFT, O., KERR, R., PATEL, D., ZHANG, W., AL-JASSAR, C., DAVITER, T., MILLSON, S. H., THALASSINOS, K. & VAUGHAN, C. K. 2017. The crystal structure of the Sgt1-Skp1 complex: the link between Hsp90 and both SCF E3 ubiquitin ligases and kinetochores. *Sci Rep,* 7**,** 41626.

WILLMUND, F., DEL ALAMO, M., PECHMANN, S., CHEN, T., ALBANESE, V., DAMMER, E. B., PENG, J. & FRYDMAN, J. 2013. The cotranslational function of ribosome-associated Hsp70 in eukaryotic protein homeostasis. *Cell,* 152**,** 196-209.

WU, C. C., NAVEEN, V., CHIEN, C. H., CHANG, Y. W. & HSIAO, C. D. 2012. Crystal structure of DnaK protein complexed with nucleotide exchange factor GrpE in DnaK chaperone system: insight into intermolecular communication. *J. Biol. Chem.,* 287.

YAN, M., LI, J. & SHA, B. 2011. Structural analysis of the Sil1-Bip complex reveals the mechanism for Sil1 to function as a nucleotide-exchange factor. *Biochem. J.,* 438.

YAN, W. & CRAIG, E. A. 1999. The glycine-phenylalanine-rich region determines the specificity of the yeast Hsp40 Sis1. *Mol. Cell. Biol.,* 19.

YANG, J., ROE, S. M., CLIFF, M. J., WILLIAMS, M. A., LADBURY, J. E., COHEN, P. T. W. & BARFORD, D. 2005. Molecular basis for TPR domain-mediated regulation of protein phosphatase 5. *EMBO Journal,* 24**,** 1-10.

YOKOM, A. L., GATES, S. N., JACKREL, M. E., MACK, K. L., SU, M., SHORTER, J. & SOUTHWORTH, D. R. 2016. Spiral architecture of the Hsp104 disaggregase reveals the basis for polypeptide translocation. *Nat Struct Mol Biol,* 23**,** 830-7.

ZABKA, M., LESNIAK, W., PRUS, W., KUZNICKI, J. & FILIPEK, A. 2008. Sgt1 has co-chaperone properties and is up-regulated by heat shock. *Biochem Biophys Res Commun,* 370**,** 179-83.

ZAHN, M. 2013. Structural studies on the forward and reverse binding modes of peptides to the chaperone DnaK. *J. Mol. Biol.,* 425.

ZHANG, M., BOTER, M., LI, K., KADOTA, Y., PANARETOU, B., PRODROMOU, C., SHIRASU, K. & PEARL, L. H. 2008. Structural and functional coupling of Hsp90- and Sgt1-centred multi-protein complexes. *EMBO J,* 27**,** 2789-98.

ZHANG, Y., SINNING, I. & ROSPERT, S. 2017. Two chaperones locked in an embrace: structure and function of the ribosome-associated complex RAC. *Nat Struct Mol Biol,* 24**,** 611-619.

ZHAO, R., DAVEY, M., HSU, Y. C., KAPLANEK, P., TONG, A., PARSONS, A. B., KROGAN, N., CAGNEY, G., MAI, D., GREENBLATT, J., BOONE, C., EMILI, A. & HOURY, W. A. 2005. Navigating the chaperone network: An integrative map of physical and genetic interactions mediated by the hsp90 chaperone. *Cell,* 120**,** 715-727.

ZHAO, R., KAKIHARA, Y., GRIBUN, A., HUEN, J., YANG, G., KHANNA, M., COSTANZO, M., BROST, R. L., BOONE, C., HUGHES, T. R., YIP, C. M. & HOURY, W. A. 2008. Molecular chaperone Hsp90 stabilizes Pih1/Nop17 to maintain R2TP complex activity that regulates snoRNA accumulation. *Journal of Cell Biology,* 180**,** 563-578.

ZHENG, N. & SHABEK, N. 2017. Ubiquitin Ligases: Structure, Function, and Regulation. *Annu Rev Biochem,* 86**,** 129-157.

ZHENG, Y. H., MA, Y. Y., DING, Y., CHEN, X. Q. & GAO, G. X. 2018. An insight into new strategies to combat antifungal drug resistance. *Drug Des Devel Ther,* 12**,** 3807-3816.

ZHU, X. 1996. Structural analysis of substrate binding by the molecular chaperone DnaK. *Science,* 272.

ZIERER, B. K., RÜBBELKE, M., TIPPEL, F., MADL, T., SCHOPF, F. H., RUTZ, D. A., RICHTER, K., SATTLER, M. & BUCHNER, J. 2016. Importance of cycle timing for the function of the molecular chaperone Hsp90. *Nature Structural and Molecular Biology,* 23**,** 1020-1028.

ZOU, X., JI, C., WANG, L., WU, M., ZHENG, H., XU, J., JIN, F., GU, S., YING, K., XIE, Y. & MAO, Y. 2004. Molecular cloning and characterization of SGT1.2, a novel splice variant of Homo sapiens SGT1. *DNA Seq,* 15**,** 140-3.

ZUEHLKE, A. D. & JOHNSON, J. L. 2012. Chaperoning the chaperone: A role for the co-chaperone Cpr7 in modulating Hsp90 function in Saccharomyces cerevisiae. *Genetics,* 191**,** 805-814.

ZUEHLKE, A. D., MOSES, M. A. & NECKERS, L. 2018. Heat shock protein 90: Its inhibition and function. *Philosophical Transactions of the Royal Society B: Biological Sciences,* 373.

ZUEHLKE, A. D., REIDY, M., LIN, C., LAPOINTE, P., ALSOMAIRY, S., LEE, D. J., RIVERA-MARQUEZ, G. M., BEEBE, K., PRINCE, T., LEE, S., TREPEL, J. B., XU, W., JOHNSON, J., MASISON, D. & NECKERS, L. 2017. An Hsp90 co-chaperone protein in yeast is functionally replaced by site-specific posttranslational modification in humans. *Nature Communications,* 8.

ZUIDERWEG, E. R., HIGHTOWER, L. E. & GESTWICKI, J. E. 2017. The remarkable multivalency of the Hsp70 chaperones. *Cell Stress Chaperones,* 22.

11. Publications

Florian H Schopf, Eva M Huber, Christopher Dodt, Abraham Lopez, Maximilian M Biebl, Daniel A Rutz, Moritz Mühlhofer, Gesa Richter, Tobias Madl, Michael Sattler, Michael Groll, & Johannes Buchner; (2019); The co-chaperone Cns1 and the recruiter protein Hgh1 link Hsp90 to translation elongation via chaperoning elongation factor 2. Mol Cell, 74, 73-78.

12. Acknowledgement

Diese Dissertation wurde am Lehrstuhl für Biotechnologie der Technischen Universität München unter Aufsicht von Prof. Dr. Johannes Buchner angefertigt.

Zu aller erst möchte ich Prof. Dr. Johannes Buchner danken für die Möglichkeit meine Promotion an dem Lehrstuhl für Biotechnologie durchzuführen. Ich möchte Johannes für die Unterstützung und Diskussion in allen Fragen danken. Außerdem für das Bereitstellen der materiellen Möglichkeiten jegliche Experimente durchzuführen und Kontakte zu Kooperationspartner zu knüpfen. Insgesamt möchte ich mich für die stetige Unterstützung und die großartige Arbeitsatmosphäre bedanken. Darüber hinaus möchte ich mich für die Möglichkeit bedanken, dass ich an den Hsp90-Konferenzen sowie der CSHL-Konferenz und den SFB1035-Meetings teilnehmen konnte.

Ich möchte Prof. Dr. Michael Sattler und Dr. Abraham Lopez für die Zusammenarbeit bei den NMR-Experimenten und den wissenschaftlichen Austausch sehr danken.

Ein großes Dankeschön möchte ich an den ganzen Lehrstuhl Biotechnologie richten. Ich möchte aktuellen und ehemaligen Kollegen herzlich danken für die nicht nur lehrreichen sondern auch sehr schönen und lustigen vergangenen vier Jahre. Vielen Dank an Frau Rubinstein, die sich stets um alle organisatorischen Anliegen kümmerte und immer das Beste für einen wollte. Zudem möchte ich Frau Hilber danken für die Unterstützung in weiteren organisatorischen Anliegen. Außerdem möchte ich Bettina Richter, Anja Osterauer, Laura Meier, Ruby Khan und Florian Rührnößl für die stetige Unterstützung im Labor danken. Florian Rührnößl möchte ich zudem für die Zusammenarbeit bei den HDX-Experimenten danken.

Herzlichen Dank möchte ich auch an Moritz für die Zusammenarbeit bei den MS-Experimenten richten. Ich möchte mich bei Jannis, Pamina, Moritz und Maxi bedanken, die mich von Anfang an gemeinsam, freundschaftlich durch die Promotion begleitet haben. Außerdem möchte ich mich für nicht immer fruchtbare aber dafür immer schöne Diskussionsrunden bei Tuan, Georg, Ramona und Maxi bedanken. Auch möchte ich mich bei Benji und Jannis für die gelegentliche Kreativpause am Kicker bedanken. Darüber hinaus möchte ich mich bei den Alumni Florian Schopf, Daniel Rutz und Benedikt Weber herzlichst bedanken, die mir den Einstieg in die Promotion erleichtert haben und mich in meiner Anfangszeit und darüber hinaus in Freundschaft begleitet haben. Zudem möchte ich Max und Marie-Lena vom Lehrstuhl für Synthetische Biochemie danken nicht nur für den wissenschaftlichen Austausch, sondern besonders auch für die freundschaftliche Unterstützung.

Ich möchte auch meinen Freunden außerhalb des Arbeitskreises für die stetige Unterstützung danken.

Danke Mama, Papa und Katti für absolut alles.

13. Declaration

Hereby I, Christopher Marius Dodt, declare that this thesis was prepared by me independently, without use of other resources or references than stated here. The work has not been presented to any examination board yet.

Hiermit erkläre ich, Christopher Marius Dodt, dass die vorliegende Arbeit selbständig verfasst wurde. Dabei wurden keine anderen als die angegebenen Hilfsmittel oder Quellen verwendet. Die Arbeit wurde noch keiner Prüfungskommission vorgelegt.

Christopher Marius Dodt